SYNERGISTIC AND DOSE RATE EFFECTS IN BORON NEUTRON CAPTURE THERAPY

by

BEN PHOENIX

A thesis submitted to
The University of Birmingham
for the degree of
DOCTOR OF PHILOSOPHY

School of Physics and Astronomy
The University of Birmingham

March 2012

Abstract

An investigation of the factors affecting the biological effectiveness of neutron beams suitable for Boron Neutron Capture Therapy (BNCT) has been carried out. This has focused on two main areas of current uncertainty. The primary experimental work described in this thesis concerns the degree of interaction, if any, between biological damage caused by low Linear Energy Transfer(LET) radiation and that caused by high LET radiation. The second area investigated concerns the biological impact of delivering a BNCT irradiation at differing dose rates.

Previously published work by McNally *et al*[1] suggested that the biological effect of irradiation with photons and alpha particles together may be greater than suggested by the combined response to the single fields. This would have implications for BNCT as treatment irradiations are a mix of different radiation qualities. Results of extending the quasi-simultaneous exposures of McNally *et al* to truly simultaneous exposures with alpha particles and photons are presented in this thesis.

In mixed ^{60}Co photon and ^{238}Pu alpha particle irradiations, no synergistic effect was observed above the response from the separate components. Maximum alpha particle doses delivered were 2.54 Gy. In mixed 250 kVp X-ray and ^{238}Pu alpha particle exposures, no synergy effect was seen with 2.54 Gy of alpha particles delivered to the cells. At the 3.18Gy alpha particle dose level, significantly lower cell survival was observed than would be predicted from survival in single fields. The mixed field data was compared to various published model treatments of synergistic effect. No model was found to fit the mixed field data, either presented here or by McNally *et al*, at all alpha particle dose levels.

The second area of experimental work concerned the dose rate effect in BNCT treatment beams. The principle that low LET radiation delivered at high dose rates is more biologically effective, for a given dose, than radiation delivered at low dose rates is well established [2]. How this principle applies to mixed field irradiations, such as those found in BNCT treatments, is less clear.

Dose rate experiments on cell survival in the Massachusetts Institute of Technology (MIT) Fission Converter neutron beam have been carried out. Cells loaded with boric acid were exposed to the beam inside a water phantom at dose rate differing by a factor of approximately 15. A dose rate effect was observed at both of the irradiation depths used, although this was only clearly significant at 50 mm depth within the phantom. Analysis of the data demonstrates that the effect observed was too large to explained solely by a dose rate effect within the photon component.

Following the same protocol as the MIT experiments, cells were also exposed to the Birmingham accelerator based epithermal neutron beam in the presence of 50 μg per gram concentrations of enriched boric acid. Survival data collected for the Birmingham beam were in agreement with previously published work by Gabel *et al* [3], with no account made for dose rate effects. This suggests that no significant dose rate effect was observed at this boron concentration.

The implications of these results are discussed in the context of clinical applications of BNCT.

Acknowledgements

Many thanks to all of the Birmingham BNCT and Medical Physics team for their help, support and advice during my time working on this project. In particular to my supervisors Andrew Mill and Stuart Green who have taught me everything I know about cell culture and radiation dosimetry, and who were always available when needed. Thanks also to Monty Charles and Cecile Wojnecki for their helpful advice. The dynamitron measurements were enabled by the hard work and expertise of its operators; thanks to John Lowe and Greg Wood. All of the supporting dosimetry for the work with neutron beams was provided by Zamir Ghani, to whom I am extremely grateful.

The MRC team of Mark Hill, David Stevens and James Thompson provided facilities, consumables and knowledge which allowed the various mixed field irradiations to take place. Thanks to them for this and for making the whole experience an enjoyable one.

The measurements at MIT would not have been possible without the help and cooperation of the MIT reactor technicians and operators. Particular thanks to Tom Newton and Tom Bork for working long days running the beam, Gil Westmeyer and Victor Lelyveld for the use of their lab and Matthew Davidson and Jacquelyn Yanch for providing cells, incubators and advice. A special mention also to Rachel Batista for handling much of the logistics and ordering that made the project possible. Thanks to the EPSRC for providing funding for this project.

Final thanks to my wonderful girlfriend Evelyn Miles for looking after me and keeping me sane during the final stages of this project.

Contents

List of Figures

List of Tables

Chapter 1

INTRODUCTION

Radiotherapy is the use of ionising radiation to treat cancerous tumours. Conventional external beam radiotherapy is performed using photons and electrons, generated by linear accelerators in all modern facilities. It relies on precise imaging of the tumour volume, typically via X-ray Computed Tomography (CT) scans. Doses to tumour are maximised, while minimising doses to surrounding healthy tissue, via multiple overlapping radiation fields and manipulating the shape of the fields through the use of multileaf collimators [4].

Recently there has been much development of ion beam sources for use in external beam radiotherapy. The advantage of ion beams is that they have a very sharp Bragg peak, the position of which can be tuned using accelerator energy adjustments, allowing very precise delivery of much of the ions energy in a well defined volume. This makes it possible to deliver very high tumour doses with reduced doses to healthy tissue.

Boron Neutron Capture Therapy (BNCT) is unusual in that it uses an external neutron beam combined with an internal chemical agent to provide a radiation dose to a tumour. As the name implies, the internal agent is a compound containing ^{10}B. This has a very high capture cross-section for neutrons in the thermal and epithermal energy range as shown in figure 1.1. The details of the boron capture reaction are shown below:

$$^{10}B + n \longrightarrow ^{7}Li + ^{4}He \qquad (2.79MeV) \tag{1.0.1}$$

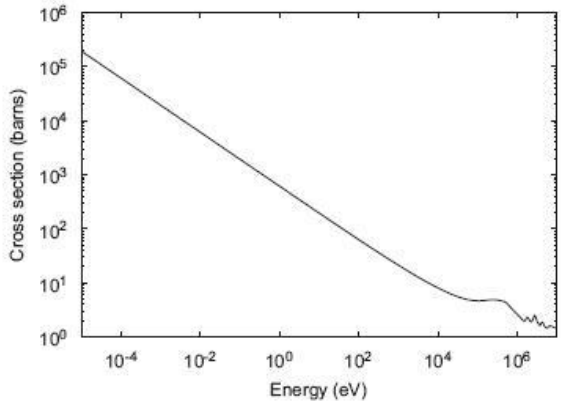

Figure 1.1: *Neutron capture cross-section for* ^{10}B *[5]*

$$^{10}B + n \longrightarrow ^{7}\,Li^{*} + ^{4}\,He \qquad (2.32MeV) \tag{1.0.2}$$

Around 94% of the reactions result in the Li being left in the ground state (1.0.2) [5].

This capture reaction has the advantage that its reaction products have extremely high Linear Energy Transfer (LET) resulting in very short ranges in tissue. This means that the dose delivered by each reaction is confined to a few cells, allowing large differentials in dose between tissue with high boron concentrations and tissue with low concentrations. Boron has a further advantage in that its atomic mass is similar to carbon allowing it to be substituted for carbon in a range of organic compounds. It also has a low toxicity [6].

The targeted nature of BNCT means that it is particularly suited to treating some types of tumour for which existing treatment modalities are problematic. Particularly of interest is the treatment of Glioblastoma Multiforme (GBM), the most aggressive form of glioma [7]. The prognosis for patients with GBM is generally very poor, with median patient survival of around 12 months. This is largely due to the frequency of tumour recurrence after surgical resection [8]. This recurrence is common because of the infiltration of otherwise healthy tissue by tumour tendrils. Treatment is complicated by the resistance of the malignant cells to damage, inability of most treatment compounds to cross the blood brain barrier, the susceptibility of the brain to damage and the poor repair capacity of brain

tissue. Maximum doses to tumour of ∼65Gy, delivered in 2Gy fractions, are required for conventional treatment. [9] This dose is limited by dose to the healthy brain tissue and associated toxicity.

1.1 History of BNCT for Glioblastoma Multiforme

The first clinical trial of BNCT was carried out at Brookhaven National Laboratory(BNL). Ten GBM patients who had previously had their tumours surgically debulked, were irradiated using a thermal beam from the reactor. Borax, delivered intravenously at doses of up to 200 mg/kg, was used as the boron carrying agent. Five patients received a single radiation dose, and the remaining 5 were given the treatment in 2 to 4 fractions. Results were disappointing; there were complications with radiation erosion of the patients scalps and all patients died from 6 to 21 weeks after treatment [10]. This was a typical survival time for glioblastoma patients in the 1950s regardless of treatment methodology.

A second series, comprising 9 malignant glioma patients, was treated with a less toxic borate preparation, sodium pentaborate with D-glucose in the molar ratio 2:1.[11] While survival times were somewhat improved compared to the first series, with median survival rising from 97 to 147 days, there were still significant problems with radiation damage to the scalp. Attempts to reduce this with the aid of pressure bandages in later patients were unsuccessful [12]. In the third series of nine patients treated at Brookhaven, in order to reduce radiation dose to the scalp, the pentaborate solution was delivered directly to the internal carotid artery of the tumour-bearing hemisphere of the patients. While these patients showed no signs of severe radiation dermatitis exhibited by previous groups their median survival was on a par with group one; 96 days.

The second trial was carried out at the Massachusetts Institute of Technology (MIT)'s reactor, which had just been constructed. To address the issues with scalp damage patients in the second trial had the scalp and bone flaps which were created in their prior surgery

turned down to expose tumour containing brain directly to the thermal beam. A new compound, p-carboxyphenylboronic acid, was used as the boron carrier compound in 16 of the 18 patients treated. The final two were treated using sodium perhydrodecaborate. Both compounds were administered intravenously. These were compounds found to have better tumour:brain boron ratios in animal models [13].

Again, results were disappointing. All patients died 10 days to 11.5 months after irradiation. Poor tumour control was shown and extensive necrosis of brain tissue found in a number of cases [14].

The extremely poor outcomes of these initial trials can be attributed mainly to the boron compounds used. They had poor tumour specificity which resulted in large doses to the healthy brain and critically, the vasculature. It is this dose which likely lead to the extensive necrosis observed. The problem was compounded by the lack of a rapid diagnostic method to establish boron levels in the blood. The neutron beams used were also far from optimal, having a thermal spectrum and exhibiting poor penetration into tissue.

Following these initial trials, in 1968, a large series of clinical studies headed by Hiroshi Hatanaka was begun in Japan. These were initially based at the Hitachi Training Reactor (HTR) but eventually irradiations took place at a number of reactor sites across the country. Sulfhydryl borane (BSH) was used as the boron carrying compound administered via a slow infusion, usually intra-arterially, but in later cases intravenously. All irradiations were carried out using a thermal beam with scalp and a skull flap removed. In later cases the void space after tumour resection was maintained by the insertion of an air filled sphere, normally a ping pong ball. This allowed for greater thermal neutron penetration into deeper regions of the tumour. The results from 149 patients, 64 with glioblastoma, are presented in [15]. Analysis by Hatanaka and Nakagawa of various patient sub groups showed improved long term survival rates over patients receiving conventional treatment. Analysis by Laramore *et al* of a small sub-group of patients from the United States, treated in Japan, found results in line with those expected from conventional treatment with no improvement attributable

to BNCT [16].

Improvements in boron compounds through the 1980's, such as the development of boronophenylalanine-fructose, spurred further trials worldwide. These new compounds exhibited both low toxicity and high tumour:normal tissue boron ratios [17]. Development of treatment facilities to deliver neutrons at epithermal (1 eV to 10 keV) energy levels instead of thermal energy levels was also carried out. This increase in beam energy results in higher doses at clinically relevant depths in tissue while reducing skin doses.

Between 1994 and 1999 at the Brookhaven National Laboratory (BNL) 53 patients were treated using a newly epithermal neutron beam. The boron compound used was BPA-fructose. Treatments with varying numbers of fields and at different dose levels were performed [18]. The initial 37 subjects treated had similar clinical outcomes to historical controls with minimal side effects [19]. Problems with side effects such as Central Nervous System(CNS) toxicity, increased as the dose was escalated. The time to progression and survival of subjects in the later protocols, with higher doses and multiple fields, did not compare favourably with historical controls. This lack of positive correlation between favourable clinical outcomes and increasing exposure was taken as indirect proof that benefits from BNCT may be realised at low neutron exposures. This study also exposed the main issue with BPA-fructose; it's poor solubility. This lead to requirements for very large volumes of fluid to patients and some instances of the compound crystallising out of solution [18]. Over the same time period as the BNL study a phase I trial at MIT, with 22 patients treated, was carried out. While some toxicity effects were observed results were generally good. Of the 17 patients for whom Magnetic Resonance Imaging (MRI) follow up studies were available, 11 exhibited marked reduction in tumour volume [20].

Since 2005 the bar has been significantly raised when comparing BNCT results to clinical outcomes from standard treatment. This is due to the widespread adoption of temozolomide as a chemotherapy agent in the treatment of GBM. Results from Stupp *et al* [21] comparing temozolomide plus radiotherapy to radiotherapy alone, in a randomised study of 573

patients, can be seen in figure 1.2.

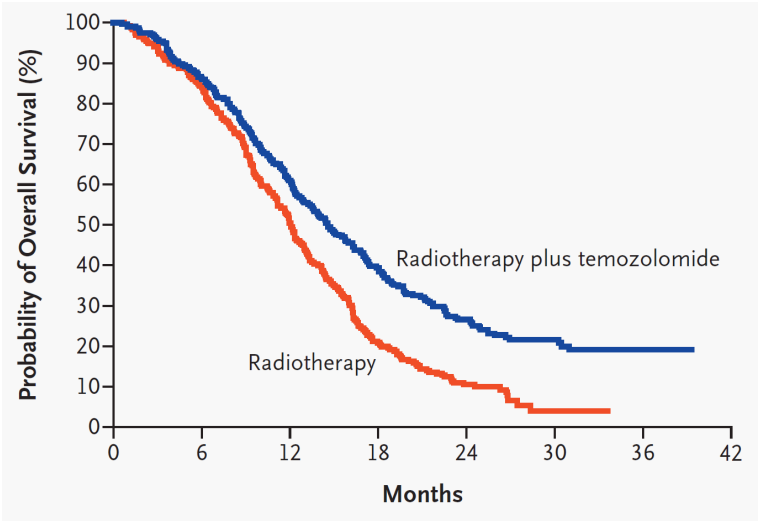

Figure 1.2: *Clinical trial data for conventional radiotherapy treatment of GBM with and without temozolomide, taken from [21]*

Over the past decade a number of further BNCT for GBM trials have been carried out worldwide. At the R2-0 research reactor at Studsvik, Sweden 30 patients were irradiated in a Phase II trial. BPA-fructose was given to patients at higher levels than ever before; doses of 900 mg kg^{-1} [22]. Results demonstrate that BNCT offers a treatment that is at least as effective as conventional radiotherapy alone. Further analysis suggests that for patients with poor response to telozolomide a possible clinical advantage of BNCT over combined telozolomide and radiotherapy was suggested [23]. A small phase I study on the LVR-15 reactor in the Czech Republic has been carried out, using BSH as the boron agent and assessing the limiting toxicity of the BNCT treatment [24]. Five patients received BSH and were exposed to the epithermal beam. Tolerance appeared good but patient numbers were not high enough to form definitive conclusions.

Extensive clinical work has been carried out at the FIR-1 reactor in Helsinki, Finland. BPA-Fructose was used as the boron loading agent and patients were exposed to an epithermal beam. Initial results from Joensuu *et al* were presented in [25] and appeared to demonstrate effectiveness at least equal to conventional treatments. Studies are still ongo-

ing with the facility treating around 1 patient a week, mainly with head and neck cancer or recurrent GBM. A number of BNCT clinical projects are still underway in Japan with recent clinical results being published by Yamamoto *et al* for irradiations, with BSH, on the Japan Research Reactor 4 [26]. Outcomes were consistent with those of conventional radiotherapy treatments. Current work from Yamamoto's group focuses on conventional photon therapy combined with BNCT. Twenty one newly diagnosed GBM patients have been treated with BNCT at the Kyoto University Reactor (KUR) utilising a combination of BPA and BSH as the boron carrying agents. Of the 21, 10 received BNCT alone while 11 received a combination of BNCT and conventional radiation therapy. THe BNCT alone group had a median survival of 15.6 months. The mixed group had a median survival of 23.5 months [26].

Another current trial is at the recruiting stage in Taiwan. This will be a study treating recurrent head and neck cancers using BPA and the Tsing Hua Open-Pool Reactor (THOR) epithermal neutron beam [27]. It is based at the Taipei Veterans General Hospital.

The future of BNCT is reliant on further development of the boron containing compounds. Current clinical work focuses on improving the uptake and retention of these compounds. Human pharmacokinetic and laboratory base trials at the University Hospital, Birmingham of BPA with Mannitol, a compound which disrupts the blood-brain barrier, along with various pre-loading and administration strategies are ongoing and are showing promising results. Patients in the cohorts receiving an additional mannitol bolus are showing approximately double the boron levels, in their extra cellular fluid of the brain, compared to the group which did not receive a bolus. The levels in the first patient to receive the additional mannitol and have BPA administered interarterially appear to show a further doubling, that is four times that found in the no bolus and conventionally administered BPA group [28].

Clinical application will be facilitated by the drive towards suitable accelerator sources for hospital based treatment. Such accelerators are under development worldwide and some,

such as the newly completed Cyclotron-Based Epithermal Neutron Source (C-BENS) [29] are likely to enter the clinical trial phase over the next few years.

1.2 Dose effect uncertainties in BNCT

1.2.1 Beam composition and synergistic effects

All neutron beams, regardless of source, consist of a mix of neutrons with other radiation types. This includes photons, both from the initial neutron production mechanism and capture within various materials. There is also likely to be a significant proton dose from capture reactions. In the case of BNCT neutrons not captured in the boron also provide additional dose. These neutrons have a range of energies. The largest capture reaction contributors to dose are likely to be from nitrogen and hydrogen, both abundant in tissue. These are detailed below;

$$^{1}H + n \longrightarrow ^{2} H + \gamma \qquad (2.25MeV)$$
$$^{12}N + n \longrightarrow ^{12} C + p \qquad (580keV)$$

Relative Biological Effectiveness (RBE) factors have been determined, albeit with large uncertainties, for the individual components [30]. However, these take no account of any possible interaction between the different components, which could result in a greater biological effect than would be the case for independent action of the different radiation types present. What the effect of such interactions, if any, would be is not clear. Such interactions would introduce treatment planning complexity and make the comparison of clinical results between facilities problematic. There have been a number of publications reporting the effects of mixed radiation fields. Unfortunately the evidence is not clear, with many authors reporting synergism [31][32][33][34] [35][36][1][37] and others no effect [38][39][40][41]. In

some cases experimenters have used sequential irradiations, neutrons followed by X-rays for example, while in just a few cases have experimenters used truly simultaneous irradiations as would be the case in BNCT. A literature review of work in this area can be found on page 47.

1.3 Boron Compounds for BNCT

BNCT relies on delivery of boron containing agents to the tumour tissue to be treated; levels of at least 20 μg of boron per g [42] must be achieved. It also requires a clear differential in boron levels in tumour vs levels in healthy brain and blood. These levels and ratio of boron level in tumour to healthy tissue must be maintained over the course of the irradiation. Initial BNCT clinical trials used sodium tetraborate (borax) as their boron delivery agent [43] [44]. This compound was inexpensive, readily available and had low toxicity. Unfortunately it had poor tumour targeting and washed out of cells quickly. It is thought that this played a large role in the unsuccessful outcome of the early trials. Efforts were quickly undertaken to find more suitable compounds.

An amino acid, p-boronophenylalanine (BPA), was synthesised in the late 1950's with BNCT applications in mind [45]. It's structure is shown in figure 1.3. Early compound screening efforts were concerned with compounds which accumulated in tumours but could

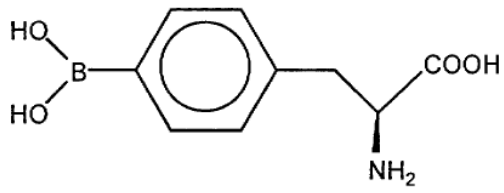

L-BPA

(*p*-borono-L-phenylalanine)

Figure 1.3: *The p-boronophenylalanine (BPA) molecule*

not cross the blood brain barrier into normal brain tissue. This lead to BPA being initially rejected as a therapeutic compound as it readily crossed over. However, the similarity of BPA to melanin precursors lead to it's application in treatment of melanomas after it was shown to accumulate preferentially in melanoma cells[46]. Following this work, Coderre and co-workers demonstrated firstly that BPA was accumulated by non melanoma tumour cells [47], and subsequently control of gliosarcomas in a rat model [48]. The accumulation of BPA in the tumour appears to be related to the increased rate of amino acid transport at the cell membrane. Studies such as [49] demonstrated an incorporation rate in tumour four times that in healthy tissue. Preferential accumulation was also demonstrated in tumour cells away from the main tumour body. Accumulation in such infiltrating cells is necessary for successful treatment of tumours such as glioblastoma multiforme and is likely related to the ability of BPA to cross the blood brain barrier. BPA has since been used in human clinical trials of BNCT all over the world.

More recent work on BPA has concentrated on the uptake mechanism and implications this may have in therapeutic applications. A number of researchers [50] [51] [52] have data that suggest that the BPA uptake is directly related to cell replication, with the quiescent cell population not actively taking up boron. If this is the case in glioblastoma multiforme typically only around 10% of the tumour cell population will be in cycle and taking up BPA [53]. As the boron reaction product range is low, only a small fraction of the tumorous cells will receive the prescribed dose and treatment is unlikely to be successful. At variance with this conclusion is a study by Detta and Cruickshank *et al* [54] at Birmingham. This work focuses on the role of L-Amino Acid Transporter-1 (LAT-1) in BPA uptake. Cell from fresh tumour explants were labelled for proliferating cell nuclear antigen (PCNA), which is an antigen that is expressed in the nuclei of cells during the DNA synthesis phase of the cell cycle. They were also labelled for LAT-1 expression. It was found that PCNA expression and LAT-1 expression were independent, with on average $\sim$70% of the tumour cells expressing LAT-1. In addition, it was found that BPA uptake was inhibited by LAT-1

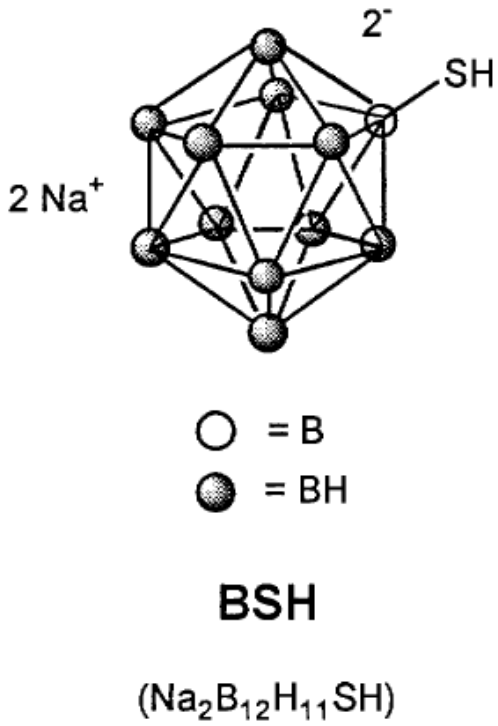

Figure 1.4: *The sulfhydryl borane(BSH) molecule*

dependent substrates and known inhibitors. These results indicated that this transporter plays an important role in BPA uptake in glioma cells. It also demonstrated that, for successful clinical outcomes, the on average ∼30% of tumour cells which do not take up BPA must be targeted using a different methodology.

The other boron compound which has seen widespread clinical interest and application is sulfhydryl borane (BSH), pictured in figure 1.4. Like BPA, BSH was first considered for use in BNCT in the 1960's [13]. Unlike BPA, BSH is unable to cross the blood brain barrier. Accumulation is still possible in intracranial tumours, via diffusion from blood, as they lack a complete blood brain barrier. Tumour to normal blood boron ratios of 1.3:1 to 2:1 have been demonstrated in patients for BSH [55]. Boron levels in infiltrating cells are much lower than in the main tumour mass.

Future compounds for BNCT are still being actively developed, with the compounds of most current interest being groups of boron loaded porphyrins and liposomes [56]. These

have shown large tumour to healthy brain uptake ratios in rat models, 30 or more in some cases [57]. Development is a long process and potential clinical effectiveness of compounds is hard to asses without data for distribution of the boron which is taken up, both at a gross tissue level and on a cellular scale.

Bioavailability of the boron compound used and their half life after delivery is a big consideration. While this is somewhat dependant on the compound, some work has been carried out utilising varied delivery mechanisms and blood brain barrier disruptors in order to maximise the amount of compound available for uptake by tumorous cells [58]. Clinical work is ongoing in this area at Birmingham [59] with a new BPA-Mannitol formulation, assessing the effects of inter-arterial delivery and giving the compound along with an additional Mannitol bolus.

It has also been demonstrated in animal tumour cell models [60] that pre-loading with compounds such as L-tyrosine can stimulate uptake of BPA. An extension of this work, in explanted human tumours, is currently being undertaken at Birmingham.

In dose response cell biology studies of BNCT the compound of choice is generally boron-10 enriched boric acid. As the accumulation ratio, the ratio of boron in cells to growth medium, is unity for boric acid [61] the boron levels inside the cells is easily determined. This allows the dose from boron capture to be calculated easily. Boric acid was used in all of the boron loaded cell survival experiments detailed in this report.

1.4 Neutron Sources for BNCT

In order to deliver the doses required for BNCT over a reasonable time period a high neutron flux is required; approximately $10^9 ncm^{-2}s$. Realistically this restricts the choice of sources to either a fission reactor or a high current particle accelerator with a suitable target. The spectrum of the neutron flux is also a design concern. Thermal neutrons, with an energy of approximately 0.025 eV, are required at the treatment depths. This requires irradiation with epithermal neutrons, energy from approximately 1 eV to 10 keV, with the final moderation down to thermal energies happening inside tissue. The range of neutron energies in a reactor is very large. Figure 1.5 shows the prompt fission spectrum for thermal fission of uranium-235, with a probability peak at 0.7 MeV and an average of 2MeV. Other isotopes present in the reactor have different fission spectra and there are contributions from fast fission and delayed neutrons. Typically a BNCT beam will have a combination of filters, which capture neutrons outside of the desired energy range, and moderating material. A suitable material for moderation has a very low capture cross section for neutrons, a high scattering cross section and consists of light nuclei leading to large energy losses in each collision. The moderator assembly will also contain materials designed to reduce the gamma ray component of the beam, as large amounts are produced in the reactor core directly from fission, from neutron capture reactions and from decay of fission daughter products.

The BNCT beam at the MITR-II is unusual in that it does not use neutrons directly from the core. Instead, leakage neutrons from the core are incident on an array of 11 MITR-II fuel elements held in a tank to one side of the core; see figure 1.6. This assembly is separated from the core by a system of shutters allowing a beam which is easily switchable without affecting normal reactor operation. This beam assembly was specifically designed for BNCT and has very low gamma and fast neutron contamination of the beam. It also has a purpose built patient irradiation room shown in figure 1.7. While this beam was not designed to have a variable dose rate, it is possible to reduce the dose rate by not fully opening the shutter. This allows for a change in flux without a change in beam spectra. Due to the

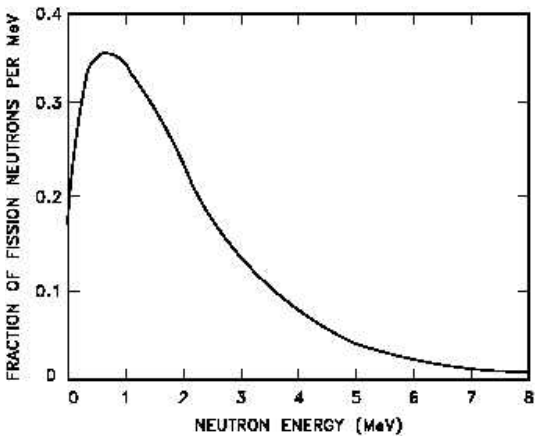

Figure 1.5: *Prompt fission neutron energy spectrum for thermal fission of uranium-235 from [62]*

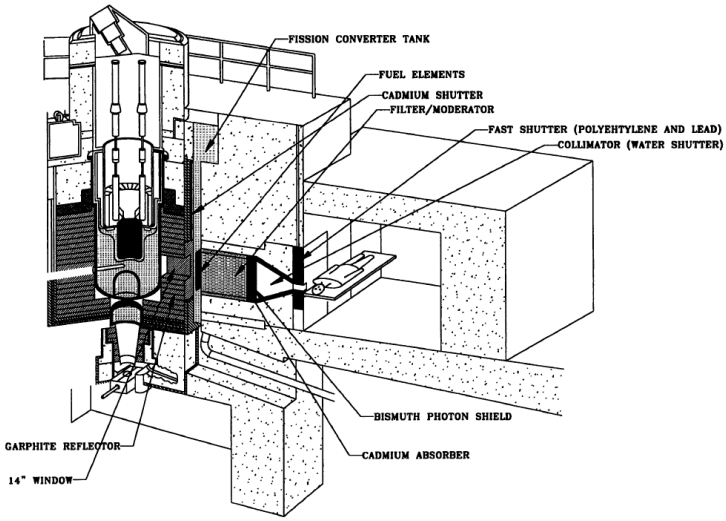

Figure 1.6: *Isometric view of the MIT BNCT beam facility [63]*

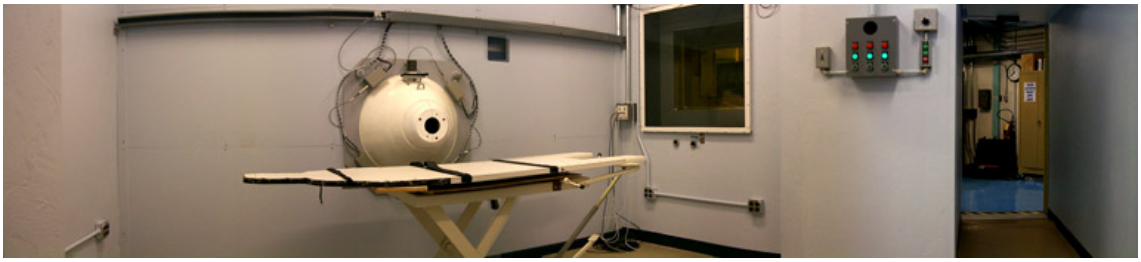

Figure 1.7: *Inside of the MIT treatment room [64]*

nature of a low energy neutron beam and the large distance between the shutter and the beam aperture, the beam profile across the aperture remains flat even for a small shutter opening.

All clinical trials of BNCT carried out so far have used reactors as a source of neutrons. Reactors can produce extremely large fluxes and are very reliable, however they are extremely expensive, large and have a poor public perception. These factors suggest that accelerators are more suitable for an in hospital application of BNCT. With the widespread adoption of linear accelerators for photon therapy, and now synchrotrons and cyclotrons for proton and carbon ion therapy, there is also greater clinical experience with and acceptance of accelerators. An accelerator design would use a proton beam onto a light nuclei target surrounded by an appropriate moderator assembly. Birmingham's Dynamitron accelerator would be typical of accelerators designed for this application. A 2.8MeV, 1mA proton beam is used to irradiate a 4cm diameter thick lithium target on a copper backing, which is cooled by a submerged jet heavy water system. The cooling system is the ultimate limit of beam power as lithium has very poor thermal properties. Work is ongoing at various sites to manufacture circulating liquid lithium targets to solve these issues [65]. Birmingham are currently (March 2012) in the process of testing a potential upgrade to their target cooling system to cope with loads of 15 kW+ utilising a novel 'binary ice cooling system'. This makes use of a suspension of ice crystals of tens of μm in volume, suspended in water containing a freezing point depressant.

Neutrons are generated by the Li(p,n) reaction. Neutron energies are dictated by the kinematics of the neutron source reaction and are therefore known; 820 keV at 90° and 1.2 MeV at 0°. This low peak neutron energy allows for an extremely compact moderator and filter assembly when compared to a reactor beam. There is also intrinsically a much lower gamma component to the beam. The moderator assembly is pictured in figure 1.8; the assembly is an approximately 75 cm cube.

While the dose rates of the Birmingham and MIT beam are different by a factor of

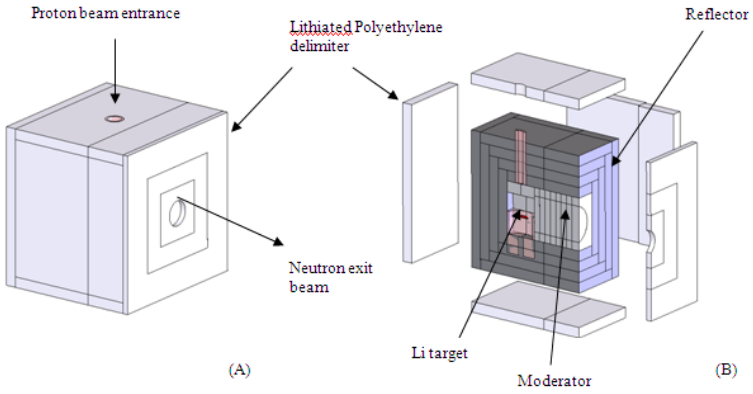

Figure 1.8: *Schematic of the Birmingham filter-moderator assembly [66]*

15 or more, the dose components delivered to tumour are similar as both are close to the ideal for BNCT, that is, maximum epithermal neutron delivery while minimising all other components. This is illustrated by figure 1.9.

A different approach to accelerator based BNCT is being pioneered by Kyoto University and Sumitomo Heavy Industries in Japan. Rather than a dynamitron, a 30 MeV cyclotron with a water cooled beryllium target is being utilised. Commissioning is complete and initial radiobiology studies are in progress [67].

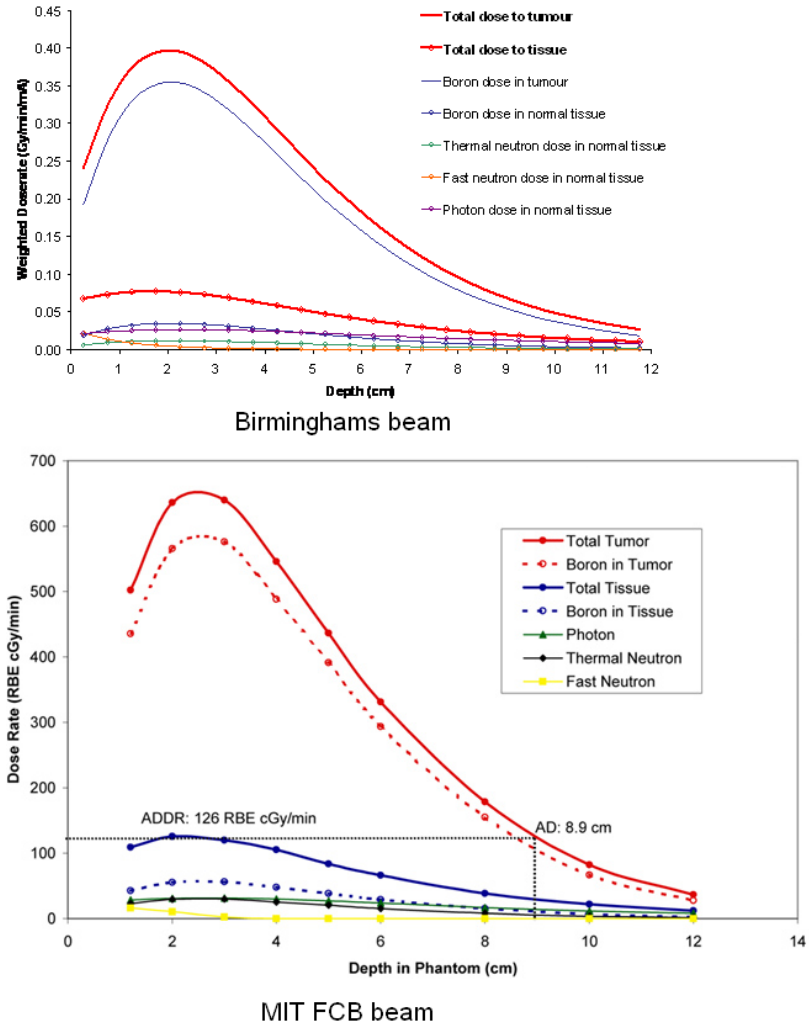

Figure 1.9: *Dose profiles for MIT and Birmingham treatment beams. Boron values are 15 µg per g and 52.5 µg per g in normal and tumour tissues, respectively. Birmingham profile from [66], MIT from [64]*

1.5 Scope of this thesis

While considerable progress has been made in the clinical application of BNCT the number of patients irradiated at any one site, with an identical beam, has remained relatively small. The complex biological effect of a mixed field beam makes direct intercomparison of these results difficult. This also hampers the application of lessons learned at one BNCT facility to others. It is clear that further work on the fundamental biology which dictates the response to a given BNCT treatment beam is required.

The two major uncertainties that remain when considering doses delivered in BNCT are the influence of the dose rate effect and any synergistic interaction between different beam components.

Currently dose rate effect is solely accounted for by an estimated 'Dose Reduction Factor' applied to the gamma ray proportion of the beam. This is factor that weights the gamma fraction of the beam, typically by 0.5-0.7 [27] [68] [69] to account for the reduction in effect by giving the gamma rays at a low dose rate. The dose rate is substantially lower in most cases than the 5Gy min^{-1} used in modern x-ray radiotherapy. This magnitude of this dose rate factor is derived by considering the response of cell lines, such as HeLa, to different dose rates of photons [70].

A direct dose rate effectiveness comparison for all combined beam components has not been carried out. This study attempts to address this, presenting the results of a measurement campaign carried out at the MIT reactor at two dose rates.

The power of the MIT Fission Converter Beam (FCB) can be varied by adjusting the position of a beam shutter. This allows the beam dose rate to be varied while leaving the other beam characteristics the same, something which would not necessarily be the case if the beam power was altered by controlling the power level of the reactor itself. The potential to vary the dose rate in this manner makes it unique among reactor based BNCT beams. V79 cells were irradiated, in the presence of boric acid, at full beam dose rate and a rate of approximately 1/15th of the full dose rate. The details of this experiment are described in

chapter 4. In addition to the MIT data, the result of cell irradiations using the Birmingham Dynamitron accelerator beam are also presented.

The work of McNally *et al* [1] and others suggests that when alpha particles and photons are delivered together the resulting biological effect is greater than might be expected from the two radiations delivered separately. This has implications for clinical BNCT, where a large fraction of the dose is delivered by alpha particles combined with photons. Relative biological weighting factors for beam components have been derived assuming no interaction between the different radiation qualities. Using a unique irradiation set-up at the Medical Research Council, cell survival experiments with controlled doses of photons and alpha particles delivered truly simultaneously have been carried out for the first time. The results will be presented here and discussed in the context of BNCT.

Chapter 2

BASIC RADIOBIOLOGY CONCEPTS AND METHODOLOGY

2.1 Biological Effect of Ionising Radiation

As the name suggests, ionising radiation is radiation which is capable of forming ions within the material being studied. The various types of radiation encountered in radiotherapy and radiobiology interact with tissue and lead to ionisation events in different ways.

Photons interact with matter via a number of different mechanisms dependant on their incident energy. At low energies, the photoelectric effect is dominant. The incident photon is absorbed by an atom and an energetic photo-electron is ejected. This electron will have an energy equal to the difference between the energy of the incident photon and the binding energy of the electron in its original shell. For high enough energy electrons the most probable origin for photo-electrons is the most tightly bound shells, the K shell of the atom. As the absorber atom is now in an ionised state with a vacancy in a bound shell, which is filled via absorption of a free electron and/or rearrangement of electrons within the shells, photoelectric absorption can lead to the emission of further photons in the form of characteristic X-rays.

At higher energies Compton scattering is the dominant mechanism. This interaction takes place between the incident photon and an electron of the material it is incident upon.

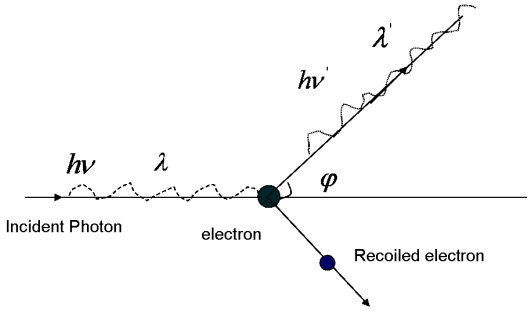

Figure 2.1: *Compton scattering (from [71])*

The gamma ray is deflected through some angle, θ, with respect to its original direction and transfers some of its energy to the electron. As any scattering angle is possible, the energy transfer can be anything from zero to a large proportion of the original gamma ray energy.

The two extreme scattering cases are at $\theta = 0$, where very little of the gamma ray energy is transferred, and $\theta = \pi$ where the gamma ray is backscattered and the maximum energy possible in a single interaction is transferred (figure 2.1). Normally all scattering angles are possible and a continuum of energy transfer ranging from zero to this maximum is observable.

Electrons ejected in the various photon interactions can themselves lead to further ionisation events.

Charged particles travelling through a medium primarily interact via Coulomb scattering with orbital electrons. In the case of light particles such as electrons, these interactions can cause large deflections in the path of the particle and large losses of kinetic energy by the incident electron.

Using a conservation of energy/momentum argument it can be demonstrated that, in a head-on elastic collision between a heavy particle, such as an alpha, and an electron, the proportion of kinetic energy lost by the heavy particle is small. For a 5 MeV alpha particle it is 2.7 keV ([5]). It follows that many such collisions are required to slow the heavy particle significantly. In a glancing collision the heavy particle will only be deflected by a very small amount. This means that heavy particles tend to follow more or less straight paths.

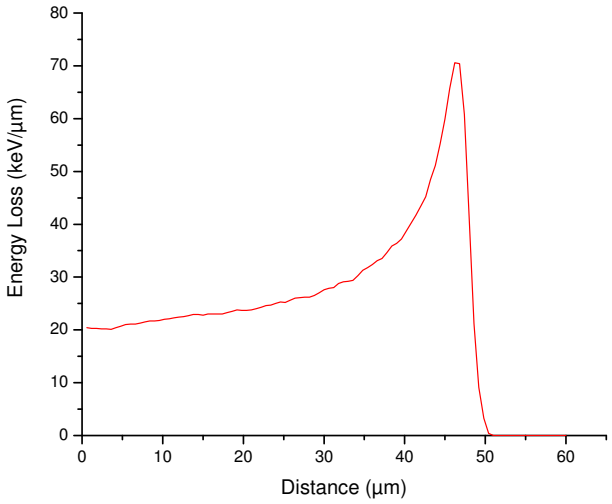

Figure 2.2: *Energy loss of 1.46 MeV alpha particles with distance in water. Calculated in SRIM[72]*

As the means of interaction of charged particles is the Coulomb force, which has an infinite range, the particles interact simultaneously and continuously with many electrons along their path. This leads to charged particles having a well defined mean range. In BNCT this is particularly important as it means that the alpha particle and lithium nucleus produced in the boron capture reaction have a short, well defined range of a few cell diameters at most and produce many ionisation events along their short track.

How the energy is deposited along the track is important; higher amounts of energy deposited are equivalent to higher numbers of ionisation events. As the interaction cross section rises as energy decreases, large proportions of the particles energy are deposited towards the end of it's path. This can be seen clearly in a plot of energy loss with distance, or Bragg curve, as in figure 2.2.

As they are uncharged, neutrons interact with the nuclei of material directly via a series of elastic scattering reactions. Energy is lost by the incident neutron in each collision, with energy transferred depending on the mass of the scattering nucleus and calculable through simple conservation of momentum. As the velocity of the neutrons reduces to thermal levels

(∼0.025 eV), capture reactions become dominant. The products of these capture reactions cause further ionisation events.

2.1.1 Linear Energy Transfer (LET)

Linear energy transfer is defined as the average energy deposited by a particle per unit length of its track in a given material. High LET particles have tracks with more densely clustered ionisation events and cause damage which is harder for cells to repair; see figure 2.3.

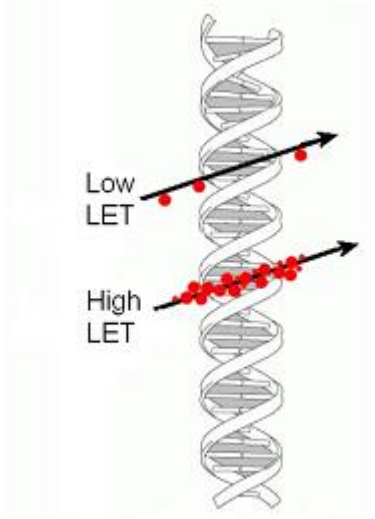

Figure 2.3: *Ionisation events across a DNA double helix, low vs high LET [73]*

In reality LET is an average value and particles with a given LET have a wide range of energies.

2.1.2 Relative Biological Effectiveness (RBE)

Relative biological effectiveness is a measure of the effect on a biological system of a type of radiation, relative to some reference radiation. It is always given for a specific endpoint (effect). Normally, the reference radiation used is 250 kV X-rays.

$$RBE = \frac{Dose\ of\ reference\ radiation}{Dose\ of\ test\ radiation} \tag{2.1.1}$$

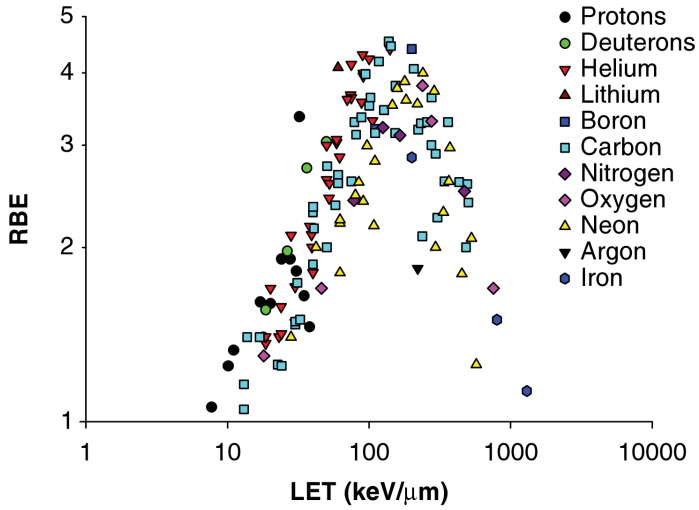

Figure 2.4: *Measured RBE compared with particle LET in V79, CHO and T1 cell lines. Taken from [74]*

RBE tends to increase with LET. This is to be expected as low LET, sparsely ionising, radiation produces damage which is more readily repaired. However there is a peak value of LET above which RBE no longer increases; above this value each cell exposed is experiencing more ionisation events than are required to bring about cell death. This can be seen clearly in figure 2.4 which compares particle LET with a wide range of experimentally determined RBE's.

As it is derived from a set of experimental results it is important to define exactly the doses, end point used and all other experimental factors when using a given RBE [75].

A calculated RBE only applies at the dose point it was calculated at; RBE tends to decrease with increasing dose. This is illustrated for typical alpha particle survival responses in figure 2.5.

This can be particularly important in all areas of high LET radiotherapy, with doses delivered in a number of fractions, particularly when the dose per fraction is varied, as a naive application of RBE can lead to patients receiving a higher equivalent dose than intended. In order to account for this effect and allow biologically meaningful calculations

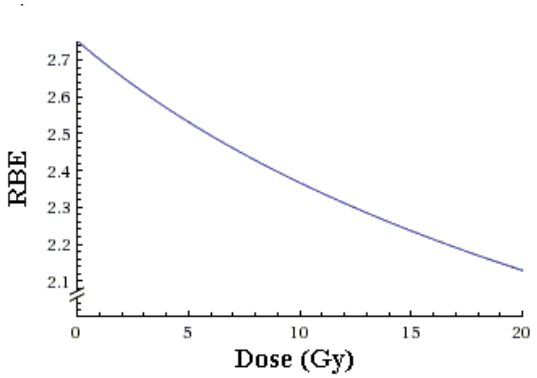

Figure 2.5: *Variation of RBE with alpha particle dose. Calculated for the alpha particle / X-ray data presented in reference [1]*

to be made the concepts of RBE_{max} and RBE_{min} have been introduced [76].

RBE of a high LET irradiation is derived from the dose to produce a given biological effect, compared to a low LET irradiation. For a single dose;

$$\alpha_L d_L \beta_L d_L^2 = \alpha_H d_H \beta_H d_H^2 \tag{2.1.2}$$

Where d is dose, alpha and beta are constants and the H and L subscripts refer to high and low LET radiations respectively. RBE is at a maximum when dose is close to zero and the quadratic terms become negligible;

$$\alpha_L d_L = \alpha_H d_H \tag{2.1.3}$$

$$RBE \rightarrow RBE_{max} = d_L/d_H = \alpha_H/\alpha_L \tag{2.1.4}$$

RBE is at a minimum when doses are large, and the quadratic terms dominate;

$$\beta_L d_L^2 = \beta_H d_H^2 \tag{2.1.5}$$

$$RBE \rightarrow RBE_{min} = d_L/d_H = \sqrt{\beta_H/\beta_L} \tag{2.1.6}$$

The assumption of the Theory of Dual Radiation Action (TRDA)[77] is that β is constant with LET and that RBE_{Min} is therefore unity for all radiation types. This has been challenged via analysis of various cell survival experiments [78] [79] but the generalised trend of RBE_{min} with LET is not yet clear.

2.1.3 Compound Biological Effectiveness (CBE)

The concept of RBE is valid only when the quantity absorbed dose can be defined, that is when the averaging implied by energy deposited per unit mass is applicable. For the boron dose in BNCT the concept of absorbed dose is not valid because of the inhomogeneous distribution of the boron compounds and the short range of the boron capture reaction products. Therefore the RBE cannot be defined and the influence of an inhomogeneous distribution of the boron atoms cannot be determined.

Only the product of two components, RBE and boron distribution, can be assessed for a given experimental system. It is therefore standard to refer to 'Compound Biological Effectiveness' (CBE) [80] when discussing weighted doses in BNCT. This is defined as the true, geometry-independent, RBE for the boron capture particles multiplied by some factor unique to a given tissue type and boron compound. Given CBE's relationship to RBE, CBE values also vary with dose.

To date all clinical BNCT treatments have been given in small numbers of large, high dose, fractions and have used fixed values of CBE in their treatment plans.

2.2 Dose rate effects

Low LET radiation that is delivered at high dose rates has a larger biological effect than the same low LET radiation delivered at lower dose rates. There are two separate mechanisms responsible for this effect. The classical dose rate effect is the result of sub-lethal radiation damage being repaired over the course of a long irradiation. The second potential dose rate effect mechanism is due to cell proliferation over the course of the radiation exposure. If the exposure is long relative to the length of the mitotic cycle cell births may partly cancel out cell deaths. The dose rate effect is illustrated in figure 2.6, with the same cell line exhibiting markedly different responses to the same dose delivered at differing rates.

The magnitude of the dose rate effect varies with cell line. This can be understood with reference to the Linear-Quadratic model of cell survival discussed in section 2.3.2. For single event killing, represented by $e^{-\alpha D}$ in the linear quadratic model, no repair is possible. In the case of two event killing, initial sub-lethal damage is compounded into lethal damage by a second ionising event. As the initial damage is repairable the amount of lethal two event damage is dictated by the frequency of ionising events in some critical volume. This implies that cells with small α / β ratios will exhibit more of a dose rate response than cells with large α / β ratios.

Dose rate effects in tumour tissue tend to be much smaller than that exhibited in healthy tissue. Tumours normally have high α / β ratios in the range 6-14 Gy while low α / β values of 1.5-5 Gy have been observed for late responding normal tissues [82]. A tumour line with minimal dose rate response is shown in figure 2.7

No dose rate effect is seen with high LET radiation; it is normally assumed that there is minimal sub-lethal damage to repair. However, this is an oversimplification. Hill *et al*[84] demonstrated that alpha particles are more effective per unit dose than X-rays even in repair deficient cells. They also demonstrated that cells, which shared the same parent line, with differing repair pathway deficiencies exhibited differing degrees of alpha particle sensitivity. This implies that there is significant repair of high LET, alpha particle induced damage.

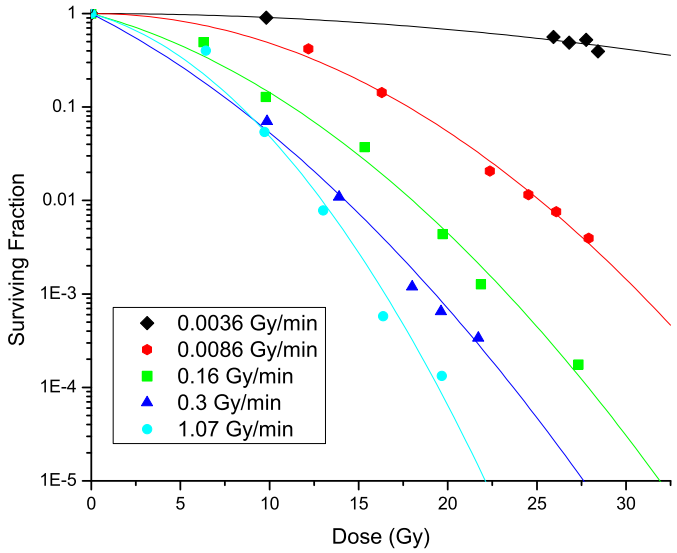

Figure 2.6: *Survival curves for CHL-F cells exposed to* ^{60}Co *gamma rays at varying dose rates* in vitro. *Taken from [81]*

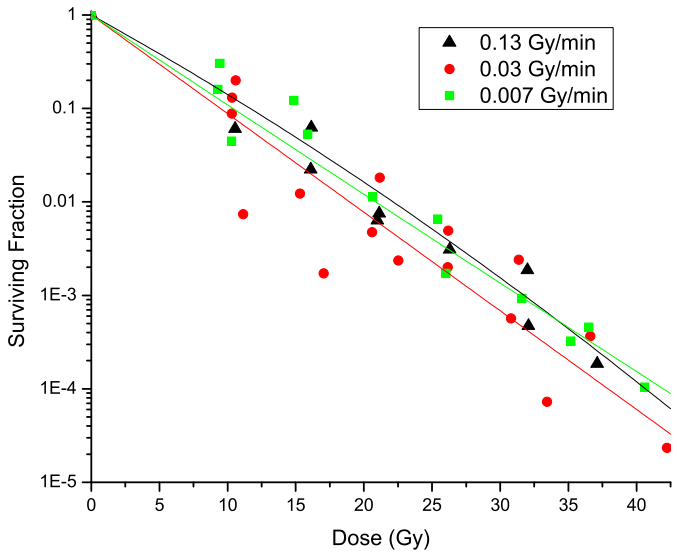

Figure 2.7: *Survival curves for cells from the KHT sarcoma in mice, irradiated* in situ *and introduced into recipient mice. Replotted from [83]*

In BNCT, at high boron concentrations, the majority of the dose is delivered by high LET components. The precise fraction varies with the treatment beam parameters but in the Birmingham epithermal beam, at levels of 50 μg/g of boron-10, approximately 85% of the dose is delivered by the high LET boron capture products. It might be expected that, at high boron concentrations, there is minimal dose rate effect in BNCT. However, there is a lack of *in vitro* and *in vivo* data to support this assumption. This study was aimed to address this issue.

2.3 Practical biology common to both studies

The mixed field irradiation study and the BNCT beam dose rate study shared common methodology. Both were clonogenic survival studies, using the same cell line and similar handling techniques. With this in mind, common elements to both studies are described here instead of repetition within the appropriate chapters.

2.3.1 Cell Survival Studies

Biological assays are always carried out with reference to some carefully defined endpoint. In the context of survival studies, this is normally the ability to reproduce for a number of generations after exposure to the compound or radiation being investigated. Choosing continued clonogenic reproductive ability as the endpoint provides a way of quantifying the response of a cell line to the radiation dose delivered in the laboratory. In practice this is performed by introducing known numbers of cells to a suitable growth medium post exposure. The cells are then left for long enough for visible colonies of greater than 50 cells to form, these are counted and then compared to the number of cells introduced. The survival fraction calculated by this method is then adjusted by the plating efficiency, the fraction of cells forming colonies in unirradiated controls.

In all cases where cells were irradiated as single cell layers, cells were left for 2 hours post-irradiation. This was to allow time for all repair of sub-lethal damage to be completed before cells were processed. This time period can be justified with reference to the work of Reddy *et al* [85]. Their experimental work involved irradiating V79 cells with 250 kV X-rays, incubating the cells in medium then replacing the medium with hypertonic saline at different time intervals. Hypertonic saline had previously been demonstrated to fix, that is make permanent, unrepaired damage in cells [86] [87]. Their data is shown in figure 2.8. They derived an expression for repair time, or time to reach a plateau of cell survival, for log-phase V79 cells;

$$t_R = (6.04 \pm 0.3)D \tag{2.3.1}$$

Where D was x-ray dose and t_R, time to reach plateau.

In all studies presented in this report, cells post-irradiation were introduced into 90 mm Petri dishes at densities calculated to give approximately 200 colonies per dish. Five dishes were used per dose point. Where the expected survival was not well known cells were plated out at a range of densities.

This methodology requires cell numbers to be known with a good degree of precision. Cells in suspension were counted using a Coulter Counter. This device pushes a sample through an aperture and measures resistance change allowing particle size to be calculated [88]. It then records the number of particles above some preset threshold. With V79 cells this was set to 8 μm. To obtain an accurate count it was important to obtain a single cell suspension, avoiding clumping. Counts were periodically checked via a manual count using a haemocytometer.

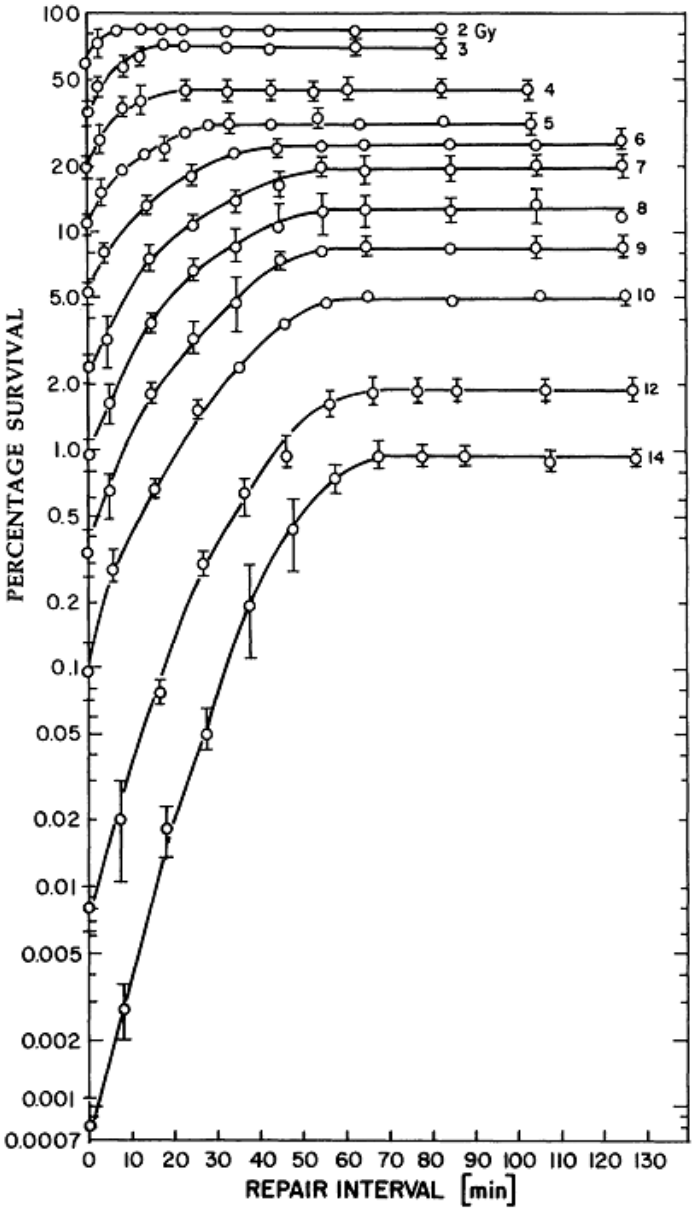

Figure 2.8: *Kinetics of recovery under growth conditions measured by treating cells with 0.5 M saline at various repair intervals after irradiation with X-rays. The number next to each curve represents the dose in Gy. Taken from [85]*

2.3.2 Survival Curves

The conventional way to present survival study data of this type is a log-linear plot of cell survival fraction against dose as shown in figure 2.9. Normally, as shown, curves of this type are fitted with a linear quadratic model. This model assumes that cell death is brought about either by a single lethal event or the accumulation of damage from sub lethal events. If these are independent then, $S = S_1 S_2$ when S_1 is single event killing, $e^{-\alpha D}$ and S_2 is two event killing $e^{-\beta D^2}$. Hence, $S = e^{-(\alpha D + \beta D^2)}$ where S is the surviving fraction after a dose of D has been delivered, alpha and beta are constants.

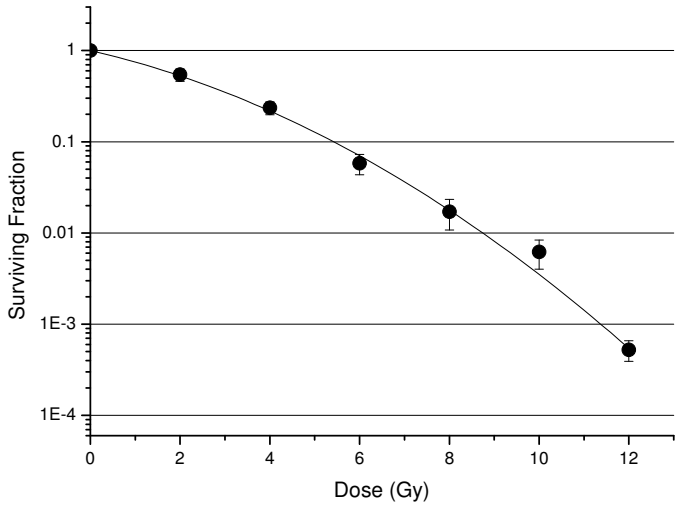

Figure 2.9: *Example cell survival curve. Experimental data for V79 cells exposed to 250kVp X-rays. Fitted linear quadratic function with* α *=0.259* $\pm$ *0.03Gy*$^{-1}$ *and* β *=0.03* $\pm$ *0.003Gy*$^{-2}$

Extensions of this theory to apply to mixed field irradiations separate the alpha and beta constants of the high and low LET radiation and attempt to describe any synergistic effects seen. Early work was published by Zaider and Rossi [89]. The model presented in this paper introduced terms into the survival curve fitting equations to explicitly account for temporal effects such as repair of sub-lethal damage and interaction between sub-lethal damage from different radiations. This model and others are discussed in more detail and compared to experimental results on page 93.

Compound	Lonza Catalogue number	Percentage of complete medium
DMEM	BE12-614F	87.635
L-Glutamine 200mM in 0.85 % NaCl	BE17-605E	1.753
Gentamicin sulphate 50 μg per ml	BE17-5187	0.096
Non-Essensial Amino Acids(NEAA)	BE13-114E	0.876
Foetal Bovine Serum	DE14-801F	9.640

Table 2.1: *Complete cell growth medium constituents*

2.3.3 Cell Culture Consumables

When grown *in vitro* a growth medium is used to provide water, salts, glucose, amino acids and other essentials for cell growth. Practically this involves a prepared solution to which perishable elements are added immediately prior to use in culture. The culture medium used throughout the cell survival experiments detailed in this report was Dulbeccos Modified Eagle's Medium (DMEM). This is a standard, widely used medium. The DMEM used was purchased from Lonza bioscience as were all other liquid consumables. Various other compounds are added to the base medium, as detailed in table 2.1. These are growth essentials along with an antibiotic to help suppress infections of the cell population.

Foetal Bovine Serum (FBS) is the portion of plasma remaining after coagulation of blood. As an extracted biological product it can demonstrate significant variation in composition between different suppliers and even between different batches from the same supplier. It is normal practice to use the same batch of FBS throughout a series of cell experiments. This was the case for all of the experiments carried out at the Medical Research Council (MRC) described later in this report.

Unfortunately restrictions on the import and export of products derived from cattle meant that this was not possible for the biological comparison of the treatment beams at Birmingham and MIT, detailed in chapter 4. Fortunately the V79 cell line used did not appear particularly sensitive to small changes in medium composition. Plating efficiency at Birmingham was 0.515 ± 0.06 while at MIT it was 0.494 ± 0.04. These plating efficiencies were both somewhat lower than is usual for V79 cells with > 0.8 regularly observed in other experiments by the author. The lower plating efficiency was thought to be due to the

presence of boric acid in the medium.

2.3.4 Cell Line

For all experiments described in this report the cell line used was V79-4. This is a sub line of the V79 cell line. V79's were first developed in 1958 from the lung tissue of a male Chinese hamster. V79-4's were isolated in 1966. They have a very high plating efficiency, typically greater than 80%, and a short doubling time of around 12 hours [90]. They are very robust cells and routine handling of them is very straightforward. This cell line has been used extensively in radiobiology work.

Stocks of V79 cells for the mixed field experiments described from page 71 onwards, were obtained from stocks held at the Medical Research Council laboratories. A single vial of approximately 3×10^6 cells was thawed and cultured. The resulting cell population was placed into culture medium containing dimethyl sulfoxide (DMSO) and divided into vials. These vials were then slow frozen and stored at liquid nitrogen temperatures until required.

The V79 cells used for the dose rate comparison study, described in chapter 4, were obtained from professor Jacqueline Yanch's group at MIT. A single vial of approximately 1×10^6 cells was thawed and cultured. Cells from this culture were then used immediately in the MIT irradiations. A flask of viable cells was then transported back to the UK, further cultured, and vials frozen for use in the Birmingham series of irradiations.

2.4 Weighted Doses in BNCT

As discussed on page 20, Relative Biological Effectiveness is an important concept in radiobiology. As traditionally formulated however, it is only a function of radiation LET. In BNCT treatment situations it is more useful to refer to Compound Biological Effectiveness (CBE) [91]. This concept was introduced as the effect of a BNCT irradiation is strongly dominated by the accumulation of boron in the cells being irradiated. In addition to the gross tissue/tumour boron uptake ratios, microdistribution within the cells is extremely important. Simulations have shown that irradiations with boron in the nucleus are more damaging than the same amount of boron universally distributed [92]. CBE is calculated in the same way as RBE in that it is a ratio of doses to produce some given end point, with reference to a 250 kV photon dose. It has the further qualification that it is specific to a given boron compound.

RBE varies with dose but BNCT treatment plans have historically applied a single, fixed, RBE/CBE value for each dose component when calculating equivalent doses. This has been justified with reference to the fact that BNCT is typically delivered in a single large dose [30]. If a different clinical strategy is adopted for BNCT, and a series of small dose fractions are delivered, then consideration will need to be given to how best apply CBE's and RBE's derived from large single dose exposures.

2.4.1 In Tumour

A number of studies have determined CBE factors in cell lines *in vitro*. Initial studies irradiated cells in attachment. Davis *et al* [93] irradiated HeLa cells, incubated in varying concentrations of boric acid, using the MIT reactor thermal neutron beam. Their results are shown in figure 2.10. A CBE factor of 3.7 was calculated. Dose deposited by the capture reaction in the cells was calculated via a computer program which was complicated by the non-spherical nature of the attached cells and various assumptions were made. Specifically

	in vitro			*in vivo*		
Irradiation	SF=0.1	SF=0.01	SF=0.001	SF=0.1	SF=0.01	SF=0.001
Thermal beam	2.6	2.6	2.6	2.1	2.3	2.5
Thermal beam minus photons	3.7	3.7	3.8	2.8	3.2	3.5
BPA	9.8	7.8	6.7	4	3.8	3.6
BSH	3.1	2.9	2.8	-	-	-
Boric acid	3.4	3.4	3.3	-	-	-

Table 2.2: *CBE factors for 9L gliosarcoma cells, figures from [48]. CBE change with dose was small, as the corresponding X-ray curve was nearly linear in this region; corresponding X-ray doses were* > 10 *Gy (*in vitro*) and >8Gy (*in vivo*).*

the assumption that all borated media was removed and capture could only take place within the cells themselves. As a layer of a few tens of microns effectively represents an infinite borated layer, due to the short range of the reaction products, the assumption of no boronated medium surrounding the cells may not have been correct.

Gabel *et al* [3] used V79 cells in suspension, loaded with enriched boric acid at varying concentrations and irradiated with thermal neutrons using the Medical Research Reactor at Brookhaven. Their results are shown in figure 2.11. By comparing the boron loaded results to the survival without boron present, RBE values at different survival levels could be derived and a calculated V79 survival curve produced as shown in figure 2.12. A combined RBE factor of 2.3 ± 0.3 at low survival was calculated for the boron reaction products. An extension of this work was derivation of CBE factors for boric acid, BPA and BSH in rat 9L gliosarcoma cells. Cells were irradiated both *in vitro* and *in vivo* using the Brookhaven thermal beam [48]. This comprehensive study attempted to derive RBE factors for all BNCT beam components. Results are shown in figures 2.13 and 2.14. Calculated values for CBE are shown in table 2.2.

The CBE factors for boric acid and BSH were similar to those stated in other published work [3] but were found to be extremely high for BPA. These factors assumed that the amount of boron inside the cells was equal to the concentration in the medium. This was shown to be an unwarranted assumption by Capala *et al* [61]. This work used a rapid

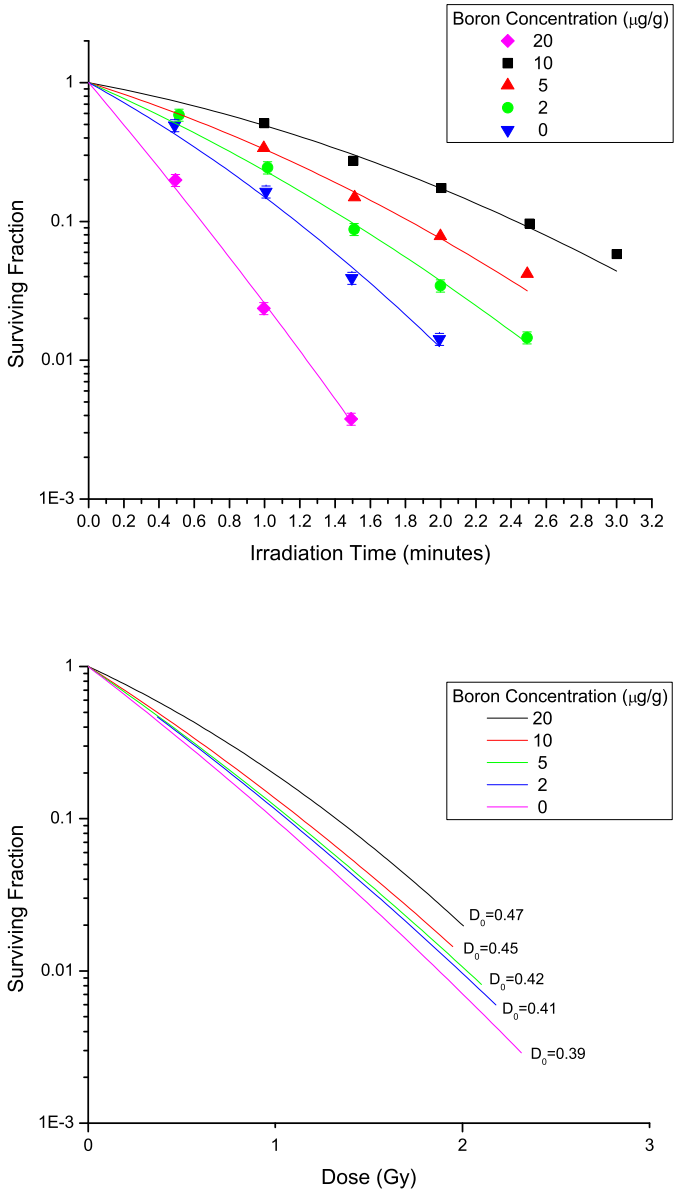

Figure 2.10: *HeLa cells irradiated at MIT in a thermal neutron beam, in the presence of boric acid, at varying concentrations, replotted from [93]*

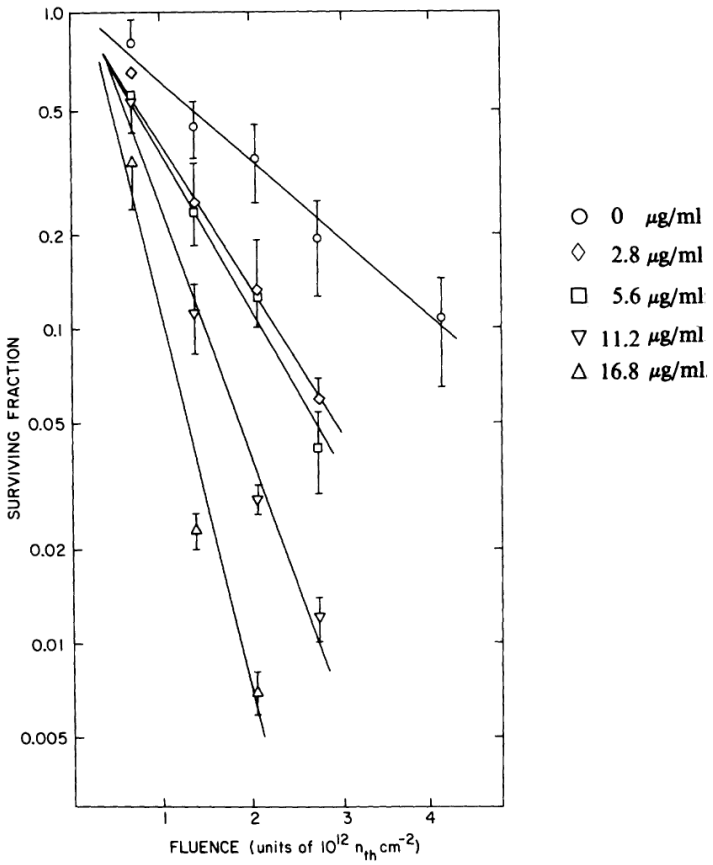

Figure 2.11: *V79 irradiated at Brookhaven, using a thermal neutron beam, in the presence of boric acid at varying concentrations. Taken from [3].*

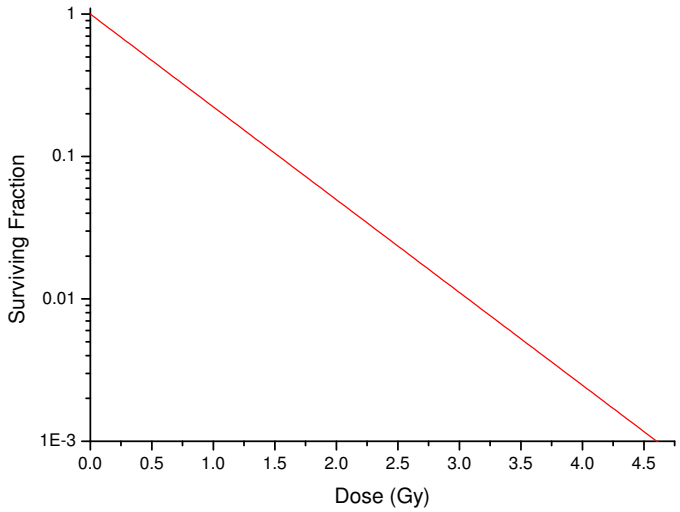

Figure 2.12: *Calculated V79 survival curve for the* $^{10}B(n,\alpha)^{7}Li$ *reaction. Replotted from [3]. Function is* $S = e^{-1.5D}$.

centrifuge filtration technique to strip away medium containing boron and allow direct measurement of only intracellular levels. The results are shown in figure 2.15. When the doses used in [48] are adjusted to account for the ∼3 times higher boron doses the average CBE factor for BPA reduced to 3.8 [91].

The factor of 3.8 for boron dose, with BPA, in tumour tissue has been widely adopted in the BNCT community and used in treatment planning in clinical trials all over the world.

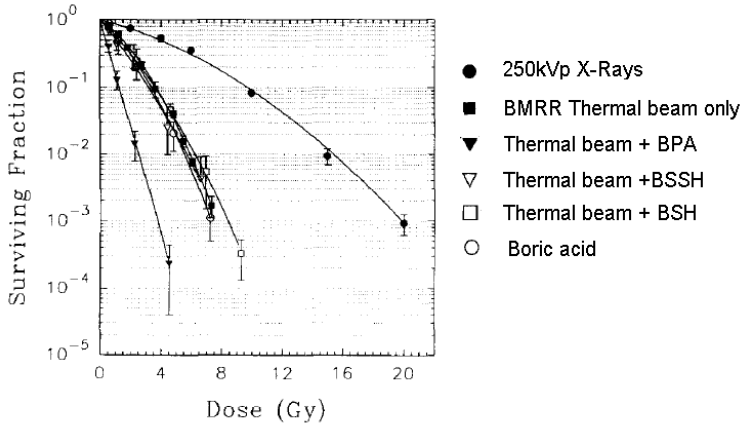

Figure 2.13: *Clonogenic survival of 9L gliosarcoma cells as a function of dose following in vitro irradiation with 250 kVp X-rays, BMRR thermal neutron beam alone, or BMRR thermal neutron beam combined with the boron compounds. Taken from [94].*

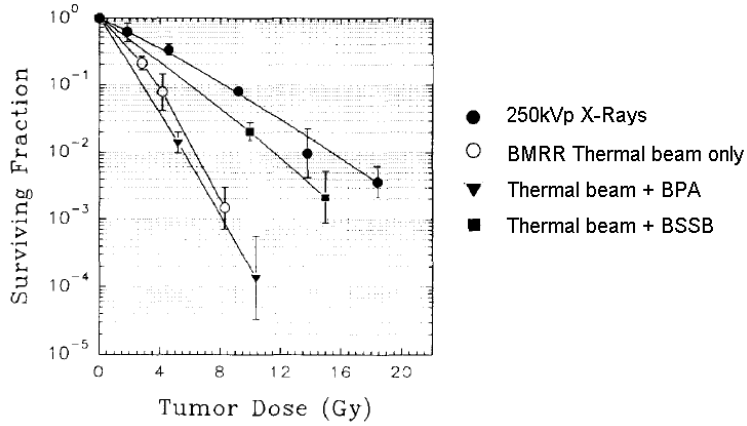

Figure 2.14: *Clonogenic cell survival determined in vitro following irradiation of tumours in vivo. Intracerebral 9L gliosarcomas were irradiated with either 250 kVp X-rays, BMRR thermal neutron beam alone, or BMRR thermal neutron beam following administration of either BPA or BSSB. Taken from [94].*

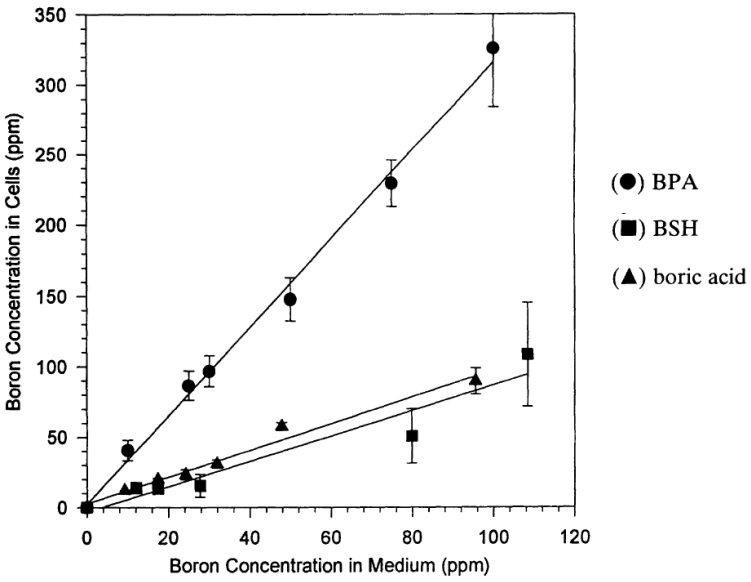

Figure 2.15: *Boron concentration in cells after incubation in various compounds, from [61]*

2.4.2 In Skin

The tolerance limit for skin is generally taken as 18 Gy photon-equivalent delivered in a single fraction [95] [96]. Above this level permanent damage to the underlying dermis results and leads to necrosis. There have been a number of *in vivo* studies which attempt to quantify RBE or CBE, in skin, for a number of end points. A summary of the calculated factors is shown in table 2.3. It is clear that the CBE factor is strongly dependant on the endpoint used and other experimental conditions. It is also apparent that the CBE in humans [97] and the CBE in rats [98] is different, even with the same compound and beam conditions. It has been suggested that this could be due to the structural differences in vascular supply [91].

Skin is not a limiting factor in BNCT treatment, with epithermal beams and BPA or BSH. The dose required to create significant skin damage, as indicated in dog experiments, exceeds the dose required to cause serious central nervous system damage [102]. This is almost certainly due to the characteristics of the neutron beam; provided it is epithermal it delivers peak dose 20+ mm below the skin.

Irradiation	Tissue	End Point	RBE	CBE	Paper
Thermal neutrons only	Rat skin	moist desquamation	3.5 ±0.2		[98]
Thermal neutrons only	Pig skin	moist desquamation	3.9		[99]
SP+thermal neutrons	Pig skin	moist desquamation		2.3	[99]
BPA+thermal neutrons	Rat skin	moist desquamation		3.7 ±0.7	[98]
BPA+thermal neutrons	Rat skin	dermal necrosis		0.73 ±0.42	[98]
BPA+thermal neutrons	Hamster skin	moist desquamation		2.4	[100]
BPA+thermal neutrons	Human skin	moist desquamation		2.5	[97]
BSH+thermal neutrons	Rat skin	moist desquamation		0.55 ±0.06	[98]
BSH+thermal neutrons	Rat skin	dermal necrosis		0.86 ±0.08	[98]
BSH+epithermal neutrons	Dog skin	moist desquamation		0.51	[101] from [91]
BSH+epithermal neutrons	Dog skin	dermal necrosis		0.52	[101] from [91]

Table 2.3: *Experimentally determined skin RBE and CBE factors from [91]*

2.4.3 In Central Nervous System (CNS)

Damage to the Central Nervous System (CNS) is normally quantified by damage to specific cell populations, the functioning of which can be assessed by various functional and histopathological tests [91]. There have been conflicting reports on which of these populations is of the most importance in terms of damage delivered during BNCT treatment; elements of the bulk CNS tissue or the vascular system.

Morris *et al* [103] exploited the fact that BSH is excluded from bulk CNS tissue and confined to the vascular system by the blood brain barrier to selectively irradiate the CNS vascular system of healthy Fischer rats. The histopathological results from this selective thermal neutron plus BSH irradiation were compared to the results from irradiations with thermal neutrons alone or thermal neutrons plus BPA. Results were similar in all three cases, suggesting that vasculature and the endothelial cells in particular are the critical target. The results also mirror damage found in conventional photon radiotherapy. This is supported by more recent work specifically undertaken to compare the importance of glial stem cell damage to vascular endothelial damage in white matter necrosis by Coderre *et al* [107].

A result of the domination of vascular system damage in BNCT is the relatively low RBE values for CNS, in BSH loaded irradiations, as seen in table 2.4. This can be explained by considering the geometry of the brain capillary system. The smallest capillaries are 8μm with a wall thickness of 0.1 to 0.3 μm. The range of the boron capture products means that some capture events within the capillaries will deposit the majority of their energy outside. Rydin *et al* demonstrated that the fraction of the dose received by the blood vessel wall was one-third to one-fifth that delivered to an infinite pool of blood, depending on the diameter of the vessel [108]. For BPA loaded systems there is a contribution to this dose from capture in the surrounding tissue.

It is clear from the varying CBE values in table 2.4 that the CBE is strongly dependent on experimental conditions. Based on the work in [103] a brain tissue CBE of 1.3 was used in planning for clinical trials at Brookhaven, MIT and elsewhere [109] [110].

Irradiation	Number of fractions	Tissue	End Point	RBE	CBE	Reference
Thermal beam proton component	1	Rat spinal cord	myeloparesis	1.8		[103]
Epithermal beam proton component	1	Dog brain	brain necrosis	4.4		[104]
BSH + epithermal beam	1	Dog brain	MRI changes		0.27-0.49	[104]
BSH + epithermal beam	1	Dog brain	brain necrosis		0.37-0.55	[104]
BSH + epithermal beam	1	Dog brain	MRI changes/brain necrosis		1.1	[104]
Thermal beam	1	Rat spinal cord	myeloparesis	1.4 ±		[103]
BSH + thermal beam	1	Rat spinal cord	myeloparesis		0.52 ±0.03	[105]
BPA + thermal beam	1	Rat spinal cord	myeloparesis		1.33 ±0.16	[103]
BPA + thermal beam	1	Rat spinal cord	myeloparesis		1.34 ±0.13	[106]
Thermal beam	2	Rat spinal cord	myeloparesis	1.76 ±0.03		[106]
BSH + thermal beam	2	Rat spinal cord	myeloparesis		0.6 ±0.04	[105]
BPA + thermal beam	2	Rat spinal cord	myeloparesis		1.7 ±0.2	[106]
Thermal beam	4	Rat spinal cord	myeloparesis	2.46 ±0,1		[106]
BSH + themal beam	4	Rat spinal cord	myeloparesis		0.81 ±0.06	[105]
BPA + thermal beam	4	Rat spinal cord	myeloparesis		2.46 ±0.29	[106]

Table 2.4: *Experimentally determined CBE in central nervous system [91]*

The variance between various experimental results shows that relative biological effectiveness and compound biological effectiveness in BNCT are not simple quantities to evaluate. Values derived in all tissues seem to depend strongly on the beam used and, more significantly, on the distribution of the boron compounds used. It is obvious that caution needs to be exercised when comparing biological and clinical results obtained under different beam conditions.

Chapter 3

MIXED FIELD IRRADIATIONS

3.1 Previously Published Work

There have been a number of investigations involving irradiation of cell cultures with mixed high and low LET fields. In the case of mixed fields of neutrons and photons there have been a large number of publications, in part due to clinical interest in fast neutron therapy. Work by Ngo *et al* [31], using 25 MeV fast neutrons and 250 kVp X-rays with the V79 cell line, showed lower survival level when the fractions were given immediately following each other compared to allowing repair post neutron irradiation, see figure 3.1. In the 'immediate' case cells were kept on ice in between the fractions to minimise repair.

This work supported the earlier findings of Railton *et al* [37], who found a similar effect when irradiating Chinese Hamster Ovary (CHO) cells with deuterium-tritium fusion neutrons and cobalt-60 gamma rays. The synergism was also demonstrated in V79 cells, again with Deuterium-Tritium fusion neutrons and Cobalt-60 gamma rays, by Higgins *et al* [32] [33]. A further study using V79's by McNally *et al* [34] showed that the synergistic effect was present for a range of neutron priming doses.

In support of the evidence of an effect *in vitro* is a study by Joiner *et al* [35] which demonstrated a synergistic interaction between 140 kVp X-rays and 3 MeV neutrons given simultaneously *in vivo*. The model used was appearance of visible skin effects in mouse feet.

	Radiation types	Cell line	LET of high LET component (keV/micron)	High LET dose range (Gy)	Low LET dose range(Gy) (Gy)	High LET dose rate (Gy/min)	Low LET dose rate (Gy/min)	Temperature of cells during exposure	Delay between exposures	Synergistic effect seen?
Barrendson *et al*[38]	200kVp X-ray + alpha particles	T1		0.5, 1	0-5	1.2	2.6	20 °C	None stated	No
	200kVp X-ray + alpha particles	T1		0.5, 1	0-5	5.4	0.45	20 °C	None stated	No
Bird *et al*[39]	50kVp X-ray + deuterons	V79	50	2, 5.6	0-16	¡60	24	room temperature	<5 minutes	Yes
	50kVp X-ray + ^{3}He ions	V79	96	2, 5.6	0-16	¡60	24	room temperature	<5 minutes	Yes
	50kVp X-ray + ^{3}He ions	V79	160	4	0-16	¡60	24	room temperature	<5 minutes	Yes
McNally *et al*[1]	250kVp X-ray + alpha particles	V79	140	0.5	0-11	0.35	3	room temperature	3-4 minutes	No
	250kVp X-ray + alpha particles	V79	140	2	0-11	0.35	3	room temperature	3-4 minutes	Yes
	250kVp X-ray + alpha particles	V79	140	2.5	0-11	0.35	3	room temperature	3-4 minutes	Yes
Demizu *et al*[40]	4MeV X-ray + carbon ion	HSG	46.6	0.8, 2, 3, 4.4	0-8	Not stated	Not stated	room temperature	<15 minutes	No
Furusawa *et al*[41]	150kVp X-ray + ^{40}Ar	V79	86	0.5,1,1.5	0-5	1	1	room temperature	None	No
	150kVp X-ray + ^{28}Si	V79	150	0.5,1,1.5	0-5	1	1	room temperature	None	No
	150kVp X-ray + ^{56}Fe	V79	442	0.5,1,1.5	0-5	1	1	room temperature	None	Yes

Table 3.1: *Summary of previously published mixed ion - photon cell survival experiments*

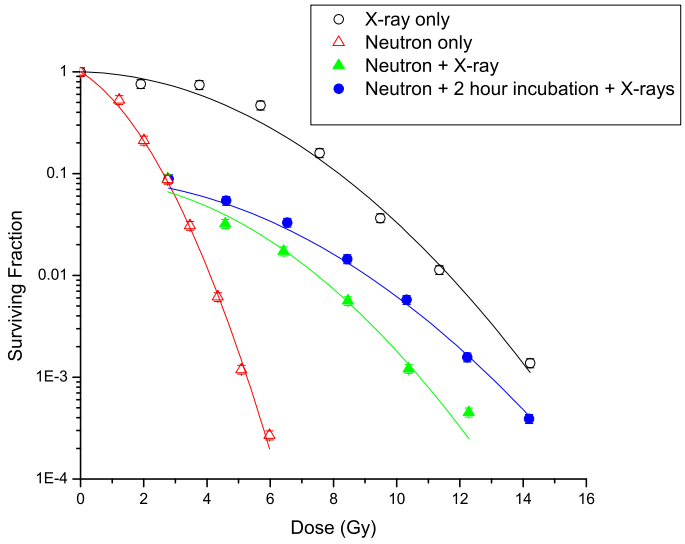

Figure 3.1: *Single-dose and fractionated-dose survival curves of V79-AL162 Chinese hamster cells obtained with JANUS neutrons and X-rays. Replotted from [31]*

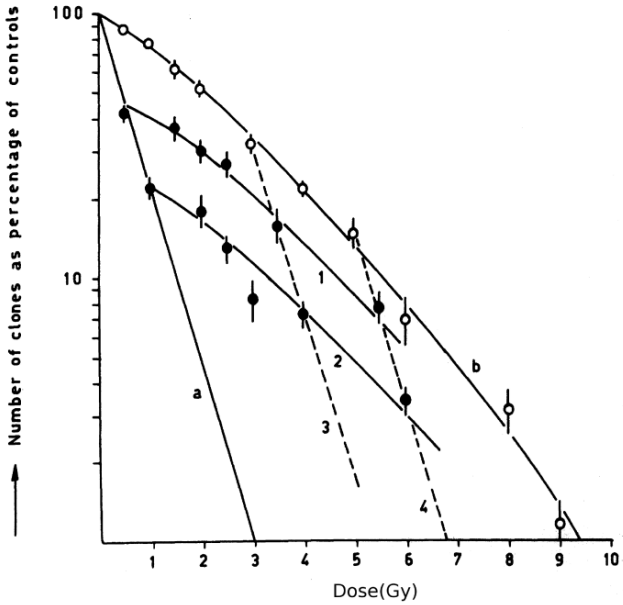

Figure 3.2: *Effects of combined α and X-ray radiation. Taken from [38]. Curve 1: 0.5 Gy α plus 0, 1, 1.5, 2, 3 and 5 Gy of X-ray. Curve 2: 1 Gy α plus 0, 1, 1.5, 2, 3 and 5 Gy of X-ray. Curve 3: 3 Gy of X-ray plus 0, 0.5 and 1 Gy of α. Curve 4: 5gy of X-ray plus 0, 0.5 and 1 Gy of α.*

From these studies the evidence seems consistent that there is an interaction between the damage delivered by fast neutrons and photons. In the case of mixed fields of photons and alpha particles, or other heavy ions, the picture is much less clear.

Early work by Barendsen *et al* [38] in the 1960's showed that for sequential irradiation with polonium-210 alpha particles and 200 kVp X-rays there was no deviance from the survival results predicted by giving the fractions individually (figure 3.2). The cells used were human origin kidney cells, irradiated while attached to thin based dishes.

This work was taken as supporting evidence that, in an exponential cell survival situation such as that given by a high LET alpha particle beam, there is no sub-lethal damage in the survivors. Without such damage there is no mechanism for synergistic interaction between the high and low LET components.

Work by Bird *et al* [39] sequentially exposed V79 cells to 50 kV X-rays and either deuterons or ^3He ions. A synergistic effect was found, with lower cell survival in the mixed irradiations than would be expected from the individual fractions. This effect was present for all of the different high LET fractions tested and increased in magnitude with dosage of the high LET fraction. Example data is shown in figure 3.3

In addition to these mammalian cell data, Murthy *et al* [36] found that in diploid yeast cells there was a synergistic effect when cobalt-60 gamma rays and polonium alpha particles were given together.

The most comprehensive mixed alpha particle and photon investigation to date is perhaps found in McNally *et al* (1988) [1], the method and results are worth examining in some detail. The motivation for the study was to repeat the work mentioned earlier [38] with the high LET component making up a higher fraction of the total dose delivered. Previous studies with neutrons [34] had suggested that the doses employed were too low to show the synergistic effect. The cells used were the V79 line, cultured in standard complete growth medium. The cells were plated out in appropriate numbers, given expected survival, into dishes several hours before irradiation. Doses of 0.5, 2 or 2.5 Gy of alpha particles were

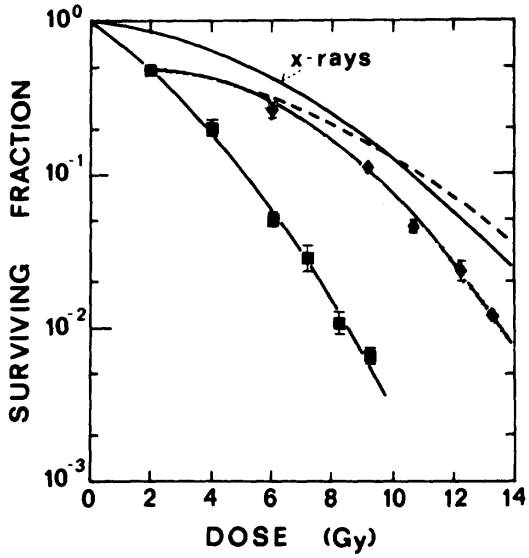

Figure 3.3: *Survival data for late-S V79 cells irradiated with 50 keV per μm LET deuterons alone (black squares), or with graded doses of X-rays after a 2-Gy dose of deuteron ions (black diamonds). The continuous line is the X-ray only survival curve and the dashed line shows the predicted mixed field survival from the separate components. [39]*

given alone, and combined with a range of X-ray doses. The combination was not truly simultaneous; the 'priming' alpha particle dose was delivered followed by the X-rays several minutes later. Alpha particles were delivered by a plutonium-238 source as described in [111] and X-rays by a 250 kV machine with a hardening filter. Their results are shown in figure 3.4. The implications are clearer when normalised results are shown, as in figure 3.5. This figure shows the mixed dose survival data adjusted with the alpha particle only data. If there was no synergistic effect the curves would overlap each other and the X-ray only curve, within uncertainties. It is obvious that a synergistic effect is visible in the 2 Gy and 2.5 Gy alpha priming dose data which is more pronounced at higher doses. The authors conclude that alpha particles can cause damage that interacts with X-ray damage leading to a lower survival in the mixed case than would be expected from the fractions given separately.

Recently, there has been renewed interest in the effect of mixed-field irradiations as they may be of interest in the rapidly expanding clinical field of carbon ion therapy which utilises high LET particles. Combining this therapy with traditional photon radiotherapy may

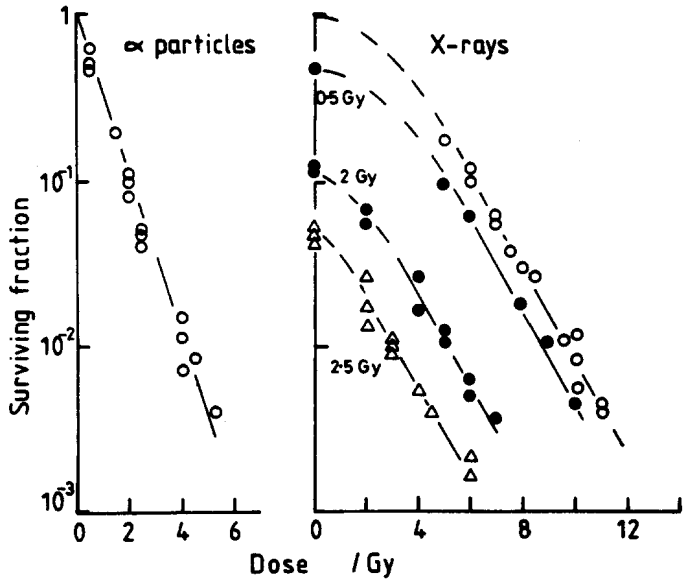

Figure 3.4: *Survival curves for V79 cells exposed to a-particles, X-rays, or X-rays after priming a-particle doses of 0.5, 2 or 2.5 Gy. Taken from [1]*

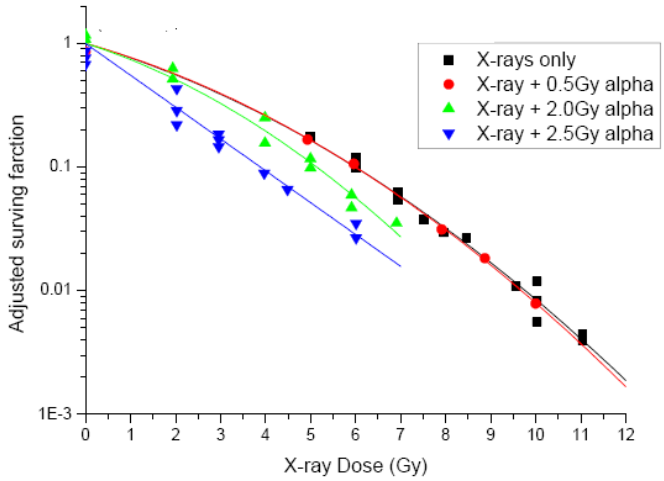

Figure 3.5: *Survival curves for cells exposed to alpha particles, X-rays, or X-rays after priming a-particle doses of 0.5, 2 or 2.5 Gy. The X-ray plus alpha data is normalised - the surviving fraction at each point is divided by the surviving fraction of the appropriate alpha only data. Re-plotted from data in [1]*

produce complicated treatment planning scenarios if a synergistic effect is seen. Demizu *et al* [40] irradiated human salivary gland (HSG) cancer cells with a mix of 320 MeV carbon ions and 4 MeV X-rays. It was found that the two radiation qualities acted in a simple additive fashion and no synergistic effect was seen. Furusawa et al [41] exposed V79 cells to X-rays combined with various heavy ions; ^{40}Ar, ^{28}Si and ^{56}Fe. Unlike many previous investigations their irradiations were truly simultaneous, with high LET dose rates matched to their X-ray dose rates. No synergistic effect was seen with the ^{40}Ar or ^{28}Si ions. A statistically significant synergistic effect was seen with the very high LET ^{56}Fe ions. However, the authors noted that this effect was very small and strongly depended on the fitting functions used. A summary of the various photon-ion simultaneous exposures, with mammalian cell lines, is given in table 3.1.

It is assumed by theoretical explanations of the synergistic effect observed by McNally *et al* [1] and others that the lowered cell survival is the result of interactions between sub lethal lesions produced by the two radiation qualities [112]. The threshold for observing an effect, observed by McNally *et al*, and proposed as an explanation for Barendsen *et al* not observing a synergistic interaction suggests that the level of effect is small and difficult to observe at higher cell survival levels. A series of experiments have been carried out to clarify the question of synergism between alpha particles and photons, particularly in the case of truly simultaneous irradiation. They will be described in the rest of this chapter.

3.2 Radiation Sources and Set-up

The initial experiments detailed in this report were carried out at the Medical Research Council (MRC) at Harwell. They utilised one of the facility's cobalt 60 sources in conjunction with a plutonium 238 alpha particle irradiator. The cobalt sources are pencil style sources attached to Teleflex for handling, which allows them to be inserted into the fixed irradiation position, inside the irradiation cells, remotely. In the case of these experiments a rig was assembled which positioned the source approximately 300 mm above the cell layer to be irradiated, as seen in figure 3.6. When in position the cobalt source used provides a dose rate of 2.6 Gy per minute. There was a small amount of transit dose, at a much lower dose rate, as the source moved on the Teleflex from the shielded bunker to the lighthouse. This dose was included in the total dose delivered to the cells and was less than 0.1 Gy in all cases.

Photon dosimetry was carried out with the assistance of James Thompson at the MRC. Gamma dosimetry was provided by a Thermo Scientific NE2670 Farmer dosimeter using a model 2581A ionisation chamber. This is a standard 0.6 cm^3 'thimble' type, cylindrical graphite chamber as described by Aird and Farmer [113] and shown in figure 3.7. Temperature and pressure compensation were built into the dosimeter. Dose rate was checked at the start and end of each day of irradiations. The dosimeter used is regularly calibrated and checked as part of the MRCs normal auditing procedures. For dose measurements the ionisation chamber is held in a dummy cell dish filled with an appropriate amount of distilled water to simulate the cell growth medium. This allowed a direct measure of dose rate at the cell layer in identical conditions to the cell irradiations themselves. The positioning of the chamber and design of the shutter jig ensured that dose from scattered X-rays measured in the chamber set-up was the same as that in the cell irradiation set-up. The jig, with ionisation chamber, is shown schematically in figure 3.8.

Actual dose delivered to the cells was calculated from the measured dose rate and time of exposure. This exposure time was electronically controlled by a purpose built micro-

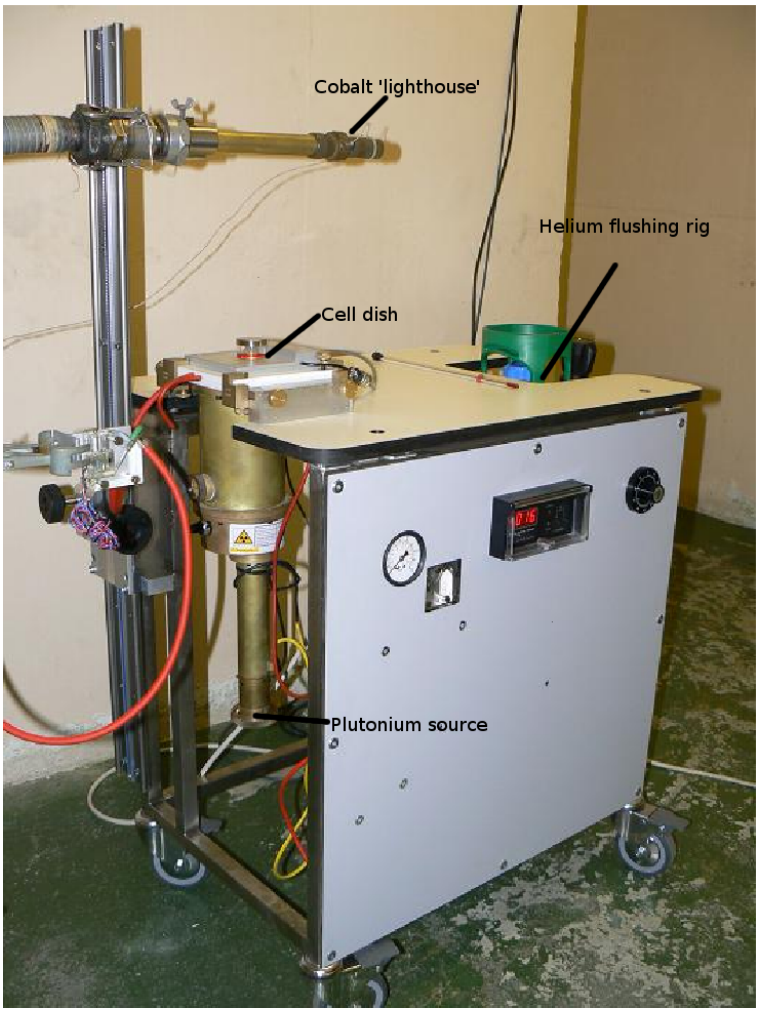

Figure 3.6: *Photograph of the mixed alpha particle and gamma ray setup*

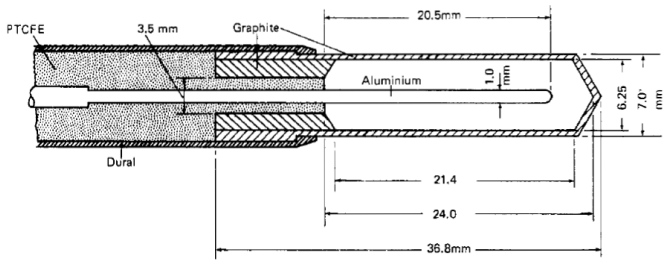

Figure 3.7: *Schematic of a Farmer type ionisation chamber. Taken from [113]*

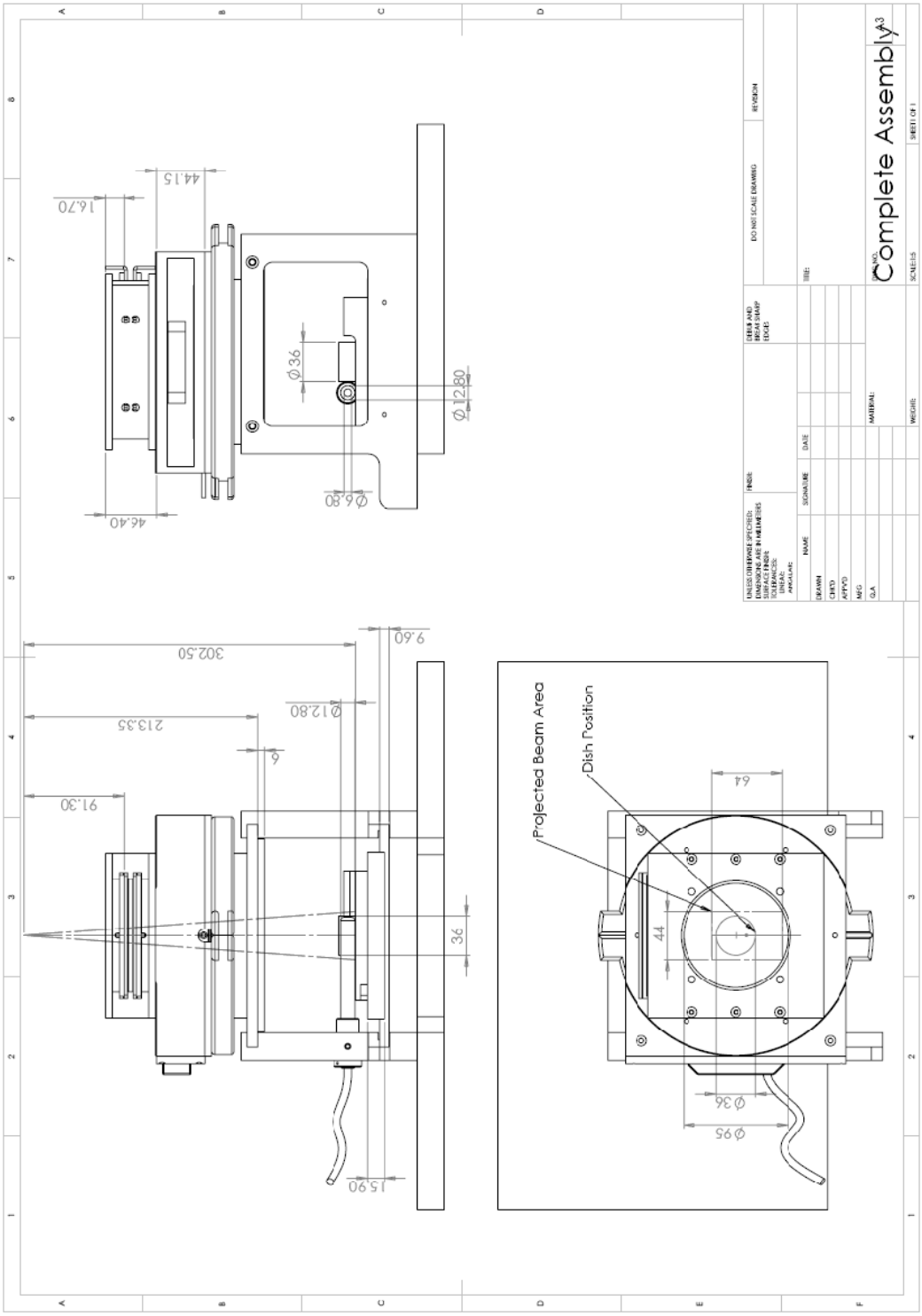

Figure 3.8: *CAD drawing of the jig used to position 250kV X-ray irradiation head for cell dish irradiations*

controller with a timing error of less than ten milliseconds.

The plutonium irradiator used was the setup described in Goodhead *et al* [114] as shown in figure 3.9. It consists of a plutonium coated platinum disk held inside a helium atmosphere. Distance from the source to the cell layer is variable. This changes the path length within the helium and consequently allows the energy of the alpha particles, at the cell layer, to be varied as described by the Bethe-Bloch formula (equation 3.2.1).

$$\frac{dE}{dx} = \frac{4\pi}{m_e c^2} \cdot \frac{nz^2}{\beta^2} \cdot \left(\frac{e^2}{4\pi\varepsilon_0}\right)^2 \cdot \left[\ln\left(\frac{2m_e c^2\beta^2}{I \cdot (1-\beta^2)}\right) - \beta^2\right] \tag{3.2.1}$$

Where;

$\beta = v/c$

v velocity of the particle

E energy of the particle

x distance travelled by the particle

c speed of light

z particle charge

e charge of the electron

m_e rest mass of the electron

n electron density of the target

I mean excitation potential of the target

e_0 vacuum permittivity

There is also a variable diameter aperture positioned above the source and various sector plates that can be positioned below the cell layer. The aperture allows the dose rate to be lowered while the sector plate allows for uniform irradiation when a rotating sample wheel is fitted. For these irradiations the largest aperture was used, with no sector plate, in all cases. This source has been used extensively at the MRC and its characteristics are well known. In it's standard configuration the source is positioned 65 mm below the chamber window. After traversing 65 mm of helium, 3 mm of air and two 0.35 mg cm^{-2} mylar windows the alpha

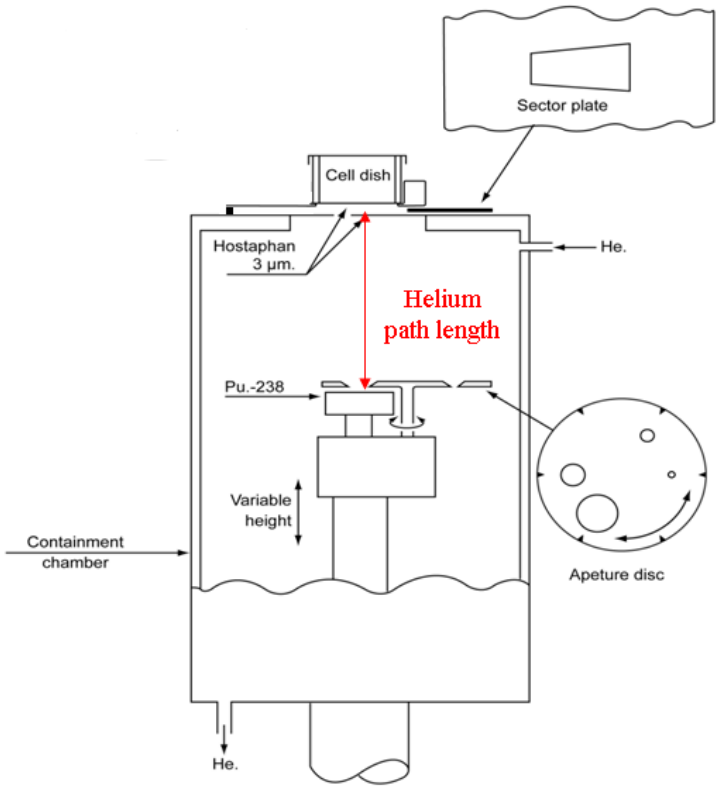

Figure 3.9: *Schematic of the MRC Plutonium irradiator*

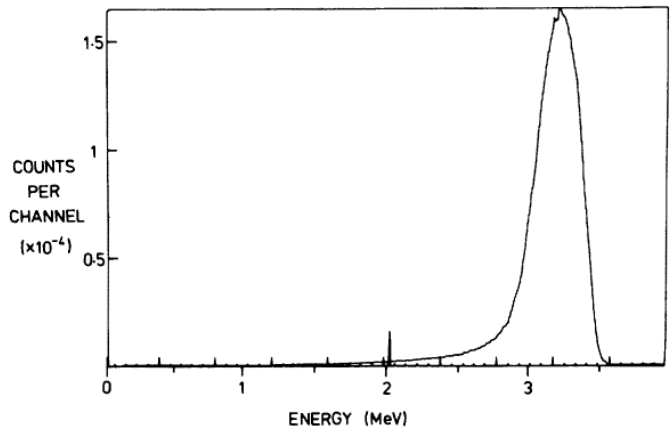

Figure 3.10: *Energy spectrum of alpha particles in the position of the irradiated cells, as measured with a silicon detector masked with a 0.9 mm diameter aperture. Taken from [115]*

particles have a measured mean spectral energy of 3.15 MeV and with spectrum peak energy of 3.23 MeV as shown in figure 3.10. These measurements, taken with a silicon detector, are detailed by Thacker *et al* in reference [115]. A conversion of this energy spectrum to LET in water gives an average, at the cell layer, of 127 keV μm^{-1}.

A modification to the set-up was made specifically for these experiments; a fast shutter was added between the source and the cell layer. The gap between the shutter and the top of the existing setup was continually flushed with helium over the course of the irradiation. As this set-up was a minor modification from the usual configuration of this source, it was modelled using the TRIM [72] code to check that the LET of the alpha particles at the cell layer was similar to that used in previous work. This code modelled the transport of the alpha particles through 65mm of helium, 2.5 μm of mylar, 5mm of helium then a final 2.5 μm of mylar. The LET as the alpha particle traverses the different layers is shown in figure 3.12. The cell layer in this case is modelled as a layer of water 7 μm thick.

The average LET across the cell layer was calculated as 123 keV μm^{-1}. This small difference in LET is not expected to make a significant difference to the biological effect of the alpha particles [74]. This is illustrated by figure 2.4 on page 24. An attempt to quantify the difference in biological effect was made by fitting a log-normal distribution to the peak

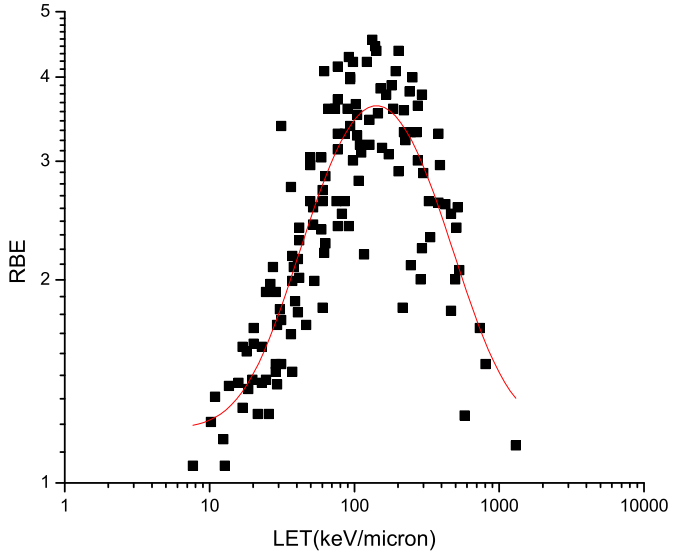

Figure 3.11: *Pooled data for particle LET vs RBE in V79 CHO and T1 cell lines. Replotted from data in [74]. Fitted line is a log-normal curve generated in Origin.*

in the pooled RBE-LET data using Origin, as shown in figure 3.11. This is not presented as having any relationship to the physical RBE-LET relation; it is just a convenient function to fit the data in the region of interest. This suggests a shift from a predicted RBE of 3.61 to 3.60 for a change in LET from 127 keV μm^{-1} to 123 keV μm^{-1}.

An appropriate number of open vs closed cycles of the shutter were used in each experiment to ensure that the prescribed alpha particle dose in the experiment was delivered over the same time period as the gamma ray dose. Alpha particle dose rate was measured using CR39 film held in a dummy cell dish. Several films were irradiated over the course of each day of experiments to provide an accurate measure of the dose rate being delivered.

All alpha dosimetry was carried out by James Thompson at the MRC. He followed the CR39 methodology described by Cartright *et al* in reference [116]. Discs of CR39 were placed in a dish identical to those used for the cell irradiations before being exposed to the alpha particles. Tracks created by the ions were enlarged by etching in 40% NaOH for 4 hours so that they were visible under a microscope. The number of tracks in a given

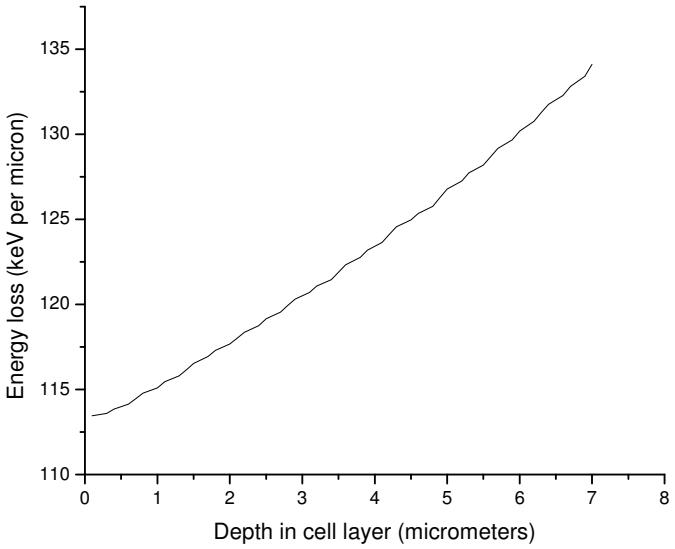

Figure 3.12: *LET across the cell monolayer in a hostaphan dish for the MRC alpha particle source. Calculated with TRIM [72]*

area were then electronically counted using an ImageJ macro. Some dose points were also counted manually and compared to the electronic results; agreement within 1.1% was found. A example microscope image of CR39 tracks, with highlighting from ImageJ, is shown in figure 3.13. Dose in Gray was calculated from this counted track density per unit area and a calibration factor as described in equation 3.2.2. This is a dosimetry method used routinely at the MRC.

$$Dose = \frac{19.424 \times Track\ count}{Area\ of\ region\ counted} \tag{3.2.2}$$

One drawback of the CR39 dosimetry method is that, at high doses, tracks can overlap. This could produce an underestimate of dose delivered. All dosimetry was carried out with maximum doses of approximately 0.7 Gy to eliminate this effect. As with the photons, doses in cell irradiations were calculated from the measured dose rate along with the irradiation time.

Initially it was believed that the dose delivered during the shutters open and close cycle

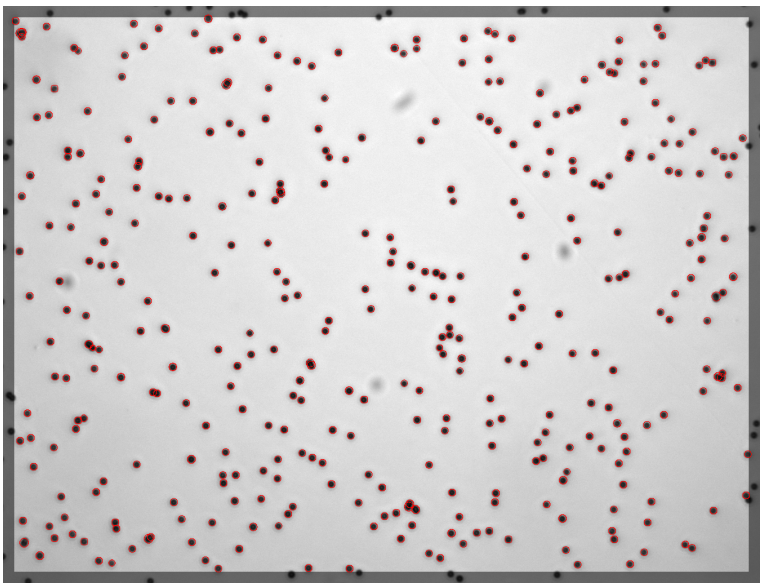

Figure 3.13: *Example image of CR39 alpha particle tracks after etching. Red highlighting is a feature of the ImageJ track counting algorithm.*

time would not be significant and dose planning was carried out under this assumption. Reviewing the CR39 dosimetry data demonstrated that this was not the case, with an additional dose of approximately 8x10^{-3} Gy per shutter cycle. This equated to a 27% rise in average dose from initial estimates. This also introduced a variation in dose across the dish. With square shutter leaves this variation would be present in one direction, y, but not in the other, x. With an iris mechanism shutter the variation would be equal in all radial directions. In reality the shutter leaves are curved and the dose variation lies somewhere in between the two extremes, with the variation in dose along x being somewhat lower than the variation across y. This dose variation, for an example irradiation with ∼0.7 Gy, is illustrated in figure 3.14

This variation factor introduced some additional uncertainty in the dose across the dish. Taking just the x variation, maximum dose in the central region was 6% higher than the average with a corresponding drop in the dose at the edges of the dish. Averaging both X and y variation, the maximum dose was 5% higher. As stated, due to the shape of the shutter, the actual variation from the average lies somewhere between these two values.

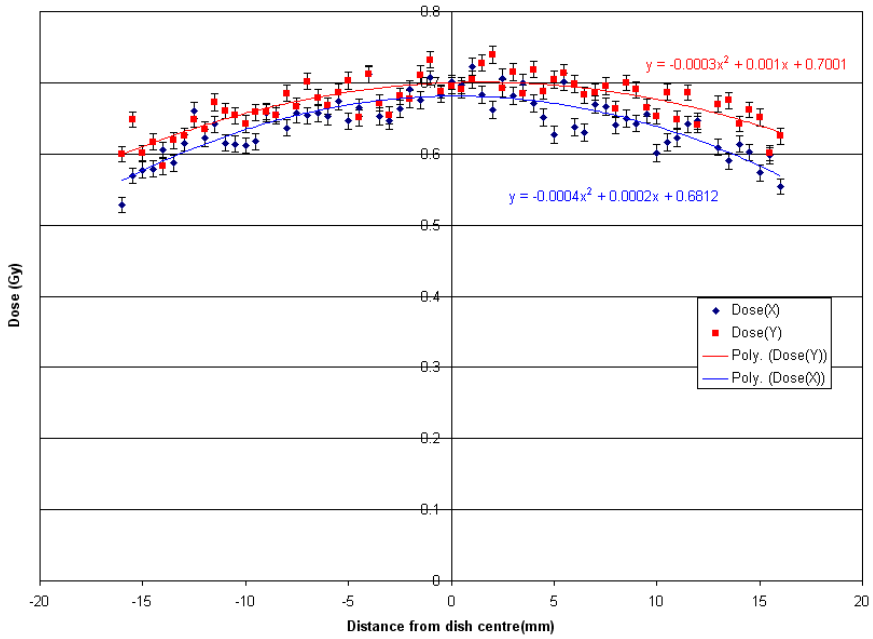

Figure 3.14: *Alpha particle dose variation, measured by CR39 track counting, across a hostaphan dish.*

The second series of experiments described in this report utilised the same alpha particle source as described above. The gamma ray source was replaced with a 250 kVp X-ray set with a hardening filter consisting of 0.6 mm of tin, 0.25 mm of copper and 1.0 mm of aluminium. With this filter in place the dose rate at the cell layer was 1.49 Gy/min at 15 mA. The irradiation head was positioned above the cell layer, see figure 3.15. X-ray dosimetry was again provided by the Farmer dosimeter and alpha dosimetry by CR39 discs. While a detailed spectrum of this X-ray source was not recorded, the half value layer was measured as 2.8 mm of copper.

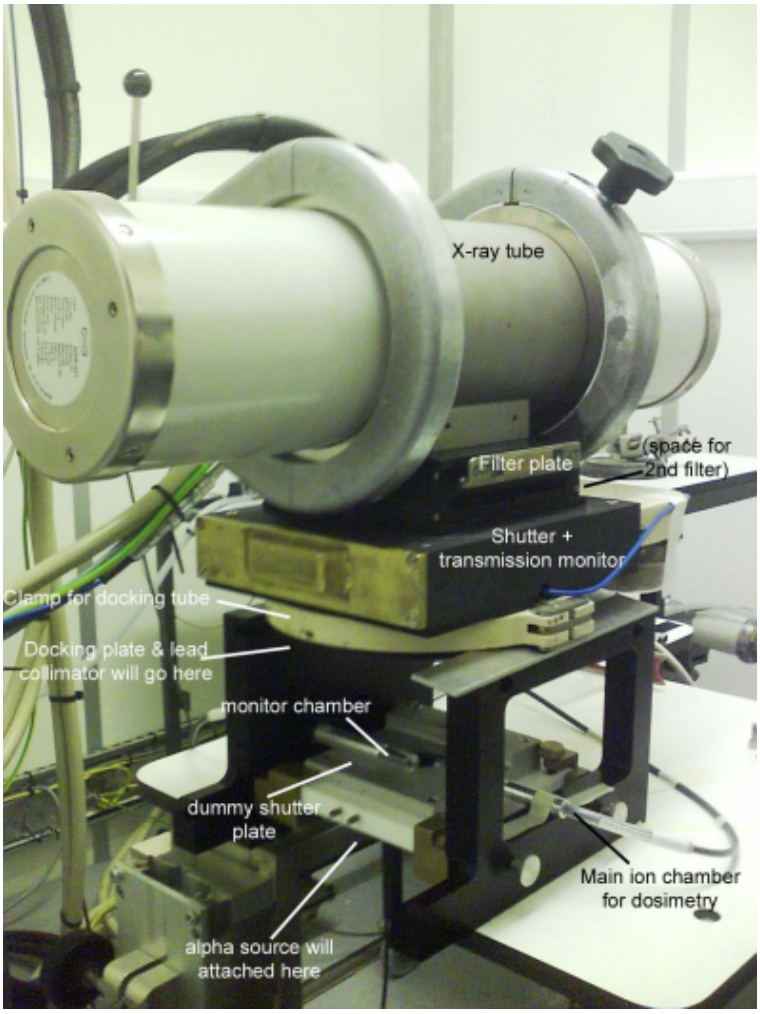

Figure 3.15: *Photograph of the mixed alpha particle and X-ray setup*

3.3 Cell Protocol

The protocol in each set of experiments was similar. Cell culture dishes were prepared 40-48 hours prior to irradiation. 2×10^5 cells were plated out into each dish in 2 ml of complete growth medium. The dishes used consist of a glass ring with a layer of polyethylene terephthalate (Mylar), serving as a base, attached with epoxy resin as in figure 3.16. The cell layer is grown directly on the Mylar.

Immediately prior to irradiation several dishes were selected randomly, the cells stained with a fluorescent dye and viewed using a confocal microscope. This allowed a check on how uniform a monolayer has formed, with stacks of cells being clearly visible. An example image is shown in figure 3.17. This is important as the alpha particles deposit a large fraction of their energy in the first cell they interact with. Cells above the first layer would receive a much reduced alpha particle dose. After examination under the microscope the stained dishes were discarded.

Ideally all cell cultures irradiated would be a monolayer to avoid any dose reduction effects. Unfortunately this requirement is in conflict with the requirement to have enough cells per irradiation to provide the required seeding for colony assays. The propensity for V79's to stack up even at relatively low densities was also an issue. With this in mind, cells were seeded at varying densities and observed 48 hours later. From these observations the

Figure 3.16: *Thin based Mylar dish*

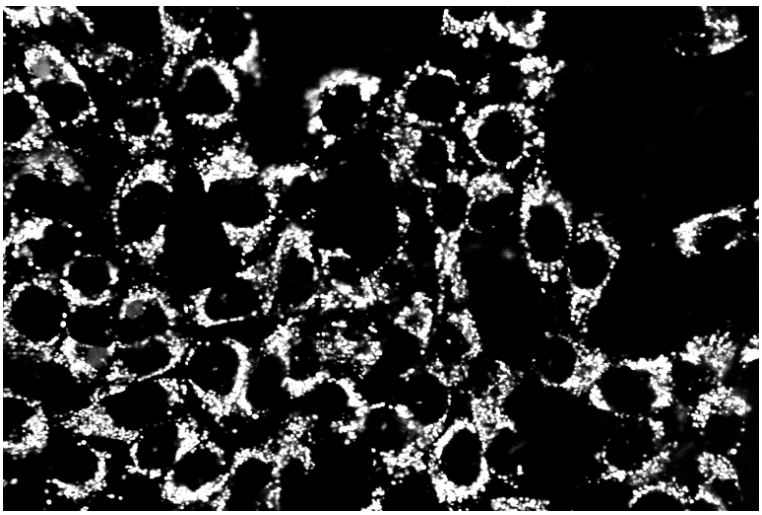

Figure 3.17: *Confocal microscope image of V79 cells stained with fluorescent dye*

density of 2×10^5 cells seeded was chosen as it provided sufficient cells for the subsequent experimental work with minimal stacking.

Cell dishes were removed from the incubator immediately prior to irradiations. The control dishes were removed for a similar time period to that needed for the irradiations. Post-irradiation the dishes are returned to the incubator for 2 hours prior to processing. Cells from the edges of the dish were discarded, due to possible alpha particle dose uncertainties. This was accomplished by cutting out the centre of the Mylar using a specially designed cutter; see figure 3.18. These Mylar disks were then placed in trypsin to remove the cells, which were then handled as described in the clonogenic cell survival study section on page 30.

In the case of the gamma ray experiments, the cells were handled in triplets comprised of cells exposed to gamma rays only, alpha particles only and a mix of alpha particles and gammas. An unirradiated control was used with each triplet. In the X-ray experiments the cells were handled in quartets with the order during the day and the grouping randomised. Two unirradiated controls were used and handled at different points during the day.

In order to provide the required gamma ray build up in the cobalt-60 exposures, 24 hours prior to irradiation an additional 2 ml of complete cell growth medium was added to the cell

Figure 3.18: *Cutter for removing the centre section of irradiated Mylar dishes*

dishes.

There was no provision for incubation of cells *in situ* so temperature of the medium, and cell layer, was not controlled during the experiment. As temperature can have a significant effect on cell repair rate [117] [118] an experiment to quantify the temperature drop over the course of the irradiations was carried out. In the case of cobalt exposures, there was also a significant delay between removal of cultures from the incubator and the irradiation commencing due to the distance from the culture lab to the cobalt source. Attempts were also made to simulate this.

Dummy dishes containing 2ml or 4ml of distilled water and a K-type thermocouple (RS part number 444-1247) were prepared and preheated in an incubator to 37 ℃. To simulate the Cobalt-60 irradiations, dishes containing 4ml were removed from the incubator and left at room temperature for ten minutes before being placed in an insulated box held at 10 ℃. Temperature measurements were then made. To simulate the X-ray irradiation conditions the dishes containing 2ml were removed from the incubator and held at room temperature, with temperature measurements beginning two minutes after removal. Temperatures were logged using a National Instruments NI9213 thermocouple module and a simple data logging application written in Labview. Results are shown in figure 3.19. As expected, a marked difference in cooling rates due to the differing temperature of the surroundings is observed.

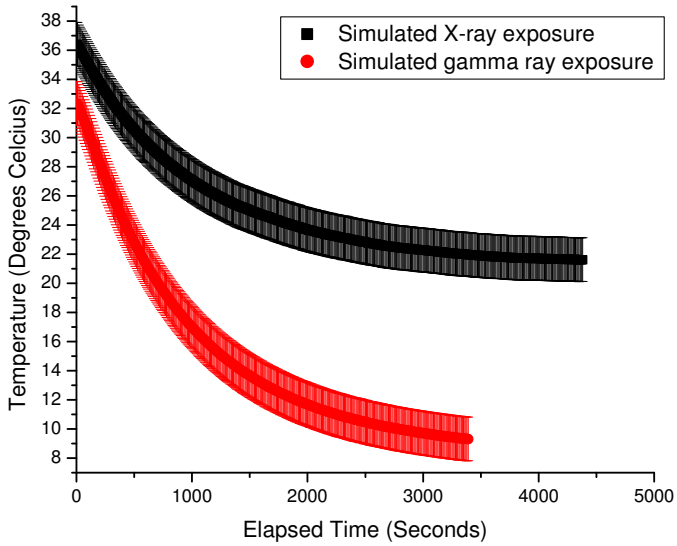

Figure 3.19: *Temperature of mylar based cell dishes over irradiation time in mixed alpha, photon cell survival experiments. A difference in cooling rate is observed as the X-ray exposures were carried out in a 20 degree Celsius environment, as opposed to 10 degrees for the cobalt exposures.*

The longest irradiation time in the case of the gamma ray exposures was less than ten minutes. According to the data shown in 3.19, this corresponds to a lowest temperature at the end of irradiation of 21.4 ℃. In the X-ray case, the longest irradiations were less than fifteen minutes corresponding to a lowest temperature at the end of irradiation of 23.6 ℃.

Even when such a temperature drop is maintained for 24 hours or more post exposure, little difference in cell response is seen [119]. In the context of an experiment including a 2 hour post irradiation incubation it was not expected to have had an observable effect on cell repair.

3.4 Calculation of Uncertainties

In all results presented in this report, cell survival uncertainties shown are calculated as one Standard Error, taken as the Standard Deviation in the survival measurements divided by the square root of the number of independent survival measurements.

$$SE = \frac{SD}{\sqrt{N}} \tag{3.4.1}$$

Each independent measurement is the mean number of colonies in the five dishes plated per dose value.

Uncertainty in photon doses are calculated by multiplying the uncertainty in irradiation time by the dose rate. These errors, when combined with the uncertainty in the dose rate itself, are typically small enough not to be visible on plots. In the case of the irradiations using cobalt-60 sources the additional uncertainty in dose from the transit time of the source is also incorporated. Errors in alpha particle doses are the combination of error introduced by irradiation time plus dose rate uncertainty, as with the photon doses, and the error due to shutter cycle time. The error from the shutter cycle time could not be calculated precisely. Plotted values are the calculated dish average dose ± 6%. This is likely to represent the extremes of dish centre dose vs dish edge dose in the worst case of square edged shutters.

Uncertainties in calculated values are based on the uncertainties in the values which were used in the function to calculate them. Normal error propagation rules were followed [120].

3.5 Curve fitting

Unless stated otherwise, all survival curves plotted in this report were fitted using Origin 6.1 or OriginPro 8 from OriginLab[121]. Origin minimises the difference between the experimental observations and the curve generated by a theoretical, user supplied, function. This is referred to as a chi squared minimisation fit. Chi squared is calculated as shown in equation 3.5.1.

$$\chi^2 = w_i \sum i = 1^n y_i - y_i^t h \tag{3.5.1}$$

y_i is the observed value, y_t is associated theoretical value and w_i the weighting factor.

Generally, the survival curve fitted followed the linear-quadratic model;

$$S = e^{-(\alpha D + \beta D^2)} \tag{3.5.2}$$

Minimising χ^2 requires iteration of the free parameters in the theoretical fitting function, in this case α and β. Such an optimising iteration is not as straightforward as it might appear as there are potential pitfalls such as local minimums of the χ^2 function. Origin utilises the Levenberg-Marquardt algorithm as described in reference [122].

A check of Origins fitting methodology was carried out using both Excels 'Solver functionality and an independent FORTRAN program. Excel uses a Generalized Reduced Gradient (GRG2) algorithm for its minima search as described by Lasdon [123]. The FORTRAN program implemented a more straightforward algorithm to solve for a minimum of a parabolic function, as described in [124]. This program can be found in appendix 1. In all cases tested it was found that all three independent methods, when given the same data, arrived at the same fitting function. This indicated that the fits provided by Origin were reliable.

Stated uncertainties in fitted parameters were provided by Origin and are derived from the sum of the squares of the deviations from each data point to the fitted line. Details of the calculation can be found in the Origin user manual [125].

3.6 Results and Discussion

3.6.1 Single Field Exposures

Alpha Particles

A comparison of single field alpha particle exposures with previously published data is shown in figure 3.20. The data show slightly lower survival at all levels than previously published data from Thacker *et al* [111], McNally *et al* [1] and Folkard *et al* [126] as shown in figure 3.20 and table 3.2. However, this is somewhat exaggerated by the levelling off of cell survival at higher doses and the resulting effect on the survival curves. A plot of the data sets for doses under 3.5Gy is shown in figure 3.21, with fitting parameters in table 3.3. Within the 95% confidence intervals the fitted curves for the current study, McNally *et al*'s and Folkard *at al*'s data all overlap. All three data sets show lower survival than that observed by Thacker *et al* [111].

The observed agreement at low dose with the two published data sets, but disagreement when higher dose responses are included suggest that cell handling techniques may account for the difference. McNally *et al* exposed their cells at low concentrations, then cultured the cells in the same dishes for their colony assay without discarding cells at the periphery. Any shielding effect at the edges of the dish would have therefore resulted in a small population receiving a reduced dose. Barendsen *et al* [38] noted a 'levelling off' effect at high alpha particle doses which they attributed to cells improperly attached to dish bases receiving a lower dose. This is another possible explanation for the observed difference, with the single field experiment described here not producing low enough survival levels for the effect to be observed. Better agreement is seen with the data of Hill *et al* [84]. An expanded comparison is shown in figure 3.22. This alpha particle data was generated using the same mylar based dish system as the current study, with the same source. While this data shows slightly lower survival at higher doses, the uncertainties in the fits overlap with uncertainties in the current data.

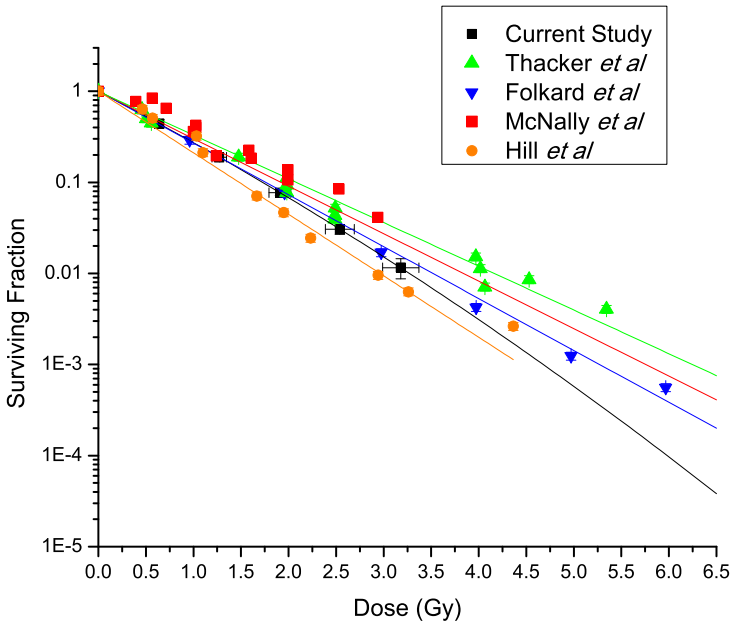

Figure 3.20: *V79 cell survival after irradiation with alpha particles compared with historic data from Thacker et al [111], McNally et al [1], Hill* et al*[84] and Folkard et al [126]*

	Alpha (Gy $^{-1}$)	**Beta (Gy $^{-2}$)**
Current Study	1.2486 ± 0.101	0.0487 ± 0.0015
Thacker et al	1.2 ± 0.0256	-
McNally et al	1.106 ± 0.1963	-
Folkard et al	1.3105 ± 0.097	0.0001 ± 0.0206
Hill et al	1.5548 ± 0.15	-

Table 3.2: *V79 survival when exposed to alpha particles. Fitted values of alpha and beta for figure 3.20, values for published data taken from the appropriate papers.*

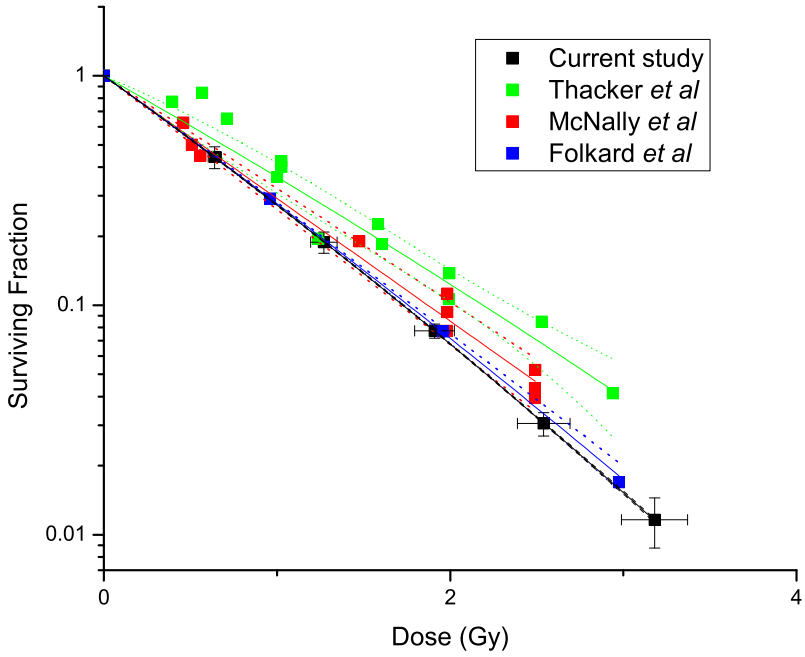

Figure 3.21: *Comparison of v79 cell survival after alpha particle irradiation, at doses under 3.5Gy, with historic data from McNally et al [1] and Folkard et al [126]. Solid lines are Origins fit lines to the data while dotted lines indicate 95% confidence levels for the fit lines of the same colour.*

	Alpha (Gy $^{-1}$)	**Beta (Gy $^{-2}$)**
Current Study	1.2486 ± 0.101	0.0487 ± 0.0015
Thacker et al	0.9855 ± 0.0574	0.03047±0.026
McNally et al	1.243 ± 0.007	-
Folkard et al	1.3105 ± 0.097	0.0001 ± 0.0206

Table 3.3: *Fit parameters for figure 3.21. Irradiation of V79 cells with alpha particles, doses of less than 3.5Gy*

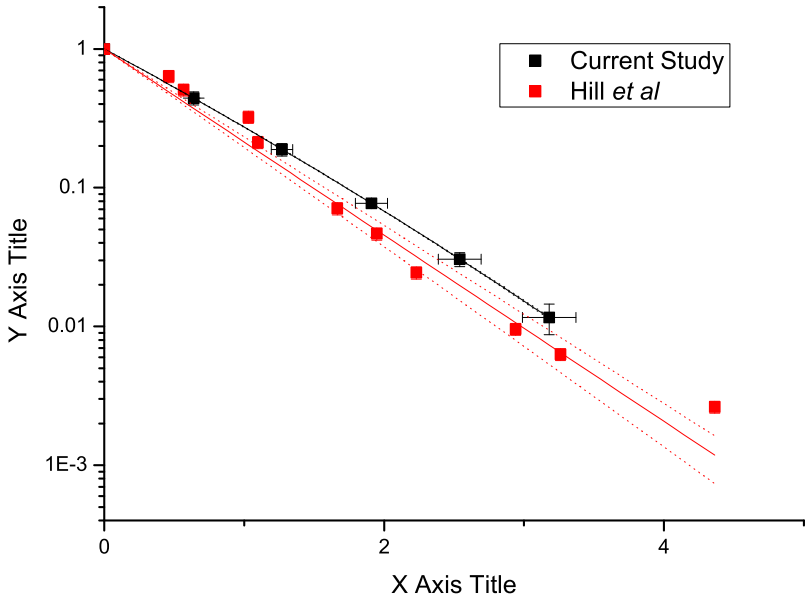

Figure 3.22: *Comparison of alpha particle survival with historic data from Hill* et al *[84]. Solid lines indicate linear quadratic fits to the data of the same colour, dashed lines the 95% confidence intervals of the associated fit. Fit to Hill* et al *data has coefficients* α*=1.545* $\pm$ *0.039 and* β*=0. Fit to the current study with parameters as in table 3.2.*

Gamma Rays

Results of single field gamma ray irradiation is shown in figure 3.23. These data also show a lower survival fraction than presented in some previous published work [32] [127], as shown in figure 3.23. While this difference from the low dose rate exposures in [32] is expected, due to the dose rate effect, the reason for the difference from published exposures at similar dose rates by Mitchell *et al* [127] and Girigoswami *et al* [128] is not clear. Better agreement is shown with the data of Winzel *et al* [129] and Schalla *et al* [130].

It has been demonstrated that V79 cells radiosensitivity can be affected by a variety of cell culture factors and their morphology during irradiation. A number of authors have reported that V79 cells grown in suspension and irradiated as clusters have a greater capacity for repair, and lower radiosensitivity, than cells grown and irradiated as a monolayer or single cells [131] [132] [133]. It has also been reported that sensitivity to DNA denaturation

in V79 is related to cell shape by Olive *et al* [134]. Reddy *et al* [135] reported differing radiosensitivity with serum concentration in medium, and also with cells exposed to trypsin, and related the observed difference between spheroids and monolayers to this.

While cell conditions in the experiments detailed here were similar to some literature exposures, and nominally identical to others, it is inevitable that factors such as small differences in medium composition exist between laboratories. Cells in this experiment were also, unusually, cultivated and exposed on mylar as opposed to a more conventional cell culture substrate.

As the mechanisms affecting radiosensitivity are thought to be repair related, differences in response are expressed more clearly in the low LET data than the high LET.

While doses are, in theory, intercomparable between the various experiments dosimetry techniques and gamma ray build up are often not fully documented for published work. There may therefore be some differences in actual gamma ray dose delivered to the cell level between the studies, at a given reported dose. Such differences, however, are likely to be small and probably do not account for variation observed.

Irradiating at low temperature produces similar effects to irradiating at a very large dose rate and can produce greater cell kill than an identical irradiation at room temperature. The irradiation room itself was at 10 ℃. While an experiment was carried out to quantify temperature drop in the cell dish being irradiated, as described in section 3.3, this may have underestimated the true temperature drop which was not directly measured. This suspicion is given some weight by the fact that the historic irradiations which most closely matched this experiments survival levels, for a given dose, (Winzel *et al*[129]) were carried out with the cells on ice at 4 ℃.

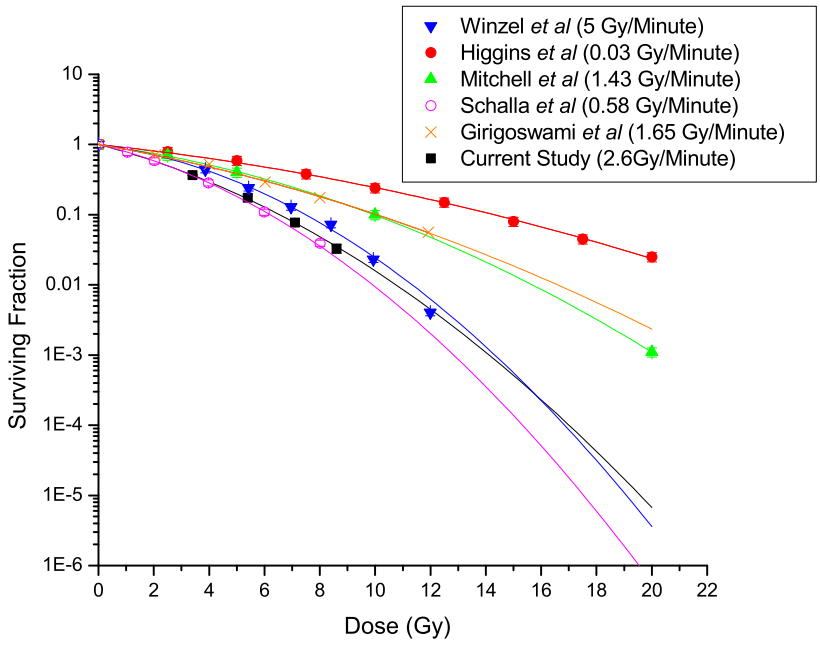

Figure 3.23: *Comparison of V79 cell survival, when exposed to gamma rays, with historic data from Higgins* et al *[32], Winzel* et el *[129], Schalla* et al *[130], Girigoswami* et al *[128] and Mitchell* et al *[127].*

	Alpha (Gy $^{-1}$)	**Beta (Gy $^{-2}$)**
Current Study	0.2332 ± 0.0040	0.0180 ± 0.0008
Higgins *et al*	0.0955 ± 0.0173	0.0046 ± 0.0011
Mitchell *et al*	0.1231 ± 0.0034	0.0109 ± 0.0002
Schalla *et al*	0.2150 ± 0.0031	0.0252 ± 0.0009
Winzel *et al*	0.1380 ± 0.0138	0.0096 ± 0.0025
Girigoswami *et al*	0.1543 ± 0.2171	0.0074 ± 0.0220

Table 3.4: *Values of alpha and beta for figure 3.23. V79 survival when exposed to* ^{60}*Co gamma rays. Values taken from published papers for historic data. Fits to the experimental data presented here were calculated in Origin, along with the associated uncertainties.*

X-rays

A comparison between the X-ray survival data and some previously published work with V79 cells is shown in figure 3.24. Although the survival appears somewhat lower than that reported by McNally et al [1], the fitted alpha parameter is the same, within the calculated error bounds, as shown in table 3.5. There is a small difference in beta. The observed difference in beta is clearly visible in figure 3.25 with the 95% uncertainty bounds of the fitted lines overlapping at lower doses and diverging at high dose. Both sets of data show lower survival than that reported by a number of other authors.

As with the single field gamma ray data, the reason for the difference in observed survival from some values presented in the literature is not entirely clear. Differences in beam hardness between the experiments are small, and X-ray dosimetry techniques are routine, leaving cell handling and culture protocols as the most likely explanation. The data presented from Gabel *et al* [55], Folkard *et al* [126] and Chapman *et al* [136] are for v79s grown and irradiated in conventional tissue culture conditions. The current study and two others where the v79 cells were irradiated and/or cultured on mylar bases, Belli *et al* [137] and McNally *et al* [1], show better agreement. This may indicate that the growing conditions in these experiments affected their response to irradiation. At odds with this conclusion is the data from Thacker *et al* [111] for cells also grown on mylar. However, these data have large published uncertainties.

Temperature was unlikely to be a factor in these exposures, as the irradiation room was at 20 degrees Celsius or higher.

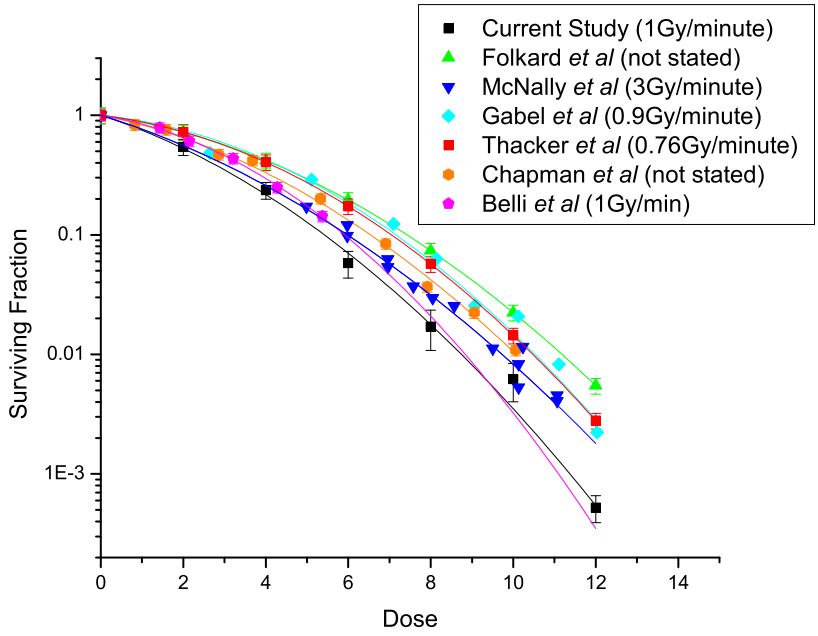

Figure 3.24: *Comparison of V79 cell survival after exposure to x-rays with historic data from Thacker et al [111], McNally et al [1], Belli* et al*[137], Gabel* et al*[3], Chapman* et al*[136] and Folkard* et al *[126]*

	Alpha (Gy $^{-1}$)	**Beta (Gy $^{-2}$)**
Current Study	0.2587 ±0.0309	0.0307 ±0.0032
Thacker *et al*[111]	0.0789 ±0.0467	0.0373 ±0.0092
McNally *et al*[1]	0.2801 ±0.0286	0.0194 ±0.0025
Folkard *et al*[126]	0.1100 ±0.032	0.0270 ±0.0058
Belli *et al*[137]	0.1248 ±0.0156	0.0448 ±0.0035
Chapman *et al*[136]	0.1582 ±0.0236	0.0297 ±0.0029
Gabel *et al*[3]	0.0763 ±0.0474	0.03432 ±0.0047

Table 3.5: *Fit parameters for figure 3.24. Cell survival after exposure to X-rays. Values taken from published papers for historic data. Fits to the experimental data presented here were calculated in Origin, along with the associated uncertainties.*

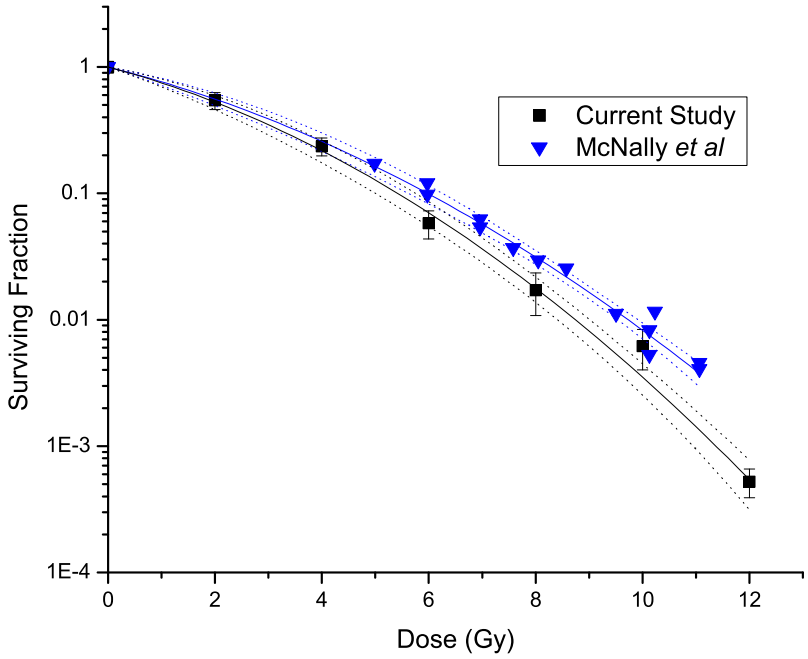

Figure 3.25: *Comparison of V79 survival response with the work of McNally* et al*[1]. Fitted line parameters as shown in table 3.5, confidence bounds calculated in Origin.*

3.6.2 Mixed Field Exposures

Gamma Rays and Alpha Particles

The results of the combined gamma ray and alpha particle irradiations are shown in figure 3.26. For this series of irradiations the corresponding doses of high and low LET radiations were chosen to give approximate identical effects (surviving fraction), based on previous work. These doses were chosen as a starting point due to the fact that in healthy tissue in BNCT, with a boron concentration of 15 ppm, receives approximately half of it's weighted dose from alpha particles.

Each of the points on the graph represents between 3 and 5 individual experimental determinations, which were carried out over a 5 week period. As described in the experimental protocol, the cells were incubated for 2 hours post irradiation to allow for repair processes to complete.

Figure 3.27 shows a comparison between the mixed field experimental data and calculated values which correspond to the effect of the two radiation qualities behaving in a strictly additive fashion. 'Additive' here, and in this rest of this document, is used in the same sense as used by Suzuki [138] in his mixed field work; the additive values were calculated from (alpha particle only surviving fraction) $\times$ (gamma ray surviving fraction) at each point. Comparing the two data sets of data points shows no significant differences. This is also the case when comparing the fit parameters, as shown in table 3.6.

	Alpha (Gy^{-1})	Beta (Gy^{-2})
Mixed alpha and gamma	0.3672 $\pm$ 0.0345	0.02543 $\pm$ 0.0041
Expected mixed field (no synergy)	0.3748 $\pm$ 0.0491	0.0213 $\pm$ 0.005
Alpha only	1.2486 $\pm$ 0.101	0.0487 $\pm$ 0.0015
Gamma only	0.2332 $\pm$ 0.004	0.018 $\pm$ 0.0008

Table 3.6: *Fit parameters for curves shown in 3.26 and 3.27. Fits to V79 cell survival in alpha particle, gamma ray and mixed fields calculated in Origin.*

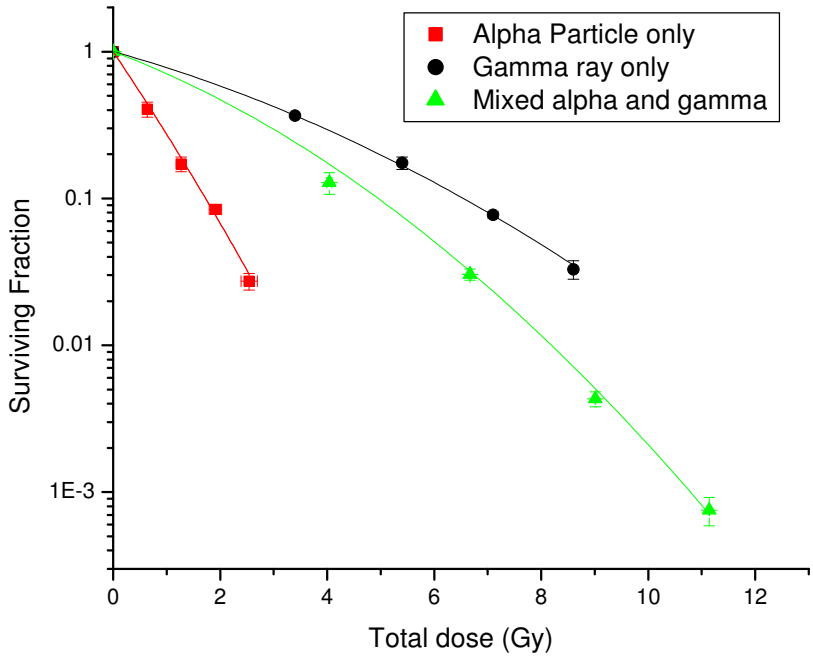

Figure 3.26: *Survival data for mixed gamma ray and alpha particle irradiations*

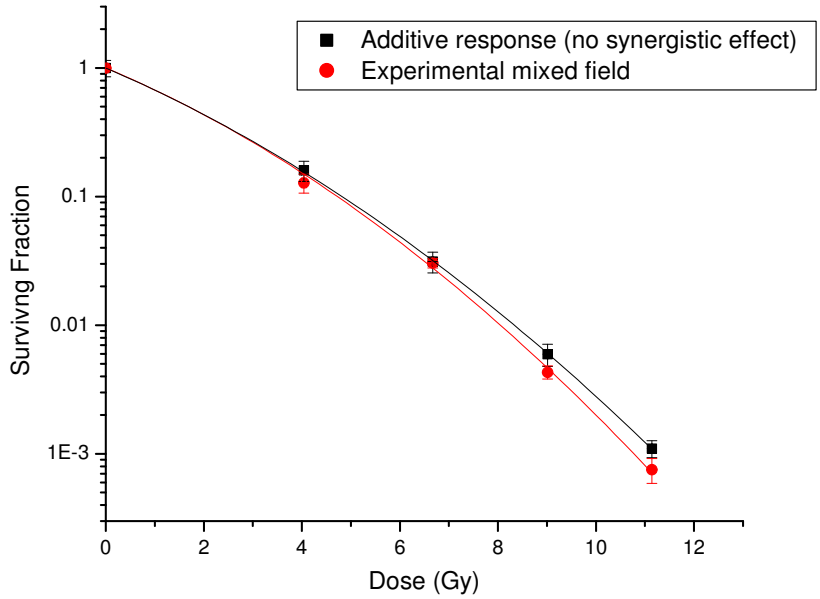

Figure 3.27: *Comparison between experimental mixed gamma ray and alpha particle irradiation data and additive response from the fields given separately*

X-Rays and Alpha Particles

The results of the combined 250 kV X-ray and alpha particle irradiations are shown in figure 3.28. Each of these data points represents the mean of between 5 and 13 experimental determinations. In order to make any variance from the expected, additive behaviour clear the data is replotted in figure 3.29. In this plot the mixed field data sets have been divided by the appropriate alpha particle only survival value, as calculated from the fitted curve. This allows any synergistic behaviour to be seen as a deviation from the X-ray only curve.

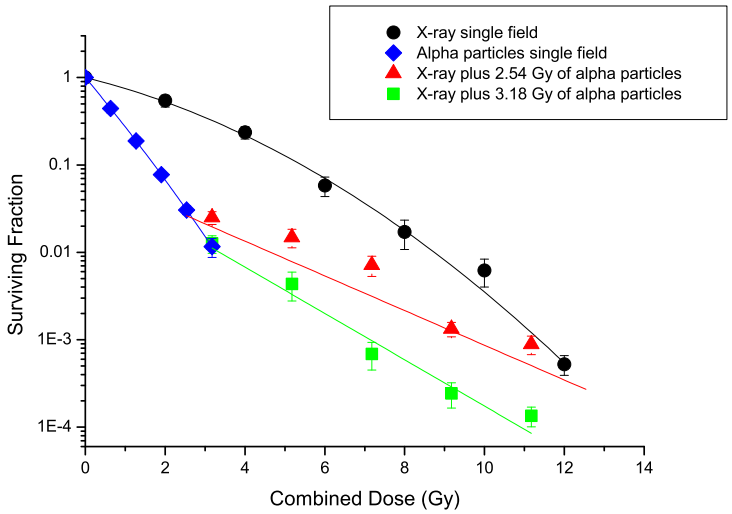

Figure 3.28: *V79 cell survival in mixed LET fields. Fitted lines are linear-quadratic functions.*

	Alpha (Gy $^{-1}$)	**Beta (Gy $^{-2}$)**
X-ray only	0.2587 ± 0.0309	0.0307±0.0032
X-ray with 2.54Gy alpha	0.4480 ± 0.0214	-
X-ray with 3.18Gy alpha	0.6383 ± 0.0390	-

Table 3.7: *Fitted values of alpha and beta for the curves in figures 3.28 and 3.29. Survival data for v79 cells. V79 survival after exposure to mixed X-ray and alpha particle fields. Mixed curves adjusted by dividing by the alpha particle only response. Values derived from a weighted chi squared fit of the linear quadratic function.*

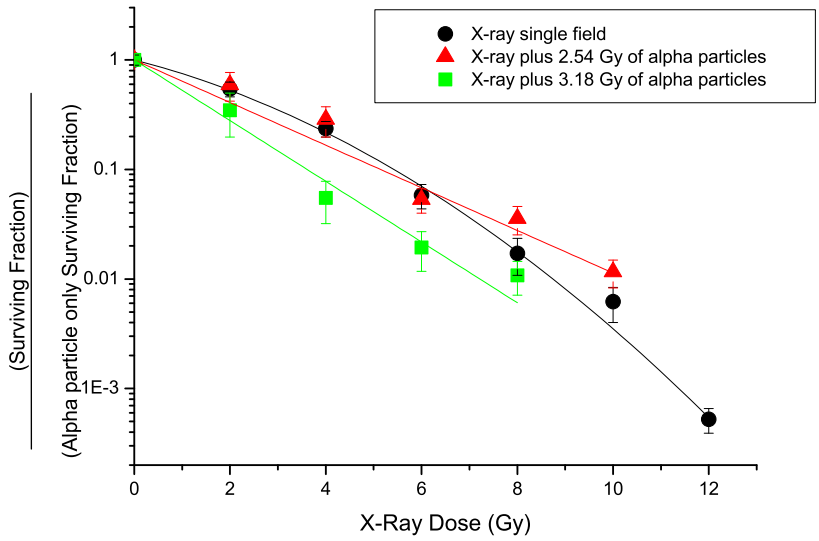

Figure 3.29: *Re-plot of mixed X-ray and alpha particle irradiations to show synergistic effect. V79 cell survival in mixed LET fields. Fitted lines are linear-quadratic functions. Mixed curves adjusted by dividing by the alpha particle only response.*

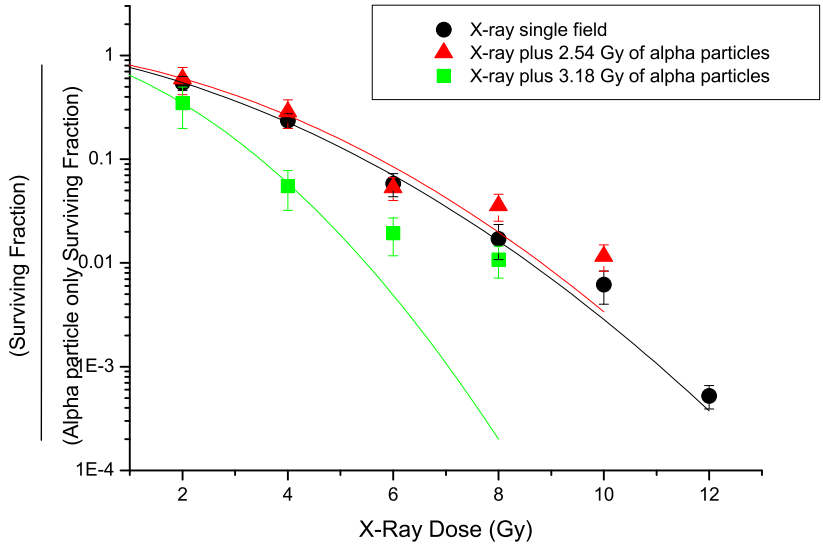

Figure 3.30: *Re-plot of mixed gamma ray and alpha particle irradiations to show synergistic effect. Mixed curves adjusted by dividing by the alpha particle only response. Fit lines from unweighted chi squared minimisation.*

	Alpha (Gy $^{-1}$)	Beta (Gy $^{-2}$)
X-ray only	0.2294 ± 0.0125	0.0357 ± 0.0037
X-ray with 2.54Gy alpha	0.1756 ± 0.0323	0.0393 ± 0.0093
X-ray with 3.18Gy alpha	0.3520 ± 0.0534	0.0891 ± 0.0232

Table 3.8: *Fitted values of alpha and beta for the curves in figure 3.30. Values derived from an unweighted chi squared fit of the linear quadratic function. Mixed curves adjusted by dividing by the alpha particle only response.*

It appears from the plot in figure 3.29 that the mixed irradiation, with a 3.18 Gy dose of alphas, shows a strong synergistic effect. There appears to be no significant synergistic effect for the mixed field with 2.54 Gy of alphas. However, comparing the fitted curve parameters (table 3.7) suggests that there is a synergistic effect in both cases. Some caution is required when interpreting these fits as the parameters are strongly dependent on the way the data is weighted in the fitting calculation. Re-fitting the data without error weighting, as shown in figure 3.30 and table 3.8, produces fits which are not significantly different for the X-ray only and 2.54 Gy alphas with X-rays. The fit to 3.18 Gy mixed data remains significantly different.

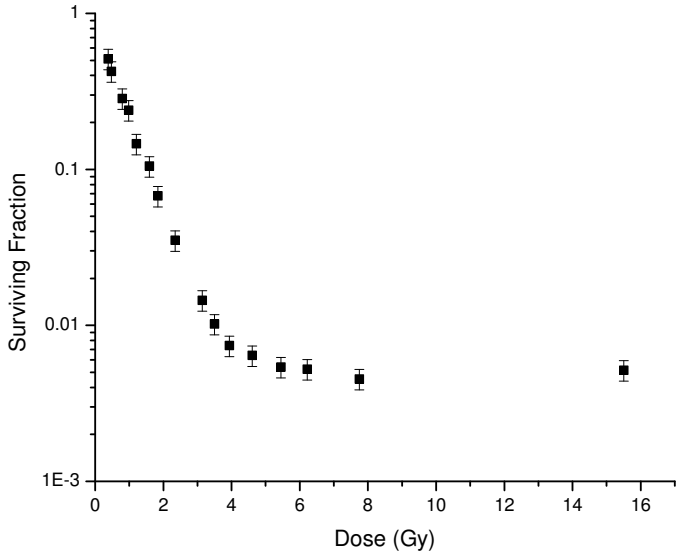

Figure 3.31: *Re-plot of cell survival data for human kidney cells of human origin irradiated with alpha particles taken from [38].*

Results are complicated further by the fact that at the lowest survival levels there appears to be some 'levelling off' of the survival curve. As mentioned in section 3.6.1, a similar effect was noted by Barendsen *et al* [38] when carrying out their alpha particle irradiations at doses greater than 3.5 Gy. Part of their data has been reproduced in figure 3.31. Their proposed explanation was a small sub population of cells, which did not adhere to the base of their dishes, and received a much reduced alpha particle dose. A similar effect may be visible in the data presented in this report, although with a much smaller population than was observed by Barrendson *et al*. The data for the mixed irradiation, with 3.18Gy of alpha particles, was refitted with the lowest survival data point excluded from the fitting calculation. The results are shown in figure 3.32. It is clear, from referring to the fit parameters in table 3.9, that excluding the last point does not have a significant effect on the fit.

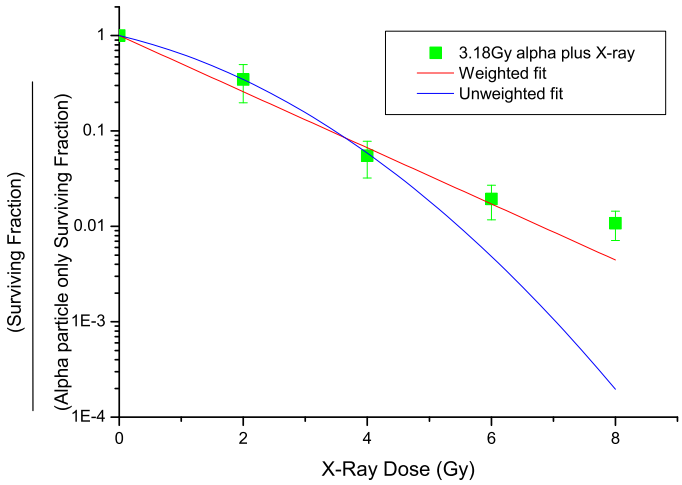

Figure 3.32: *Re-plot of mixed gamma ray and 3.18 Gy alpha particle irradiations to show synergistic effect. V79 survival data. Fit lines from weighted and unweighted chi squared minimisation with the lowest survival point excluded from the fitting calculation.*

	Alpha (Gy $^{-2}$)	Beta (Gy $^{-2}$)
Weighted	0.6772 ± 0.0557	-
Unweighted	0.3510 ± 0.0536	0.0896 ± 0.0233

Table 3.9: *Fitted values of alpha and beta for the curves in figure 3.32. Fit lines from weighted and unweighted chi squared minimisation with the lowest survival point excluded from the fitting calculation.*

3.6.3 Statistical Comparison of Data

Each of the groups of independent measurements corresponding to the mixed 2.54Gy and 3.18Gy alpha plus X-ray curves has been compared to the equivalent expected 'additive' result using a t-test. The t statistic was calculated form the difference between the two group means, divided by the standard error of the difference from the means;

$$t = \frac{\bar{x}_T - \bar{x}_C}{SE(\bar{x}_T - \bar{x}_C)} \tag{3.6.1}$$

From the values in table 3.10 it is apparent that there is no statistically significant difference between the expected response to the mixed field data, with 2.54 Gy of alpha particles, and the experimental data.

X-ray dose (Gy)	**Alpha dose (Gy)**	**t**	**DOF**	**value for 95/% confidence**
2	2.54	-0.493	13	1.771
4	2.54	-0.755	15	1.753
6	2.54	-0.641	11	1.796
8	2.54	0.988	15	1.753
10	2.54	1.640	15	1.753
2	3.18	-1.128	12	1.782
4	3.18	**-2.978**	14	1.761
6	3.18	**-1.846**	10	1.812
8	3.18	-0.796	15	1.753

Table 3.10: *t-test results for mixed field data*

In the case of the mixed field data with 3.18 Gy of alpha particles there is a significant difference from the expected response with both 4 Gy and 6 Gy of X-rays. The lack of significance at 8 Gy, and the marginal significance at 6 Gy, is likely an artifact of the levelling of the survival curve discussed earlier.

3.7 Comparison of Mixed Field Results with Published Data

A plot of the X-ray mixed field data presented in this report, along with the results published by McNally *et al* can be seen in figure 3.33. While the survival levels in the McNally *et al* 2.5 Gy data and the 2.54 Gy exposure presented in this report are similar, in the region of doses explored in the McNally experiment, the fitted lines diverge at higher doses. The difference in survival seen in the single field exposures between the two studies also leads to a large difference in the expected mixed field survivals and therefore in the magnitude of the observed synergistic effect.

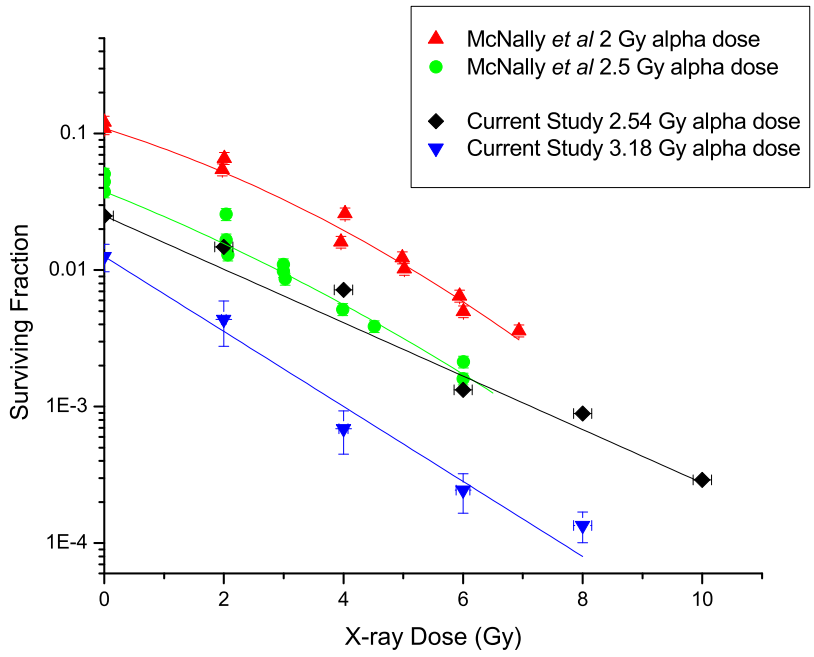

[!ht]

Figure 3.33: *Comparison of v79 cell survival in mixed x-ray/alpha particle fields with previously published work by McNally* et al*[1].*

McNally *et al* observed a synergistic effect at two of their alpha particle dose points, 2Gy and 2.5Gy (figure 3.5 on page 52). Synergy leading to higher than anticipated cell kill was only seen at 3.18Gy and not at 2.54Gy of alphas in our recent work (figure 3.29 on page 83).

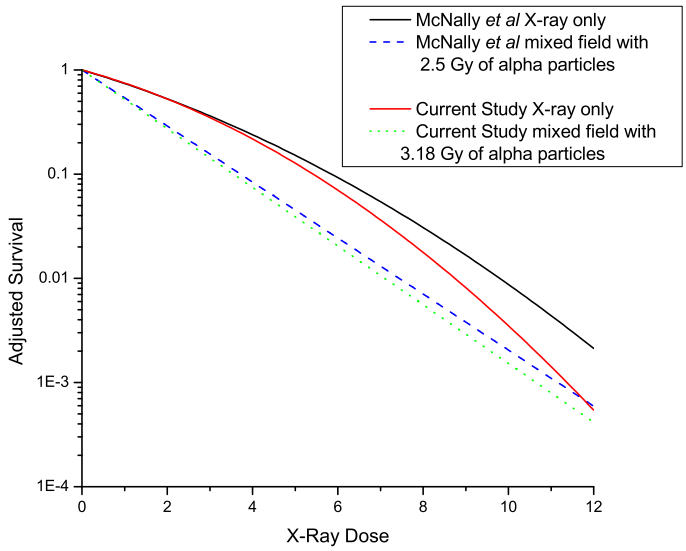

Figure 3.34: *Comparison of fitted x-ray survival curves with fitted mixed field survival curves. Data for the mixed field case was generated by dividing the experimental mixed field data by the appropriate single field alpha survival value.*

The level of synergistic effect can be seen in figure 3.34. This is a plot of the curves fitted to the X-ray response in each study along with a plot of a linear quadratic fit to (the mixed field survival)/(single field alpha survival).

The change in response in McNally *et al*'s 2.5Gy and the current 3.18Gy exposure was similar in that both showed a purely exponential response to the mixed field exposure. This differs from what would be expected from a simplistic multiplication; (single field alpha survival) $\times$ (single field X-ray response) for a single alpha particle dose, as this function leads to a shouldered curve. The level of synergistic effect therefore varies over the x-ray dose range. A comparison of synergistic effect, or 'additional cell kill', is shown in figure 3.35, calculated from the curves in figure 3.34. This curve is a plot of difference between the observed mixed field response, divided by the appropriate alpha survival, and the single field x-ray data. The difference is plotted as a fraction of x-ray response so 1 corresponds to the X-ray survival level, 2 to half the x-ray survival level and so on. Finding the maximum value of the functions in Mathematica gives a low LET fraction of 0.67 for the data presented here

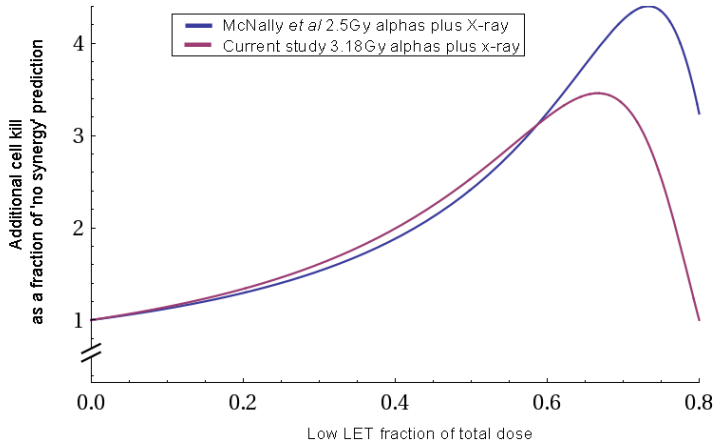

Figure 3.35: *Plot of observed synergistic effect against low LET fraction for v79 cell exposures. Data generated from fitted curves to X-ray single field data and to the fitted mixed field curves from 3.34*

and 0.77 for McNally *et al*s work. These correspond to X-ray doses of 6.36 Gy and 6.76 Gy.

The reason for the differences in which alpha particle doses exhibited a synergistic effect, and the level of synergistic effect, between the two studies is not clear. There were some differences in experimental protocol between the studies. Perhaps the most obvious is the truly simultaneous nature of the more recent irradiations. McNally *et al* performed a quasi-simultaneous irradiation where one radiation quality was delivered, the cells were maintained at 4 °C for a brief period before exposure to the second radiation type.

There were a number of differences in cell handling technique. Rather than irradiating a cell monolayer and diluting the cells for colony growth, McNally *et al* introduced an appropriate number of cells into the dishes pre-irradiation and the colonies were grown in the irradiated dishes. This could have introduced a reduction in true alpha particle dose delivered, through a shielding effect at the dish edges. Examination of the single field alpha particle doses suggests that this effect, if present, is small at the alpha particle doses of interest ($\leq$ 2.5 Gy).

The technique of plating the cells into mylar based dishes 48hr prior to exposure adopted in this study was based on experience at the MRC with this methodology and published work which used the same technique [111][139]. There is some suggestion in these papers by

Thacker *et al* and Raju *et al* that V79 cells grown on mylar take significant amounts time to assume the 'flattened' morphology of cells attached to a surface. McNally *et al* plated their cells onto mylar four to six hours prior to alpha particle irradiation. If the cells were not flat at the time of irradiation the path length of the alpha particles through the cells, and consequently the dose delivered for a given flux, would be higher than that for flat cells. Again, examination of single field alpha survival suggests that this effect would not explain the difference observed in the dual field cases.

Dose rates were different between the two studies. McNally *et al* delivered the photon dose at 3 Gy min^{-1} as opposed to 1 Gy min^{-1} in the recent work. Alpha particles were delivered at 0.3 Gy min^{-1}. The alpha dose rate in the recent work varied, as the alpha irradiation time was matched to the photon irradiation time. The maximum was 1.59 Gy min^{-1} and the minimum 0.254 Gy min^{-1}. The longest exposures were 12 minutes, the shortest 2 minutes. These dose rate differences would not normally be expected to produce significantly differences in survival in single field experiments as they would both be considered 'acute'. Ling *et al* have demonstrated that some dose rate effect is present above 1 Gy min^{-1}, with a difference observed between 10 Gy min^{-1} and 1 Gy min^{-1} at the same dose. The effect observed was small, 1% or less at the photon dose levels considered in the current work [140].

Frank *et al* [141] demonstrated that cells with differing morphologies, spheroids or monolayers, expressed differing degrees of dose rate effect. They postulated that the spheroid status confers greater protection against lesion fixation or misrepair. If the synergistic effect is more sensitive to dose rate than single field photon exposures and if, as suspected, the morphology of the cells between the two studies was somewhat different then this may provide some explanations for the differing levels of synergy seen. Further studies at varying dose rates are required for greater understanding of the effect.

This potential difference in repair between the two studies is reflected in the differing alpha/beta ratios seen in the single field X-ray exposures. McNally *et al* obtained a value

of 14.4 ± 2.4 Gy compared to a value of 8.4 ± 1.3 Gy in our more recent work. This ratio indicates the dose where alpha mediated cell kill is equal to beta mediated cell kill. Lower ratios therefore indicate a survival response with a larger contribution from multiple event, potentially repairable, damage. If the synergistic effect is repair dependant then the conditions responsible for this difference, seen in the single fields, could also account for the differences seen in mixed field responses.

Uncertainties over the origin of the synergistic effect make drawing definitive conclusions difficult. Further discussion of potential synergistic mechanisms can be found it section 3.9.

3.8 Comparison with Theoretical Predictions

3.8.1 Linear-Quadratic Based

There have been a number of attempts to treat the proposed synergistic interaction between different radiation qualities theoretically. Zaider and Rossi [89] used The Theory of Dual Radiation Action (TDRA) [142] as a starting point. The base assumption of the TDRA is that ionizing radiation produces 'sub-lesions' at a rate proportional to the specific energy, z. Pairs of these sub-lesions produce lesions and the number of lesions is proportional to the observed colonogenic survival.

Following the approach presented in [112], the yield of sublesions is cz where c is a constant. Taking A as the probability of interaction between two sublesions, the yield of lesions is therefore;

$$\epsilon(z) = Ac^2z^2 = kz^2 \tag{3.8.1}$$

where $k = Ac^2$.

The specific energy is a stochastic quantity and for an absorbed dose of D the average number of lesions can be expressed as;

$$\epsilon(D) = \int \epsilon(z) f(z;D) dz \tag{3.8.2}$$

$f(z;D)dz$ is the probability, dependent on dose, that the specific energy lies between z and $z + dz$. It is defined so that;

$$\int f(z;D)dz = 1, \int zf(z;D)dz = D \tag{3.8.3}$$

It was shown by Kellerer and Rossi in [143] that $\epsilon(D)$ can be expressed as;

$$\epsilon(D) = k(\zeta D + D^2) \tag{3.8.4}$$

ζ is the dose mean of the specific energy deposited in single events.

Choosing an appropriate constant k such that;

$$\alpha = k\zeta, \beta = k \tag{3.8.5}$$

allows survival fractions to be calculated from;

$$S = e^{-\alpha D - \beta D^2} \tag{3.8.6}$$

With two doses of radiation, D_1 and D_2, with specific energies z_1 and z_2 the yield of sublesions is $c_1 z_1$ and $c_2 z_2$. Equation 3.8.2 can then be rewritten to give the yield of lesions in the two dose case;

$$\epsilon(z_1, z_2) = A(c_1 z_1 + c_2 z_2)^2 = (k_1^{1/2} z_1 + k_2^{1/2} z_2)^2 \tag{3.8.7}$$

$$\epsilon(D_1, D_2) = \int\int \epsilon(z_1, z_2) f(z_1, z_2; D_1, D_2) dz_1 dz_2 \tag{3.8.8}$$

As z1 and z2 are independent scholastic variables the probability function can be written as;

$$f(z_1, z_2; D_1, D_2) = f1(z_1; D) f2(z_2; D_2) \tag{3.8.9}$$

Using 3.8.3 and 3.8.4 this gives;

$$\epsilon D_1, D_2 = k_1 \zeta_1 D_1 + k_2 \zeta_2 D_2 + (k_1^{1/2} D_1 + k_2^{1/2} D_2)^2 \tag{3.8.10}$$

and the surviving fraction can be calculated from

$$S = e^{-(\alpha_1 D_1 + \beta_1 D_1^2 + \alpha_2 D_2 + \beta_2 D_2^2 + 2(\beta_1 \beta_2)^{1/2} D_1 D_2)} \tag{3.8.11}$$

The expected synergistic effect is reflected in the difference between equations 3.8.6 and 3.8.11; the $2(\beta_1\beta_2)^{1/2}D_1D_2$ term. Zaider and Rossi referred to this as the interference term. It suggests that an interaction between the sub-lesions produced by each radiation type interact, to produce more lethal damage than would be expected from the two irradiations given separately.

This treatment of sequential irradiations implies that the order in which the two irradiations are given is irrelevant. This is in agreement with the experimental findings of McNally *et al*[34] [144] with neutrons and X-rays. No significant difference in survival was found between X-rays followed by neutrons, neutrons followed by x-rays or both given simultaneously. Similar results were shown by Suzuki [145].

The theoretical predictions of equation 3.8.11 can be compared to experimental mixed field data through obtaining values for the $\alpha_1, \alpha_2, \beta_1$ and β_2 constants from single field irradiations. Using the alpha and beta values arrived at using weighted chi squared fitting (table 3.7) modelled vs experimental results for 2.54 Gy of alpha particles plus photons and 3.18 Gy of alpha particles plus photons are shown in figures 3.36 and 3.37 respectively.

It is clear that the Zaider-Rossi model is an excellent fit to the mixed field survival data with 3.18Gy of alpha particles. For the 2.54 Gy of alpha particles the model predicts lower survival than was observed experimentally. Uncertainties in these Zaider-Rossi plots and all further model plots were calculated from the uncertainties in the single field alpha and beta values.

Suzuki [145][146] modified the Zaider and Rossi model to apply to various mixed field irradiation regimes. They also presented experimental data to demonstrate that the order of irradiation in sequential mixed field exposures is not significant. The model presented in the paper included terms to account for cell recovery during the course of irradiation. This extension allowed them to explain the variation in observation of synergistic effects between Higgins *et al* [147] and McNally *et al*[144], with neutron-photon mixed fields, as due to differences in dose rates. The model, as derived in [145] is;

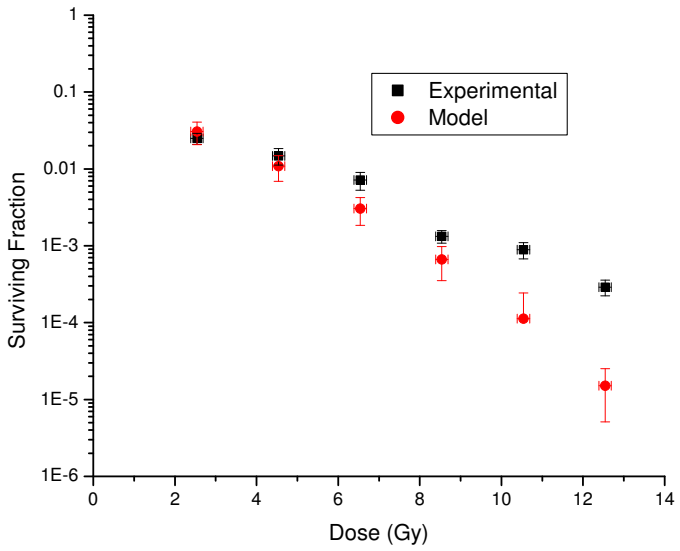

Figure 3.36: *Comparison of experimental mixed field results for 2.54Gy of alpha particles plus photons with the Zaider Rossi model. Parameters for the Zaider-Rossi model were taken from the fits shown in table 3.8*

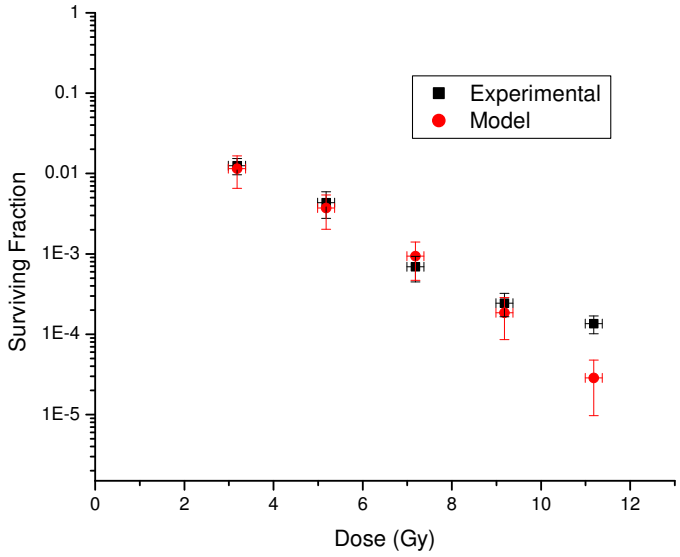

Figure 3.37: *Comparison of experimental mixed field results for 3.18Gy of alpha particles plus photons with the Zaider Rossi model. Parameters for the Zaider Rossi model were taken from the fits shown in table 3.8*

$$S = \exp\left[-\left(\frac{\alpha_1 a_1 D}{a_1 + a_2} + \frac{\alpha_2 a_2 D}{a_1 + a_2} + \frac{q_1 \beta_1 a_1^2 D^2}{(a_1 + a_2)^2} + \frac{q_2 \beta_2 a_2^2 D^2}{(a_1 + a_2)^2} + 2q_{12}(D,T)\sqrt{\beta_1 \beta_2}\frac{a_1 a_2 D^2}{(a_1 + a_2)^2}\right)\right] \tag{3.8.12}$$

Where D is total dose, a_1 and a_2 are the relative dose rates of the two radiation types.

α_1,α_2,β_1 and β_2 are the constants determined by fitting curves to the single field irradiation data.

q_1,q_2 and q_{12} are cell repair related reduction factors. In the special case of simultaneous irradiation $q_1 = q_2 = q_{12}$ and is given by;

$$q_{12} = \left(\frac{t_0}{t}\right)^2\left[\exp\left(\frac{t}{t_0}\right)\left(1 - \exp -\left(\frac{t}{t_0}\right)\right)^2 + \exp -\left(\frac{t}{t_0}\right) - \exp\left(\frac{t}{t_0}\right) + \frac{2t}{t_0}\right] \tag{3.8.13}$$

t is the irradiation time.

t_0 is referred to, somewhat confusingly, by Suzuki as the 'time constant for recovery'. This formulation of cell recovery is based on the work of Kellerer and Rossi, in 'The theory of dual radiation action' [148], who refer to the same factor as recovery time.

Kellerer and Rossi's treatment of dose rate dependent recovery introduces a reduction factor applied to the β term in their linear-quadratic formula. A function $\tau(t)$ was introduced, which determines the interaction probability as a function of the time interval between the formation of two sublesions. This is assumed to be exponential, that is;

$$\tau(t) = e^{\left(\frac{-t}{t_0}\right)} \tag{3.8.14}$$

Their formula for a reduction factor q(T), derived in reference [148], for a continuous irradiation of duration T and dose D can be written;

$$q(T) = \frac{2t_0}{T} - \left(\frac{2t_0^2(1 - e^{T/t_0})}{T^2}\right)D^2 \tag{3.8.15}$$

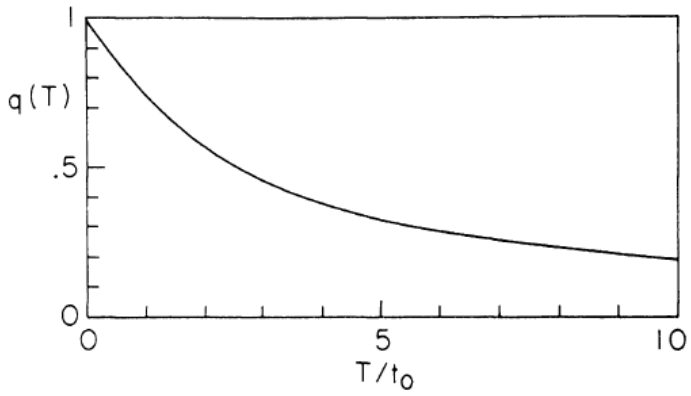

Figure 3.38: *Plot of reduction factor of the beta term as a function of irradiation time T and recovery time t_0[148]*

The function for cell survival therefore becomes;

$$S = e^{-(\alpha D + q(T)\beta D^2)} \tag{3.8.16}$$

A plot of reduction factor against the ratio of exposure time to recovery time is shown in figure 3.38. At the limit of $T/t_0 \rightarrow 0$ equation 3.8.16 reduces to the standard linear quadratic function. At the limit where $T/t_0 \rightarrow \infty$ the beta term is insignificant and the survival function is reduced to a simple exponential. This effect of the beta component tending to zero has been observed in cell experiments, as illustrated in figure 3.39.

Zaider and Brenner arrive at a value of t_0 for V79 cells of 78.6 minutes [150]. This is a value obtained by by fitting a survival function, which accounts for repair in the intertrack (beta) term, to single field photon exposures at differing dose rates R;

$$S(D) = \exp -(\alpha D + \beta q(D,R) D^2) \tag{3.8.17}$$

$$q(D,R) = 2t_0 R/D - 2(t_0 R/D)^2[1 - exp(-D/t_0 R)] \tag{3.8.18}$$

A comparison of the 'Extended Zaider-Rossi model' to the experimental data presented

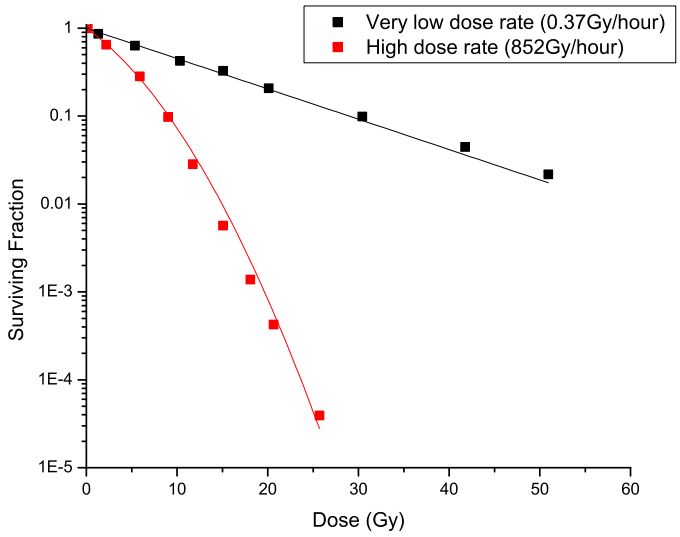

Figure 3.39: *Plot of survival response of V79 cells to varying 250 kV X-ray dose rates. The low dose rate has an exponential response, with fitted constants in the linear quadratic function of* $\alpha = 0.0794 \pm 0.002$ *and negligible* β*. Fitted constants for the acute exposure were* $\alpha = 0.1687 \pm 0.0119$ *and* $\beta = 0.0093 \pm 0.002$*. Data replotted from [149].*

in this report is shown in 3.40 and 3.41. Values of $\alpha_1, \alpha_2, \beta_1$ and β_2 were obtained by fitting the single field data. A t_0 of 78.6 was used.

There are no large differences in survival levels predicted by the extended Zaider-Rossi compared to the standard Zaider-Rossi model for the dose rates utilised in the irradiations detailed in this report or in the work presented in [1]. The irradiation time is small compared to the recovery time. It is likely that Suzuki's treatment of repair is something of an oversimplification for all dose rates, as it is assumed that the repair is LET independent. This has been disproved experimentally by Belli *et al* [151] and others; see figure 3.42. There is instead significant evidence that the level of repairable damage is related to the complexity of the damage, which is in turn related to the ionisation track structure of the radiation inducing it. This is discussed further in section 3.9.

The statistical approach of the TDRA, on which the Zaider-Rossi model is based, implies that the biological effect is expressed immediately after dose deposition and disregards cell

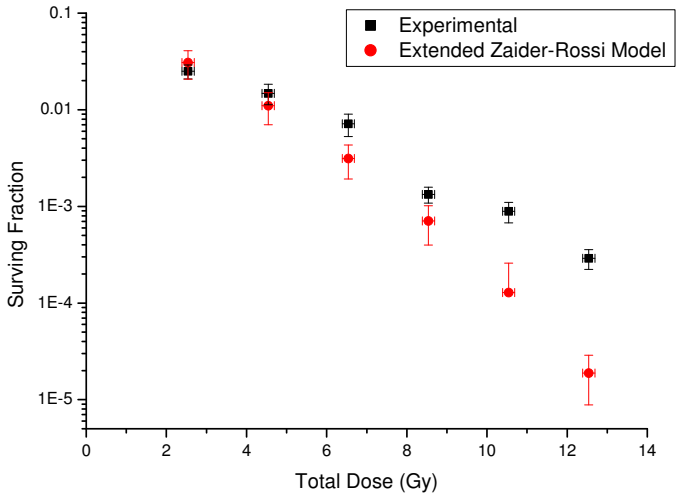

Figure 3.40: *Comparison of experimental mixed field results for 2.54 Gy of alpha particles plus photons with the Extended Zaider-Rossi model. Parameters for the Zaider-Rossi model were taken from the fits shown in table 3.8 on page 84 along with the associated uncertainties. Doses are total dose delivered to the cells.*

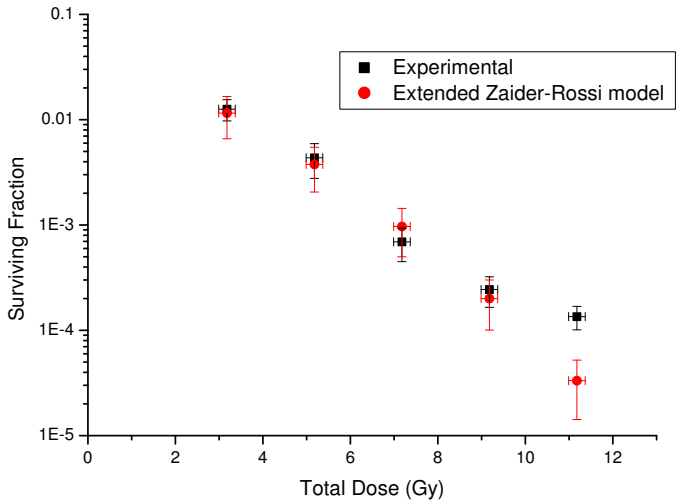

Figure 3.41: *Comparison of experimental mixed field results for 3.18 Gy of alpha particles plus photons with the Extended Zaider-Rossi model. Parameters for the Zaider-Rossi model were taken from the fits shown in table 3.8 on page 84 along with the associated uncertainties. Doses are total dose delivered to the cells.*

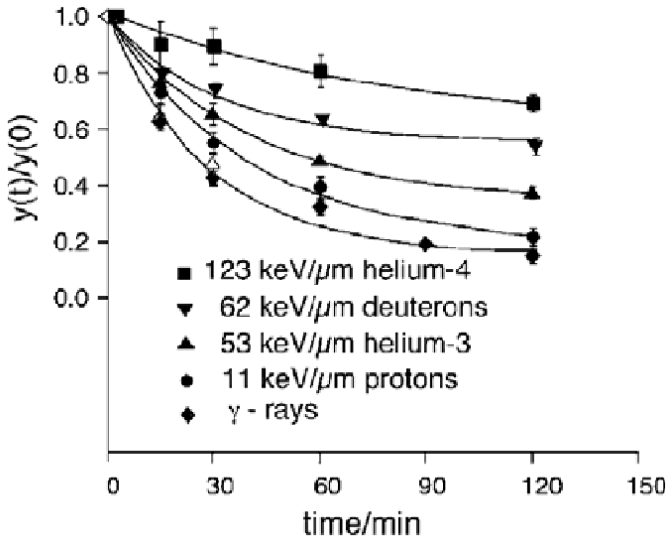

Figure 3.42: *Repair of double strand breaks with time vs LET, in V79 cells. Taken from [151]*

repair kinetics. More recent models of cell survival such as the Microdosimetric-Kinetic (MK) model proposed by Hawkins [152] attempt to combine more sophisticated modelling of repair and injury processes with a microdosimetric description of radiation energy deposition. These models have been further extended in various ways [153] [154] to attempt account for the repair mechanisms dependance on LET. Ultimately these models are limited in their usefulness due to the large number of parameters which are difficult to determine experimentally.

The Zaider-Rossi approach may overemphasise the non zero beta constant in the fit to the single field alpha particle data presented in this report. It is often assumed that a high LET alpha particle survival curve is exponential with a beta value of zero. Refitting the alpha particle data with beta constrained to zero, as shown in figure 3.43, gave an alpha value of 1.356 $\pm$ 0.012 Gy_{-1}. The quality of fit is reduced from the unconstrained case, with a reduced χ^2 of 0.2382 vs 0.0014 for the unconstrained case. The reduction is not significant as both fits are within experimental uncertainty. Re-plots of the Zaider-Rossi model with this revised value can be seen in 3.44 and 3.45. The model is a good match for the 2.54 Gy data but predicts higher survival than is seen experimentally in the 3.18 Gy

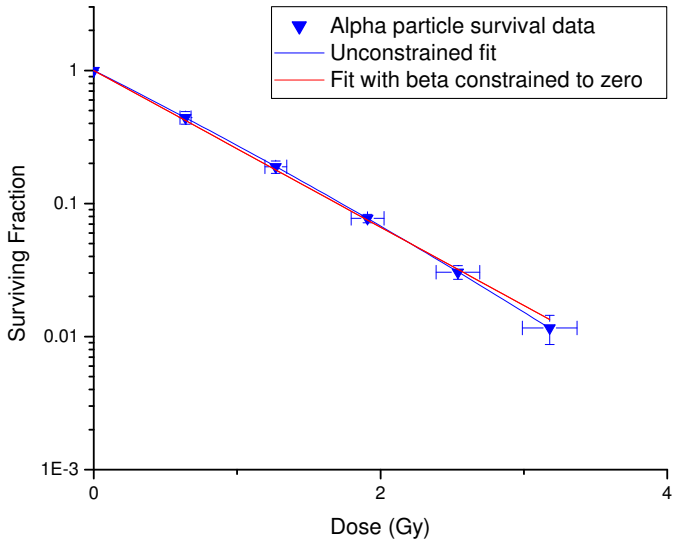

Figure 3.43: *Comparison of unconstrained linear quandratic fit and constrained fit to single field alpha particle survival data. Constrained fit parameters were α=1.356, β=0 with beta fixed*

alpha mixed field data. This is to be expected as with a zero β_2 term the interference term in the Zaider-Rossi model is zero, no synergistic effect is predicted and the model reduces to the two single field curve results multiplied together.

The reduction to zero of the interference term in the Zaider-Rossi, and extended Zaider-Rossi, model for zero β is the explanation for the lack of agreement at higher alpha particle dose levels with the work of McNally *et al.* The Zaider-Rossi model, using the parameters from the single field data in [1], predicts a response with no large synergistic effect at a dose of 2.5 Gy or 3 Gy of alpha particles. This at variance with the experimental results presented by McNally *et al.* A comparison between the data presented by McNally *et al* and the Zaider-Rossi model at this level can be seen in figure 3.46.

In the fitted models presented so far the values of the coefficients in the linear quadratic function have been derived from fitting both α and β to single field data. This has yielded values of α_{High},β_{High} from the alpha particle irradiations and α_{Low},β_{Low} from the X-ray irradiations. However, the TDRA predicts that high LET radiation increases the linear, α,

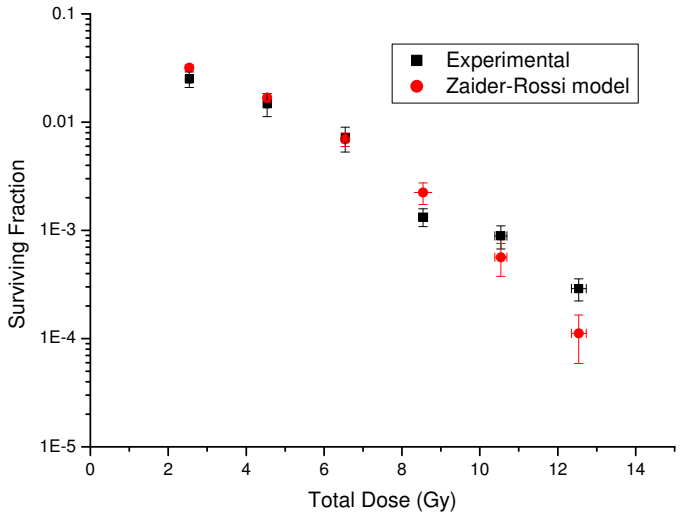

Figure 3.44: *Comparison of experimental mixed field results for 2.54 Gy of alpha particles plus photons with the Zaider-Rossi model. Parameters for the Zaider-Rossi model were taken from the X-ray fits shown in table 3.8 on page 84. Single field alpha particle parameters were α=1.356, β=0*

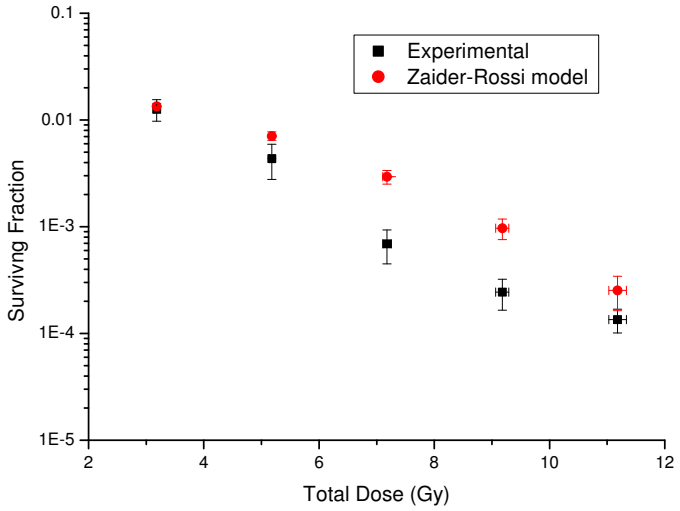

Figure 3.45: *Comparison of experimental mixed field results for 3.18 Gy of alpha particles plus photons with the Zaider-Rossi model. Parameters for the Zaider-Rossi model were taken from the X-ray fits shown in table 3.8 on page 84. Single field alpha particle parameters were α=1.356, β=0*

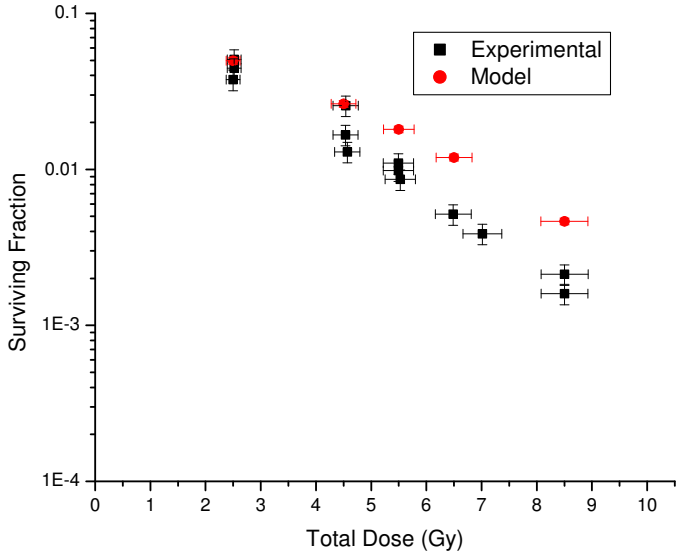

Figure 3.46: *Comparison of experimental mixed field results for 2.5Gy of alpha particles plus photons with the Zaider Rossi model. Experimental data replotted from figures presented in [1] and model parameters were taken from fits to the single field data in the same reference.*

component of radiation damage without changing the quadratic term, β [142] [76]. This implies survival in the high-LET case can be predicted by;

$$S_{High} = e^{-(\alpha_{High} D_{High} + \beta_{Low} D_{High}^2)} \tag{3.8.19}$$

Where S_{High} is cell survival, α_{High} is the linear coefficient for high LET, β_{Low} is the quadratic coefficient found at low LET and D_{High} is dose of high LET radiation delivered.

To determine α_{High} for the alpha particles, used in both the current study and the work of McNally *et al*, the single field data was re-fitted with beta constrained to the value of β_{Low}. The results are shown in table 3.11. The extended Zaider-Rossi model was recalculated for each mixed field case, using these values. Results for the current study are shown in figure 3.47. It is clear that this methodology produces a predicted response much closer to that which was observed by McNally at lower alpha particle doses. The model still under predicts cell kill for the highest alpha particle dose delivered by McNally *et al* (2.5 Gy).

	Alpha (Gy $^{-1}$)	Beta(Gy $^{-2}$)
Current study	1.2876	0.0307
McNally *et al*	1.1111	0.0194

Table 3.11: *Fit parameters for single field alpha particle survival data when beta is constrained to the value of* β_{Low}

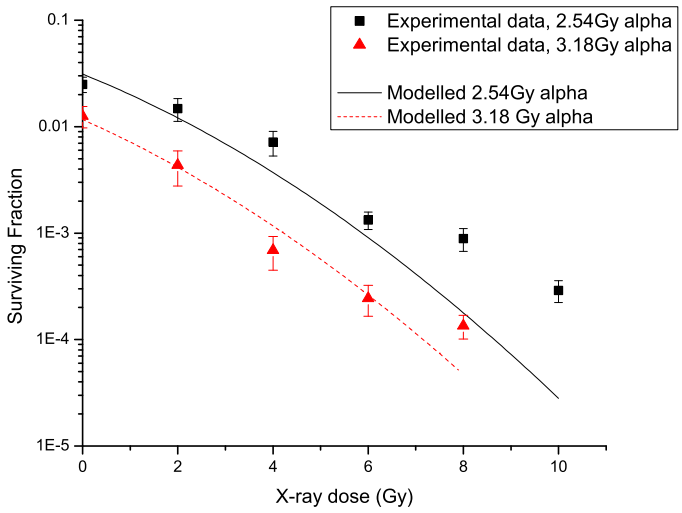

Figure 3.47: *Comparison of the Zaider-Rossi model with experimental mixed field results for irradiation with alpha particles plus photons. Co-efficients for the model are as stated in table 3.11*

Similar model predictions for the irradiations presented in this report are found using β_{Low} for both levels of LET instead of β_{Low} and β_{high}. Both approaches predict lower cell survival in the 2.54Gy alpha mixed case than is observed experimentally while being in good agreement for the 3.18Gy of alpha particles dose level.

There is some suggestion from re-analysis of historic fast neutron survival data that rather than being fixed with LET the beta constant may actually increase with increasing LET [78]. If this was the case in the mixed field exposures then model comparisons with McNally *et al*'s higher alpha dose, mixed field, data would be improved.

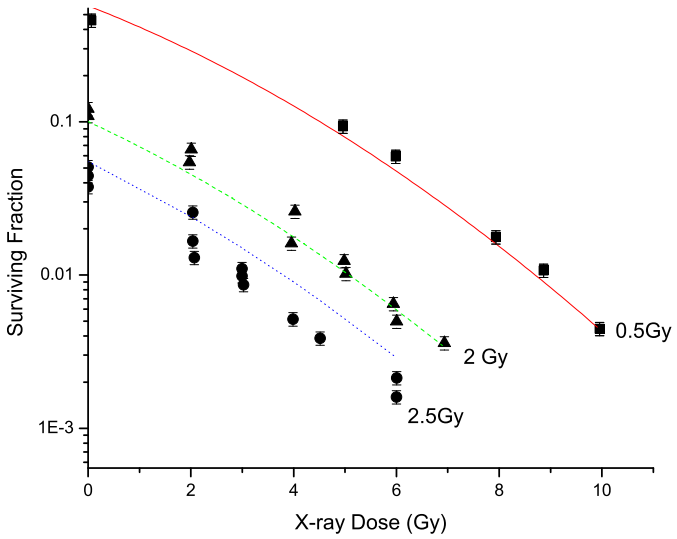

Figure 3.48: *Comparison of the Zaider-Rossi model with experimental mixed field results taken from [1]. Plotted points are the experimental data and lines are the associated model. Numbers indicated the alpha particle dose delivered in addition to the photons. Coefficients for the model areas are as stated in table 3.11.*

3.8.2 Lesion Additivity Model

A different approach to predicting survival in a mixed field irradiation to that of Zaider and Rossi was introduced by Lam [155]. This model has as it's central assumption some intermediate stage in the cell inactivation path, where different types of lesion precursors produced by different radiations become indistinguishable and therefore additive. It also assumed that precursors competing to produce lesions have equal probabilities and that lesion precursors reach the intermediate stage concurrently if delivered within a sufficiently short time [156]. The model derived in [155] can be stated as;

$$RBE_{mix} = \sum_i f_i RBE_i \tag{3.8.20}$$

where f_i is the fraction of radiation, with an RBE of RBE_i at the effect level being considered. Predicted cell survival curves can be constructed by calculating RBE_mix across a range of doses.

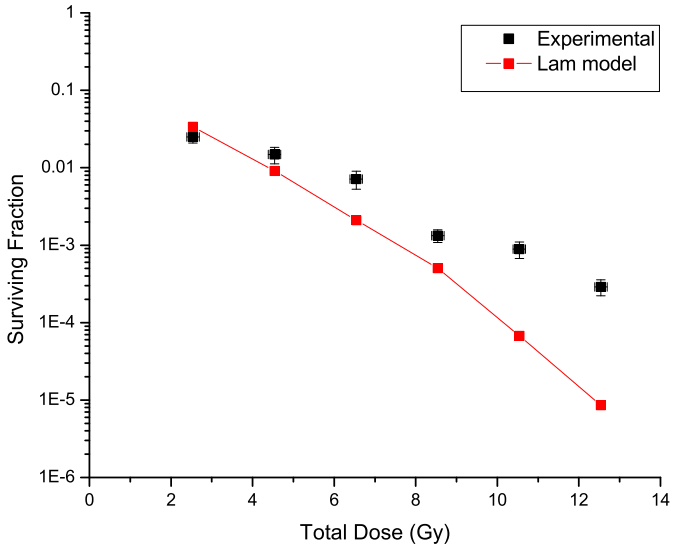

Figure 3.49: *Comparison of the Lam* et al *lesion model[155] with survival data from mixed X-ray / 2.54 Gy alpha particle exposures*

Figures 3.49 and 3.50 show a comparison between predicted survival values calculated with the Lam model and experimental work. As with the Zaider-Rossi models good agreement is seen for the data with 3.18Gy of alpha particles, at lower x-ray doses, and poor agreement at 2.54 Gy. To produce the model fits an alpha particle RBE was calculated at each survival level based on the linear-quadratic fits to the single field X-ray and alpha particle data. Poorer agreement is seen at higher doses in the 3.18 Gy of alpha particles case than was seen with the Zaider-Rossi model. This was due to the model predicting a larger degree of curvature than the purely exponential response of the Zaider-Rossi prediction.

This similarity between predictions of the Lam model and the ZR model found here was also reported by Tilly *et al* when comparing them to combined gamma ray, nitrogen ion exposures [156].

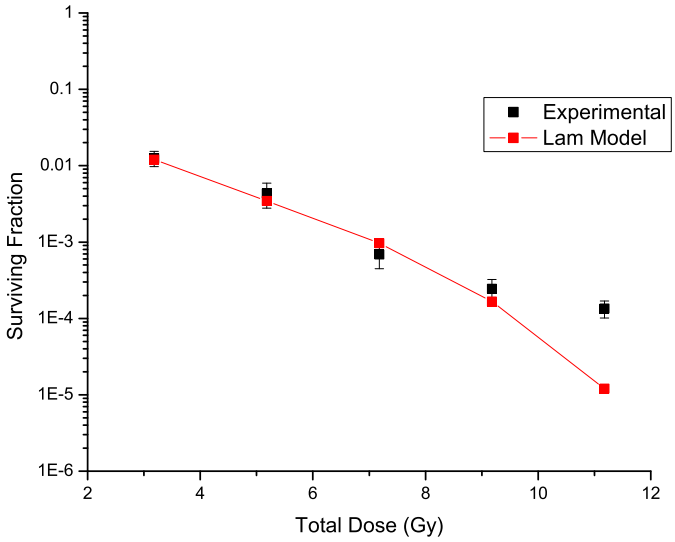

Figure 3.50: *Comparison of the Lam* et al *lesion model[155] with survival data from mixed x-ray / 3.18 Gy alpha particle exposures*

3.9 Mechanism of Synergy

There are several mechanisms which could conceptually lead to a synergistic survival response in cells exposed to two radiation fields. Possibilities could include an overall increase in the level of damage, an interaction between existing damage resulting in damage more effective at causing cell death and an impairment or prevention of damage repair.

As the level of damage is proportional to absorbed dose in a cell, it is hard to see how a mixed field would introduce any 'extra' damage which could account for synergy. The amount of DNA damage has been observed to be proportional to the energy deposited. However, here is significant evidence that it is not the absolute level of damage but rather the local complexity of damage which dictates a cells response. The ionisation track structure is thought therefore to account for the difference in biological effect, for a given dose, seen between high LET ions and low LET photons [157]. High LET radiation deposits most of its energy in the form of relatively small numbers of densely ionising tracks through a cell compared to much more sparsely ionising electron tracks, produced in large numbers by X-rays, and distributed randomly throughout a cell. These different energy depositions are reflected in the distributions of DNA damage [158]. Thanks to modern antibody staining techniques, the differences in density of DNA damage can now be directly observed. Phosphorylation of histone protein H2AX on serine 139 occurs at sites flanking Double Strand Breaks (DSB) and can provide a measure of the number of DSBs within a cell [159]. It also provides an informative visualisation of the location of the damage sites [160]. An example of images produced using this technique and an illustration of the track differences between radiation of differing qualities can be seen in figure 3.51.

The idea that damage from low and high LET tracks could interact, increasing local complexity of damage and producing more damage clusters, is an appealing explanation for synergy. However, this is unlikely. The complexity in question, which dictates the likelihood of a DSB being repairable, involves additional damage within a few DNA base pairs of a DSB. Monte Carlo track structure models suggest that this additional damage is present in

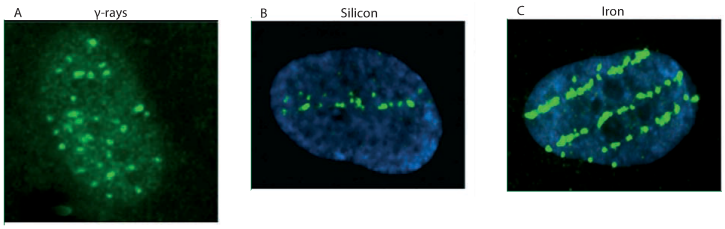

Figure 3.51: *Formation of fluorescent γ-H2AX clusters in irradiated human fibroblasts, at 10 min post-irradiation, with (A) 2 Gy of g rays, (B) 0.5 Gy of 54 keV/mm silicon ions, or (C) 0.5 Gy of 176 keV/mm iron ions. Each panel shows the DAPI-stained nucleus(blue)and anti-g-H2AX antibody (green) [161].*

	Energy	SSB/DSB	SSB complex/simple	DSB complex/simple
Electrons	0.3 keV	11	0.12	0.28
Electrons	1keV	13	0.11	0.32
Electrons	10 keV	30	0.05	0.23
Electrons	100keV	30	0.04	0.2
α particles	2 MeV	2	0.27	0.73
α particles	4 MeV	3	0.23	0.61

Table 3.12: *Clustered DNA damage from different radiation qualities. Complex SSB are defined as single-strand breaks with additional break(s) on the same strand. Complex DSB are double-strand breaks with additional break(s) on one or both strands. The values for electrons are for full slowing down tracks of the stated starting energy; the values for alpha particles are for track segments of the stated energy/. From [162].*

approximately 20% of higher energy X-ray DSB's and 60% or more of high LET α DSB's - see table 3.12. The small dimensions of these clusters leads to the conclusion that clustered damage is produced almost exclusively within single tracks. The probability of separate tracks overlapping within the nanometre scale in question is negligible even at very high doses [162].

Interference with normal cell repair processes has long been proposed as a mechanism for synergy. While some efforts have been made to investigate this, with delayed cell plating and separation of the two dose components in time [31][34], little insight into the mechanism has been gained. It was demonstrated that with a separation of several hours between irradiation qualities independent action was observed. This lead to a suggestion that there was some element of interactive damage, which was itself repairable [31].

A recent study by Staff *et al* [163] applied γ-H2AX staining assays to mixed field ex-

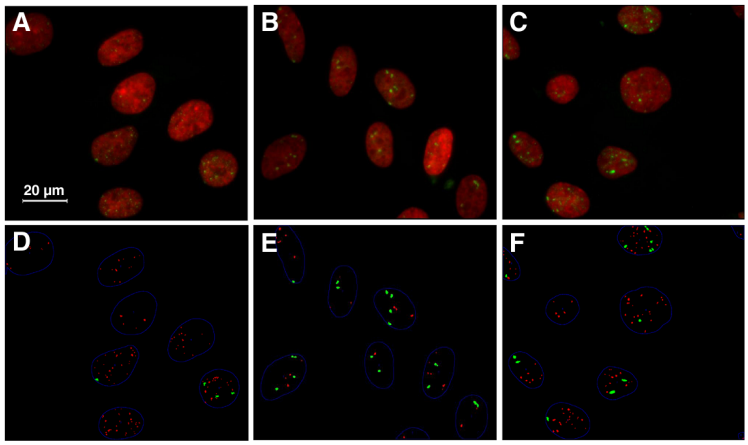

Figure 3.52: *Original fluorescence microscope images and program output images for γ-H2AX labelled VH10 cells irradiated with X-rays (A and D), alpha particles (B and E) and a mixture (C and F). Top row are original images and the bottom row program output. Red dots in the program output indicate small foci, green indicate large. From [163].*

posures. They exposed VH10 human fibroblast cells to 190kV X-rays and ^{241}Am alpha particles, with an LET entering the cell layer ranging from 100 keVμm to 172 keVμm. Doses used were 0.13, 0.27 and 0.32 Gy alpha particles, 0.20, 0.40 and 0.80 Gy X rays and 0.27, 0.53 and 0.80 Gy mixed beams, with 25% of the dose contributed by alpha particles. The alpha irradiation was delivered perpendicularly to the cell layer so, after staining, alpha particle cell traversals were visible as single large gamma-H2A X Ionising Radiation Induced Foci (IRIF). Small individual IRIF's were not distinguishable within the track. Previous results using 3D analysis of carbon ion tracks found approximately 15 IRIF's within each of these large foci. Therefore, to avoid under-counting IRIF's and facilitate analysis, IRIF's within their results were classified automatically in software into small foci (SF) or large foci (LF) groups, depending on area. Numbers of large foci were well matched to number of cell traversals, calculated from fluence and cell area, indicating that each LF in the alpha case corresponded to a single alpha track. Sample images, along with classification program output can be seen in figure 3.52.

In analysis of their mixed field data Staaf *et al*'s [163] most significant findings were related to repair kinetics. They found that, for large foci, significant differences between experimental responses to the mixed field and predictions from single field data were observed.

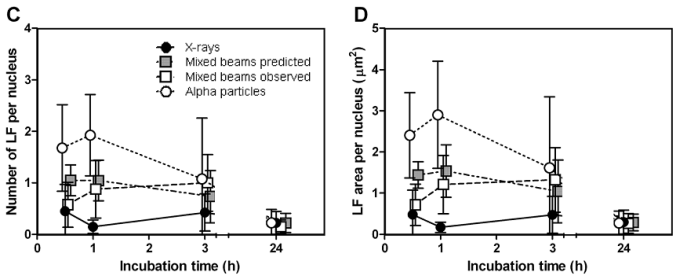

Figure 3.53: *Dose response and repair kinetics for summarised gamma-H2AX foci number and total area per nucleus for VH10 cells. Cells were exposed to 0.27 Gy alpha particles, 0.8 Gy X-rays and 0.13 + 0.40 Gy mixed beams of alpha particles and X-rays. Taken from [163].*

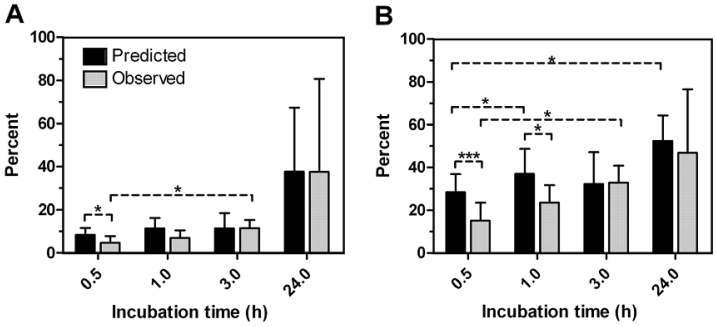

Figure 3.54: *Dose response and repair kinetics for summarised gamma-H2AX foci number and total area per nucleus for VH10 cells. Large gamma-H2AX foci data replotted as a percentage of total gamma-H2AX foci. Cells were exposed to 0.13 +0.40 Gy mixed beams of alpha particles and X-rays. * = significant, p≤0.05. *** = significant, p≤0.001. Taken from [163].*

The frequency and area of large foci were initially lower than predicted and increased during the first 3 hours of repair, at variance with predictions. Response had returned to expected levels after 24 hours. This data can be seen in figure 3.53. The same data is replotted, with number of large foci as a percentage of total IRIF, in figure 3.54.

It was concluded that the repair kinetics of large foci, indicative of complex damage sites, in cells irradiated with a mixed beam of alpha particles and X-rays was significantly different from predictions based on the effect of the single dose components. The initial phosphorylation of the damage, indicated by area of visible foci, along particle tracks was slower than expected. This was taken as an indication that the presence of low LET damage delayed the DNA damage response to high LET damage.

These results are interesting and seem to confirm that the mechanism of synergy is related to interference in the repair of DSB's. This is the first study directly investigating DNA

damage and repair after mixed beam exposure so it is likely that, in the coming years, similar DNA damage assay studies will provide a wealth of useful data to help fully understand the synergistic interaction.

3.10 Summary

It is clear that, in some dose regimes, damage from high and low LET radiation does interact in a way that produces higher levels of biological effect than might be expected from single field exposures. The mechanism of interaction is less clear. When considering the data presented by McNally *et al* [1] and that which is presented in this report, it appears that the level of synergistic effect is very sensitive to the experimental conditions.

To fully explore the mechanism which leads to increased cell kill in mixed field exposures more data are required. As the work of Staaf *et al* [163] seems to indicate that the synergy mechanism changes the repair response, further repair related investigations would seem to be warranted. An experiment, such as that carried out by Nandanuri *et al*[85] with photons, where cell repair is effectively stopped at different time points after irradiation could yield valuable information about the synergistic effect. Experiments with wider spreads of dose rate, in both radiation qualities, may also yield interesting results. Development of the irradiation rig described in section 3.2 is underway to allow for incubation of cells *in situ*, allowing for the possibility of long exposure times. Similarly experiments such as those performed by Hill *et al*[84] with alpha particles, using cells with the same parent line but different repair deficiencies, would help shed light on which specific DNA repair mechanisms are involved.

Regardless of the physical basis of the synergy, use can still be made of models when considering the biological effect of doses from mixed high and low LET fields. The Zaider Rossi formulation is particularly useful as α/β ratios are widely available for many tissues of clinical interest. The Linear Quadratic equation is used in a similar manner, as the basis for determining the effect of elongation or fractionation of radiation therapy [164], despite debate over it's physical origins. Caution has to be exercised as, while the Zaider-Rossi model fits some data sets well, there is significant disagreement with other experimentally observed results. Again, further work is required to understand these findings.

More complex track structure models such as the Local Effect Model (LEM) are finding

use in treatment planning for carbon ion therapy. The current iteration (LEM III) has introduced DNA damage clustering to improve fitting to experimental data. It is possible that, in the future, similar computational models can be extended to include the synergistic effect.

Chapter 4

EPITHERMAL NEUTRON BEAMS

4.1 Neutron Dosimetry

4.2 General Methodology

Dosimetry in BNCT is not straight forward. There are four major contributions to dose in a BNCT treatment [165];

1. **Boron dose.** This is the dose arising from the $^{10}B(n,\alpha)^{7}Li$ reaction. The mean energy deposited is approximately 2.33 MeV. The 477 keV gamma ray produced by the de-excitation of the ^{7}Li in the majority of the reactions is not considered as part of the dose component.

2. **Photon dose.** The majority of the photon dose arises from the capture of thermal neutrons in tissue. The $^{1}H(n,\gamma)^{2}H$ reaction emits a 2.2 MeV gamma ray. Further contributions are from neutron capture in other materials and non-nuclear processes such as Compton scattering.

3. **Neutron dose.** Neutrons of epithermal or higher energies scattering from hydrogen, result in recoiling hydrogen nuclei. Energy from these 'recoil protons' and other neutron induced reactions which deposit their energy locally, such as the $^{12}C(n,\alpha)$ reaction, are included in this dose component.

4. **Nitrogen dose.** Thermal neutron capture in ^{14}N produces the $^{14}N(n,p)^{14}C$ reaction. Dose results from the energy deposited by the proton and the recoiling ^{14}C.

It is not possible to measure all of these dose components directly. The approach taken is to determine the thermal neutron flux experimentally and derive the other related and dependant doses from known factors and a computational model. Practically this generally involves irradiating a series of metal foils and measuring the resulting activity using a gamma ray detector. These are the most precise dosimetry measurements available in BNCT. Direct fast neutron and gamma ray doses are generally derived from measurements with the paired ionisation chamber technique. The results from this are subject to large uncertainties [166].

The interaction rate of a neutron with energy E with an atom is equal to the product of fluence rate $\phi(E)$ and cross-section $\sigma(E)$. The reaction rate per atom of such a process is this product integrated over the full energy range, as shown in equation 4.2.1.

$$R = \int \phi(E)\sigma(E)dE \tag{4.2.1}$$

Thermal fluence rate is defined as shown in equation 4.2.2, that is the neutron reaction rate that produces the reaction rate R when multiplied by the cross section for neutrons of speed 2200 m/s;

$$R = \phi_0\sigma_0 \tag{4.2.2}$$

The dosimetry used in this report used reaction rates induced in gold and manganese foils as a measurement technique. Dilute foils are used to minimise self-shielding effects. Reaction rates in these foils can be approximated as shown in equations 4.2.3 and 4.2.4 [165].

$$R_{Mn} = \phi_0\sigma_{0,Mn} + \phi_{epi}I_{Mn} \tag{4.2.3}$$

$$R_{Au} = \phi_0 \sigma_{0,Au} + \phi_{epi} I_{Au} \tag{4.2.4}$$

Where I is the resonance integral defined as shown in equation 4.2.5.

$$I = \int_{0.55eV}^{\infty} \frac{\sigma(E)}{E} dE \tag{4.2.5}$$

Solving equations 4.2.3 and 4.2.4 allows thermal and epithermal fluence rates to be calculated.

$$\phi_0 = \frac{I_{Au} R_{Mn} - I_{Mn} R_{Au}}{I_{Au} \phi_{0,Mn} - I_{Mn} \sigma_{0,Au}} \tag{4.2.6}$$

$$\phi_{epi} = \frac{\sigma_{0,Mn} R_{Au} - \sigma_{0,Au} R_{Mn}}{I_{Au} \sigma_{0,Mn} - I_{Mn} \sigma_{0,Au}} \tag{4.2.7}$$

When a complete simulation of fluence at different depths is available the above approximations do not need to be used. Instead measured values for reaction rate can be used to scale the theoretical fluences appropriately.

A secondary measure of thermal neutron fluence can be arrived at using the cadmium difference method as described in Rogus *et al* [167]. This involves exposing gold foils and gold foils with cadmium covers to separate the activation of gold induced by thermal and epithermal neutrons. The reaction rate of a gold detector with cadmium cover can be expressed as shown in equation 4.2.8. F_{Cd} is a correction factor for absorption of epithermal neutrons in cadmium, equal to 1 as a first approximation.

$$(R_{Au})_{Cd} = F_{Cd} \phi_{epi} I_{Au} \tag{4.2.8}$$

$$\phi_0 = [R_{Au} - (R_{Au})_{Cd})] \sigma_{0,Au}] \tag{4.2.9}$$

4.3 Dosimetry for this Report

All experimental and theoretical dosimetry was carried out by Zamir Ghani. A comprehensive description of the work undertaken can be found in his PhD thesis [168]. A summary is presented here.

4.3.1 Dosimetry in the Large Water Phantom

The majority of the neutron exposures described in this report were carried out in the 'Large water phantom' shown in figure 4.1. The beam enters the phantom through the area of reduced thickness Perspex which is slightly larger than the area of the beam port.

To derive the doses used in the cell survival experiments, using the Birmingham dynamitron, which are described in this report a Monte Carlo N Particle (MCNP) model was used. This model incorporated the geometry of the target and its surroundings including the beam moderator and the water phantom; see figure 4.2. The initial neutron spectra produced in the lithium target was represented by a source definition originally produced by Z. Ghani[169]. Fluence at a number of depths in the water phantom was tallied. This fluence was then converted to dose using the energy dependant kerma factors published by Goorley *et al* [170].

To provide empirical scaling factors pairs of dilute (1% by weight, in aluminium) manganese and gold foils were fixed at a range of depths within the same water phantom being used for the cell measurements. A perspex jig ensured repeatability of positioning within ±1mm. This assembly was then irradiated using the dynamitron beam.

Post irradiation activity in the foils was measured using a high purity germanium detector (HPGe). Photo peak efficiency of the detector was calculated by measuring efficiency for a set of calibration sources, of known activity, and interpolating to give the efficiency at the energy of the characteristic gold and manganese photo peaks. These are 411 keV and 847 keV respectively. Measured gold and manganese activities were then used to calculate

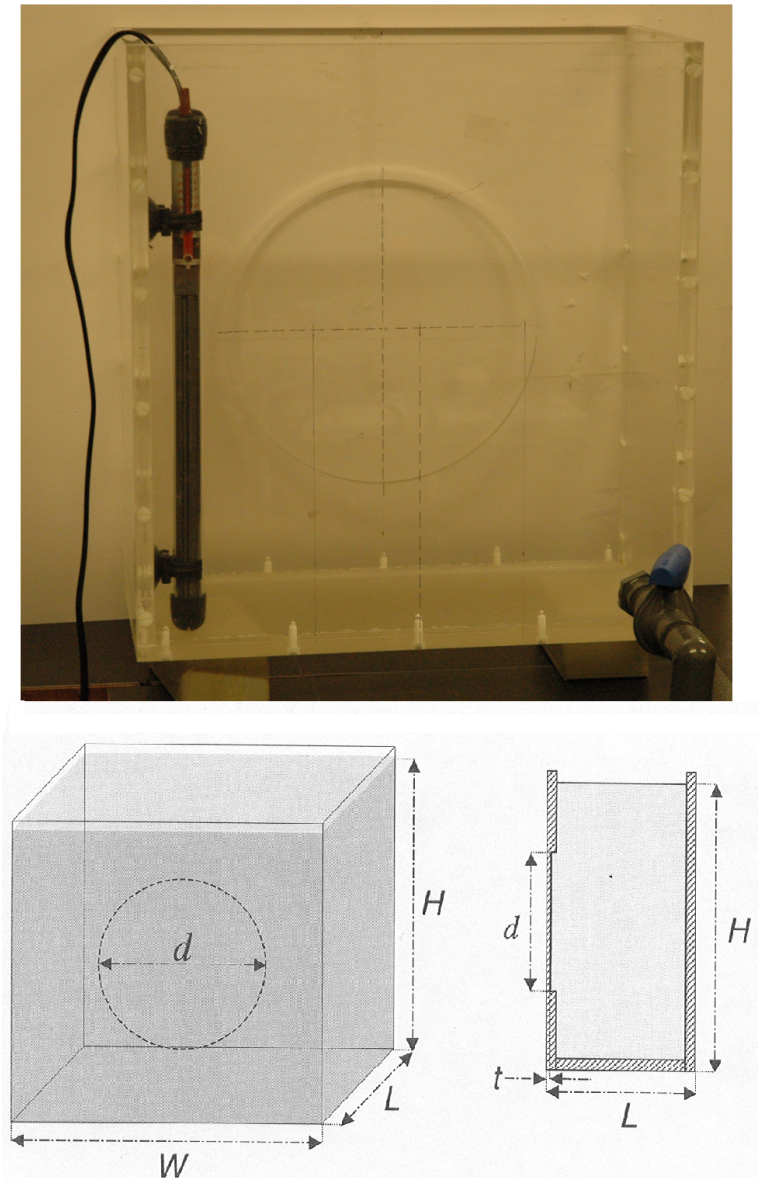

Figure 4.1: *Large water phantom. 40 cm × 43 cm × 20cm (W×H×L). D=15cm with a thickness of 5mm*

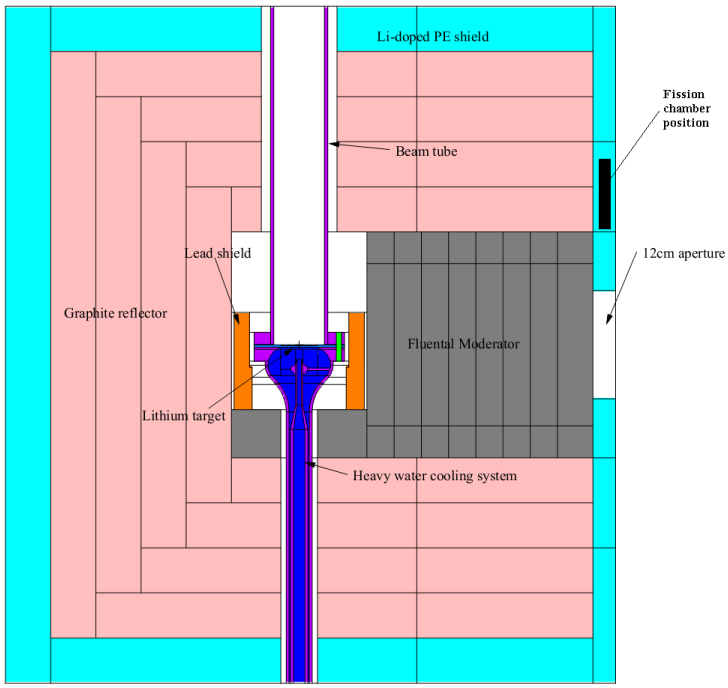

Figure 4.2: *Output of MCNP file geometry used for dose calculations with the Birmingham BNCT beam.*

^{14}N reaction rates using the approach developed by Freudenreich [171] and described in 'Recommendations for the Dosimetry of Boron Neutron Capture Therapy (BNCT)' [165];

$$R(^{14}N) = [-6 \times 10^{-4} \times \frac{R(Au)}{R(Mn)} + 0.141] \times R(Mn) \tag{4.3.1}$$

Dose rate values, at 935 μA, derived from foil measurements for a nitrogen fraction of 1.1% are shown in table 4.1. Uncertainties in the calculated reaction rates derive from uncertainties in the gamma ray counts, taken as $\sqrt{N}$ where N is the total number of counts and from uncertainties in the efficiency calculation. A long enough counting time was used in each case to reduce this error to 5% of the total. Uncertainties in the dose rate were calculated from these values. A comparison between the MCNP simulated thermal dose and the measured values at the same beam current is shown in figure 4.3. The simulated dose has been scaled by a factor of 0.4 but the shape of the curve is in good agreement.

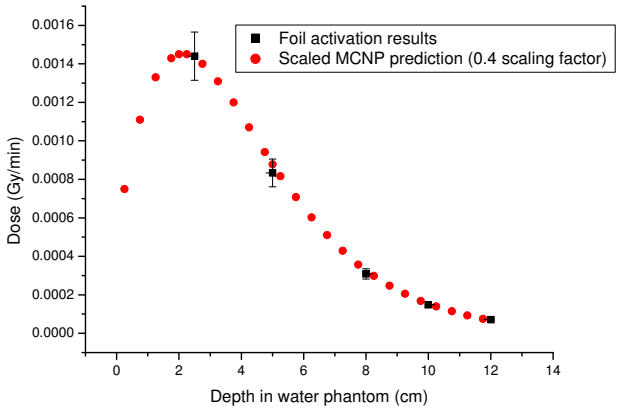

Figure 4.3: *^{14}N depth dose curve for thermal neutrons in the Birmingham dynamitron BNCT beam. Dilute foil activation measurements compared to MNCP simulation. Simulated results have been scaled by a factor of 0.4*

Practically, dose rates for cell irradiations in both beams are scaled to a reference neutron count rate rather than time. At Birmingham this is provided by a U235 fission chamber located in the front of the dynamitron beam shaping assembly. This is chosen as scaling reference for several reasons. Firstly dynamitron proton current is not reliably reproducible and secondly target neutron yield, the number of neutrons produced per incident proton, can vary between exposures. Using a neutron count reference as opposed to absolute time avoids any uncertainties introduced by these factors. Similarly dose rates at MIT were scaled to one of the FCB's monitoring fission counters. A dose per monitor unit value is therefore arrived at and multiplied by the recorded monitoring units during the cell radiation exposures.

The MCNP simulation is based on the theoretical yield for the Li(p,n) reaction for a given proton current. The size of the scaling factor to experimental values is determined by a number of factors which modify this yield. The target itself consists of a 40 mm diameter lithium disk on a copper backing. Proton current onto this target is measured by a Keithley electrometer. It was originally envisioned that collimation would constrain the proton beam to the lithium region and that all current measured would therefore represent protons impacting the lithium. This has proved not to be the case and often a significant portion of

Depth in phantom (cm)	RR(Mn) /atom	RR(Au) /atom	R(^{14}N)	Kerma	Dose - Gy/min	Uncertainty in dose - Gy/min
2.5	1.90E-15	1.98E-14	2.56E-16	2.40E-05	1.44E-03	1.25E-04
5	1.09E-15	9.38E-15	1.48E-16	1.39E-05	8.33E-04	7.21E-05
8	4.04E-16	3.16E-15	5.51E-17	5.16E-06	3.09E-04	2.68E-05
10	1.93E-16	1.44E-15	2.63E-17	2.46E-06	1.48E-04	1.28E-05
12	9.24E-17	6.83E-16	1.26E-17	1.18E-06	7.09E-05	6.14E-06

Table 4.1: *Dose rate values in the Birmingham BNCT beam, at 935 μA proton current, derived from foil measurements for a nitrogen fraction of 2.2%*

the proton current is wasted on bare copper regions. This was readily observable on a target removed from the machine. Tests comparing an unrastered beam at low beam currents showed that yields of $\sim$ 0.07 fission neutron counts per recorded proton were achievable compared to typical values of $\sim$0.04 for high current, rastered beams. Deterioration of the lithium target layer is another factor which may account for lower observed experimental neutron doses. Visual inspection of used targets suggests that this is a small factor with little observable degradation.

A further independent check of the Birmingham dosimetry has been provided by direct measurement of the gamma dose component using a Magnesium-Argon ionisation chamber. This was carried out as a summer project by Turki Alzahrani assisted by Zamir Ghani, Cecile Wojnecki and the author. Full details are available in Turki Alzahranis's MSc thesis [172]. Results are shown in figure 4.4 compared to the scaled MCNP predicted values. The scaling factor was somewhat different in this case as these measurements were carried out after some changes had been made to beam alignment, with a new target. As with the foil irradiation work there is good agreement between the shape of the experimental gamma depth dose curve and the MCNP prediction.

The source definition and precise MCNP geometry input deck were unavailable for the MIT Fission Converter Beam. Instead published results for were used for comparison with experimental measurements carried out in conjunction will cell measurements. The values used were presented by Riley *et al* in reference [173]. The same foil irradiation protocol was followed as in the Birmingham BNCT beam. Results of the comparison, for an assumed nitrogen content of 3.4%, are shown in figure 4.5. This value for nitrogen content, equivalent to muscle [174], was used to match the published MIT calculations. The foil, and cell, irradiations used for dosimetry in this report were carried out at 3.5 MWt. This is due to the fact that the irradiations were carried out in the summer, with high ambient temperatures, and the reactor power was limited by the capacity of its heat exchangers. Two scaling methods for the 5 MWt reference doses are shown. One was scaled by a simple $\frac{3.5}{5}$ factor.

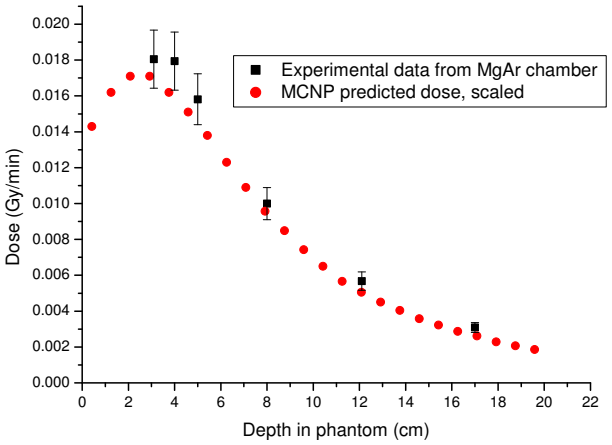

Figure 4.4: *Comparison of gamma ray measurements using a MgAr ionisation chamber with MCNP predicted values in the BIrmingham BNCT beam. MCNP results are scaled by a factor of 0.68*

The other is scaled by comparing the monitoring fission chamber counts in the two cases. The differences can be explained by several factors. The MIT reactor was refuelled, increasing fluxes by 20%, and the FCB beam line was extended by ∼1cm to allow fitment of an optional Lithium filter [175]. The additional flux from new fuel would be observable in the fission monitoring chambers but the reduction in flux at the beam port, from the increased distance from the source, would not.

A comparison between doses measured independently by the cadmium difference foil activation method and the Freudenreich method [171] are shown in figure 4.6. The dose rates measured by the two methodologies agree within 5% at all depths. Details of the Freudenreich method are provided in the previous section (page 116 onwards). The cadmium difference method relies on measuring neutron activation in gold foils with and without cadmium shields. The cadmium absorbs neutrons below about 0.5 eV, the two data sets therefore allow thermal neutron activation to be distinguished from activation by higher energies.

The beam from the FCB was used at two dose rates for cell irradiations. This was not

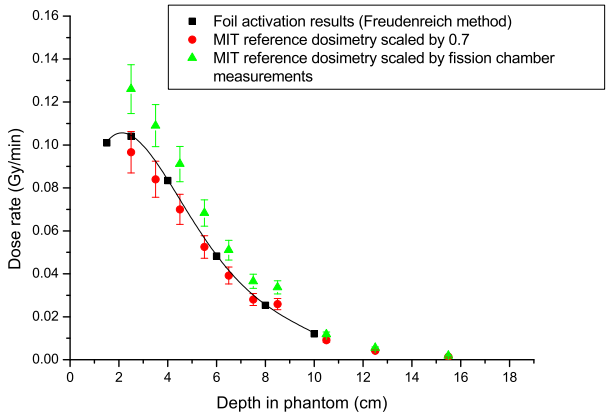

Figure 4.5: *^{14}N depth dose curve for thermal neutrons in the MIT FCB. Dilute foil activation measurements compared to historical MIT measurements. Historical measurements are scaled to account for differing reactor power levels*

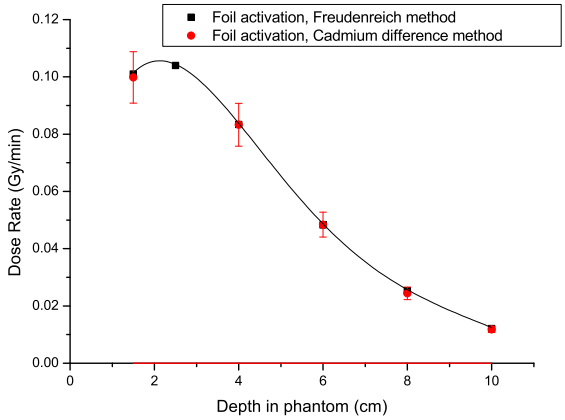

Figure 4.6: *Comparison between ^{14}N depth dose curves measured by two different foil activation methodologies in the MIT FCB beam*

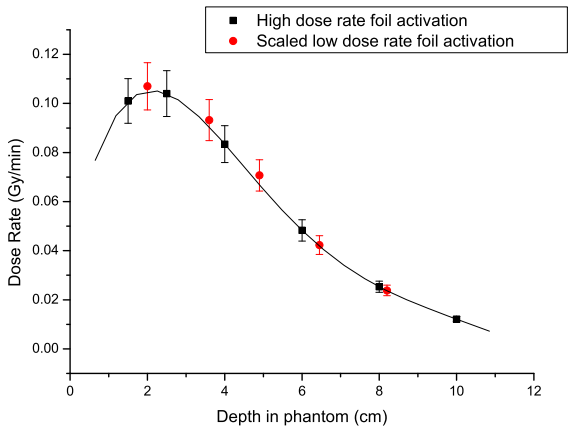

Figure 4.7: *Comparison between ^{14}N depth dose curves measured at two dose rates in the MIT FCB beam. Doses were measured by the Freudenreich method of foil activation. Low dose rate data scaled by a factor of 13.44*

expected to change the ratio of dose components. This was due to the fact that apparent power of the FCB was controlled via the position of a shutter rather than by directly varying the reactor power. The equivalence of the thermal dose was checked with a further foil activation experiment using the Freudenreich method [171]. A comparison between the low and high dose exposures is shown in figure 4.7. The low dose rate activities were scaled up by a factor of 13.44, calculated from the ratio of the fission chamber monitoring counts recorded for each case. There was excellent agreement between the two experimental data sets.

Some further correction factors in the calculated dose values to cells were required. All doses considered so far were calculated and measured by foils at the centre point of the beam output port. The beam profile at both Birmingham and MIT is not flat across the port and reduces towards the periphery; see figure 4.8 for an illustration of the effect. With 50 mm width cell growth flasks and a 1 2cm beam aperture the non-uniformity is not negligible. In addition, when considering cells irradiated in flasks, the effect of the boronated cell medium on the neutron flux has to be considered. For the Birmingham beam a modified MCNP file including the flask geometry was constructed to quantify these effects. The resulting scaling

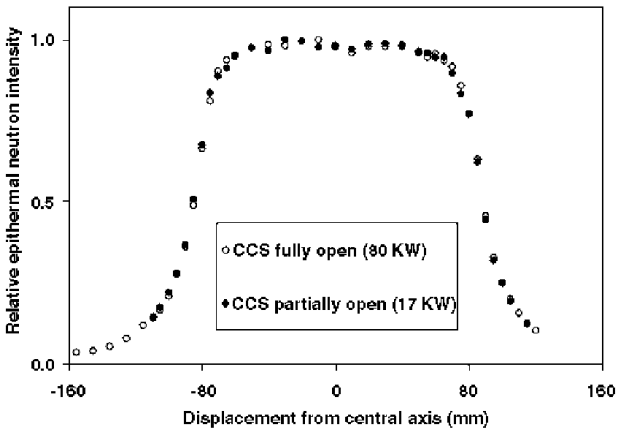

Figure 4.8: *Collimator cross-plane profile measured for the MIT FCB using a small volume fission counter in air. Power levels refer to FCB power; 80kW is equivalent to a reactor power of 4.8MWt. Data is normalised to 1 at maximum observed intensity in each case. Taken from reference [173].*

factors can be seen in table 4.2. In the case of MIT a correction factor for the beam non uniformity was calculated using the off axis foil activation measurements presented in [173]. Boron perturbation factors were assumed to be the same as in the Birmingham beam.

To derive total doses to cells levels of various neutron capture agents need to be known in order to scale the thermal neutron dose. In cell culture experiments there is some uncertainty in the nitrogen, $^{14}N(n,p)^{14}C$, contribution. In brain the nitrogen content is well established at 2.2% [174] . The value for cell lines is less well known. Gabel *et al* [3] established the nitrogen content of V79 cells as 1.7% by weight. DMEM cell culture medium is approximately 0.9% by weight without additives. The nitrogen content of FBS is unknown and is likely to vary between batches. There is a further complication in that the range of the released proton, which delivers the majority of the dose, is 12.8 μm or of the order of one cell diameter in water. This means that the dose to a cell is due both to the nitrogen inside and in the medium surrounding it. As the nitrogen content of these two regions is not the same, charged particle equilibrium can not be assumed and accurate determination of the dose would require a complex microdosimetry calculation. Following the approach of Mason [73] Gabel *et al*'s [92] value of 1.7% by weight for V79's was used and an average

Dose component	Boron capture (50ppm ^{10}B)	rel. uncert.	Thermal neutron	rel. uncert.	Fast neutron	rel. uncert.	Photon	rel. uncert.
Flask with 50ppm boron, 2cm depth	1.95E-17	6.00E-04	3.97E-17	6.00E-04	1.26E-17	1.90E-03	3.32E-16	6.00E-04
Flask with no boron, 2cm depth	2.08E-17	6.00E-04	4.25E-17	6.00E-04	1.33E-17	1.80E-03	3.12E-16	6.00E-04
Ratio	**1.07**		**1.07**		**1.06**		**0.94**	
flaska 5cm	1.02E-17	8.00E-04	2.11E-17	8.00E-04	1.11E-18	5.90E-03	2.62E-16	6.00E-04
flaskn 5cm	1.17E-17	7.00E-04	2.42E-17	7.00E-04	1.24E-18	5.60E-03	2.54E-16	6.00E-04
Ratio	**1.15**		**1.15**		**1.12**		**0.97**	

Table 4.2: *Correction factors due to the presence of boron in cell medium and non uniformity of the neutron beam for Birmingham and MIT's BNCT beams*

nitrogen content overall of 1.1% was used for dosimetry purposes.

As identical cells were handled similarly at both MIT and Birmingham an exact nitrogen concentration is not necessarily required for a comparison provided that the same assumed concentration and methodology is used for both beams. In any case, for cells loaded with 50 ppm ^{10}B, the nitrogen dose is a small contribution to the total at the depths considered. It is calculated, via the scaled MCNP results, to be less than 3% in all cases.

Typical dose rates per second for each dose component, calculated from scaled MCNP simulations, in both epithermal beams are shown in table 4.3.

Dose per Monitor Unit (Gy)					
	Boron (50ppm)	Thermal neutron (1%N)	Fast neutron	Photon	Total Physical Dose
Birmingham, 20mm depth	1.95E-07	3.62E-09	3.06E-09	5.72E-08	2.59E-07
Birmingham, 50mm depth	1.17E-07	4.82E-09	2.63E-10	4.81E-08	1.70E-07
MIT, 20mm depth	1.63E-05	2.96E-07	3.31E-07	4.27E-06	2.12E-05
MIT, 50mm depth	9.91E-06	1.80E-07	9.31E-08	3.58E-06	1.38E-05
Dose as a percentage of total dose					
Birmingham, 20mm depth	75.36%	1.40%	1.18%	22.06%	100.00%
Birmingham, 50mm depth	68.70%	2.84%	0.15%	28.30%	100.00%
MIT, 20mm depth	76.91%	1.40%	1.56%	20.13%	100.00%
MIT, 50mm depth	71.99%	1.31%	0.68%	26.03%	100.00%

Table 4.3: *Dose conversion factors for Birmingham and MIT's BNCT beams in the full scatter water phantom.*

4.3.2 Monolayer Correction Factors

A further correction factor is required due to irradiating the cells while they are attached to a surface. As this surface does not contain boron the dose from boron capture reactions is reduced, something which is not accounted for in a simple fluence to boron dose calculation. Cells in suspension also adopt a different shape from cells attached to a surface, with markedly different nuclear areas and thicknesses for ions to traverse.

Experimental and theoretical work in this area has been carried out by Charlton *et al* [176]. In their paper they present survival data for V79 cells in both attachment and suspension surrounded by growth medium containing an alpha emitter (^{212}Bi) in varying concentrations. This data is replotted in figure 4.9. A model for calculating cell survival, from previously obtained D_0, values is also presented in the paper.

The Charlton *et al* model [176] relies on a Monte Carlo simulation of alpha particle traversals of the nucleus to determine a distribution of doses delivered and corresponding LET's. A look up table of D_0 vs LET constructed from historic V79 alpha particle experimental data is then used to determine expected survival.

A similar Monte Carlo model has been implemented in MatLab, by Zamir Ghani, for boron neutron capture events. Cell size and nuclear area distributions, as shown in figure 4.10, were taken from the work of Hill *et al* [84]. For these simulations the distributions were randomly sampled via a table lookup method. Again based on the work of Hill *et al*, cell nuclei were taken to have a mean nuclear thickness to cell thickness ration of 0.8; a typical cell cross section is shown in 4.11.

The Boron capture cross-section is peaked at a very low neutron energy (less than 0.5eV[5]). This means that the initial neutron energy contributes little to the final energy of the reaction products, which carry a combined kinetic energy of 2.79 MeV or 2.31 MeV depending on decay mode. This means that, to simplify the calculation, both particles can be assumed to be emitted 'back to back' and the resulting pair of ion tracks treated as a single track with varying LET along it's length. This is illustrated in figure 4.12 where

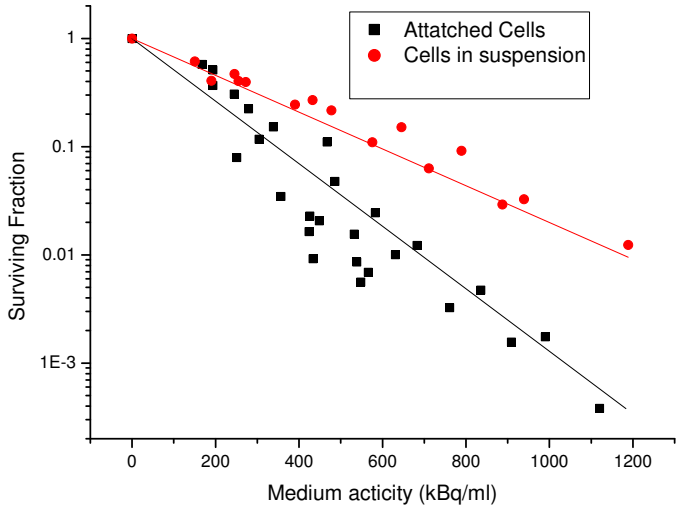

Figure 4.9: *Comparison of cell survival for cells in attachment and suspension in medium containing ^{212}Bi. Data replotted from values in [176]. Fit lines are exponential fits taken from the paper.*

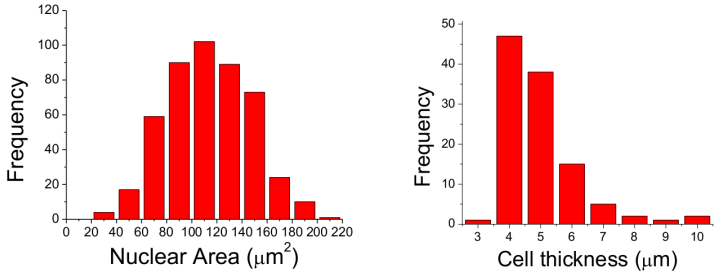

Figure 4.10: *Cell area and thickness distributions for attached V79 cells obtained from confocal microscope images. From reference [84]*

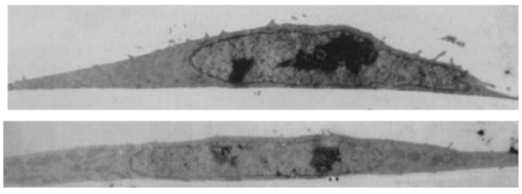

Figure 4.11: *Electron Microscope image of a sectioned V79 cell from [84]*

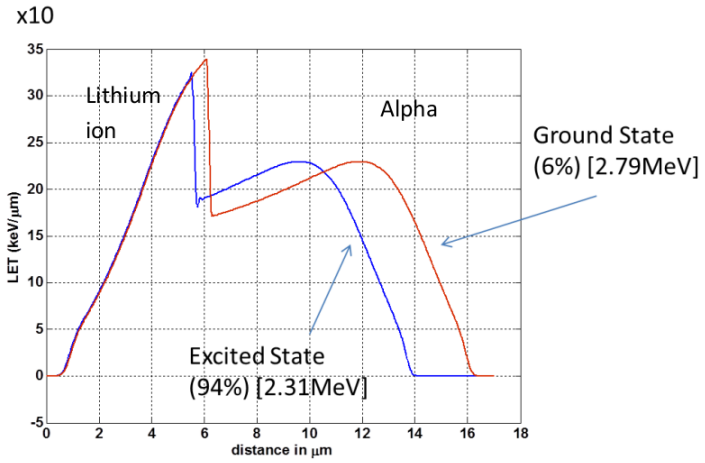

Figure 4.12: *Back to back particle LET as a function of distance from the boron capture event. Taken from [168].*

tracks of the individual ions have been simulated in TRIM then combined.

To perform dose calculations, random populations of ion tracks are created. Each of these ion tracks is checked for intersection with simulated cells. The chord length of these intersections, across the cell nucleus, is calculated. An integral lookup up function is then used to obtain a value for energy deposited in the cell traversal. The lookup function consists of the integral of the LET/stopping power distribution of the two particles over their combined range. The difference between the entrance and exit 'lookup' is equal to the energy deposited in the cell.

Example results of a simulation comparing absorbed doses in a suspended cell to doses in one attached to a non-boron containing boundary can be seen in 4.13. The boundary was defined such that the cell nucleus sat with it's surface 10% of the total cell height away from the boundary (approximately 0.3 μm). The results can be seen converging on a stable solution as the number of particle histories increases. By comparing the ratio of absorbed doses with cells attached to a surface and one with cells in suspension a scaling factor for the boron dose of 0.77 $\pm$ 0.05 was derived.

The quoted uncertainty was a statistical error calculated from the Monte Carlo simulation. Further detailed discussions of possible sources of error in these calculations, more

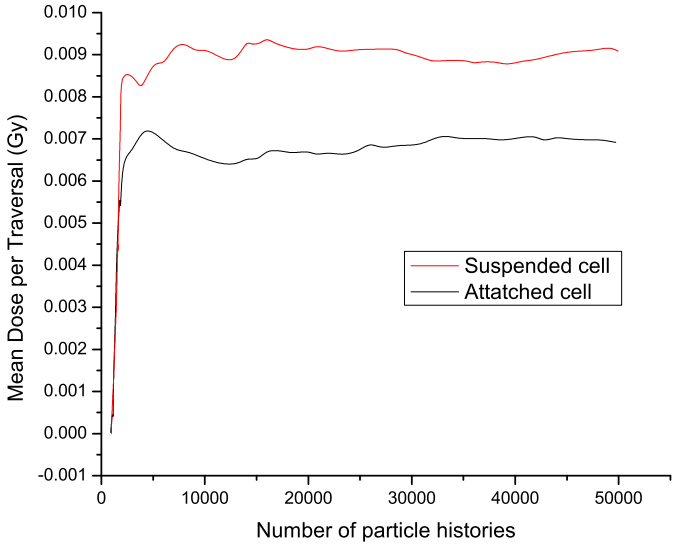

Figure 4.13: *Tally results for mean energy deposited per source particle in two different cell systems. Replotted from [168]*

details of the algorithms used and the results of extensive code validation tests can be found in Chapter 7 of Zamir Ghani's thesis [168].

Direct experimental investigations of these simulations can be found in section 4.7.1 on page 168.

4.3.3 Dosimetry in the 'Radiobiology Phantom'

All cell survival measurements carried out by Anna Mason took place in a non-standard water phantom [73]. Cell survival measurements for comparison against this work were carried out in the same phantom. Again, doses to cells were determined by scaling MCNP values to foil measurements. As irradiations were carried out in small vials, on-axis, no off-axis or perturbation corrections were used. Conversion factors are shown in 4.4.

Dose per Monitor Unit					
Depth in Phantom	Boron (50ppm)	Thermal neutron (1% N)	Fast neutron	Photon	Total Physical Dose (Gy)
20mm	8.62E-08	3.52E-09	1.11E-09	2.18E-08	1.13E-07
30mm	7.70E-08	3.16E-09	4.99E-10	2.04E-08	1.01E-07
50mm	4.78E-08	1.97E-09	8.31E-11	1.67E-08	6.65E-08
Dose as a percentage of total dose					
20mm	76.57%	3.13%	0.99%	19.32%	100.00%
30mm	76.19%	3.13%	0.49%	20.19%	100.00%
50mm	71.83%	2.97%	0.12%	25.07%	100.00%

Table 4.4: *Dose conversion factors for Birmingham's BNCT beam using the RadB phantom*

Figure 4.14: *Birmingham's Radiobiology phantom*

4.4 Initial Cell Survival Experiments at Birmingham

Initial irradiations using the Birmingham dynamitron were an attempt to reproduce and expand on work by Anna Mason [73]. Irradiations were carried out inside the 'Radiobiology Phantom' which is unique to Birmingham; see figure 4.14 on page 137. This phantom has a central rod into which 1.5 ml vials can be inserted at fixed depths. This central rod is rotated via an electric motor, ensuring that cells in solution do not settle and receive an even dose. The phantom is water filled and has connections for an external circulating water bath, allowing temperature to be selected across a wide range.

Irradiation takes place through the end of the phantom with the beam orientated along the long axis. The lines visible in 4.14 are for aligning with the dynamitron beam port.

4.4.1 Comparison With Historic Data

Following the technique described in Anna Mason's thesis [73], V79 cells were introduced into vials at a concentration of 5×10^5 cells per ml immediately prior to irradiations. They were then inserted into the RadB phantom. The cells were held at 4°C throughout the irradiations by chilling the water inside the phantom. Post-irradiation the cells were handled as described in the Cell Survival Studies section on page 30. Results for irradiations at the 3 depths within the phantom are shown in figures 4.15, 4.16 and 4.17. The two data sets are in good agreement, within experimental uncertainties.

In order for dose rate effects to be seen clearly, it was desirable for irradiations to take place at 37 °C to allow for cell repair during the course of the irradiation. There were concerns that this would require modification of the irradiation technique. At 4 °C there is very little, or no, cell proliferation but this is clearly not the case at 37 °C. To address concerns that this may cause problems with cells in suspension at high concentrations, a survival study with unirradiated cells plated out at different time intervals was carried out. This data is presented in figure 4.18.

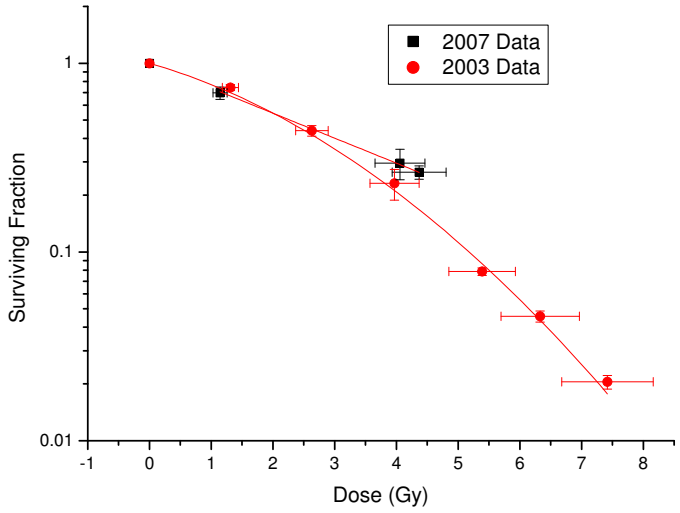

Figure 4.15: *V79 cell survival at 4° C, 20 mm depth in the RadB phantom. 2003 data from [73]. Fitted with the linear quadratic function; values of alpha and beta can be found in table 4.5.*

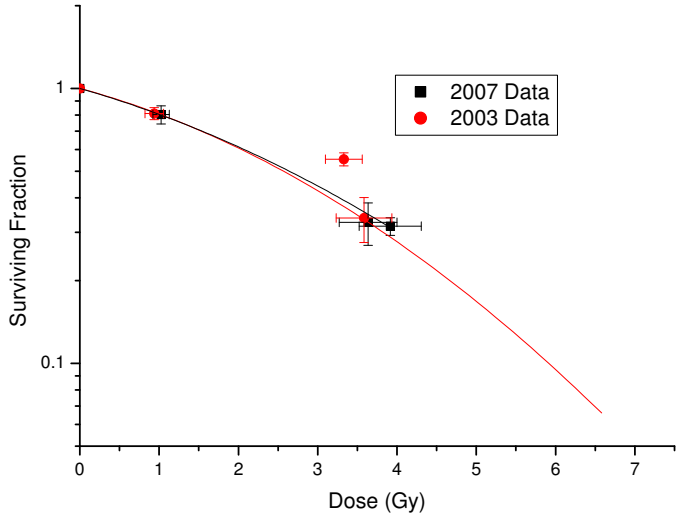

Figure 4.16: *V79 cell survival at 4° C, 35 mm depth in the RadB phantom. 2003 data from [73]. Fitted with the linear quadratic function; values of alpha and beta can be found in table 4.5.*

It is clear that high concentrations of cells left for long time periods in the irradiation vials have their survival adversely affected. This is likely due to the cells inability to regulate the pH of their surroundings and depletion of various vital survival elements within the media.

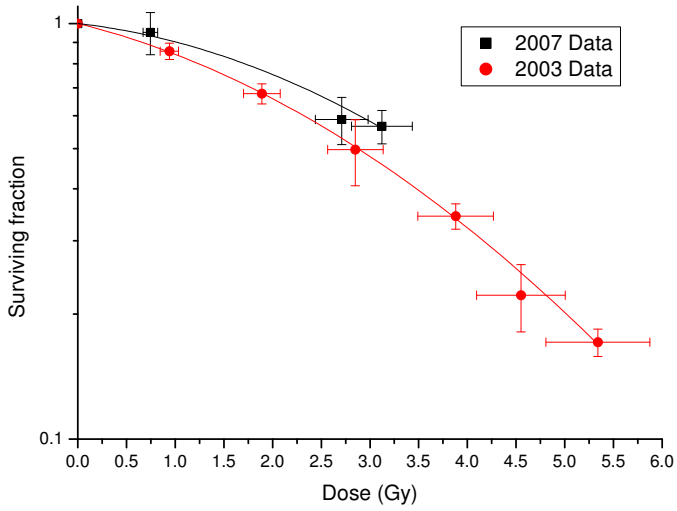

Figure 4.17: *V79 cell survival at 4° C, 50 mm depth in the RadB phantom. 2003 data from [73]. Fitted with the linear quadratic function; values of alpha and beta can be found in table 4.5.*

	Alpha (Gy^{-1})	**Beta (Gy^{-2}**
2007 data (this report)		
20mm	0.3046 ± 0.0169	-
35mm	0.1898 ± 0.09	0.0275 ± 0.0230
50mm	0.0624 ± 0.093	0.3951 ± 0.0306
2005 data from [73]		
20mm	0.1810 ± 0.0278	0.0517 ± 0.0052
35mm	0.1782 ± 0.0275	0.03571 ± 0.0051
50mm	0.1335 ± 0.0334	0.0374 ± 0.0075

Table 4.5: *Fitted values in the linear quadratic function for figures 4.15, 4.16 and 4.17. Data fitted is for V79 cells, irradiated at 4 ℃, in the 'RadB' phantom using the Birmingham BNCT beam*

With this in mind it was decided that any irradiations at 37 °C in this system should be at a maximum cell concentration of 1×10^5 cells per ml and limited to less than 5 hours duration.

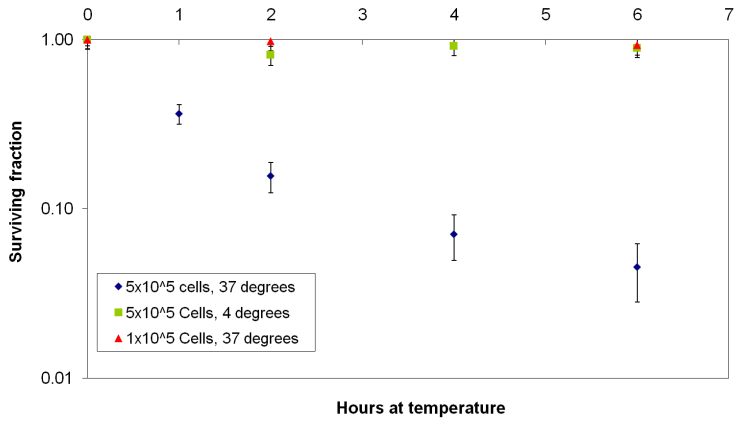

Figure 4.18: *Survival over time of cells held in suspension in 1.5ml vials. Cells held in normal growth medium*

4.4.2 New Irradiation Phantom Design

It was evident that the previously described Radiobiology Phantom (RadB) had a number of flaws. The limit on cell concentration with the phantom at 37° C, as discussed in the previous section, imposed a limit on the lowest realistic survival levels which could be investigated. There is also a significant dose uncertainty, linked to the position uncertainty of the cells. This arose both due to the movement of the cells in suspension, across a 5mm diameter vial, and poor tolerances in the rod holding the vials. As can be seen in figure 4.19 relatively small changes in cell position can lead to large changes in flux and consequently dose.

In addition to the intrinsic dose uncertainty it introduces, the RadB phantom had a number of other practical experimental issues. Changeover of cell vials between irradiation runs was time consuming as it required removal of the bolted on phantom end cap. Inadvertant damage to, or contamination of, the cell vials was common during changeover due to the design of the rod retaining them. The phantom was also unique to the Birmingham facility. With these flaws in mind, and the desire to create a simple biological protocol for the inter-comparison of BNCT facilities, a new cell irradiation set up was designed and constructed. Rather than a specialised, unique, phantom it was decided that the more standard large water phantom should be utilised. As pictured in figure 4.1, on page 120, this phantom is a

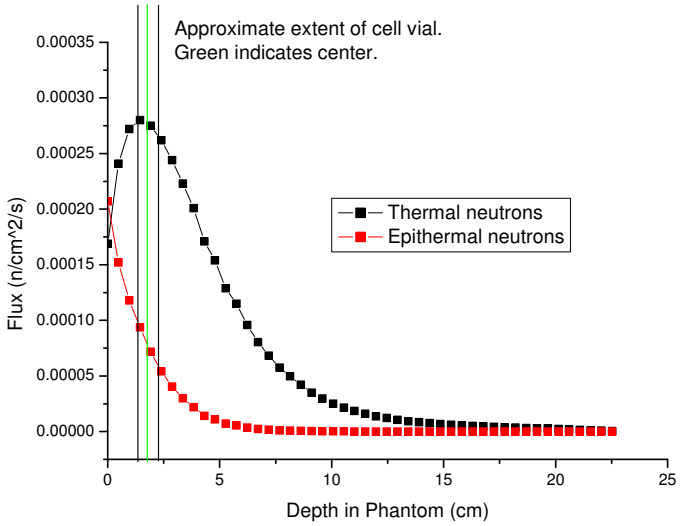

Figure 4.19: *Thermal and epithermal neutron flux variation with dose in the RadB phantom [169]*

large rectangular box constructed of 12 mm perspex, with a thin 5mm thick front window which matches up with the beam port. This is the phantom design specified in the Petten dosimetry methods report, followed by many BNCT centres worldwide[165]. It is therefore likely that most, if not all, BNCT facilities will posses a similar phantom used for beam dosimetry. Rather than irradiate in vials it was decided to use 25cm^2 culture flasks. These allowed for irradiation of a monolayer, not a suspension, and allowed a sufficient volume of medium for the cells to remain healthy over extended time periods. To hold the flasks in position in the phantom a perspex jig was constructed. This was designed to allow quick changeover of flasks between irradiations, allow for irradiation at any depth and to be easily replicable at any BNCT site. This jig is shown in figure 4.20. This design was proposed as a suitable design for use in biology intercomparions, by the author, at the 13^{th} International Congress On Neutron Capture Therapy in 2009.

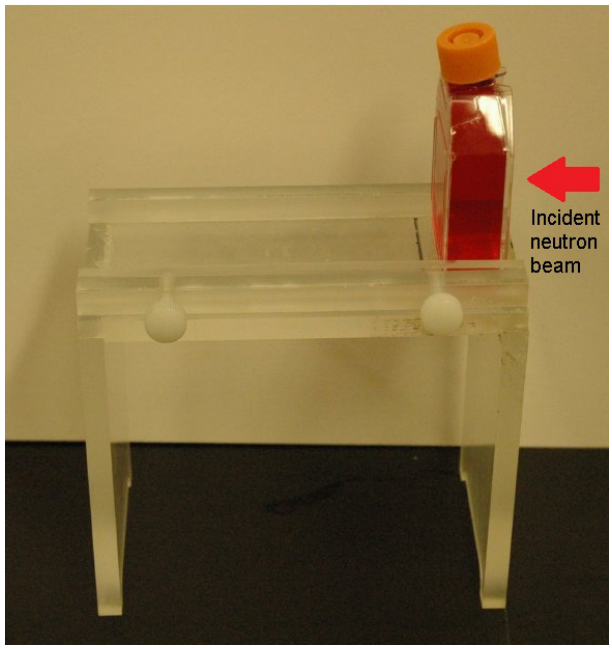

Figure 4.20: *Jig to hold flasks in position inside the large water phantom*

4.5 Biological Comparison of MIT and Birmingham Treatment Beams

4.5.1 Cell Preparation and Irradiation

The cell preparation prior to irradiation was identical at both sites. Stock V79 cells were thawed and cultured for a number of days. 48 hours prior to irradiation, 5 x 10^5 cells in 5 ml of medium were introduced into standard Corning T25 flasks. These were then cultured in a 5% CO_2, humid atmosphere at 37°C. 16 hours prior to irradiation the medium was removed and replaced with medium loaded with 50 ppm ^{10}B using enriched boric acid. Immediately prior to irradiation the flasks were completely filled with this boron loaded medium and the flask tops replaced with non-filter caps. Two controls for each day of experiments were used and treated identically to all other dose points. After irradiation the cells were incubated for 2 hours to allow for repair prior to processing. Flasks were irradiated at two distances from the beam port simultaneously using the jig shown in figure 4.20. The lowest depth was selected as it is close to the ideal peak clinical treatment depth. Originally it was intended that all irradiations would be carried out at 37°Cwith temperature in the phantom controlled by an aquarium heater linked to a digital temperature controller. Due to a failure of the original heating element, the water phantom irradiations were carried out at 34°C instead of 37°C. The effect on cell repair of this difference over the course of the irradiations is believed to be minor. Dose delivered was controlled on a time basis during irradiations and exact dose calculated later from recorded fission chamber counts.

4.6 Results of Biology Comparison

4.6.1 Birmingham

Results of irradiations using the epithermal beam from Birmingham's dynamitron accelerator are shown in figure 4.21. Each point represents a single evaluation, with mean survival calculated from 5 Petri dishes. Evaluations from the same exposure plated at different densities are shown as separate points. Mean total physical dose rate, before off axis corrections, for these exposures was 0.042 Gy min^{-1} at 20 mm depth.

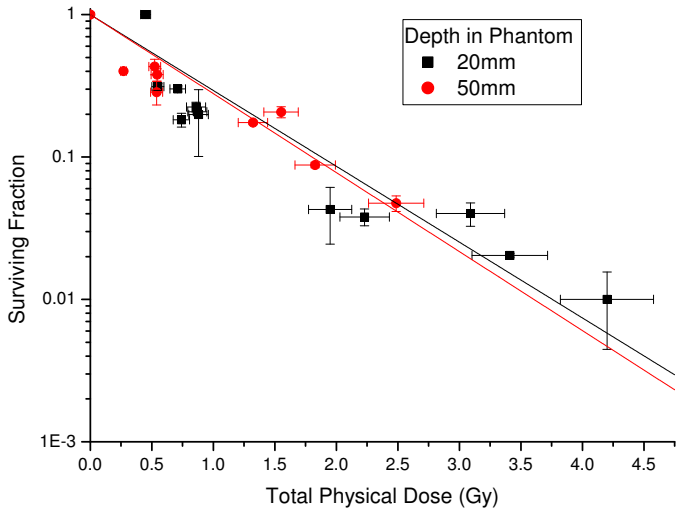

Figure 4.21: *V79 cell survival, in the large rectangular phantom, in Birmingham's epithermal beam. Cells loaded with 50 μg per g boric acid. Fit parameters can be found in table 4.6*

	20mm	50mm
Alpha (Gy^{-1})	1.226 $\pm$ 0.08	1.277 $\pm$ 0.10
Beta (Gy^{-2})	-	-

Table 4.6: *Fit parameters for figure 4.21. V79 survival, loaded with 50 ppm boron, irradiated in the Birmingham epithermal beam. Fitted with the linear quadratic function*

As might be expected from the similar dose component mixes at these depths the survival response is very similar at both 20 mm and 50 mm. Gabel *et al* [3] presented survival data

	Alpha (Gy^{-1})	Beta (Gy^{-2})
Boron capture	1.5 ± 0.15	-
Nitrogen capture	1.29 ± 0.23	-
Photon	0.2332 ± 0.004	0.018 ± 0.0008
Fast neutron	1.18 ± 0.2	-

Table 4.7: *Summary of constants used with equation 4.6.1 to produce predicted survival data for V79 cells in a BNCT beam. Taken from fits to data presented in references [3] and [34]*

for V79 cells exposed to various elements of a typical BNCT beam. This data, data from photon exposures presented in this report and fast neutron survival data from [34] was used to calculate expected survival using the following equation;

$$SF = e^{-(\alpha_p D_p + \beta_p D_p^2)} e^{-(\alpha_n D_n + \beta_n D_n^2)} e^{-(\alpha_t D_t + \beta_t D_t^2)} e^{-(\alpha_B D_B + \beta_B D_B^2)} \tag{4.6.1}$$

The subscripts refer to the various dose components. p is photon, n is fast neutron, t is thermal neutron (Nitrogen capture) and B is the dose from the boron capture reaction. The various constants used are summarised in table 4.7.

A comparison using this methodology is shown in figure 4.22. The survival predicted from Gabel *et al*'s work is an excellent match to the 20mm depth data, with the prediction overlaying the linear quadratic fit to the data. The predicted 50mm survival is somewhat higher than was observed experimentally.

When appropriate fractional doses, from table 4.3 on page 131, and fitted constants from table 4.7 are substituted into equation 4.6.1 it reduces to a linear-quadratic. Values of alpha and beta for this function are shown in table 4.8.

	Alpha (Gy^{-1})	Beta (Gy^{-2})
20mm	1.21452 $\pm$ 0.11	0.00026 $\pm$ 0.0002
50mm	1.13 $\pm$ 0.1	0.00246 $\pm$ 0.0003

Table 4.8: *Values of constants in the linear-quadractic function in mixed fields at two depths, in the large water phantom, in Birmingham's epithermal beam. Values and uncertainties calculated from the constants in table 4.7.*

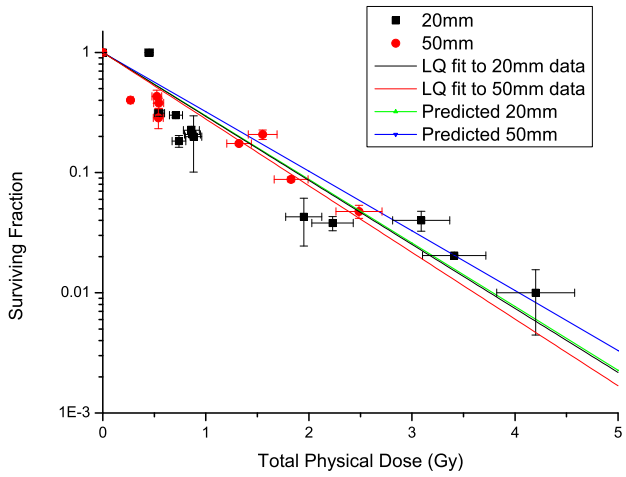

Figure 4.22: *V79 cell survival, in the large rectangular phantom, in Birmingham's epithermal beam. Cells loaded with 50μg per g boric acid. Experimental results compared with predictions from previously published RBE values. Constants used are shown in table 4.7*

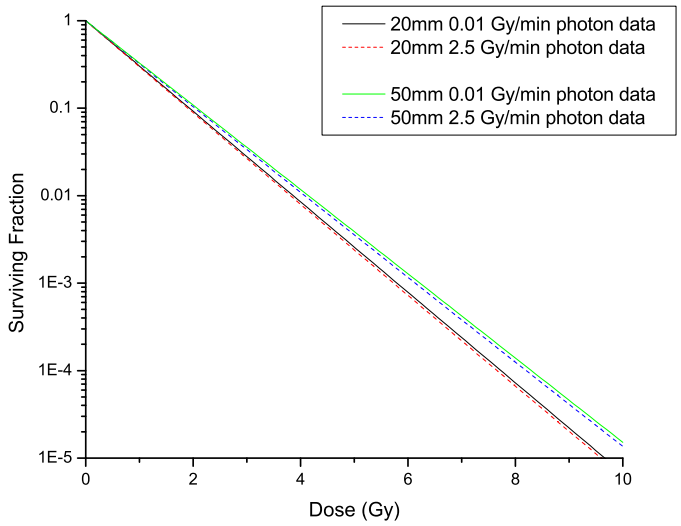

Figure 4.23: *Comparison of predicted cell kill in Birminghams epithermal beam, with differing fitted values for the photon component. Photon data taken from reference 2.6*

The constants for the photon component of the beam, in table 4.7, are taken from cobalt-60 exposures detailed earlier in this report (Chapter 3). These values are likely to be an overestimate of cell kill by the photons, as the dose rate the irradiation were delivered at was 1 Gy min^{-1} compared to approximately 0.01 Gy min^{-1} for the photon component in the epithermal beam. The result of using fit parameters from a lower photon dose rate to predict response is shown in figure 4.23. In this case the photon constants used were taken from an experiment which exposed V79 cells to 250 kV X-rays at 0.01 Gy min^{-1} [149]. Due to the small contribution to total cell kill from the photon component at this boron fraction, little difference is seen in overall predicted biological effect.

4.6.2 MIT

Results of irradiations using the MIT Fission Converter Beam at full output are shown in figure 4.24. Mean total dose rate, before off axis corrections, at 20 mm depth for these exposures was 1.788 Gy min^{-1}. Exposures using the MIT FCB at reduced dose rate, of 0.135 Gy min^{-1} at 20 mm, are shown in figure 4.25.

It is clear that the survival levels are much higher than would be expected for the stated doses, with RBE's of less than 1 when compared to 250 kV X-rays. This is illustrated in figure 4.26 where the fitted lines from figures 4.24 and 4.25 are plotted alongside 250 kV X-ray survival data. The 50 mm high dose rate data shows the lowest survival of the groups studied; RBE's for this data are shown in table 4.10. This response suggests a large systematic error in either the stated doses or the levels of cell survival.

As the plating efficiency was low in these experiments, compared to the authors other work with V79's, this was considered as a possibility to explain this result. It is clear that it some cases the low plating efficiency results in artificially high survival, >1 in one case. Figure 4.27 shows a comparison between two sets of data at the same dose rate and depth, with different plating efficiencies. These were 0.27 and 0.56 respectively. Survival is plotted against irradiation time allowing a comparison regardless of total dose delivered. The similarity of the two data sets, despite the approximate factor of two difference in plating efficiency, suggests that plating efficiency alone is not responsible for the high survival levels. Similar results were found comparing plating efficiencies within the other data sets.

Incident neutron fluxes from the reactor were monitored by a number of independent fission counters which, as may be expected in a reactor facility, are frequently checked and

	20mm	50mm	20mm low dose rate	50mm low dose rate
Alpha (Gy^{-1})	0.3090 ± 0.0233	0.3385 ± 0.0270	0.2114 ± 0.0863	0.1539 ± 0.0556
Beta (Gy^{-2})	-		0.0010 ± 0.0060	0.00081 ± 0.0060

Table 4.9: *Fitting factors for figures 4.24 and 4.25. Fitted linear quadratic function to survival data for V79. Doses based on cells loaded with 50ppm boric acid. Irradiations carried out in the large water phantom.*

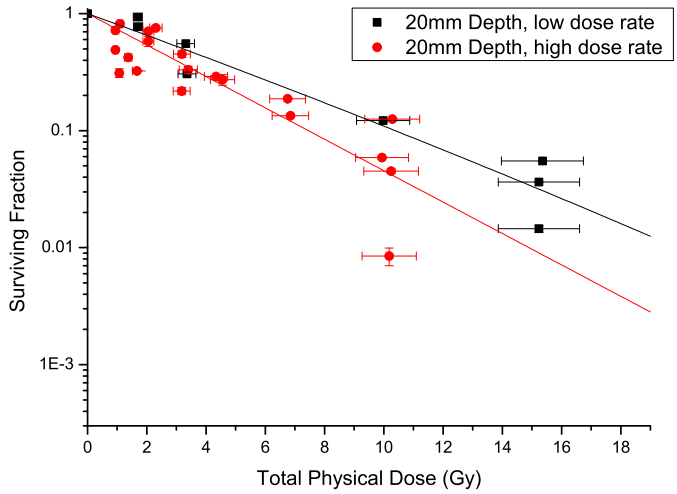

Figure 4.24: *V79 cell survival, at 20mm depth in the large rectangular phantom, in MIT's epithermal neutron beam at varying dose rates. Doses based on cells loaded with 50ppm boric acid. Fit parameters can be found in table 4.9.*

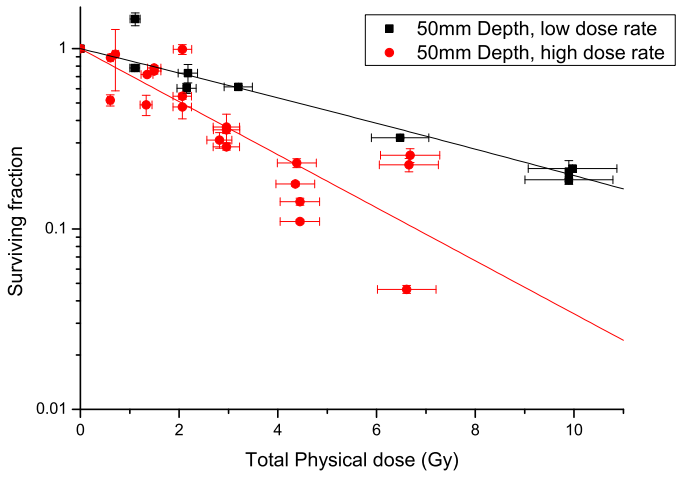

Figure 4.25: *V79 cell survival, at 50mm depth in the large rectangular phantom, in MIT's epithermal neutron beam at varying dose rates. Doses based on cells loaded with 50ppm boric acid. Fit parameters can be found in table 4.9.*

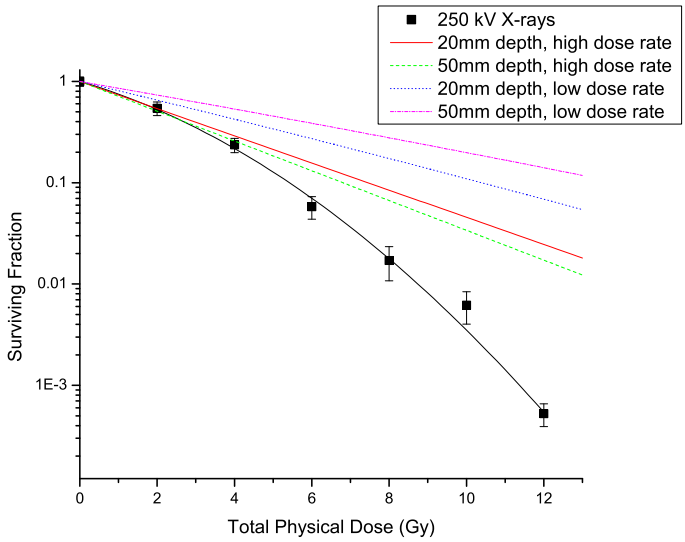

Figure 4.26: *Comparison of 250kV X-ray survival data with fits to experimental data from MIT's epithermal beam exposures. The 250kV experimental system is detailed in the previous chapter. MIT fits as in table 4.9*

Survival level	X-ray dose	50mm, high dose rate dose	RBE
0.1	5.42	6.80	0.80
0.01	8.74	13.60	0.64
0.001	11.37	20.41	0.56

Table 4.10: *Calculated RBE's for exposures in the MIT epithermal beam, at high dose rate. 50 ppm boron level assumed. Doses calculated from fitted curve data presented in table 4.9 and X-ray curve from table 3.5 on page 78.*

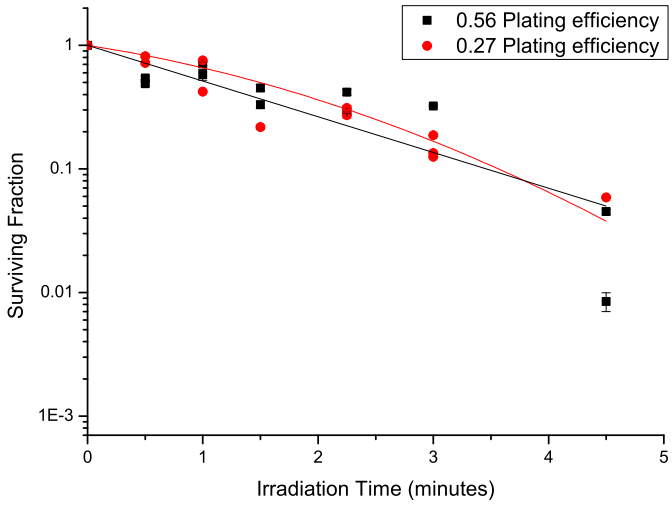

Figure 4.27: *V79 cell survival in the large rectangular phantom in MIT's epithermal beam at full dose rate. Comparison of two data sets with different plating efficiencies*

calibrated. Thermal neutron doses were measured using two standard techniques which, as described in section 4.3, were in good agreement with each other and showed only minor differences from MIT's reference dosimetry.

The most likely explanation for the results therefore lies in the calculated dose values, specifically the dose from boron capture products. Due to export restrictions a different supply of ^{10}B enriched boric acid was used at MIT than at Birmingham and a new stock solution was prepared in saline. The boric acid dilution is straightforward. 3.08 g of 99% enriched boric acid, H_3BO_3, is added to 500 ml of saline to give a 1000 μg ml^{-1} stock solution. This is then diluted at 20:1 in complete cell growth medium for use in experiments. It has hard to see how a dilution error could be introduced. The most likely explanation is thought to be that the boric acid supplied at MIT was not enriched and instead had the natural isotope ratio of 19.9% ^{10}B with 80.1% ^{11}B. Unfortunately boron analysis for the cell solutions was unavailable. All cells were incubated using the same stock solution and therefore can be assumed to have had the same boron levels. Consequently, all cells would receive the same physical dose for a given thermal neutron flux. With this in mind the two dose rates

can still be usefully compared despite the uncertainty over absolute dose levels. Plots of the data with two axis, representing the two assumed boron concentrations, can be found in figures 4.28 and 4.29.

A comparison of the survival data, assuming 10 ppm boron, with the published work of Gabel *et al* [3] is shown in figures 4.30 and 4.31. Dose rates at this boron level were 0.911 Gy min^{-1} and 0.067 Gy min^{-1}. Fitted values for this data can be found in table 4.11. As described in the preceding section, the predicted curves are produced using equation 4.6.1 with values of the constants from table 4.7 on page 146.

4.6.3 Comparison of Data Sets for Differing Dose Rates

To establish if the differences between survival at the high and low dose rates in the MIT beam were statistically significant they were compared using an f-test.

An f-test is normally used to compare two different models fitted to one data set. The two models are fitted and goodness of fit is quantified as the sum of squares of the deviations of the data points from the model. Complexity of the model is quantified by degrees of freedom; the number of data points minus the number of parameters fit by the model. If the alternative, more complicated, model is correct the increase in the sum of squares going from the complex to the simple model is greater than the relative increase in the degrees of freedom.

In this case the f-test is used to see if the differences between two sets of data are statistically significant. The two data sets and the data combined into a single set are all fitted with the same model. Hence the null hypothesis is that there is no significant difference between the two data sets. The degrees of freedom and sum of squares of the two separate fits and the combined fit are compared as in equation 4.6.2 taken from [122]. This f-test value, along with the appropriate degrees of freedom, was used to look up a p-value using Microsoft Excels FDIST command. The resulting values are shown in table 4.12.

This result suggests that there is a significant dose rate effect at both depths.

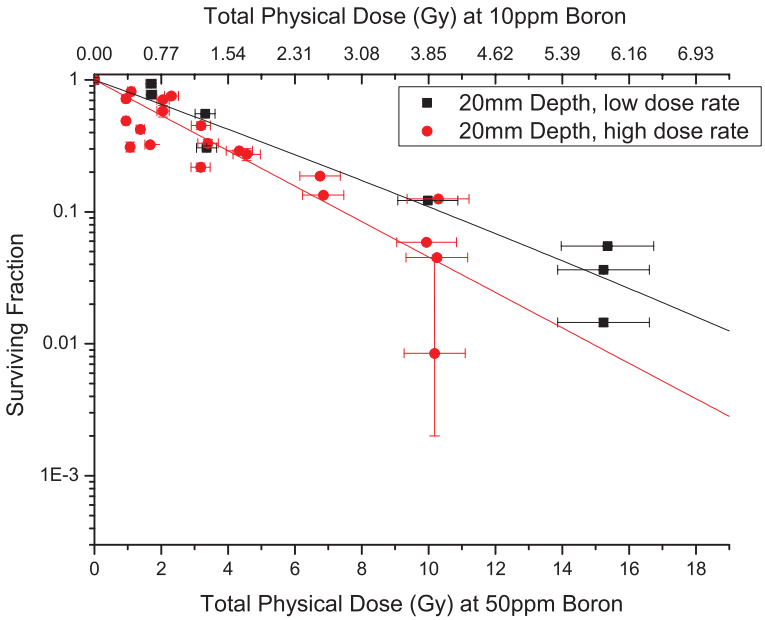

Figure 4.28: *V79 cell survival, at 20 mm depth in the large rectangular phantom, in MIT's epithermal neutron beam at varying dose rates. Doses for two assumed boron levels are shown.*

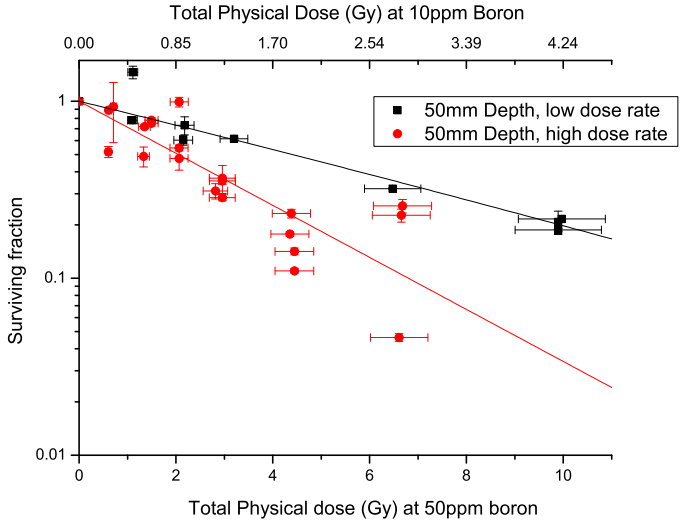

Figure 4.29: *V79 cell survival, at 50 mm depth in the large rectangular phantom, in MIT's epithermal neutron beam at varying dose rates. Doses for two assumed boron levels are shown.*

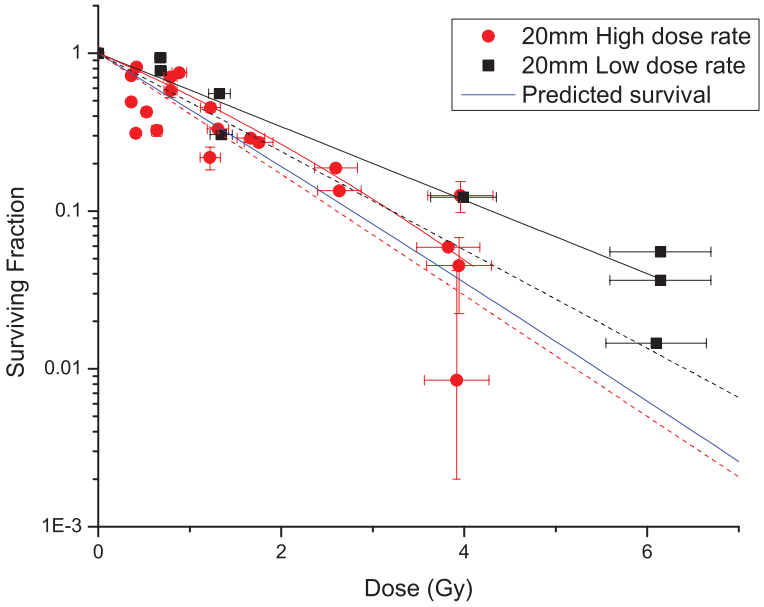

Figure 4.30: *Comparison between experimental results and calculated values from Gabel* et al *[3]. 10 ppm boron is assumed. Cell data from 20 mm depth in the large water phantom, irradiated in the FCB. Fitting factors can be found in table 4.11; solid lines indicate weighted fits, dashed unweighted.*

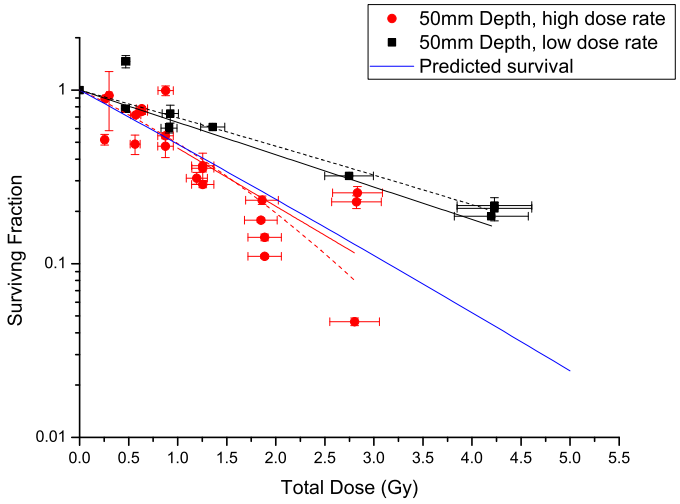

Figure 4.31: *Comparison between experimental results and calculated values from Gabel* et al *[3]. 10 ppm boron is assumed. Cell data from 50 mm depth in the large water phantom, irradiated in the FCB. Fitting factors can be found in table 4.11; solid lines indicate weighted fits, dashed unweighted.*

20mm Depth		
	Alpha (Gy $^{-1}$)	**Beta (Gy $^{-2}$)**
Weighted		
High dose rate	0.5750 ± 0.0032	0.0448 ± 0.0017
Low dose rate	0.4539 ± 0.2432	0.0132 ± 0.0394
Combined	0.6176 ± 0.1090	0.0156 ± 0.0589
Unweighted		
High dose rate	0.8633 ± 0.0032	-
Low dose rate	0.7176 ± 0.0596	-
Combined	0.6480 ± 0.0395	-
50mm Depth		
	Alpha (Gy $^{-1}$)	**Beta (Gy $^{-2}$)**
Weighted		
High dose rate	0.7705 ± 0.1468	-
Low dose rate	0.4288 ± 0.0052	-
Combined	0.6176 ± 0.1090	0.0156 ± 0.0589
Unweighted		
High dose rate	0.6049 ± 0.2026	0.1055 ± 0.1519
Low dose rate	0.3640 ± 0.1310	0.0040 ± 0.0332
Combined	0.5553 ± 0.1520	

Table 4.11: *Fitted values to V79 survival data irradiated in the large water phantom using the MIT FCB. 10ppm boron assumed.*

$$F = \frac{\frac{(SS_{Combined} - SS_{Separate})}{(DF_{Combined} - DF_{Separate})}}{\frac{SS_{Separate}}{DF_{Separate}}} \tag{4.6.2}$$

	Weighted fit	Unweighted fit
20mm	1.22E-04	7.92E-04
50mm	7.54E-05	1.20E-03

Table 4.12: *p-values from an f-test comparing the fits to independent high and low dose rate sets to a fit to the pooled data set. The null hypothesis was that there is no significant difference between the fits.*

As discussed earlier in this report all curves plotted in this report were fitted to the data sets using OriginPro from OriginLab. In addition to producing a best fit, Origin is capable of calculating confidence bands for the fit at any given point. A value y, for a confidence level α, confidence intervals are;

$$\hat{y} \pm t_{\frac{\alpha}{2}}(Estimated\ standard\ error\ of\ \hat{y}) \tag{4.6.3}$$

$t_{\frac{\alpha}{2}}$ is the critical value of the t-distribution.

For a chosen confidence level, the confidence bands show the limits of all possible fitted lines for the given data. For example, for a chosen 95% level it is possible to say that there is 95% confidence that the best-fit line lies within the confidence bands[125].

Plots of data from both depths in the phantom is plotted with fitted lines and associated confidence intervals in figures 4.32 and 4.33. The 50 mm data shows a significant difference between the two different dose rates; the 95% confidence intervals do not overlap. The 20 mm data shows no significant difference between the fitted lines.

The differing conclusions of the two methods of comparing the data sets may be due to the influence of 'outliers' within the data. With small data sets, the F-test calculation is very sensitive to such points. As an F test compares the difference in sum-of-squares with the difference expected by chance, it can be skewed if one or both fitted data sets have large differences from the predicted values for some points. Figure 4.34 shows a plot illustrating the difference between observed experimental values and the weighted fit value as a fraction of the observed value. The data shows a number of points where the deviation from the model is large compared to the recorded experimental errors.

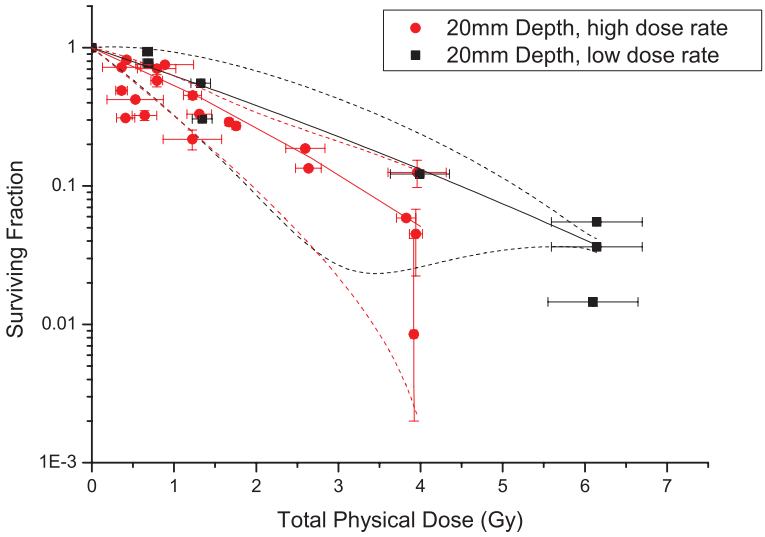

Figure 4.32: *V79 cell survival, at 20 mm depth in the large rectangular phantom, in MIT's epithermal neutron beam at varying dose rates. 10ppm boron assumed. Solid lines indicate fitted linear quadratic functions; constants as in table 4.11. Dotted lines indicate 95% confidence intervals in the fits.*

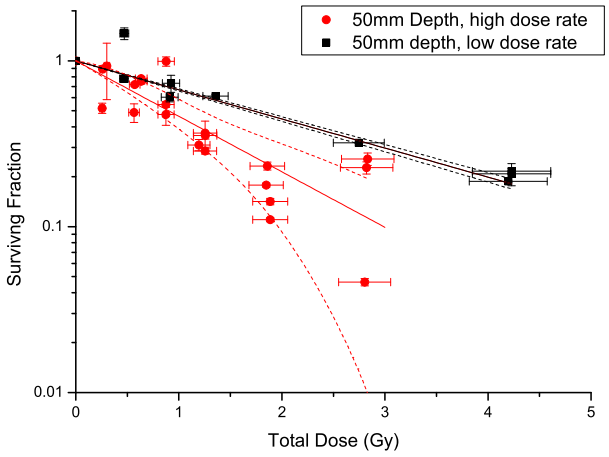

Figure 4.33: *V79 cell survival, at 50 mm depth in the large rectangular phantom, in MIT's epithermal neutron beam at varying dose rates. 10ppm boron assumed. Solid lines indicate fitted linear quadratic functions; constants as in table 4.11. Dotted lines indicate 95% confidence intervals in the fits.*

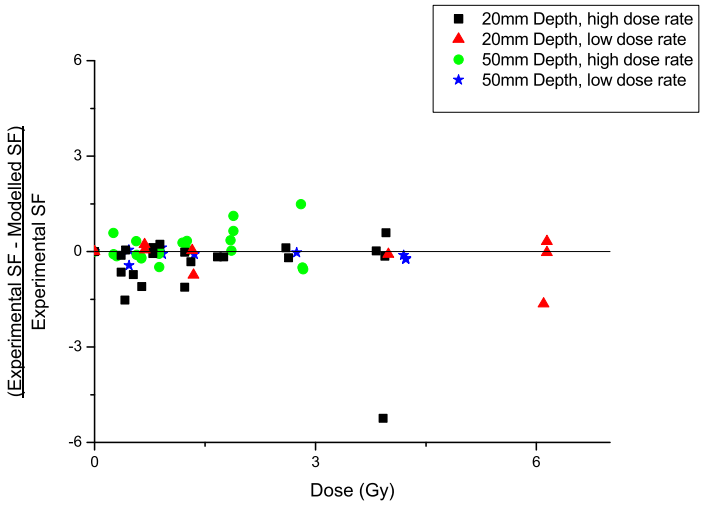

Figure 4.34: *Comparison of values predicted by fitted linear quadratic functions with experimental data, at varying depth and dose rate. Survival data for V79 cells irradiated in the MIT epithermal beam.*

	Photon	Thermal Neutron	Fast Neutron	Boron
20mm depth	52.33%	3.63%	4.06%	39.98%
50mm depth	61.38%	3.08%	1.59%	33.95%

Table 4.13: *Fractional contributions to physical dose, in the FCB, at 10ppm boron. Percentages calculated as described in section 4.3 on page 119, from data provided by Zamir Ghani[168]*

4.6.4 Comparison With Published V79 Dose Rate Data

V79 cells have a large 'shoulder' region in their survival curves when exposed to X-ray radiation and show a large dose rate effect.

In the classic dose rate effect differing survival levels with dose rate, at a given dose, are assumed to result from longer irradiation times allowing more sub-lethal damage to be repaired over the course of the irradiation. High LET radiation is assumed to show no dose rate effect, as cell kill is dominated by unrepairable damage [177]. In a mixed field such as that found in BNCT it may therefore be expected that any dose rate effect is due only to repair of the photon component. Proportions of the different dose fractions are shown in table 4.13.

As seen in the previous section in figures 4.30 and 4.30 on page 155, the high dose rate survival data is a good match, when uncertainties are considered, to predictions made from previously published data when using an acute ($\sim$1 Gy Min^{-1}) dose rate photon component. Actual photon dose rates in the FCB were 0.034$\pm$0.001 Gy Min^{-1} and 0.45 $\pm$0.1 Gy Min^{-1} for the low and high dose rates respectively. Bedford *et al* [149] presented data for V79 cells irradiated with cesium-137 gamma rays (661.7 keV) at a wide range of dose rates. Their data are replotted in figure 4.35.

Predictions of cell survival using fits to Bedford *et al*'s 0.026 GyMin^{-1} and 14.2 GyMin^{-1} data are shown in figures 4.36 and 4.37. All other beam components were modelled using the constants in table 4.7 on page 146. Modelling methodology was the same as described in section 4.6.1. As with the higher dose rate photon data, predicted survival is similar to that observer in the higher dose rate exposures but lower than observed at the low dose rate.

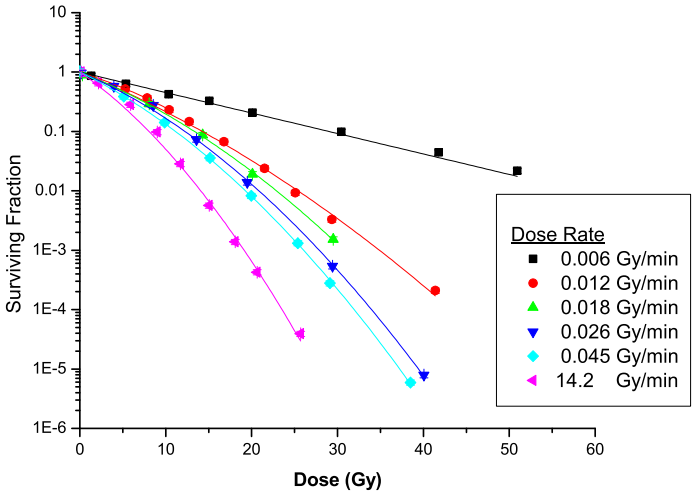

Figure 4.35: *Survival data for V79 cells exposed to gamma rays at varying dose rate. Replotted from reference [149], fits generated in Origin. Fitted parameters can be found in table 4.14.*

Dose/min (Gy)	Alpha (Gy $^{-1}$)	Beta (Gy $^{-2}$)
0.006	0.0794 ± 0.0057	-
0.012	0.1361 ± 0.0077	0.0018 ± 0.003
0.018	0.1327 ± 0.0079	0.0030 ± 0.003
0.026	0.1410 ± 0.0063	0.0038 ± 0.0002
0.045	0.1629 ± 0.0039	0.0039 ± 0.0001
14.2	0.2315 ± 0.0211	0.0068 ± 0.0011

Table 4.14: *Parameters fitted to the gamma ray survival data of Bedford* et al*[149], plotted in figure 4.35*

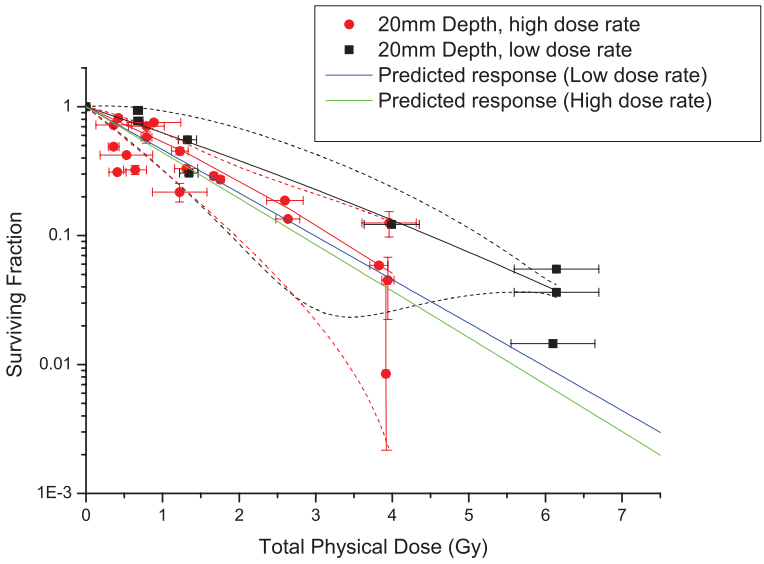

Figure 4.36: *Comparison between experimental results and calculated values. 10 ppm boron is assumed. Cell data from 20 mm depth in the large water phantom, irradiated in the FCB. Fitting factors can be found in table 4.11; solid lines indicate weighted fits, dashed unweighted. High and low dose rate predictions based on combination of photon data from Bedford* et al *[149] and factors from table 4.7*

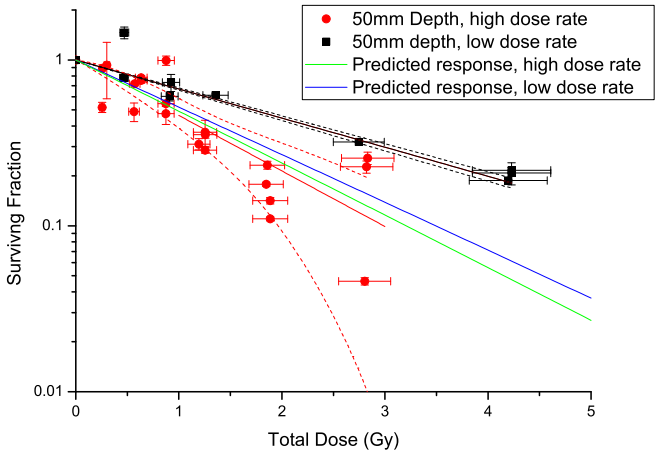

Figure 4.37: *Comparison between experimental results and calculated values. 10 ppm boron is assumed. Cell data from 50 mm depth in the large water phantom, irradiated in the FCB. Fitting factors can be found in table 4.11; solid lines indicate weighted fits, dashed unweighted. High and low dose rate predictions based on combination of photon data from Bedford* et al *[149] and factors from table 4.7*

20mm Depth SF	**0.37**	**0.1**	**0.01**
High dose rate	1.54 ± 0.01 Gy	3.20 ± 0.02 Gy	5.58 ± 0.05 Gy
Low dose rate	2.07 ± 1.00 Gy	4.50 ± 2.30 Gy	8.20 ± 4.60 Gy
Ratio	0.74 ± 0.34	0.71 ± 0.35	0.68 ± 0.36
50mm Depth SF	**0.37**	**0.1**	**0.01**
High dose rate	1.29 ± 0.24 Gy	2.99 ± 0.56 Gy	6.00 ± 1.10 Gy
Low dose rate	2.46 ± 0.02 Gy	5.37 ± 0.07 Gy	10.74 ± 0.13 Gy
Ratio	0.524 ± 0.10	0.56 ± 0.10 Gy	0.56 ± 0.1

Table 4.15: *Dose values to produce different levels of survival. Calculated from weighted fits to V79 survival data with 10ppm boron, in the large water phantom, in the MIT FCB*

A further comparison can be made to published data by considering the ratio of doses required to produce a given biological effect between the two dose rates. Table 4.15 shows the results of this calculation for the MIT FCB exposures. Table 4.16 shows a similar calculation for the data of Bedford *et al.* Ratios of (Dose Required)/(Acute Dose Required) are tabulated to allow comparison between the two dose rate experiments.

These calculations of effect vs dose show clearly that the observed dose rate effect at 20 mm is insignificant; a ratio of (Dose Required)/(Acute Dose Required) of 1 within the uncertainties at the 95% level. The data from 50 mm depth shows a significant, and large, dose rate effect. The photon component has dose rates of 0.034 ± 0.001 Gy Min^{-1} and 0.45 ±0.1 Gy Min^{-1} at this boron level. Comparing the observed effect with that of the photon dose rate effect quantified by Bedford *et al*, the reduction in cell kill at low dose rate is greater than would be expected even if all of the physical dose components were repairable to the same degree as photons.

A final useful comparison can be made using Mitchell *et al*'s data. Their lowest dose rate exposure, at 0.006 Gy Min^{-1}, can be assumed to be the upper limit of repair for low LET radiation. That is, all repairable sub-lethal damage can be assumed to be repaired in this case. Therefore, using the fit for this data as the constants for the photon component in 4.6.1 gives a predicted response for a combined irradiation where all possible repair of

SF	0.37	0.1	0.01
Dose/min			
0.006	12.52 ± 0.89	29.00 ± 2.1	58.10 ± 4.10
0.012	6.72 ± 0.33	14.26 ± 0.64	25.40 ± 1.10
0.018	6.53 ± 0.31	13.34 ± 0.56	22.90 ± 0.91
0.026	6.06 ± 0.21	12.25 ± 0.35	20.85 ± 0.52
0.045	5.40 ± 0.10	11.14 ± 0.18	19.29 ± 0.28
14.2	3.86 ± 0.29	8.05 ± 0.54	14.08 ± 0.86

Table 4.16: *Dose values to produce different levels of survival. Calculated from weighted fits to data taken from Bedford* et al*[149]. V79 cells irradiated with Cs-133 gamma rays.*

SF	0.37	0.1	0.01
Dose/min			
0.006	0.310 ± 0.030	0.278 ± 0.027	0.243 ± 0.023
0.012	0.574 ± 0.051	0.565 ± 0.045	0.554 ± 0.041
0.018	0.591 ± 0.052	0.603 ± 0.048	0.615 ± 0.045
0.026	0.637 ± 0.053	0.657 ± 0.053	0.675 ± 0.045
0.045	0.715 ± 0.055	0.723 ± 0.050	0.730 ± 0.046
14.2	1	1	1

Table 4.17: *Ratios of (Dose Required)/(Acute Dose Required) for table 4.16*

the sub-lethal photon component has taken place. As can be seen from figure 4.38, higher cell kill is predicted than was observed experimentally. This result suggests that a dose rate effect is present in the other beam components.

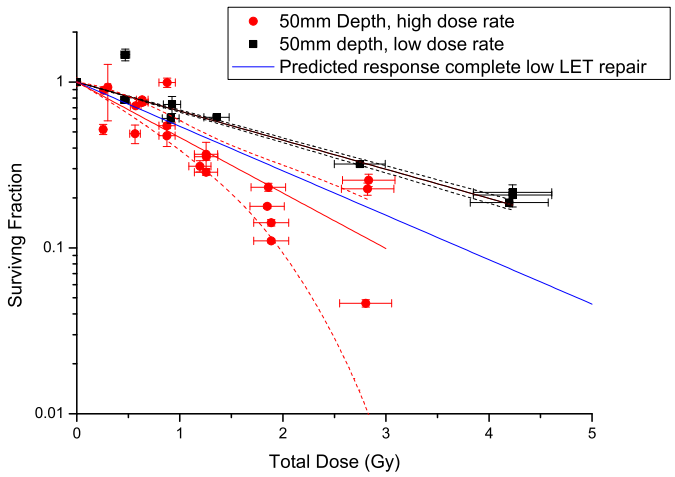

Figure 4.38: *Comparison of V79 survival at 50 mm depth, 10 ppm boron with predictions from equation 4.6.1. Photon component used is based on very low dose rate data from reference 2.6. All other components as table 4.7. Solid lines indicate fits from Origin of the LQ function, dotted lines indicate 95% confidence bounds.*

4.7 Summary

Survival values found at Birmingham, when irradiating v79 cells with 50ppm boron in an epithermal beam, are a reasonable match within uncertainties to survival values predicted from previous cell biology work. Despite the low overall dose rate of 0.042 Gy min^{-1} at 20mm, this good agreement was found without any allowance for the dose rate effect. This result suggests that any dose rate effect at this boron concentration is insignificant in the dose range investigated.

A large systematic error appears to be present in survival results recorded at MIT. The most likely explanation is that actual boron-10 concentrations in the cell system were lower than planned. Data has therefore been analysed assuming a boron-10 concentration of 10 ppm. When irradiating cells in the FCB, a dose rate effect was observed at both depths within the water phantom. However, a large spread in experimental cell survival observed means that the difference in fitted response was only significant at 50mm depth.

Comparisons with previously published results suggest that the overall dose rate effect

observed is too large to be explained solely by the effect on the low LET, photon, component. This result holds even when the conventional maximum amount of sub-lethal repair in the photon component is assumed. This implies that some degree of dose rate effect is present in the higher LET components of the beam.

How the mix of beam components effects the level of effect is not clear. There is a different mixture of components at 20 mm and 50 mm but a comparison between the two is confounded by the fact that cell survival at the two depths is not significantly different, as shown in figures 4.39 and 4.40.

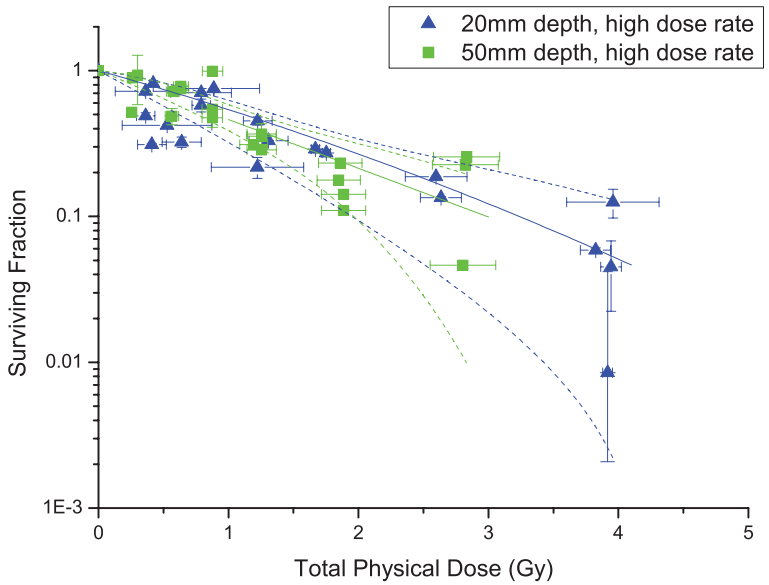

Figure 4.39: *V79 cell survival at varying depths in the large water phantom, in the MIT FCB beam. Full beam dose rate. 10 ppm boron assumed. Solid lines are fits of the LQ function, dashed lines are the 95% confidence intervals for the fits.*

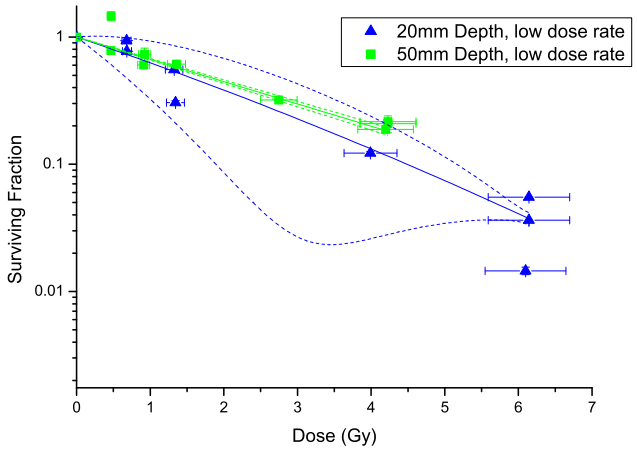

Figure 4.40: *V79 cell survival at varying depths in the large water phantom, in the MIT FCB beam. Reduced beam dose rate. 10 ppm boron assumed. Solid lines are fits of the LQ function, dashed lines are the 95% confidence intervals for the fits.*

4.7.1 Biological Quantification of the Dose Reduction in Attached Cells

A complication of the large water phantom irradiation rig, when comparing to previous work, is that with the cells in attachment they are no longer surrounded on all sides by medium. For work with boron loaded medium this suggests that there is a reduction in the dose due to boron capture products. In order to quantify the dose reduction effect a series of cell survival experiments were carried out. These utilised sealable, 0.9 μm Mylar based, glass dishes as shown in figure 4.43. The products of the ^{10}B neutron capture reaction lose their energy extremely quickly in Mylar but should still deliver a significant fraction of dose through a 0.9 μm layer. Energies for the boron capture reaction products after passing through 0.9 μm mylar are shown in figures 4.41 and 4.42. These plots were produced by simulating 10^5 particles propagating through a layer of ICRU-222 standard Mylar, $H_8C_{10}O_4$ using SRIM [72].

A similar protocol to the Birmingham and MIT flask irradiations was followed. 48 hours prior to irradiation 2 x 10^5 V79 cells were introduced into the dishes in 2 ml of complete growth medium, leading to the growth of a cell monolayer on the Mylar base. 16 hours prior to irradiation the medium was removed and replaced with medium loaded to 50 ppm with 99% ^{10}B enriched boric acid. Immediately prior to irradiation, a second dish without a base was attached to each of the dishes in which cells had been cultured. Referring to figure 4.43 the 'single sided' dishes, equivalent to flask irradiations, had region A filled with boronated medium and region B filled with normal medium. The 'double sided' dishes had both regions A and B filled with borated medium. The gassing ports, shown sealed with rubber hose, were not used in this experiment. The samples were then attached in pairs to Perspex rods to hold them in place at a fixed depth of 20 mm within the large water phantom. These were then irradiated, the Mylar cut out, and the cells cultured in the normal way for a survival study. Results are shown in table 4.18.

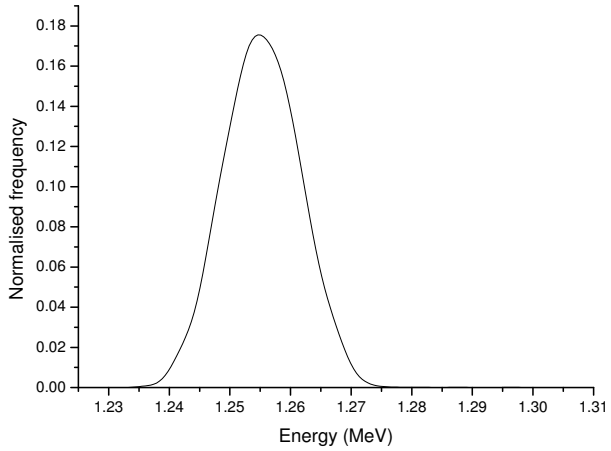

Figure 4.41: *Simulation of the energy spread of 1.47 MeV alpha particles after they have passed through a 0.9 μm mylar layer. Produced using SRIM[72]*

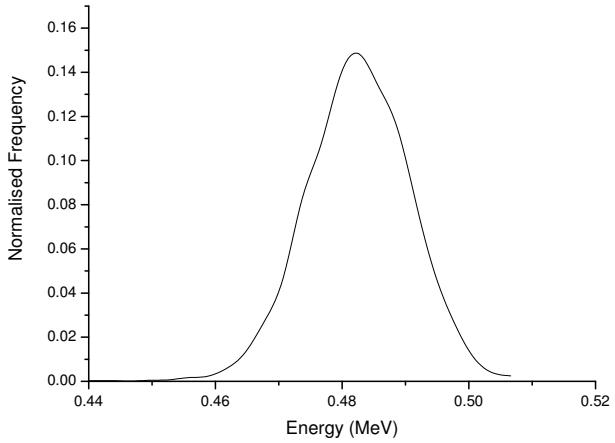

Figure 4.42: *Simulation of the energy spread of 0.84 MeV lithium ions after they have passed through a 0.9 μm mylar layer. Produced using SRIM[72]*

	Single sided	Double sided
45 minutes exposure time	0.220 $\pm$ 0.003	0.122 $\pm$ 0.008
30 minutes exposure time	0.247 $\pm$ 0.020	0.153 $\pm$ 0.007

Table 4.18: *Cell survival fractions from irradiation of V79s, in Birminghams BNCT beam, with single and double sided boron loading. Data from two separate experimental evaluations*

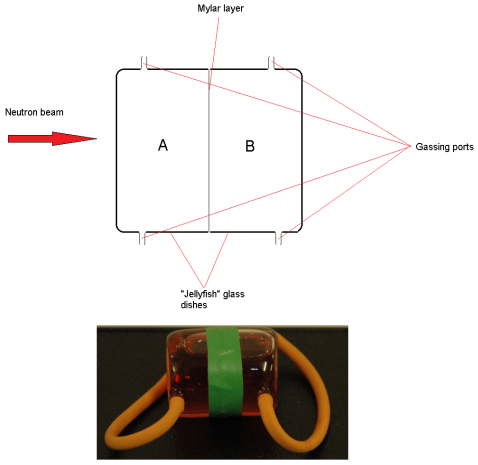

Figure 4.43: *'Jellyfish' dishes. Cells were cultivated on the A side of the mylar layer. In 'two sided' irradiations A and B contained borated medium. In 'single sided' irradiations A contained borated medium, B contained normal medium. The gassing ports were not used in this experiment and were sealed with rubber hose.*

Doses in the 'jellyfish dishes for this experiment were not known precisely at the time of writing. The necessary MCNP calculation to convert fission chamber monitor units to dose at the cell layer had not been carried out. Assuming that the dose response is similar to that delivered to T25 flasks irradiated in the same system allows a useful comparison. Boron doses required to produce the survival levels shown in table 4.18 were calculated using the fitting data from the T25 flask irradiations described in section 4.6.1. The constants used were $\alpha = 1.226 \pm 0.08$,$\beta = 0$. Solving the linear quadratic fitting function for dose, with $\beta = 0$ gives;

$$Dose = \frac{ln(\frac{1}{S})}{\alpha} \tag{4.7.1}$$

Where S is survival. Doses calculated this way are shown in table 4.19.

	Single sided dose (Gy^{-1})	Double sided dose (Gy^{-2})	Ratio of Single/Double
45 minutes	1.235 $\pm$ 0.081	1.72 $\pm$ 0.12	0.72 $\pm$ 0.07
30 minutes	1.141 $\pm$ 0.099	1.53 $\pm$ 0.15	0.75 $\pm$ 0.1

Table 4.19: *Doses estimated from surviving fractions detailed in table 4.18 for two different exposure times*

Monte Carlo calculations carried out by Zamir Ghani [168], detailed in section 4.3.2 on page 132, suggested a boron dose reduction of 0.77 ± 0.05 for cells in attachment. While this agrees with the estimated experimental dose reduction, it is important to note that the data presented here represent a single experimental observation and that the required dosimetry to fully interpret the results has not been completed.

Further modelling and experimental work in the 'jellyfish' system is ongoing.

Chapter 5

CONCLUSIONS

Work presented in this thesis has covered two main areas of radiobiology relevant to BNCT. The first was an investigation into synergistic effects when radiations of differing LET are delivered simultaneously to cells. Previously published work with high LET ions and photons is inconsistent regarding both degree of synergistic effect and whether any synergistic effect is seen at all.

A series of experiments were carried out, using a newly constructed irradiation jig built for the purpose, exposing V79 cells to mixed fields of photons and ^{238}Pu alpha particles. The motivation was to repeat and extend previous work carried out by McNally *et al* in a similar system [1]. Initial exposure using varying doses of alpha particles and ^{60}Co photons delivered simultaneously found no differences from a purely additive prediction, based on the fields given separately. The same result was seen with 2.54 Gy of alpha particles given simultaneously with X-rays. In the case of a mixed field with an alpha dose of 3.18 Gy a significant synergistic effect was seen, with lower levels of cell survival than would be expected from the same fields given separately. The level of alpha dose at which McNally *et al* observed synergy was lower, with significant effects being seen with both 2 Gy and 2.5Gy of alpha particles. The level of synergy effect seen in McNally *et al*'s results, as a deviation from predicted survival, was similar to that observed with 3.18Gy of alphas in the present study. At higher low-LET fractions ($>\sim$60%) McNally *et al* observed a larger effect.

Some published attempts to model synergistic interactions were compared to both McNally *et al*'s and the recent data. It was found that the Zaider-Rossi model [89], using constants from single field exposures, was a good fit to the data exhibiting synergy but predicted higher cell kill at the lower alpha dose than was seen experimentally. The same model was a poor fit to McNally *et al*'s data when the single field constants were used. When a non-zero beta constant, based on low LET data, was used the model fitted McNally mixed exposures with 0.5 Gy and 2 Gy of alphas well. Lower cell survival than modelled was seen in the mixed exposure with 2.5Gy of alphas. Use of the extended Zaider-Rossi model [145] and the lesion-additively model [155] produced similar results, with no model fitting either data set well at all dose levels.

The second area of uncertainty in BNCT investigated in this report was the dose rate effect. This is well characterised in single field, low LET, exposures but not in the mixed fields encountered in BNCT. A series of experiments were carried out in the MIT FCB at two dose rates differing by a factor of approximately 15. Cells were exposed at two depths, 20 mm and 50 mm, in a full scatter water phantom. A difference in response at both of the two dose rates was observed but was only clearly significant at the 50 mm depth. Analysis of the results was complicated by the fact that a large systematic error, thought to be related to boron-10 concentration, appeared to be present in the results. Analysis, with an assumed boron-10 concentration of 10 ppm, with reference to previous published work with individual beam components suggests that the magnitude of the dose rate observed was too large to be explained solely by a difference in response of the low LET component.

Further experiments in the Birmingham BNCT beam at 50 ppm boron produced cell survival levels well matched to predictions based on previous published cell culture work.

The potential impact of these findings can be explored in the context of clinical BNCT.

5.1 BNCT Treatment Planning

Treatment planning in BNCT is not a straightforward process. Simplifications in computational approach which are useful in conventional photon therapy and which have historically been applied in fast neutron therapy are of little use. This is due to the high dependence of delivered dose on the exact scattering and transport of low energy neutrons [178]. Recent approaches have focussed on probabilistic, Monte Carlo, methods of solving the dose distribution problem.

Ultimately treatment plans in BNCT are dependent on a number of assumptions and biologically derived values which have some significant uncertainties. The first is that the boron distribution within various tissues and ultimately within cells must be known with precision. Historically when calculating effect of boron doses clinically it has been assumed that boron is distributed uniformly in a tissue of a given type. This has been demonstrated to be a flawed assumption by using various techniques to directly examine boron distribution in patients. These include positron emission topography (PET) with ^{18}F labelled BPA [179] and, at a cellular level, Secondary Ion Mass Spectrometry (SIMS) imaging of tumour explants [180]. The other major assumption, related to the work presented in this report, is in determining the relative biological effect of the various BNCT dose components.

To determine a treatment dose conversion from a physical absorbed dose, as calculated by MCNP or similar, and a weighted dose is required. For comparison to standard radiotherapy this has been handled in BNCT clinical trials via a conversion to 'photon-equivalent-dose'[181], nominally the dose of photons required to produce the same clinical effect. This is calculated as;

$$D_w = (d_\gamma \times DRF) + (d_n \times RBE_n) + (d_N \times RBE_N) + ({}^{10}B \times CBE) \tag{5.1.1}$$

Where d_γ, d_n and d_N are the doses of gamma rays, fast neutrons and nitrogen capture protons respectively. DRF is the, dose rate dependent, dose reduction factor for photons

and CBE is the compound biological effectiveness. CBE, as discussed earlier in this report, is derived from the RBE of the alpha and lithium particles along with the micro distribution of boron. Historically fixed values for the various RBE's have been used.

5.1.1 Impact of Dose Reduction Factor

The DRF factor, in the photon term in equation 5.1.1, is incorporated to account for the fact that the gamma dose rate in most BNCT treatment beams is considerably lower than 1Gy min^{-1}. This means that, with long exposure times, cell repair is not insignificant. Rather than direct calculation this factor is arrived at via a somewhat ad hoc methodology of looking at photon exposures in various *in vitro* experiments and estimating a level of reduction in effect on cell survival. For some typical BNCT beams this factor has been taken as approximately 0.7 [68]. In the MIT FCB it was assumed to be 1, due to the acute gamma dose rate. Perhaps the factor most applicable to Birminghams Dynamitron beam would be the one used for early work in the MIT M67 beam, due to their similar gamma dose rates [182]. This factor was estimated as 0.5, justified by reference to Hall *et al*'s work with HeLa cells [183]. It is important to note however, that this 0.5 factor used for the M67 beam was derived with reference to cell data showing dose reduction factors of between 0.3 and 0.7. Dose reduction factors in other beams have similar uncertainties associated with their derivation.

Typical assumed clinical boron levels, with BPA, are $65\mu g^{-1}$ for tumour and 18 μg^{-1} for normal brain tissue. Typical weighting factors are RBEs of 1.0 for photons and 3.2 for neutrons, CBEs of 1.35 for boron in brain and 3.8 in tumour [173]. These factors can be used to explore the impact of varying the DRF on doses delivered. Figure 5.1 is a plot of the Birmingham accelerator beam weighted depth dose curve, in brain, with different assumed values of the DRF. To calculate the impact of this in BNCT treatments, typical BNCT treatment doses have to be considered.

Maximum BNCT treatment doses are calculated based on dose delivered to healthy brain.

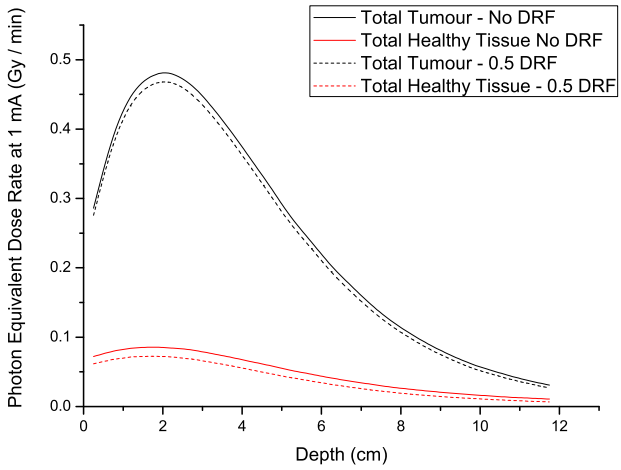

Figure 5.1: *Calculated depth dose curve for the Birmingham beam with different assumed values of the photon Dose Reduction Factor.*

Healthy brain radiation tolerance depends on the volume of brain irradiated along with the dose delivered. Widely quoted tolerance values are taken from Emami *et al* [184] and are presented in table 5.1. Any BNCT treatments are likely to be delivered either in a single fraction or a small number of large fractions. Doses in conventional photon radiotherapy are instead delivered in a number of smaller doses, typically 2 Gy per treatment. To make use of the values in 5.1 in BNCT, reference can be made to Biological Effective Dose (BED). The BED is derived from the linear quadratic function and essentially represents the physical dose required to produce a given effect if the dose were to be delivered by infinitely small doses per fraction or if the dose were delivered at an extremely low dose rate [185];

$$BED = nd[1 + \frac{d}{(\alpha/\beta)}] \tag{5.1.2}$$

Where n is the number of fractions and d is the dose per fraction. The α / β ratio is specific to the tissue being considered and gives a measure of repair capacity. As the same BED in a given tissue type can be achieved through different fractionation schedules, the normal tissue tolerance doses from [184] can be converted to a 'single fraction equivalent'

Volume of brain irradiated	$TD_{5/5}$ (Gy)	$TD_{50/5}$ (Gy)
1/3	60	75
2/3	50	65
3/3	45	60

Table 5.1: *Values for healthy brain radiation tolerance taken from [184]. $TD_{5/5}$ and $TD_{50/5}$ are the total doses (TD) producing 5% or 50% incidence of necrosis within 5 years.*

for BNCT by setting the BED's as equal, that is;

$$n_{Photon}d_{Photon}[1 + \frac{d_{Photon}}{(\alpha/\beta)}] = n_{BNCT}d_{BNCT}[1 + \frac{d_{BNCT}}{(\alpha/\beta)}] \tag{5.1.3}$$

n_{Photon} and d_{Photon} are the number of fractions and dose per fraction. n_{BNCT} and d_{BNCT} are the number of BNCT fractions and the photon-equivalent BNCT dose per fraction. Following the approach of Coderre *et al* [69], the alpha/beta ratio for brain is assumed to be 2Gy based on the work in reference [186]. This gives an equivalent single fraction dose for the 1/3 brain $TD_{5/5}$ quoted in table 5.1 of 14.5 Gy. The equivalent for 3/3 brain $TD_{5/5}$ is 11.6 Gy.

While this derivation of applicable clinical doses in BNCT is somewhat simplistic, assuming this 11.6 Gy-Eq single fraction dose is indicative of a maximum dose that would be delivered to the healthy brain in BNCT allows the impact on dose delivered, of various DRF's and other factors, to be explored. In reality the dose profile to healthy brain in BNCT is extremely complex and varies between patients. To simplify calculations for the purposes of comparison it is assumed that all dose to tumour is delivered at a fixed depth (32.5mm), and that all dose to healthy tissue is delivered at close to the dose peak (20mm). This tumour depth was chosen with reference to a recent audit of typical high grade glioma locations [187] and the healthy tissue depth was chosen as a representative 'worst case'.

Using the data from figure 5.1 with the maximum healthy tissue photon-equivalent dose of 11.6 Gy, and no photon DRF, gives a treatment time of 136 minutes. Dose to tumour would be 58.7 Gy-Eq. The same treatment time but with a DRF of 0.5 only delivers a healthy tissue dose of 9.87 Gy-Eq and a tumour dose of 56.9 Gy-Eq. This approximately

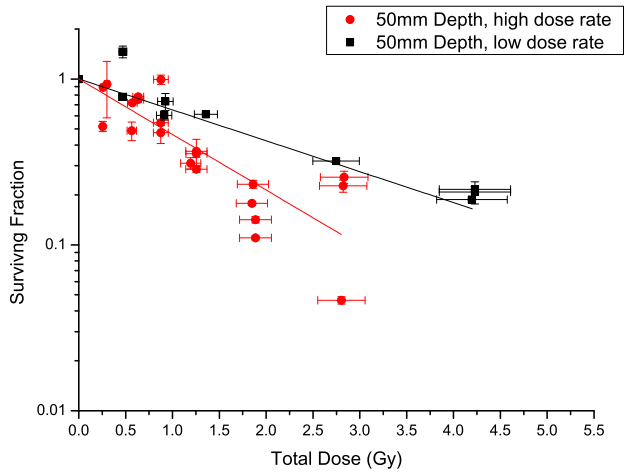

Figure 5.2: *V79 cell survival, at 50mm depth in the large rectangular phantom, in MIT's epithermal neutron beam at varying dose rates. 10ppm boron assumed. Solid lines indicate fitted linear quadratic functions; constants as in table 4.11 on page 156.*

15% shift in healthy tissue dose with DRF, for the same treatment time, suggests that caution needs to be exercised when applying this factor in treatment planning to avoid under or over dosing patients. The proportional shift in tumour dose is much smaller, due to the majority of the weighted dose being contributed by the high-LET components. This implies that a conservative estimate of the degree of dose rate sparing may be clinically justifiable, as the impact on the therapeutic dose of under-estimation is minor.

The *in vitro* dose rate work presented in chapter 4 suggests that the dose rate effect seen in BNCT exposures at low boron concentrations is larger than can be explained solely by changes in response to the photon component. The fitted V79 cell survival curves, at 50 mm depth, are reproduced in figure 5.2. If it assumed that this degree of cell sparing at low dose will be similar in healthy brain, then these figures can be used to predict the 'high dose rate equivalent' of a dose delivered at low dose rate. The cell responses seen in 5.2 have a negligible beta component in the LQ fit, so for an equivalent biological effect we can write;

$$\alpha_{LDR} D_{LDR} = \alpha_{HDR} D_{HDR} \tag{5.1.4}$$

Where α_{LDR} is the α constant for the low dose rate exposure, D_{LDR} is the dose for the low dose rate exposure. α_{HDR} is the α constant for the high dose rate exposure, D_{HDR} is the dose for the high dose rate exposure. Solving for D_{HDR} gives;

$$D_{HDR} = \frac{\alpha_{LDR} D_{LDR}}{\alpha_{HDR}} \tag{5.1.5}$$

Using the values of α_{LDR}=0.4288 and α_{HDR}=0.7705 from figure 5.2 and a D_{LDR} of 11.6 Gy-Eq allows us to calculate that giving the maximum healthy tissue dose at low dose rate is equivalent to giving only 6.5 Gy-Eq at high dose rate. Irradiations at 50 ppm of boron-10 were only carried out at a single, low, dose rate. However, results at this low dose rate matched predictions from previous cell work, with individual dose components, at high dose rate. It can therefore be inferred that any dose rate effect at this high boron concentration is negligible. Consequently the dose to tumour, at low dose rate, would remain at 58.7 Gy-Eq.

These two results raise the possibility that delivering BNCT treatments at low overall dose rates could have a significant clinical advantage, with a approximate doubling of the tumour dose being possible for the same effect on healthy tissue.

The dose rate results presented here are a small data set and have some significant issues. The most serious is the uncertainty over the apparent large error in the survival responses obtained at MIT. With this in mind, drawing firm conclusions is difficult. Future experiments are likely to use Birmingham's beam, when available, at varying dose rates and boron concentrations. Initial determinations will essentially repeat the MIT low dose rate exposures, with 10 ppm of boron-10.

5.1.2 Impact of Synergistic Effects

To date it has been assumed that the various dose components of differing LET act independently; there is no interaction term in equation 5.1.1. The data presented earlier in this report, along with the historical findings of McNally *et al* [1] demonstrate that this is not always a valid assumption. Irradiation with high and low LET radiation simultaneously can have a greater effect than is expected from the same doses, of the same radiation, given independently. The problem is how to treat this in the context of BNCT treatment planning. Hopewell *et al* [68] suggest approaching the problem by considering the synergistic effect as an increase in RBE of the photon component, in the same way the dose rate is treated as an effective decrease. This may not reflect the physical mechanism of the synergistic effect but it provides a convenient methodology to introduce a synergistic factor. Establishing the size of this 'Dose Enhancement Factor' (DEF) to account for synergy is not straightforward. It is clear both from the results presented here and by McNally *et al* [1] that the factor is different at different dose levels. This is further emphasised by the failure of Barendsen *et al* [38] to observe a synergistic effect at low alpha particle doses.

Despite the differences between the data for synergistic effects presented by McNally *et al*[1] and the data presented here there are enough similarities for some speculative conclusions about impact in BNCT to be drawn. McNally *et al* showed a strong synergistic effect with combined 2.5 Gy alpha particle and photon exposures. The more recent data shows a strong effect with 3.18 Gy of alpha particles and photons. Despite the differing alpha doses the level of effect, as a fraction of expected survival, seen in the two studies was similar when the low-LET component of the exposure made up approximately 60% or less of the total physical dose.

The data for the X-ray only data and the mixed 3.18 Gy plus X-ray curves presented in section 3.6.2 can be used to calculate values of the DEF for varying mixes. Figure 5.3 shows a plot of the X-ray data vs a curve generated by dividing the mixed field data by the corresponding alpha particle only surviving fraction. DEF at any given endpoint can then

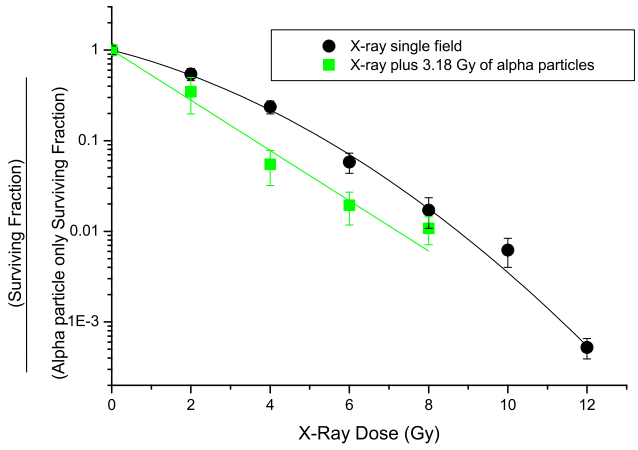

Figure 5.3: *Comparison of mixed field results with 3.18 Gy of alpha particles plus X-rays with X-ray single field data. Mixed field data has been divided by the equivalent alpha particle only, single field, survival. The difference between the curves is therefore the synergistic 'enhancement' effect.*

be calculated from the values plotted in this curve, in a similar manner to RBE, that is;

$$DEF = \frac{X - ray\ dose}{Mixed\ field\ X - ray\ dose} \tag{5.1.6}$$

For the purposes of comparison, a DEF was calculated as a function of low-LET fraction rather than absolute dose. The DEF at every point in the depth-dose curve could then be introduced into equation 5.1.1;

$$D_w = (d_\gamma \times DRF \times DEF) + (d_n \times RBE_n) + (d_N \times RBE_N) + ({}^{10}B \times CBE) \tag{5.1.7}$$

As in the DRF example, a depth dose curve accounting for synergy can then be produced. DEF at 20 mm depth with 18 ppm of boron was calculated as 1.73. The 11.6 Gy-eq for healthy tissue, as calculated earlier, therefore becomes 14.2 Gy-eq once synergy is accounted for. DEF at 32.5 mm depth with 62.5 ppm boron is calculated as 2.12, the corresponding tumour dose is 62.6 Gy-eq. DRF was assumed to be unity.

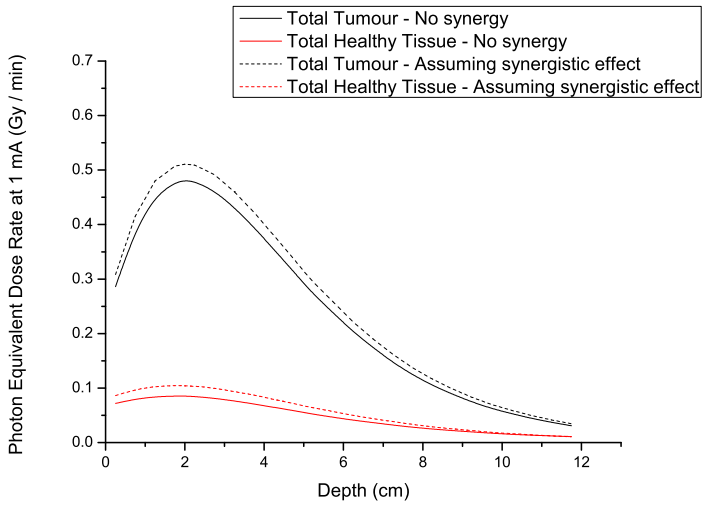

Figure 5.4: *Calculated depth dose curve for the Birmingham beam with a synergistic effect assumed and no dose rate effect*

It is unclear how directly applicable the synergy factors used to generate figure 5.4 would be in a clinical BNCT situation. Implicit in this calculation of DEF is the assumption that the degree of synergy seen is dependant on the fractions of the different LET components rather than the absolute dose. Both the present study and McNally *et al* found that the amount of synergistic effect appeared to vary significantly with total high LET dose and this has not been accounted for in the calculations presented. Investigating clinically relevant high LET doses to tumour, in mixed fields, in cell culture experiments has large practical difficulties due to the low survival levels involved. Rather than directly comparable exposures, more fundamental work understanding the mechanism of synergy will need to be carried out. Clinical dose strategies can then be based on more sophisticated models informed by this work.

5.1.3 RBE of High LET Components

Further complications are introduced by the proton and fast neutron dose components. The RBE of neutrons can vary significantly with neutron energy, from 1.7 to as high as 6 [188]. Despite this, equivalent dose calculations for BNCT where fast neutron dose is considered as

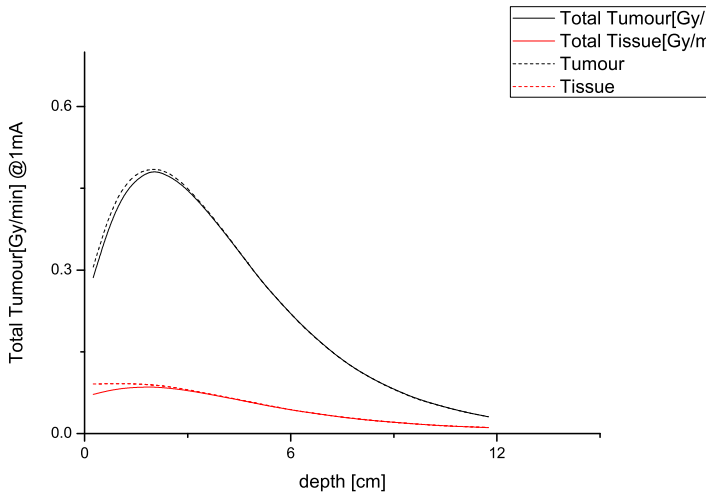

Figure 5.5: *Calculated depth dose curve for the Birmingham beam with an RBE of 6 assumed for the fast neutron component.*

a separate factor have tended to use a fixed neutron RBE. Similarly proton RBE has been shown to vary in the approximate range of 1 to 3, depending on energy, by Belli *et al* [189]. In treatment planning this dose is often combined with the fast neutron dose as a grouped high LET beam component with a single fixed RBE. This is considered a not unreasonable simplification as the high LET component is generally only of the order of 2 or 3% of the total physical dose in irradiations where clinically relevant levels of boron are present.

The impact of these RBE uncertainties can be seen in figure 5.5, where the fast neutron components of the dose have been assigned an RBE of 6.

A further potential uncertainty lies in the use of fixed RBE's for all dose components when deriving photon equivalent doses. As discussed in section 2.1.2, a given RBE is only valid for a fixed dose; RBE decreases as dose is increased. This consideration also applies to CBE. The widely used CBE value of 3.8 in tumour, quoted in this section and used for comparison, was taken as an average from experiments described in [94] where CBE was derived at *in vivo* survival levels of 0.1, 0.01 and 0.001. Corresponding CBE's were 4, 3.8 and 3.6. The small variation was due to the near linearity of the X-ray curve at these survival levels. As the doses used were relevant to single dose clinical levels (>10Gy-eq),

and BNCT tends to be delivered in a single large fraction, it has been assumed that using a fixed average of these values is a reasonable assumption [30].

If a different fractionation schedule for BNCT is adopted then uncertainties from the use of fixed RBE's and CBE's will become more of a concern. It is possible that modifications of the BED concept, intended for use in high LET therapy, may be of use in addressing these issues [190].

5.2 Summary

Based on the work presented in this thesis, both dose rate and synergistic interactions can make a significant difference to the biological effect of a given dose delivered by a BNCT beam.

In BNCT treatment planning to date dose rate has been treated only via an approximate factor introduced into the photon component when calculating total photon equivalent dose delivered. The cell culture work carried out at MIT and presented here demonstrates that this may lead to an underestimate of the degree of dose rate sparing, particularly in healthy tissue. Caution needs to be exercised when interpreting this result due to uncertainties over absolute doses delivered in the MIT beam. However, it is clear that further work is warranted in this area.

Synergistic interactions have been demonstrated in mixed X-ray and alpha particle fields, with lower cell survival observed than predicted from individual components. This is important in BNCT as, if similar levels of interaction are seen in BNCT mixed fields, photon-equivalent doses change significantly. There is evidence both from the work presented here and from previously published work [1][38] that the amount of synergistic effect seen varies according to high LET dose. There also appears to be a dependance on exact cell growth conditions.

In general the mechanism of synergy is poorly understood, although recent work on

DNA damage response in mixed fields is beginning to shed some light on the processes involved [163]. Direct measurements to quantify synergy *in vitro* at the high doses involved in therapy are impractical. Better models to account for the synergistic effect therefore need to be developed. Simple models to fit mixed field survival data of the type proposed by Zaider and Rossi [112] are not adequate in isolation for predicting the outcome of mixed field exposures. While they provide good fits to some data exhibiting a synergistic effect, other data is fitted poorly. Some improvement can be made through differing treatments of the constants used but a more complex approach is probably necessary.

Work with track structure models such as LEM has been incorporated into carbon ion treatment planning codes successfully [191]. Similar models with dose rate and synergy effects accounted for may be the correct approach for BNCT. Such models will need to be informed by considerable amounts of further fundamental biology work.

The data presented in this report emphasises the fact that radiobiology in a BNCT environment is not straightforward. Translation of clinical experiences between facilities, whether in planning or analysis of outcomes, requires reference to detailed biological work at both sites. It has been demonstrated that, due to synergistic and dose rare effects, RBE's calculated for one beam should not be simplistically transferred to another.

5.3 Future Work

Funding has been allocated under the Knowledge Transfer Secondment(KTS) scheme for a series of experiments that will build on the work presented in this report. The project will be lead by the Professor of Neurosurgery and involve cooperation with several clinical scientists based at University Hospital Birmingham. Tissue samples will be acquired during the surgical debulking of patient tumours. An identical procedure to that used in prior drug uptake studies[59] will be followed, with a number of small samples being acquired simultaneously using a side cutting needle. Ethical approval to store and carry out a study

with patient samples has already been granted (REC reference 05/Q2704/61).

Once samples have been obtained they will be prepared for tissue culture and incubated. In parallel with this, other samples will be tested for expression of the large neutral amino acid transporter (LAT1). It is believed from the work published by the Birmingham group in Cancer Research in 2009[59] that cellular uptake of the candidate drug for BNCT, boron phenylalanine (BPA), is highly dependent on LAT1 expression.

The bulk tumour samples will be incubated in BPA concentrations which are realistic for human treatments, and will then receive clinically relevant doses of neutrons. Samples prepared in parallel will be irradiated with X-rays using the standard hospital radiotherapy machines. A final group will receive X-ray irradiation and a 'boost' dose of neutrons. This group is representative of our proposed patient treatment methodology. Damage to the tumour cells will be evaluated using a γH2Ax stain to identify double strand DNA breaks, following the methodology of Merz *et al.*

In parallel with this work survival studies will be carried out using cells from the M059K and M059J cell lines, which are derived from humour tumours.

A study such as this, with greater effect shown in a human tumour system than existing treatment, is a necessity for clinical trials at Birmingham to proceed. With a sufficiently comprehensive *in vitro* study, with bulk tumour samples, an *in vivo* animal study will not be necessary to show efficacy. With recent renovation of the dynamitron completed, and appropriate medical expertise in place, an effectiveness comparison study remains the last significant obstacle to phase one patient trials beginning within the next few years.

Further work will also be carried out using the 'jellyfish' dish system described on page 168. A comprehensive dose-survival curve for single and double sided boron loading will be constructed and compared to simulations.

To reduce patient treatment times significant dynamitron upgrades are planned to increase usable proton beam current from 1mA to 5mA or more. This will require an upgrade of the target cooling system, currently limited to removing 6kW of heat continuously. A

redesign and implementation of a new, modern, ion source is also required. In parallel with these machine upgrades the beam monitoring and closely related safety systems will be comprehensive overhauled and modernised. This involves rewriting the monitoring software in the latest version of LabView from National Instruments. Outdated data acquisition cards have been replaced with newer equivalents and the target monitoring thermocouples have been checked and overhauled.

Once beam upgrades are complete survival experiments similar to those at MIT can be carried out at a range of dose rates and boron concentrations. This will provide further valuable data on the dose rate effect in BNCT treatment beams.

5.4 Publications and presentations arising from this project

Experimental work detailed in this report has been presented at the Young BNCT investigators meetings at Birmingham in 2007 and Mainz in 2009, where it received an award for best poster. It was also presented at the Associated for Radiation Research annual meeting in 2008. A paper was submitted and data presented at the 13th International Congress for Neutron Capure Therapy, 2008, which received the Fairchild Award. This paper was published in [192]. Further data was presented at the 14th ICNCT in 2010.

Papers detailing the X-ray, alpha mixed field work and the BNCT dose rate effect work are being prepared for publication.

Appendix A

FORTRAN CHI SQUARED MINIMISATION PROGRAM

Chi square fitting arrives at fit parameters by finding values that minimise the value of the Chi squared statistic;

$$\chi^2 = w_i \sum_{i=1}^{n} y_i - y_i^t h \tag{A.0.1}$$

This chi squared function has a parabolic shape around it's minimum value, as shown in figure A.1. A FORTRAN program was written which solves for the value of the minimum of such a parabola.

The program was adapted from one previously written by the author to fit a double exponential to a radioactive decay curve.

```
      program new
      implicit none
      integer i,j,k,ic/0/,direction/-1/,z
      double precision time(500),cnts(500),err(500),line(3),
     &test(500),chi(3),chibest,a,inca,
     &b,l1,l2,doexp,t/0/,abest,bbest,l1best,l2best,
     &incl1,incb,incl2,change/1e10/,dochi,hold(2),
     &vary(3),chinew/0/,prev/1e10/
      real multi,inc/1/,tolerance
      character name*16,choice*1
      logical check/.true./,firstloop/.true./,ndone/.true./,
     &nfinished/.true./,failed/.false./

C**********************************************************************
C Program body
c**********************************************************************
c get the data file name and load the values into arrays (using getdata
c subroutine)

   21 write(6,666)
   70 write(6,*) 'Please enter the data file name'
      write(6,*) '(including extension, e.g. myfile.csv)'
```

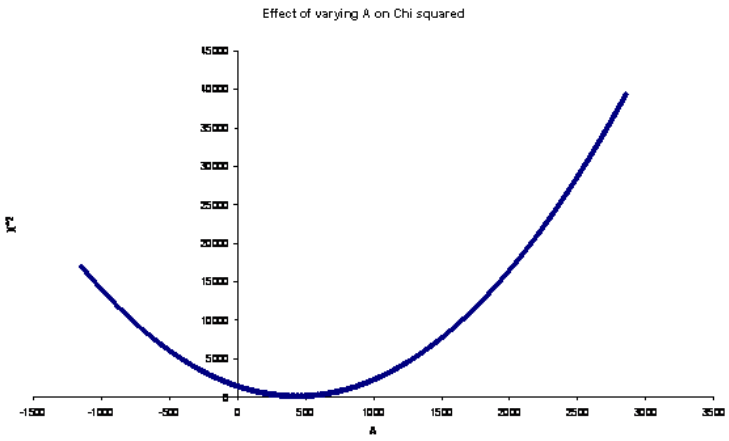

Figure A.1: *Plot showing the shape of the Chi squared function around a minimum.*

```
      write(6,*)
      write(6,*) 'All files must be in comma delimited format.'
      write(6,*) '(The example data is stored in data.csv)'
      read(*,'(a)',err=70) name
      inquire(file=name,exist=check)

      if(check) then
            call getdata(name,time,cnts,err,ic,failed)
      else
            write(6,*) 'File does not exist'
            goto 70
      endif
      if(failed) stop


c we went round the loop one too many times so array element=ic is empty
c and we need to discard it

      ic=ic-1

c Setup of initial values for increment and 'best' variables
c includes a call to guess subroutine to initialise A,B,lambda1,lambda2
c with sensible starting values

      call guess(a,b,l1,l2,cnts,time,ic)
      abest=a
      bbest=b
      l1best=l1
      l2best=l2
      inca=a/100
      incb=b/100
      incl1=l1/100
      incl2=l2/100

      do 40 k=1,ic
             t=time(k)
             test(k)=doexp(a,b,l1,l2,t)
             chinew=chinew+dochi(test(k),cnts(k),err(k))
   40 continue

      chibest=chinew

      write(6,666)
      write(6,*) 'Initial values:'
      write(6,*)'A=',a
      write(6,*)'B=',b
      write(6,*)'l1=',l1
      write(6,*)'l2=',l2
      write(6,*)'Initial chi=',chibest
      write(6,*)
      write(6,*)

c read in the tolerance value - this controls how many times the program loops

  90  write(6,*)'Please enter % change to stop iterating at'
      write(6,*)'A value of 0.1 is recommended'

      read(*,*,err=90) tolerance
```

```
      if(tolerance.le.0) goto 90
      tolerance=tolerance/100


c ******************Iteration loops block starts here**********************
c outer loop ends at 999

      do 999,while(nfinished)

c Loop to find parameter A
      chinew=0

      do 41 k=1,ic
            t=time(k)
            test(k)=doexp(a,b,l1,l2,t)
            chinew=chinew+dochi(test(k),cnts(k),err(k))
   41  continue

      chibest=chinew

c Work out direction of decreasing chi squared

      inca=inca*inc
      do 2 z=1,2
        chinew=0
        do 1 k=1,ic
             t=time(k)
             test(k)=doexp(a,b,l1,l2,t)
             chinew=chinew+dochi(test(k),cnts(k),err(k))
   1    continue
        if(chinew.gt.chibest) direction=direction*(-1)
        a=a+(inca*direction)
   2   continue
       inca=inca*direction

c Loop adds increments until chi increases

       do 4, while(ndone)
        chibest=chinew
        chinew=0
        do 3 k=1,ic
             t=time(k)
             test(k)=doexp(a,b,l1,l2,t)
             chinew=chinew+dochi(test(k),cnts(k),err(k))
   3    continue


c Keeps 3 most recent chi squares
        hold(1)=chi(2)
        hold(2)=chi(3)
        chi(3)=chinew
        chi(2)=hold(2)
        chi(1)=hold(1)

c Find the parabola minimum if there's a chi increase

        if(chinew.gt.chibest) then
         abest=a-(inca*(((chi(3)-chi(2))/(( chi(3)-
     &   (2*chi(2)))+chi(1))+0.5))))
         ndone=.false.
        endif
       a=a+inca

    4   continue
      a=abest
      ndone=.true.
      chinew=0



c Loop to find parameter B
c set chibest to appropriate (i.e. lowest so far!) value

      do 43 k=1,ic
            t=time(k)
            test(k)=doexp(a,b,l1,l2,t)
            chinew=chinew+dochi(test(k),cnts(k),err(k))
   43  continue
      chibest=chinew

c Work out direction of decreasing chi squared
      incb=incb*inc


      do 6 z=1,2
        chinew=0
        do 5 k=1,ic
             t=time(k)
             test(k)=doexp(a,b,l1,l2,t)
             chinew=chinew+dochi(test(k),cnts(k),err(k))
```

```
   5    continue
        if(chinew.gt.chibest) direction=direction*(-1)
        b=b+(incb*direction)
   6   continue

       incb=incb*direction

c Loop adds increments until chi increases

       do 8, while(ndone)
        chibest=chinew
        chinew=0
        do 7 k=1,ic
             t=time(k)
             test(k)=doexp(a,b,l1,l2,t)
             chinew=chinew+dochi(test(k),cnts(k),err(k))
   7    continue

c Keeps 3 most recent chi squares
        hold(1)=chi(2)
        hold(2)=chi(3)
        chi(3)=chinew
        chi(2)=hold(2)
        chi(1)=hold(1)

c Find the parabola minimum if there's a chi increase

        if(chinew.gt.chibest) then
         bbest=b-(incb*(((chi(3)-chi(2))/(((  chi(3)-
     &   (2*chi(2)))+chi(1))+0.5))))
         ndone=.false.
        endif
       b=b+incb

    8   continue
      b=bbest
      ndone=.true.
      chinew=0


c Loop to find parameter l1

      do 44 k=1,ic
             t=time(k)
             test(k)=doexp(a,b,l1,l2,t)
             chinew=chinew+dochi(test(k),cnts(k),err(k))
   44  continue
      chibest=chinew
c Work out direction of decreasing chi squared
      incl1=incl1*inc


      do 10 z=1,2
        chinew=0
        do 9 k=1,ic
             t=time(k)
             test(k)=doexp(a,b,l1,l2,t)
             chinew=chinew+dochi(test(k),cnts(k),err(k))
   9    continue
        if(chinew.gt.chibest) direction=direction*(-1)
        l1=l1+(incl1*direction)
   10   continue

       incl1=incl1*direction

c Loop adds increments until chi increases

       do 12, while(ndone)
        chibest=chinew
        chinew=0
        do 11 k=1,ic
             t=time(k)
             test(k)=doexp(a,b,l1,l2,t)
             chinew=chinew+dochi(test(k),cnts(k),err(k))
   11    continue


c Keeps 3 most recent chi squares
        hold(1)=chi(2)
        hold(2)=chi(3)
        chi(3)=chinew
        chi(2)=hold(2)
        chi(1)=hold(1)

c Find the parabola minimum if there's a chi increase

        if(chinew.gt.chibest) then
         l1best=l1-(incl1*(((chi(3)-chi(2))/(((  chi(3)-
     &   (2*chi(2)))+chi(1))+0.5))))
         ndone=.false.
        endif
```

```
       l1=l1+incl1

   12   continue
      l1=l1best
      ndone=.true.
      chinew=0

c Loop to find parameter l2

      do 45 k=1,ic
            t=time(k)
            test(k)=doexp(a,b,l1,l2,t)
            chinew=chinew+dochi(test(k),cnts(k),err(k))
  45  continue
      chibest=chinew

c Work out direction of decreasing chi squared

      incl2=incl2*inc
      do 14 z=1,2
        chinew=0
        do 13 k=1,ic
            t=time(k)
            test(k)=doexp(a,b,l1,l2,t)
            chinew=chinew+dochi(test(k),cnts(k),err(k))
  13    continue
        if(chinew.gt.chibest) direction=direction*(-1)
        l2=l2+(incl2*direction)
  14   continue

       incl2=incl2*direction

c Loop adds increments until chi increases

       do 16, while(ndone)
        chibest=chinew
        chinew=0
        do 15 k=1,ic
            t=time(k)
            test(k)=doexp(a,b,l1,l2,t)
            chinew=chinew+dochi(test(k),cnts(k),err(k))
  15    continue


c Keeps 3 most recent chi squares
        hold(1)=chi(2)
        hold(2)=chi(3)
        chi(3)=chinew
        chi(2)=hold(2)
        chi(1)=hold(1)

c Find the parabola minimum if there's a chi increase

        if(chinew.gt.chibest) then
         l2best=l2-(incl2*(((chi(3)-chi(2))/(((  chi(3)-
     &    (2*chi(2)))+chi(1))+0.5))))
         ndone=.false.
        endif
       l2=l2+incl2

   16   continue
      l2=l2best
      ndone=.true.
      chinew=0


c decide whether or not to stop looping

      change=(prev-chibest)*(100/prev)
      if((change.lt.tolerance).and.(change.gt.0)) nfinished=.false.

c this IF statement introduced to combat 'overshooting':
c program tended to get close to optimal value then start increasing chi again.
c I think because of the way previous chi values are stored in the chi array.
c This IF reduces the a incrementing variable until the prog is back on track

      if(change.lt.0) then
       inc=inc/2
      else
       inc=1
      endif

      prev=chibest


 999  continue
```

```
c Write out the results to screen

      write(6,*) 'A=',abest
      write(6,*) 'Lambda1=',l1best
      write(6,*) 'B=',bbest
      write(6,*) 'Lambda2=',l2best
      write(6,*)'Sum of Chi squared=',chibest
      write(6,*)'Chi squared=',(chibest/(ic-4))
      write(6,*)
  91  write(6,*)'Write results to file?(y/n)'
      read(*,601,err=91) choice

      if((choice.eq.'y').or.(choice.eq.'Y'))
     &call writeout(abest,bbest,l1best,l2best,chibest,ic)



c format statements
 601  format(a1)
 666  format(/////////////////////////////////////////)
      end


c*************************************************************

c START OF FUNCTIONS AND SUBROUTINES

c*************************************************************
c Subroutine to load in the data
c recieves the name variable which contains the filename to be read
c passes back time,cnts,err arrays, ic (number of elements) and failed
c which informs of failed data read

      subroutine getdata(name,time,cnts,err,ic,failed)
      double precision time(500),cnts(500),err(500),line(3)
      integer ic
      character name*16
      logical failed
      open(1,file=name,status='old',err=10)
      rewind(1)
      do
            write(6,*) ic
            ic=ic+1
            read(1,50,end=20,err=10) line
            time(ic)=line(1)
            cnts(ic)=line(2)
            err(ic)=line(3)

      end do
   20 close(1)
      return

   50 format(g12.0,g12.0,g12.0)
      write(6,*)
   10 write(6,*) 'Something file related is broken!'
      write(6,*) 'Most likely, that file is not of the correct'
      write(6,*) 'format or is corrupt.'
      write(6,*)
      write(6,*) 'Failing gracefully(ish).....'
      write(6,*)
      failed=.true.
      end
c*************************************************************
c Function we're using to fit
c takes a,b,l1,l2 for a given value of t
c returns a value for that point

      double precision function doexp(a,b,l1,l2,t)
      double precision a,b,l1,l2,t
      doexp=(a*exp(-l1*t))+(b*exp(-l2*t^2))
      return
      end

c*************************************************************
c Subroutine to 'guess' starting values
c recieves the cnts,time arrays and ic
c l1 and l2 are set equal to the half life
c A is set to the starting value of counts
c B is set (fairly arbitrarily) to 1/2 A

      subroutine guess(a,b,l1,l2,cnts,time,ic)
      double precision time(20),cnts(20),a,b,l1,l2
      integer i,ic
      logical unset/.true./
      a=cnts(1)
      b=a/2

      do 99 i=1,ic
       if((cnts(i).le.b).and.(unset)) then
        write(*,*) cnts(i),b
```

```
        unset=.false.
        l1=0.693/time(i+1)
        write(*,*) time(i+1)
       endif
   99 continue
      l2=l1
      return
      end
c*************************************************************
c Chi calculation function
c calculates a single chi^2 value from given t,c,e

      double precision function dochi(t,c,e)
      double precision t,c,e
      dochi=((t-c)**2)/(e**2)
      return
      end
c*************************************************************

c Subroutine to write out the data
c takes in all calculated variables, doesn't return anything

      subroutine writeout(abest,bbest,l1best,l2best,chibest,ic)
      double precision abest,bbest,l1best,l2best,chibest
      character name*12
      logical check/.false./

  75  write(6,*)'Enter file name:'
      write(6,*)'(12 characters maximum)'
      read(*,*) name
      inquire(file=name,exist=check)
      if(check) then
       write(*,*) 'Sorry, file exists already'
       goto 75
      endif
      open(2,file=name,status='new',err=76)
      rewind(2)
      write(2,*) 'A=',abest
      write(2,*) 'Lambda1=',l1best
      write(2,*) 'B=',bbest
      write(2,*) 'Lambda2=',l2best
      write(2,*)'Sum of Chi squared=',chibest
      write(2,*)'Chi squared=',(chibest/(ic-4))
      close(1)
      return

   76 write(*,*) 'Something file related is broken!'
      end
```

Appendix B

MIXED GAMMA RAY AND ALPHA PARTICLE CELL SURVIVAL DATA

Data from the mixed field exposures using the cobalt-60 source are shown in the table overleaf. Each tabulated survival value represents the mean count from five Petri dishes.

		A	B	C	D	E	Mean	Stdev
	PE	**0.89**	**0.99**	**1.01**	**1.00**	**1.00**	**0.98**	**0.05**
Alpha Dose (Gy)	**Photon Dose (Gy)**							
0.53	0	6.17E-01	3.30E-01	3.46E-01	3.74E-01	3.58E-01	4.05E-01	1.07E-01
0.00	3.4	3.62E-01	1.50E-01	3.51E-01	3.86E-01	3.67E-01	3.23E-01	8.75E-02
0.53	3.4	1.14E-01	1.20E-01	1.50E-01	2.49E-01	1.72E-01	1.61E-01	4.86E-02
1.05	0	2.19E-01	1.32E-01	1.13E-01	2.23E-01	1.72E-01	1.72E-01	4.42E-02
0.00	5.4	2.19E-01	1.48E-01	1.20E-01	2.11E-01	1.75E-01	1.75E-01	3.74E-02
1.05	5.4	3.56E-02	2.14E-02	3.42E-02	3.82E-02	3.24E-02	3.24E-02	5.81E-03
1.58	0	6.48E-02		9.79E-02	9.07E-02	8.41E-02	8.43E-02	1.23E-02
0.00	7.1	8.75E-02		7.68E-02	1.53E-01	6.78E-02	9.62E-02	3.33E-02
1.58	7.1	3.96E-03		4.67E-03	6.98E-03	5.01E-03	5.16E-03	1.12E-03
2.10	0		1.75E-02	3.71E-02		2.74E-02	2.73E-02	7.97E-03
0.00	8.6		2.01E-02	4.57E-02		3.29E-02	3.29E-02	1.05E-02
2.10	8.6		2.68E-04	1.24E-03	4.40E-04	6.46E-04	6.49E-04	3.67E-04

Table B.1: *Mixed gamma ray and alpha particle V79 cell survival data*

Appendix C

MIXED X-RAY AND ALPHA PARTICLE CELL SURVIVAL DATA

Data for the mixed field exposures using the X-ray source are presented overleaf. Each tabulated survival value corresponds to the mean count from five petri dishes.

Label		MRC	A	C	D	E	F	G	H	I	K
PE		**0.67**	**0.38**	**0.23**	**1.00**	**0.91**	**0.59**	**0.63**	**0.70**	**0.89**	**0.72**
X-ray Dose	**Alpha Dose**										
0	0	1.00E+00		1.00E+00	1.00E+00	1.00E+00	1.00E+00	1.00E+00	1.00E+00	1.00E+00	1.00E+00
2	0	2.07E-01	6.00E-01	9.72E-01	2.90E-01	8.82E-01			6.29E-01	4.06E-01	5.42E-01
4	0			2.08E-01	3.31E-01	1.53E-01	4.59E-01	4.49E-01	2.56E-01	1.18E-01	1.39E-01
6	0		5.09E-02		2.95E-02		3.57E-02		4.74E-02	2.14E-02	6.38E-02
8	0			2.71E-02	4.27E-03	6.73E-02	3.26E-03		3.50E-03		
10	0		1.27E-03	3.08E-03		2.69E-03	3.49E-03	4.83E-03			
12	0							4.70E-04			
0	2.54	2.13E-02	3.71E-02	9.32E-02	1.75E-02	2.74E-02	2.73E-02				
2	2.54	1.09E-02	2.39E-03	3.93E-02	9.05E-03	2.55E-02	1.10E-02				
4	2.54	3.84E-03	3.01E-03	7.25E-03	1.22E-02	4.65E-03	8.84E-03				
6	2.54	1.83E-03	3.97E-04	3.07E-03	7.72E-04	1.28E-03	1.70E-03				
8	2.54	3.49E-05	9.27E-04	2.97E-03	5.26E-04	1.15E-04	3.08E-03	9.45E-04			
10	2.54	2.15E-04	4.74E-05	3.71E-04	1.21E-05			5.53E-04			
0	3.18			9.71E-03				1.73E-02	9.33E-03		2.37E-02
2	3.18								6.34E-03	1.22E-03	
4	3.18								5.16E-04	6.54E-05	
6	3.18								2.25E-04	2.17E-05	
8	3.18							9.17E-05	2.00E-05	8.53E-06	

Label		L	M	N	X	Y	Z	AA	AB	AE
PE		**0.73**	**0.76**	**0.76**	**0.94**	**0.60**	**0.41**	**0.99**	**0.20**	**0.38**
X-ray Dose	**Alpha Dose**									
0	0	1.00E+00	1.00E+00			1.00E+00	1.00E+00	1.00E+00	1.00E+00	1.00E+00
2	0		7.00E-01							
4	0				8.64E-02				1.28E-01	3.44E-01
6	0		1.64E-01							
8	0	5.27E-03						3.34E-03	5.23E-02	1.10E-02
10	0				1.86E-02				2.00E-04	4.40E-04
12	0				4.15E-04	9.99E-04	1.62E-04			
0	2.54						8.33E-03	1.35E-03	4.13E-02	5.96E-02
2	2.54									
4	2.54									
6	2.54									
8	2.54			6.48E-04						
10	2.54			3.29E-04	6.21E-04			6.67E-05	8.86E-04	
0	3.18	1.55E-02				2.51E-03	1.99E-03		1.29E-02	
2	3.18	1.17E-02				4.58E-04	3.68E-04			
4	3.18	2.79E-03				1.32E-04	1.54E-04			
6	3.18	6.29E-04			3.01E-04	3.76E-05				
8	3.18	2.80E-04			2.85E-04		1.32E-04	8.33E-05	2.78E-04	

Table C.1: *Mixed 250kVp X-ray and alpha particle V79 cell survival data*

Appendix D

BIRMINGHAM NEUTRON BEAM CELL SURVIVAL DATA

The data for cells irradiated using the Birmingham dynamitron neutron beam are presented in this section. All irradiations were carried out with cells loaded with 50μg per gram enriched boric acid. Data for two depths inside the full scatter water phantom are presented; 20mm and 50mm. All survival values represent the mean count from five petri dishes. Quoted doses are the combined physical, unweighted, doses from all components.

Plating efficiency	**0.52 ±0.06**	
20mm Depth		
Total Physical Dose [Gy]	**SF**	**Uncertaintity in SF**
0.45	1.00E+00	4.00E-02
0.55	3.12E-01	1.84E-02
0.71	3.01E-01	1.46E-02
0.74	1.83E-01	2.04E-02
0.86	2.25E-01	1.78E-02
0.87	2.08E-01	4.95E-03
0.88	1.99E-01	9.79E-02
1.95	4.29E-02	1.84E-02
2.23	3.80E-02	5.11E-03
3.09	4.01E-02	7.50E-03
3.41	2.04E-02	5.79E-04
50mm Depth		
Total Physical Dose [Gy]	**SF**	**Uncertaintity in SF**
0.27	4.01E-01	1.08E-02
0.52	4.32E-01	5.39E-02
0.54	2.86E-01	5.43E-02
0.54	3.79E-01	3.73E-02
1.32	1.75E-01	5.53E-03
1.55	2.07E-01	1.87E-02
1.83	8.80E-02	4.04E-03
2.49	4.75E-02	5.95E-03

Table D.1: *Birmingham neutron beam cell survival data, cells loaded with 50µg per gram enriched boric acid*

Appendix E

MIT NEUTRON BEAM CELL SURVIVAL DATA

The data for cells irradiated using the MIT FCB, at two dose rates, are presented in this section. Data for two depths inside the full scatter water phantom, 20mm and 50mm. Quoted doses are the combined physical, unweighted, doses from all components at the stated boron level.

Raw data is included for plating efficiency comparisons.

20mm depth, high dose rate												
Total Dose (Gy) 50ppm	Total Dose (Gy) 10ppm	Irradiation time (minutes)	Plated						Mean	Survival	Adj. Survival	PE
10.18	3.92	4.5	15000	13	12	13	64	70	34.4	2.29E-03	8.47E-03	0.27
10.25	3.94	4.5	7500	110	113	92	80	63	91.6	1.22E-02	4.51E-02	0.27
9.94	3.82	4.5	15000	500	484	OG	OG	OG	492	3.28E-02	5.89E-02	0.56
10.29	3.96	3	2143	150	160	145	144	151	150	7.00E-02	1.26E-01	0.56
6.85	2.63	3	4286	301	333	331	321	320	321.2	7.49E-02	1.34E-01	0.56
6.75	2.60	3	4286	457	470	444	460	410	448.2	1.05E-01	1.88E-01	0.56
3.18	1.22	1.5	250	36	22	33	30	31	30.4	1.22E-01	2.18E-01	0.56
4.56	1.75	2	500	95	71	59	79		76	1.52E-01	2.73E-01	0.56
4.34	1.67	2	500	40	44	34	39	39	39.2	7.84E-02	2.90E-01	0.27
1.07	0.41	2	417	53	87	63	87	71	72.2	1.73E-01	3.11E-01	0.56
1.66	0.64	3	4286	368	396	412	351	350	375.4	8.76E-02	3.24E-01	0.27
3.40	1.31	1.5	250	19	17	36	20	20	22.4	8.96E-02	3.31E-01	0.27
1.37	0.53	1	214	50	53	50	51	48	50.4	2.36E-01	4.23E-01	0.56
3.18	1.23	1.5	250	19	46	27	29	32	30.6	1.22E-01	4.52E-01	0.27
0.94	0.36	0.5	190	24	21	31	23	27	25.2	1.33E-01	4.90E-01	0.27
2.05	0.79	1	214	61	16	27	30	34	33.6	1.57E-01	5.80E-01	0.27
2.05	0.79	1	214	34	37	37	47	50	41	1.92E-01	7.08E-01	0.27
0.94	0.36	0.5	190	80	91	69	72	70	76.4	4.02E-01	7.21E-01	0.56
2.30	0.89	1	214	102	90	92	75	91	90	4.21E-01	7.55E-01	0.56
1.09	0.42	0.5	188	83	83	84	77	101	85.6	4.55E-01	8.17E-01	0.56

Table E.1: *Survival of V79 cells at 20mm depth, full dose rate in the FCB.*

50mm depth, high dose rate												
Total Dose (Gy) 50ppm	Total Dose (Gy) 10ppm	Irradiation time (minutes)	Plated						Mean	Survival	Adj. Survival	PE
7.29	2.80	4.5	1500	24	20	11	19	20	18.8	1.25E-02	4.63E-02	0.27
4.90	1.89	3	1000	23	33	32	31	30	29.8	2.98E-02	1.10E-01	0.27
4.90	1.89	3	1000	37	40	50	39	26	38.4	3.84E-02	1.42E-01	0.27
4.80	1.85	3	1000	90	108	101	100	97	99.2	9.92E-02	1.78E-01	0.56
7.33	2.82	4.5	750	116	95	65	107	91	94.8	1.26E-01	2.27E-01	0.56
4.83	1.86	3	1000	120	117	160	122	128	129.4	1.29E-01	2.32E-01	0.56
7.36	2.83	4.5	1500	180	244	277	200	170	214.2	1.43E-01	2.56E-01	0.56
3.26	1.25	2	300	25	29	21	16	25	23.2	7.73E-02	2.86E-01	0.27
3.10	1.19	2	300	52					52	1.73E-01	3.11E-01	0.56
3.26	1.26	2	300	32	32	17	29	34	28.8	9.60E-02	3.55E-01	0.27
3.26	1.25	2	300	33	49	89	91	45	61.4	2.05E-01	3.67E-01	0.56
2.28	0.88	1.5	214	38	89	55	50	51	56.6	2.64E-01	4.75E-01	0.56
1.47	0.57	1	176.47	22	60	51	52	55	48	2.72E-01	4.88E-01	0.56
0.67	0.26	0.5	160	48	36	45	44	58	46.2	2.89E-01	5.18E-01	0.56
2.28	0.88	1.5	214	23	36	33	38	28	31.6	1.48E-01	5.46E-01	0.27
1.49	0.57	1	176	35	33	41	29	33	34.2	1.94E-01	7.18E-01	0.27
1.65	0.63	1	176	35	46	27	36	35	35.8	2.03E-01	7.52E-01	0.27
1.65	0.63	1	176	78	75	75	70	85	76.6	4.35E-01	7.81E-01	0.56
0.67	0.26	0.5	160	40	40	36	38	39	38.6	2.41E-01	8.91E-01	0.27
0.78	0.30	0.5	158	103	61				82	5.19E-01	9.31E-01	0.56
2.28	0.88	1.5	214	31	68	74	68	46	57.4	2.68E-01	9.91E-01	0.27

Table E.2: *Survival of V79 cells at 50mm depth, full dose rate in the FCB.*

20mm depth, low dose rate												
Total Dose (Gy) 50ppm	Total Dose (Gy) 10ppm	Irradiation time (minutes)	Plated						Mean	Survival	Adj. Survival	PE
15.85	6.10	90	15000	100	41	230	58	103	106.4	7.09E-03	1.45E-02	0.49
15.97	6.14	90	15000	359	360	355	360	361	359	2.39E-02	3.63E-02	0.66
15.97	6.14	90	15000	394	402	420	398		403.5	2.69E-02	5.51E-02	0.49
10.37	3.99	60	1000	41	75	40	70	72	59.6	5.96E-02	1.22E-01	0.49
3.49	1.34	20	214	51	43	38	33	50	43	2.01E-01	3.05E-01	0.66
3.44	1.32	20	214	49	58	65	59	58	57.8	2.70E-01	5.54E-01	0.49
1.78	0.68	10	188	75	71	75	70	64	71	3.78E-01	7.74E-01	0.49
1.76	0.68	10	188	119	110	80	166	105	116	6.17E-01	9.37E-01	0.66

Table E.3: *Survival of V79 cells at 20mm depth, reduced dose rate in the FCB.*

50mm depth, low dose rate												
Total Dose (Gy) 50ppm	Total Dose (Gy) 10ppm	Irradiation time (minutes)	Plated						Mean	Survival	Adj. Survival	PE
10.91	4.20	90	1500	131	137	142	131	145	137.2	9.15E-02	1.87E-01	0.49
10.99	4.23	90	1500	183	184	250			205.6667	1.37E-01	2.08E-01	0.66
10.99	4.23	90	750	67	77	90	80	82	79.2	1.06E-01	2.16E-01	0.49
7.14	2.75	60	1000	161	159	156	150	155	156.2	1.56E-01	3.20E-01	0.49
2.37	0.91	20	176	36	54	54	55	60	51.8	2.94E-01	6.03E-01	0.49
3.53	1.36	30	176	53	51	54			52.66667	2.99E-01	6.13E-01	0.49
2.40	0.92	20	176	80	70	120	82	72	84.8	4.82E-01	7.32E-01	0.66
1.21	0.47	10	158	67	67	52	55	60	60.2	3.81E-01	7.81E-01	0.49
1.22	0.47	10	158	158	170	169	155	108	152	9.62E-01	1.46E+00	0.66

Table E.4: *Survival of V79 cells at 50mm depth, reduced dose rate in the FCB.*

List of references

[1] Nicolas J. McNally, Jennifer de Ronde, and Melvyn Folkard. Interaction between X-ray and a-particle Damage in V79 Cells. *International Journal of Radiation Biology*, 53(6):917–920, 1988.

[2] G. Gordon Steel, Judith M. Deacon, Gillian M. Duchesne, Alan Horwich, Lloyd R. Kelland, and John H. Peacock. The dose-rate effect in human tumour cells. *Radiotherapy and Oncology*, 9(4):299 – 310, 1987.

[3] Detlef Gabel, Ralph G. Fairchild, Brje Larsson, and Hans G. Brner. The Relative Biological Effectiveness in V79 Chinese Hamster Cells of the Neutron Capture Reactions in Boron and Nitrogen. *Radiation Research*, 98(2):307–316, 1984.

[4] Lawrence S. Chin and William Regine. *Principles and Practice of Stereotactic Radiosurgery*. Springer, 2008.

[5] K S Krane. *Introductory Nuclear Physics, 2nd ed.* John Wiley and Sons, 1988.

[6] Rolf F. Barth, Jeffrey A. Coderre, M. Graa H. Vicente, and Thomas E. Blue. Boron Neutron Capture Therapy of Cancer: Current Status and Future Prospects. *Clinical Cancer Research*, 11(11):3987–4002, 2005.

[7] D. Williams Parsons, Sian Jones, Xiaosong Zhang, Jimmy Cheng-Ho Lin, Rebecca J. Leary, Philipp Angenendt, Parminder Mankoo, Hannah Carter, I-Mei Siu, Gary L. Gallia, Alessandro Olivi, Roger McLendon, B. Ahmed Rasheed, Stephen Keir, Tatiana Nikolskaya, Yuri Nikolsky, Dana A. Busam, Hanna Tekleab, Jr. Diaz, Luis A., James Hartigan, Doug R. Smith, Robert L. Strausberg, Suely Kazue Nagahashi Marie, Sueli Mieko Oba Shinjo, Hai Yan, Gregory J. Riggins, Darell D. Bigner, Rachel Karchin, Nick Papadopoulos, Giovanni Parmigiani, Bert Vogelstein, Victor E. Velculescu, and Kenneth W. Kinzler. An integrated genomic analysis of human glioblastoma multiforme. *Science*, 321(5897):1807–1812, 2008.

[8] H. Lawson, Prakash Sampath, Eileen Bohan, Michael Park, Namath Hussain, Alessandro Olivi, Jon Weingart, Lawrence Kleinberg, and Henry Brem. Interstitial chemotherapy for malignant gliomas: the Johns Hopkins experience. *Journal of Neuro-Oncology*, 83(1):61–70, 2007.

[9] Fulton DS, Urtasun RC, Scott-Brown I, Johnson ES, Mielke B, Curry B, Huyser-Wierenga D, Hanson J, and Feldstein M. Increasing radiation dose intensity using

hyperfractionation in patients with malignant glioma Final report of a prospective phase I and II dose response study. *Journal of Neuro-Oncology*, 14:63 – 72, 1992.

[10] William H. Sweet. Early history of development of boron neutron capture therapy of tumors. *Journal of Neuro-Oncology*, 33:19–26, 1997.

[11] Daniel N. Slatkin. A history of boron neutron capture therapy of brain tumours postulation of a brain radiation dose tolerance limit. *Brain*, 114(4):1609–1629, 1991.

[12] J. O. Archambeau. The effect of increasing exposures of the ^{10}b(n,α)^{7} li reaction on the skin of man. *Radiology*, 94:179–187, 1970.

[13] A. L. Soloway, R . L. Wright, and J. R. Messer. Evaluation of boron compounds for use in neutron capture therapy of brain tumors. 1. Animal investigations. *J. Pharmacol.*, 134:117–122, 1961.

[14] ARTHUR K. ASBURY, ROBERT G. OJEMANN, SURL L. NIELSEN, and WILLIAM H. SWEET. Neuropathologic study of 14 cases of malignant brain tumor treated by boron-10 slow neutron capture radiation. *Journal of Neuropathology and Experimental Neurology*, 31(2):278–303, 1972.

[15] Yoshinobu Nakagawa and Hiroshi Hatanaka. Boron neutron capture therapy: Clinical brain tumor studies. *Journal of Neuro-Oncology*, 33:105–115, 1997.

[16] George E. Laramore and Alexander M. Spence. Boron neutron capture therapy (BNCT) for high-grade gliomas of the brain: A cautionary note. *International journal of radiation oncology, biology, physics*, 36(1):241–246, 1996.

[17] Eric H. Elowitz, Richard M. Bergland, Jeffrey A. Coderre, Darrel D. Joel, Manjeet Chadha, and Arjun D. Chanana. Biodistribution of p-boronophenylalanine in patients with glioblastoma multiforme for use in boron neutron capture therapy. *Neurosurgery*, 42, 1998.

[18] Aidnag Diaz. Assessment of the results from the phase I/II boron neutron capture therapy trials at the Brookhaven National Laboratory from a clinicians point of view. *Journal of Neuro-Oncology*, 62(1):101–109, 2003.

[19] Chanana AD, Capala J, Chadha M, Coderre JA, Diaz AZ, Elowitz E H, Iwai J, Joel DD, Liu HB, Ma R, Pendzick N, Peress NS, Shady MS, Slatkin DN, Tyson GW, and Wielopolski L. Boron neutron capture therapy for glioblastoma multiforme: interim results from the phase i/ii doseescalation studies. *Neurosurgery*, 44(6):1182–1192, 1999.

[20] Paul Busse, Otto Harling, Matthew Palmer, W. Kiger, Jody Kaplan, Irving Kaplan, Cynthia Chuang, J. Goorley, Kent Riley, Thomas Newton, Gustavo Cruz, Xing-Qi Lu, and Robert Zamenhof. A critical examination of the results from the Harvard-MIT NCT program phase I clinical trial of neutron capture therapy for intracranial disease. *Journal of Neuro-Oncology*, 62(1):111–121, 2003.

[21] Roger Stupp, Warren P. Mason, Martin J. van den Bent, Michael Weller, Barbara Fisher, Martin J.B. Taphoorn, Karl Belanger, Alba A. Brandes, Christine Marosi, Ulrich Bogdahn, Jrgen Curschmann, Robert C. Janzer, Samuel K. Ludwin, Thierry Gorlia, Anouk Allgeier, Denis Lacombe, J. Gregory Cairncross, Elizabeth Eisenhauer, and Ren Mirimanoff. Radiotherapy plus Concomitant and Adjuvant Temozolomide for Glioblastoma. *New England Journal of Medicine*, 352(10):987–996, 2005.

[22] Jacek Capala, Britta H.-Stenstam, Kurt Skld, Per af Rosenschld, Valerio Giusti, Charlotta Persson, Eva Wallin, Arne Brun, Lars Franzen, Jrgen Carlsson, Leif Salford, Crister Ceberg, Bertil Persson, Luigi Pellettieri, and Roger Henriksson. Boron neutron capture therapy for glioblastoma multiforme: clinical studies in sweden. *Journal of Neuro-Oncology*, 62:135–144, 2003.

[23] K Skold, T Gorlia, L Pellettieri, V Giusti, B H-Stenstam, and J W Hopewell. Boron neutron capture therapy for newly diagnosed glioblastoma multiforme: an assessment of clinical potential. *Br J Radiol*, 83(991):596–603, 2010.

[24] J. Burian, M. Marek, J. Rataj, S. Flibor, J. Rejchrt, L. Viererbl, F. Sus, H. Honova, L. Petruzelka, K. Prokes, F. Tovarys, V. Dbaly, V. Benes, P. Kozler, J. Honzatko, I. Tomandl, and V. Mares. Report on the first patient group of the phase i bnct trial at the lvr-15 reactor. *Developments in Neuroscience. Proceedings of the 3rd International Mt. Bandai Symposium for Neuroscience*, 1259:27 – 32, 2004.

[25] Heikki Joensuu, Leena Kankaanranta, Tiina Seppälä, Iiro Auterinen, Merja Kallio, Martti Kulvik, Juha Laakso, Jyrki Vähätalo, Mika Kortesniemi, Petri Kotiluoto, Tom Serén, Johanna Karila, Antti Brander, Eija Järviluoma, Päivi Ryynänen, Anders Paetau, Inkeri Ruokonen, Heikki Minn, Mikko Tenhunen, Juha Jääskeläinen, Markus Färkkilä, and Sauli Savolainen. Boron Neutron Capture Therapy of Brain Tumors: Clinical Trials at the Finnish Facility Using Boronophenylalanine. *Journal of Neuro-Oncology*, 62(1):123–134, 2003.

[26] T. Yamamoto, A. Matsumura, K. Nakaia, Y. Shibataa, K. Endoa, F. Sakurai, T. Kishi, H. Kumada, K. Yamamoto, and Y. Toriib. Current clinical results of the Tsukuba BNCT trial. *Applied Radiation and Isotopes*, 61(5):1089–1093, 2004.

[27] C.J Tung, Y.L Wang, F.Y Hsu, S.L Chang, and Y-W.H Liu. Characteristics of the new thor epithermal neutron beam for bnct. *Applied Radiation and Isotopes*, 61(5):861 – 864, 2004.

[28] Personal communication from Dr Allah Detta.

[29] H. Tanaka, Y.Sakurai, M. Suzuki, S. Masunaga, T. Mitsumoto, K. Fujita, G. Kahino1, Y. Kinashi1, Y. Liu, M. Takada, K. Ono, and A. Maruhashi. Experimental Demonstration of Beam Characteristics for Cyclotron-Based Epithermal Neutron Source (C-BENS). *Applied Radiation and Isotopes*, 69(12):16421645, 2011.

[30] Jeffrey A. Coderre and Gerard M. Morris. The Radiation Biology of Boron Neutron Capture Therapy. *Radiation Research*, 151(1):1–18, 1999.

[31] Frank Q. H. Ngo, Antun Han, and M. M. Elkind. On the Repair of Sub-lethal Damage in V79 Chinese Hamster Cells Resulting from Irradiation with Fast Neutrons or Fast Neutrons Combined with X-rays. *International Journal of Radiation Biology*, 32(5):507 511, 1977.

[32] P. D. Higgins, Jr. P. M. DeLuca, D. W. Pearson, and M. N. Gould. V79 survival following simultaneous or sequential irradiation by 15-mev neutrons and ^{60}co photons. *Radiation Research*, 95(1):45–56, 1983.

[33] P. D. Higgins, Jr. P. M. DeLuca, and M. N. Gould. Effect of Pulsed Dose in Simultaneous and Sequential Irradiation of V-79 Cells by 14.8-MeV Neutrons and 60 Co Photons. *Radiation Research*, 99(3):591–595, 1984.

[34] Nicolas J. McNally, Jennifer de Ronde, and Margaret Hinchliffe. The Effect of Sequential Irradiation with X-rays and Fast Neutrons on the Survival of V79 Chinese Hamster Cells. *International Journal of Radiation Biology*, 45(4):301 – 310, 1984.

[35] M. C. Joiner, J. C. Bremner, J. Denekamp, and R. L. Maughan. The Interaction between X-rays and 3 MeV Neutrons in the Skin of the Mouse Foot. *International Journal of Radiation Biology*, 46(5):625 638, 1984.

[36] M. S. S. Murthy, U. Madhvanath, P. Subrahmanyam, B. S. Rao, and N. M. S. Reddy. Synergistic Effect of Simultaneous Exposure to ^{60} Co Gamma Rays and 210 Po Alpha Rays in Diploid Yeast. *Radiation Research*, 63(1):185–190, 1975.

[37] R. Railton, R. C. Lawson, and D. Porter. Interaction of gamma-ray and Neutron Effects on the Proliferative Capacity of Chinese Hamster Cells. *International Journal of Radiation Biology*, 27(1):75 82, 1975.

[38] A. J. Vergroesen G. W. Barendsen, T. L. J. Beusker and L. Budke. Effects of Different Ionizing Radiations on Human Cells in Tissue Culture: II. Biological Experiments. *Radiation Research*, 13(6):841–849, 1960.

[39] R. P. Bird, M. Zaider, H. H. Rossi, E. J. Hall, S. A. Marino, and N. Rohrig. The Sequential Irradiation of Mammalian Cells with X Rays and Charged Particles of High LET. *Radiation Research*, 93(3):444–452, 1983.

[40] Yusuke Demizu, Kazufumi Kagawa, Yasuo Ejima, Hideki Nishimura, Ryohei Sasaki, Toshinori Soejima, Toshihiro Yanou, Masakazu Shimizu, Yoshiya Furusawa, Yoshio Hishikawa, and Kazuro Sugimura. Cell biological basis for combination radiotherapy using heavy-ion beams and high-energy X-rays. *Radiotherapy and Oncology*, 71(2):207 – 211, 2004.

[41] Y. Furusawa, M. Aoki, and M. Durante. Simultaneous exposure of mammalian cells to heavy ions and x-rays. *Advances in Space Research*, 30(4):877 – 884, 2002.

[42] Albert H. Soloway, Werner Tjarks, Beverly A. Barnum, Feng-Guang Rong, Rolf F. Barth, Iwona M. Codogni, and J. Gerald Wilson. The Chemistry of Neutron Capture Therapy. *Chemical Reviews*, 98(4):1515–1562, 1998.

[43] Farr LE, Sweet WH, Robertson JS, Foster CG, Locksley HB, Sutherland DL, Mendelsohn M, and Stickley EE. Neutron-capture therapy with boron in the treatment of glioblastoma multiforme. *Am J Roentgenol*, 71:279293, 1954.

[44] J.T. Godwin, L.E. Farr, W.H. Sweet, and J.S. Robertson. Pathological study of eight patients with glioblastoma multiforme treated with by neutron capture radiation using boron 10,. *Cancer (Phil.)*, 8:601–615, 1955.

[45] H. R. Snyder, Albert J. Reedy, and Wm. J. Lennarz. Synthesis of Aromatic Boronic Acids. Aldehydo Boronic Acids and a Boronic Acid Analog of Tyrosine. *Journal of the American Chemical Society*, 80(4):835–838, 1958.

[46] Yutuka Mishima, Masamitsu Iichihashi, Susumu Hatta, Chihiro Honda, Keizo Yamamura, and Toshio Nakagawa. New Thermal Neutron Capture Therapy for Malignant Melanoma: Melanogenesis-Seeking 10B Molecule-Melanoma Cell Interaction From In Vitro to First Clinical Trial. *Pigment Cell Research*, 2(4):226–234, 1989.

[47] J. A. Coderre, J . D. Glass, R. G. Fairchild, P . L. Micca, I. Fand, and D. D. Joel. Selective delivery of boron by the melanin precursor analogue p-boronophenylalanine to tumors other than melanoma. *Cancer Research*, 50(1):138–141, 1990.

[48] Jeffrey A. Coderre, Darrel D. Joel, Peggy L. Micca, Marta M. Nawrocky, and Daniel N. Slatkin. Control of Intracerebral Gliosarcomas in Rats by Boron Neutron Capture Therapy with p-Boronophenylalanine. *Radiation Research*, 129(3):290–296, 1992.

[49] Imahori Y, Ueda S, Ohmori Y, Kusuki T, Ono K, Fujii R, and Ido T. Fluorine-18-labeled fluoroboronophenylalanine PET in patients with glioma. *Nucl Med.*, 39(2):325–33, 1998.

[50] Jeffrey A. Coderre, John D. Glass, Ralph G. Fairchild, Uma Roy, Scott Cohen, and Irwin Fand. Selective Targeting of Boronophenylalanine to Melanoma in BALB/c Mice for Neutron Capture Therapy. *Cancer Research*, 47(23):6377–6383, 1987.

[51] Ono K., Masunaga S.-I., Kinashi Y., Takagaki M., Akaboshi M., Kobayashi T., and Akuta K. Radiobiological evidence suggesting heterogeneous microdistribution of boron compounds in tumors: its relation to quiescent cell population and tumor cure in neutron capture therapy. *International Journal of Radiation Oncology*Biology*Physics*, 34:1081–1086(6), 15 March 1996.

[52] F Yoshida, A Matsumura, Y Shibata, T Yamamoto, H Nakauchi, M Okumura, and T Nose. Cell cycle dependence of boron uptake from two boron compounds used for clinical neutron capture therapy. *Cancer letters*, 187(1):135–141, 2002.

[53] R. RAGHAVAN, P. V. STEART, and R. O. WELLER. Cell proliferation patterns in the diagnosis of astrocytomas, anaplastic astrocytomas and glioblastoma multiforme: a Ki-67 study. *Neuropathology and Applied Neurobiology*, 16(2):123–133, 1990.

[54] Allah Detta and Garth S. Cruickshank. L-Amino Acid Transporter-1 and Boronophenylalanine-Based Boron Neutron Capture Therapy of Human Brain Tumors. *Cancer research*, 69:2126–32, 2009.

[55] D. Gabel, D. Preusse, D. Haritz, F. Grochulla, K. Haselsberger, H. Fankhauser, C. Ceberg, H. D. Peters, and U. Klotz. Pharmacokinetics of $Na_2B_{12}H_{11}SH$(BSH) in patients with malignant brain tumours as prerequisite for a phase I clinical trial of boron neutron capture. *Acta Neurochirurgica*, 139:606–612, 1997.

[56] M. W. Renner, M. Miura, M. W. Easson, and M. G.H. Vicente. Recent progress in the syntheses and biological evaluation of boronated porphyrins for boron neutron-capture therapy. *Anti-Cancer Agents in Medicinal Chemistry (Formerly Current Medicinal Chemistry - Anti-Cancer Agents)*, 6(2):145–157, 2006.

[57] Shinji Kawabata, Weilian Yang, RolfF. Barth, Gong Wu, Tianyao Huo, PeterJ. Binns, KentJ. Riley, Owendi Ongayi, Vijay Gottumukkala, and M.GraaH. Vicente. Convection enhanced delivery of carboranylporphyrins for neutron capture therapy of brain tumors. *Journal of Neuro-Oncology*, 103(2):175–185, 2011.

[58] R. F Barth, W . Yang, J . H. Rotaru, M . L. Moeschberger D, D. Joel, M. M. Nawrocky, J. H. Goodman, and A. H. Soloway. Boron neutron capture therapy of brain tumors: enhanced survival following intracarotid injection of either sodium borocaptate or boronophenylalanine with or without blood-brain barrier disruption. *Cancer Res.*, 57:1129–1136, 1997.

[59] G.S. Cruickshank, D. Ngoga, A. Detta, S. Green, N.D. James, C. Wojnecki, J. Doran, J. Hardie, M. Chester, N. Graham, Z. Ghani, G. Halbert, M. Elliot, S. Ford, R. Braithwaite, T.M.T. Sheehan, J. Vickerman, N. Lockyer, H. Steinfeldt, G. Croswell, A. Chopra, R. Sugar, and A. Boddy. A cancer research uk pharmacokinetic study of bpa-mannitol in patients with high grade glioma to optimise uptake parameters for clinical trials of bnct. *Applied Radiation and Isotopes*, 67(7-8, Supplement 1):S31 – S33, 2009.

[60] Manfred Papaspyrou, Ludwig E. Feinendegen, and Hans-W. Mller-Grtner. Preloading with l-tyrosine increases the uptake of boronophenylalanine in mouse melanoma cells. *Cancer Research*, 54(24):6311–6314, 1994.

[61] Jacek Capala, Michael S. Makar, and Jeffrey A. Coderre. Accumulation of Boron in Malignant and Normal Cells Incubated In Vitro with Boronophenylalanine, Mercaptoborane or Boric Acid. *Radiation Research*, 146(5):554–560, 1996.

[62] US Department of Energy. *Nuclear Physics and Reactor Theory Volume 1*, 1993.

[63] Balendra Sutharshan. *Engineering Design of a Fission Converter-Based Epithermal Beam for Neutron Capture Therapy*. PhD thesis, MIT, 1998.

[64] `http://web.mit.edu/nrl/www/bnct/bnct_home.html,retrieved29/11/2007`.

[65] S. Halfon, M. Paul, D. Steinberg, A. Nagler, A. Arenshtam, D. Kijel, I. Polacheck, and M. Srebnik. High power accelerator-based boron neutron capture with a liquid lithium target and new applications to treatment of infectious diseases. *Applied Radiation and Isotopes*, 67(7-8, Supplement 1):S278 – S281, 2009.

[66] Personal communication from Cecile Wojnecki.

[67] T. Mitsumoto, K. Fujita, T. Ogasawara, H. Tsutsui, S. Yajima, A. Maruhashi, Y. Sakurai, and H. Tanaka. Bnct system using 30 mev h^- cyclotron. *Proceedings of Cyclotrons 2010*, 2010.

[68] J.W. Hopewell, G.M.Morris, A.Schwint, and J.A.Coderre. The radiobiological principles of boron neutron capture therapy: A critical review. *Applied Radiation and Isotopes*, 69(12):17561759, 2011.

[69] Coderre JA, Hopewell JW, Turcotte JC, Riley KJ, Binns PJ, Kiger WS 3rd, and Harling OK. Tolerance of normal human brain to boron neutron capture therapy. *Applied Radiation and Isotopes*, 61(5):10831087, 2004.

[70] Matthew R. Palmer, J.Timothy Goorley, W.S. Kiger III, Paul M. Busse, Kent J. Riley, Otto K. Harling, and Robert G. Zamenhof. Treatment planning and dosimetry for the harvard-mit phase i clinical trial of cranial neutron capture therapy. *International Journal of Radiation Oncology*Biology*Physics*, 53(5):1361 – 1379, 2002.

[71] GF Knoll. *Radiation Detection and Measurement*. John Wiley and Sons, 2000.

[72] J.P. Biersack James F. Ziegler, M.D. Ziegler. Srim the stopping and range of ions in matter. *Nuclear Instruments and Methods in Physics Research Section B: Beam Interactions with Materials and Atoms*, 268(11-12):1818–1823, 2010.

[73] Mason A J. *A Biological Comparison of Epithermal Neutron Beams for BNCT*. PhD thesis, The University of Birmingham, 2004.

[74] Bassler Srensen BS, Overgaard J. In vitro rbe-let dependence for multiple particle types. *Acta Oncologica*, 50:757–762, August 2011.

[75] ICRU. Quantitative concepts and dosimetry in radiobiology (report 30). Technical report, International Commission on Radiation Units and Measurement, 1979.

[76] R.G. Dale and B. Jones. The assessment of rbe effects using the concept of biologically effective dose. *International Journal of Radiation Oncology* Biology* Physics*, 43(3):639–645, 1999.

[77] Albrecht M. Kellerer and Harald H. Rossi. A Generalized Formulation of Dual Radiation Action. *Radiation Research*, 75(3):471–488, 1978.

[78] B. Jones. The apparent increase in the β-parameter of the linear quadratic model with increased linear energy transfer during fast neutron irradiation. *British Journal of Radiology*, 83(989):433–436, 2010.

[79] DT Goodhead. Inactivation and mutation of cultured mammalian cells by aluminium characteristic ultrasoft x-rays. *International Journal of Radiation Biology*, 32(1):43–70, 1977.

[80] Morris GM, Coderre JA, Hopewell JW, Micca PL, Nawrocky MM, Liu HB, and Bywaters A. Response of the central nervous system to boron neutron capture irradiation: evaluation using rat spinal cord model. *Radiotherapy and Oncology*, 32(3):249 – 255, 1994.

[81] Joel S. Bedford and James B. Mitchell. Dose-rate effects in synchronous mammalian cells in culture. *Radiation Research*, 54(2):316–327, 1973.

[82] Fowler JF. Williams MV, Denekamp J. A review of alpha/beta ratios for experimental tumors: implications for clinical studies of altered fractionation. *Int J Radiat Oncol Biol Phys.*, 11(1):87–96, January 1985.

[83] R. P. Hill and R. S. Bush. The effect of continuous or fractionated irradiation on a murine sarcoma. *Br J Radiol*, 46:167–174, 1973.

[84] M.A. Hill, M.T. Herdman, D.L. Stevens, N.J. Jones, J. Thacker, and D.T. Goodhead. Relative sensitivities of repair-deficient mammalian cells for clonogenic survival after α-particle irradiation. *Radiation research*, 162(6):667–676, 2004.

[85] Nandanuri M. S. Reddy, Peter J. Mayer, and Christopher S. Lange. The saturated repair kinetics of chinese hamster v79 cells suggests a damage accumulation-interaction model of cell killing. *Radiation Research*, 121(3):pp. 304–311, 1990.

[86] H. Utsumi and M. M. Elkind. Potentially lethal damage versus sublethal damage: Independent repair processes in actively growing chinese hamster cells. *Radiation Research*, 77(2):pp. 346–360, 1979.

[87] G. P. Raaphorst and W. C. Dewey. A study of the repair of potentially lethal and sublethal radiation damage in chinese hamster cells exposed to extremely hypo- or hypertonic nacl solutions. *Radiation Research*, 77(2):pp. 325–340, 1979.

[88] R. W. DeBlois and C. P. Bean. Counting and sizing of submicron particles by the resistive pulse technique. *Review of Scientific Instruments*, 41(7), February 1970.

[89] M. Zaider and H. H. Rossi. The synergistic effects of different radiations. *Radiation Research*, 83(3):732–739, 1980.

[90] `http://www.cell-lines-service.de/content/e174/e1883/e2047/e1962/index_ger.html`, 11 2010.

[91] Jeffrey A. Coderre and Gerard M. Morris. The Radiation Biology of Boron Neutron Capture Therapy. *Radiation Research*, 151(1), 1999.

[92] Detlef Gabel, Sheila Foster, and Ralph G. Fairchild. The Monte Carlo Simulation of the Biological Effect of the ^{10}b(n, α)^{7}li Reaction in Cells and Tissue and Its Implication for Boron Neutron Capture Therapy. *Radiation Research*, 111(1):14–25, 1987.

[93] Michael A. Davis, John B. Little, K. M. M. S. Ayyangar, and A. R. Reddy. Relative Biological Effectiveness of the ^{10}b(n, α)^{7}li Reaction in HeLa Cells. *Radiation Research*, 43(3):534–553, 1970.

[94] Jeffrey A. Coderre, Michael S. Makar, Peggy L. Micca, Marta M. Nawrocky, Hungyuan B. Liu, Darrel D. Joel, Daniel N. Slatkin, and Howard I. Amol. Derivations of relative biological effectiveness for the high-let radiations produced during boron neutron capture irradiations of the 9l rat gliosarcoma in vitro and in vivo. *International Journal of Radiation Oncology, Biology, Physics*, 27(5):11211129, 1993.

[95] H. Fukuda, J. Hiratsuka, T. Kobayashi, Y. Sakurai, K. Yoshino, H. Karashima, K. Turu, K. Araki, Y. Mishima, and M. Ichihashi. Boron neutron capture therapy (bnct) for malignant melanoma with special reference to absorbed doses to the normal skin and tumor. *Australasian Physical and Engineering Science in Medicine*, 26(3):97–103, 2003.

[96] Daniel W Mundy, Wael Harb, and Tatjana Jevremovic. Radiation binary targeted therapy for her-2 positive breast cancers: assumptions, theoretical assessment and future directions. *Physics in Medicine and Biology*, 51:13771391, 2006.

[97] H. Fukuda, J. Hiratsuka, C. Honda, T. Kobayashi, K. Yoshino, H. Karashima, J. Takahashi, Y. Abe, K. Kanda, M. Ichihashi, and Y. Mishima. Boron Neutron Capture Therapy of Malignant Melanoma Using ^{10}B-Paraboronophenylalanine with Special Reference to Evaluation of Radiation Dose and Damage to the Normal Skin. *Radiation Research*, 138(3):435–442, 1994.

[98] Gerard M. Morris, Jeffrey A. Coderre, John W. Hopewell, Peggy L. Micca, and Mohi Rezvani. Response of rat skin to boron neutron capture therapy with p-boronophenylalanine or borocaptate sodium. *Radiotherapy and Oncology*, 32(2):144 – 153, 1994.

[99] Archambeau JO. Swine skin: a model to evaluate dose recovery from different radiations. *Basic Life Science*, 50:9–20, 1989.

[100] Junichi Hiratsuka, Hiroshi Fukuda, Tooru Kobayashi, Hiroshi Karashima, Kazuo Yoshino, Yoshinari Imajo, and Yutaka Mishima. The Relative Biological Effectiveness of ^{1}0B Neutron Capture Therapy for Early Skin Reaction in the Hamster. *Radiation Research*, 128(2):186–191, 1991.

[101] PR Gavin, CE Dehaan, MP Moore, and JP Weidner. Large animal studies on the use of bnct for the treatment of brain tumors. *Advances in Neutron Capture*, pages 469–475, 1993.

[102] Patrick R. Gavin, Susan L. Kraft, Ren Huiskamp, and Jeffrey A. Coderre. A review: CNS effects and normal tissue tolerance in dogs. *Journal of Neuro-Oncology*, 33:71–80, 1997.

[103] G. M. Morris, J. A. Coderre, J. W. Hopewell, P. L. Micca, M. M.Nawrocky, H. B. Liu, and A. Bywaters. Response of the central nervous system to boron neutron capture irradiation. Evaluation using rat spinal cord model. *Radiology and Oncology*, 32:249–255, 1994.

[104] P. R. Gavin, S . L. Kraft, R . Huiskamp, and J. A. Coderre. A review:CNS effects and normal tissue tolerance in dogs. *Journal of Neuro-Oncology*, 33:71–80, 1997.

[105] Morris G. M., Coderre J. A., Hopewell J. W., Rezvani M., Micca P. L., and Fisher C. D. Response of the central nervous system to fractionated boron neutron capture irradiation: studies with borocaptate sodium. *International Journal of Radiation Biology*, 71(2):185–192, 1997.

[106] J. A. Coderre, G. M. Morris, P. L. Micca, C. D. Fisher, and G. A.Ross. Comparative assessment of single-dose and fractionated boron neutron capture therapy. *Radiation Research*, 144(3):310–317, 1995.

[107] Jeffrey A. Coderre, Gerard M. Morris, Peggy L. Micca, John W. Hopewell, Ilja Verhagen, Bert J. Kleiboer, and Albert J. van der Kogel. Late Effects of Radiation on the Central Nervous System: Role of Vascular Endothelial Damage and Glial Stem Cell Survival. *Radiation Research*, 166(3):495–503, 2006.

[108] R A Rydin, B W Murray, and O L Deutsch. The effect of geometry on capillary wall dose for boron neutron capture therapy. *Physics in Medicine and Biology*, 21(1), 1976.

[109] M. Chadha, J. Capala, J.A. Coderre, E.H. Elowitz, J. Iwai, D.D. Joel, H.B. Liu, L. Wielopolski, and A.D. Chanana. Boron neutron-capture therapy (bnct) for glioblastoma multiforme (gbm) using the epithermal neutron beam at the brookhaven national laboratory. *International Journal of Radiation Oncology* Biology* Physics*, 40(4):829–834, 1998.

[110] J.A. Coderre, E.H. Elowitz, M. Chadha, R. Bergland, J. Capala, D.D. Joel, H.B. Liu, D.N. Slatkin, and A.D. Chanana. Boron neutron capture therapy for glioblastoma multiforme using p-boronophenylalanine and epithermal neutrons: Trial design and early clinical results. *Journal of neuro-oncology*, 33(1):141–152, 1997.

[111] J . THACKER, A. STRETCH, and D. T. GOODHEAD. The mutagenicity of a-particles from Plutonium-238. *Radiation Research*, 92:343–352, 1982.

[112] M. Zaider and H. H. Rossi. The synergistic effects of different radiations. *Radiation Research*, 83(3):732–739, September 1980.

[113] E G A Aird and F T Farmer. The design of a thimble chamber for the farmer dosemeter. *Physics in Medicine and Biology*, 17(2):169, 1972.

[114] D.T. Goodhead, D.A. Bance, A. Stretch, and R.E. Wilkinson. A Versatile Plutonium-238 Irradiator for Radiobiological Studies with α-particles. *International Journal of Radiation Biology*, 59(1):195–210, 1991.

[115] Albert Stretch John Thacker and Dudley T. Goodhead. The mutagenicity of a particles from plutonium-238. *Radiation Research*, 92(2):343–352, November 1982.

[116] B.G. Cartwright, E.K. Shirk, and P.B. Price. A nuclear-track-recording polymer of unique sensitivity and resolution. *Nuclear Instruments and Methods*, 153(2-3):457 – 460, 1978.

[117] R. J. Berry and R. Oliver. Effect of post-irradiation incubation conditions on recovery between fractionated doses of x-rays. *Nature*, 201:94 – 96, 1964.

[118] W. C. Dewey L. F. Winans and C. M. Dettor. Repair of sublethal and potentially lethal x-ray damage in synchronous chinese hamster cells. *Radiation Research*, 52:333–351, 1972.

[119] P. M. Calabro-Jones J. F. Ward, C. L. Limoli and J. Aguilera. An examination of the repair saturation hypothesis for describing shouldered survival curves. *Radiation Research*, 127:90–96, July 1991.

[120] Eric W. Weisstein. Error propagation. From MathWorld–A Wolfram Web Resource. http://mathworld.wolfram.com/ErrorPropagation.html.

[121] Origin (OriginLab, Northampton, MA).

[122] H. Motulsky and A. Christopoulos. *Fitting models to biological data using linear and nonlinear regression: a practical guide to curve fitting.* Oxford University Press, USA, 2004.

[123] L. S. Lasdon, A. D. Waren, A. Jain, and M. Ratner. Design and testing of a generalized reduced gradient code for nonlinear programming. *ACM Trans. Math. Softw.*, 4(1):34–50, March 1978.

[124] William H. Press, Saul A. Teukolsky, and William T. Vetterling. *Numerical Recipes in C, 2nd Edition.* Cambridge University Press, 1992.

[125] OriginLab, Northampton, MA. *Origin 8.5 User Manual.*

[126] M. Folkard, K.M. Prise, B. Vojnovic, S. Davies, M.J. Roper, and B.D. Michael. The irradiation of v79 mammalian cells by protons with energies below 2 mev. *International Journal of Radiation Biology*, 56(3):221–237, 1989.

[127] S. M. Bailey J. B. Mitchell, J. S. Bedford. Dose-rate effects in plateau-phase cultures of s3 hela and v79 cells. *Radiation Research*, 79:552–567, September 1979.

[128] Koyeli Bose Girigoswami and Rita Ghosh. Response to gamma irradiation in v79 cells conditioned by repeated treatment with low doses of hydrogen peroxide. *Radiation and Environmental Biophysics*, 44(2):131–137, 2005.

[129] E Winzel, EJ van der Merwe, W Groenewald, S Pistorius, JP Slabbert, L Robinson, and L Bhm. The relative biological effectiveness of 100 kv x-rays determined by the v-79 cell colony assay. *S Afr Med J*, 71(11), June 1987.

[130] S. Schalla, C. Herskind, K.H. Hver, W.J. Lorenz, and E.W. Hahn. Changes in rbe of 14-mev (d+t) neutrons for v79 cells irradiated in air and in a phantom: Is rbe enhanced near the surface? *Strahlentherapie und Onkologie*, 174(4):204–211, 1998.

[131] RE Durand and RM Sutherland. Effects of intercellular contact on repair of radiation damage. *Experimental cell research*, 71(1):75–80, 1972.

[132] RE Durand. Repair during multifraction exposures: spheroids versus monolayers. *The British Journal of Cancer. Supplement*, 6:203, 1984.

[133] D.J. Gordon, A.E. Milner, R.P. Beaney, D.J. Grdina, and A.T.M. Vaughan. The increase in radioresistance of chinese hamster cells cultured as spheroids is correlated to changes in nuclear morphology. *Radiation research*, 121(2):175–179, 1990.

[134] PL Olive, S. Vanderbyl, and SH MacPhail. Resistance to dna denaturation in irradiated chinese hamster v79 fibroblasts is linked to cell shape. *Experimental cell research*, 193(2):339–345, 1991.

[135] NMS Reddy, AFG Stevenson, and CS Lange. Trypsinization and the radiosensitivity of mitotic and log phase chinese hamster v79 cells exposed to 250 kvp x-rays. *International journal of radiation biology*, 55(1):105–117, 1989.

[136] JD Chapman, RC Urtasun, EA Blakely, KC Smith, and CA Tobias. Hypoxic cell sensitizers and heavy charged-particle radiations. *The British journal of cancer. Supplement*, 3:184, 1978.

[137] M. Belli, R. Cherubini, S. Finotto, G. Moschini, O. Sapora, G. Simone, and MA Tabocchini. Rbe-let relationship for the survival of v79 cells irradiated with low energy protons. *International journal of radiation biology*, 55(1):93–104, 1989.

[138] Shozo Suzuki. The "synergistic" action of mixed irradiation with high-let and low-let radiation. *Radiation Research*, 138(2):297–301, 1994.

[139] MR Raju, SG Carpenter, JJ Chmielewski, ME Schillaci, ME Wilder, JP Freyer, NF Johnson, PL Schor, RJ Sebring, and DT Goodhead. Radiobiology of ultrasoft x rays: I. cultured hamster cells (v79). *Radiation research*, 110(3):396–412, 1987.

[140] Stickler R. Ling CC, Spiro IJ. Dose-rate effect between 1 and 10 gy/min in mammalian cell culture. *Br J Radiol*, 57:723–728, 1984.

[141] C. Frank, K.J. Weber, P. Fritz, and M. Flentje. Increased dose-rate effect in v79-multicellular aggregates (spheroids). relation to initial dna lesions and repair. *Radiotherapy and Oncology*, 26(3):264–270, 1993.

[142] Albrecht M. Kellerer and Harald H. Rossi. A generalized formulation of dual radiation action. *Radiation Research*, 75(3):471–488, September 1978.

[143] A. M. Kellerer and H. H. Rossi. A generalized formulation of dual radiation action. *Radiation Research*, 75:471–488, 1978.

[144] Nicolas J. McNally, Jennifer De Ronde, and Margaret Hinchliffe. Survival of v79 cells following simultaneous irradiation with x-rays and neutrons in air or hypoxia. *International Journal of Radiation Biology*, 48(5):847–855, 1985.

[145] Shozo Suzuki. Survival of chinese hamster v79 cells after irradiation with a mixture of neutrons and ^{60}co γ rays: Experimental and theoretical analysis of mixed irradiation. *Radiation Research*, 133(3):327–333, 1993.

[146] Shozo Suzuki. Assessment of the action of mixed irradiation. *Environmental Health Perspectives*, 105(6), December 1997.

[147] P. D. Higgins, P. M. DeLuca Jr., D. W. Pearson, and M. N. Gould. V79 survival following simultaneous or sequential irradiation by 15-mev neutrons and ^{60}co photons. *Radiation Research*, 95(1):45–56, July 1983.

[148] A.M. Kellerer and H.H. Rossi. *The theory of dual radiation action*, page 133. North-Holland, 1972.

[149] J.B. Mitchell, J.S. Bedford, and S.M. Bailey. Dose-rate effects in mammalian cells in culture. iii. comparison of cell killing and cell proliferation during continuous irradiation for six different cell lines. *Radiation Research*, 79:537–551, September 1979.

[150] M. Zaider and D. J. Brenner. Comments on "v79 survival following simultaneous or sequential irradiation by 15-mev neutrons and 60 co photons" by higgins et al. [radiat. res. 95, 45-56 (1983)]. *Radiation Research*, 99(2):438–441, August 1984.

[151] M. Belli, R. Cherubini, M. Dalla Vecchia, V. Dini, G. Moschini, C. Signoretti, G. Simone, M. A. Tabocchini, and P. Tiveron. Dna dsb induction and rejoining in v79 cells irradiated with light ions: a constant field gel electrophoresis study. *International Journal of Radiation Biology*, 76(8):1095–1104, 2000.

[152] R. B. Hawkins. A microdosimetric-kinetic model of cell death from exposure to ionizing radiation of any let, with experimental and clinical applications. *International Journal of Radiation Biology*, 69(6):739–755, 1996.

[153] Roland B. Hawkins. A microdosimetric-kinetic model for the effect of non-poisson distribution of lethal lesions on the variation of rbe with let. *Radiation Research*, 160(1):61–69, July 2003.

[154] Krasavin EA Kozubek S. Cell sensitivity to irradiation and dna repair processes. ii. the cell sensitivity to ionizing radiation of different lets. *Neoplasma*, 31:685–95, 1984.

[155] G.K.Y. Lam. The survival response of a biological system to mixed radiations. *Radiation research*, 110(2):232–243, 1987.

[156] N. Tilly. Comparison of cell survival models for mixed let radiation. *International journal of radiation biology*, 75(2):233–243, 1999.

[157] DT Goodhead. Initial events in the cellular effects of ionizing radiations: clustered damage in dna. *International journal of radiation biology*, 65(1):7–17, 1994.

[158] PK COOPER LOBRICH and M. B. RYDBERG. Non-random distribution of dna double-strand breaks induced by particle irradiation. *International journal of radiation biology*, 70(5):493–503, 1996.

[159] A. Muslimovic, I.H. Ismail, Y. Gao, and O. Hammarsten. An optimized method for measurement of gamma-h2ax in blood mononuclear and cultured cells. *Nature protocols*, 3(7):1187–1193, 2008.

[160] F.A. Cucinotta and M. Durante. Cancer risk from exposure to galactic cosmic rays: implications for space exploration by human beings. *The lancet oncology*, 7(5):431–435, 2006.

[161] N. Desai, E. Davis, P. O'Neill, M. Durante, FA Cucinotta, and H. Wu. Immunofluorescence detection of clustered γ-h2ax foci induced by hze-particle radiation. *Radiation research*, 164(4):518–522, 2005.

[162] D.T. Goodhead. Energy deposition stochastics and track structure: what about the target? *Radiation protection dosimetry*, 122(1-4):3–15, 2006.

[163] E. Staaf, K. Brehwens, S. Haghdoost, J. Czub, and A. Wojcik. Gamma-h2ax foci in cells exposed to a mixed beam of x-rays and alpha particles. *Genome Integrity*, 3(1):8, 2012.

[164] B. Jones R. Dale. *Radiobiological Modelling in Radiation Oncology*. British Institute of Radiology, 2007.

[165] W.P. Voorbraak. Recommendations for the Dosimetry of Boron Neutron Capture Therapy (BNCT). Technical report, Petten, 2003.

[166] C. P. J. Raaijmakers, E. L. Nottelman, and B. J. Mijnheer. The neutron sensitivity of dosimeters applied to boron neutron capture therapy. *Medical Physics*, 23(1581), 1996.

[167] Ronald D. Rogus, Otto K. Harling, and Jacquelyn C. Yanch. Mixed field dosimetry of epithermal neutron beams for boron neutron capture therapy at the MITR-II research reactor. *Medical Physics*, 21(10):1611–1625, 1994.

[168] Zamir Ghani. *The Physics, Dosimetry and Microdosimetry of BNCT*. PhD thesis, The University of Birmingham, 2012.

[169] Personal communication from Zamir Ghani.

[170] J. T. Goorley and III W. S. Kiger. Reference dosimetry calculations for neutron capture therapy with comparison of analytical and voxel models. *Medical Physics*, 29, 2002.

[171] W.E. Freudenreich. Empirical relations between reaction rates of monitors activated in bnct beams. NRG report 21425/03.55288, 2003. Petten.

[172] Turki Alzahrani. Ion chamber measurements in an epithermal neutron beam. Master's thesis, The University of Birmingham, 2012.

[173] K J Riley, P J Binns, and O K Harling. Performance characteristics of the mit fission converter based epithermal neutron beam. *Physics in Medicine and Biology*, 48(7):943, 2003.

[174] ICRU. Tissue substitutes in radiation dosimetry and measurement, report 44 of the international commission on radiation units and measurements. Technical report, International Commission on Radiation Units and Measurements, 1989.

[175] Kent Riley. Personal communication.

[176] A.I. Kassis D.E. Charlton and S.J. Adelstein. A comparison of experimental and calculated survival curves for v79 cells grown as monolayers or in suspension exposed to alpha irradiation from ^{2}12bi distributed in the growth medium. *Radiation Protection Dosimetry*, 52(1-4):311–315, 1994.

[177] Eric J Hall. *Radiobiology for the Radiologist*. J.B. Lippencott Company, Philadelphia, fourth edition, 1994.

[178] David W. Nigg. Computational dosimetry and treatment planning considerations for neutron capture therapy. *Journal of Neuro-Oncology*, 62:75–86, 2003.

[179] GW Kabalka, GT Smith, JP Dyke, WS Reid, CP Longford, TG Roberts, NK Reddy, E Buonocore, and KF Hubner. Evaluation of fluorine-18-bpa-fructose for boron neutron capture treatment planning. *Journal of Nuclear Medicine*, 38:1762–1767, 1997.

[180] Subhash Chandra and Daniel R. Lorey II. Sims ion microscopy imaging of bpa and 13c15n-labeled phenylalanine in human glioblastoma cells: Relevance of subcellular scale observations to bpa-mediated boron neutron capture therapy of cancer. *International Journal of Mass Spectrometry*, 260:90–101, 2007.

[181] J. Capala, J.A. Coderre, and A.D. Chanana. A treatment planning comparison of BPA- or BSH-based bnct of malignant gliomas. *Proceedings of the 7th international symposium on neutron capture therapy for cancer*, 1996.

[182] Matthew R. Palmer, J.Timothy Goorley, W.S. Kiger III, Paul M. Busse, Kent J. Riley, Otto K. Harling, and Robert G. Zamenhof. Treatment planning and dosimetry for the harvard-mit phase i clinical trial of cranial neutron capture therapy. *International Journal of Radiation Oncology, Biology and Physics*, 53(5):13611379, 2002.

[183] E. Hall and D. Brenner. The dose-rate effect revisited, radiobiological considerations of importance in radiotherapy. *Int J Radiat Oncol Biol Phys*, 21:14031414, 1991.

[184] B. Emami, J. Lyman, A. Brown, L. Cola, M. Goitein, JE Munzenrider, B. Shank, LJ Solin, and M. Wesson. Tolerance of normal tissue to therapeutic irradiation. *International Journal of Radiation Oncology* Biology* Physics*, 21(1):109–122, 1991.

[185] B. Jones, RG Dale, C. Deehan, KI Hopkins, and DAL Morgan. The role of biologically effective dose (bed) in clinical oncology. *Clinical Oncology*, 13(2):71–81, 2001.

[186] TE Schultheiss, LE Kun, KK Ang, and LC Stephens. Radiation response of the central nervous system. *International Journal of Radiation Oncology* Biology* Physics*, 31(5):1093–1112, 1995.

[187] Personal communication from Cecile Wojnecki, data from 'Clinical Audit on Location and Size of Tumour Volumes of High Grade Glioma Patients.' Article in preparation for publication.

[188] Eric J. Hall, Judy K. Novak, Albrecht M. Kellerer, Harald H. Rossi, Stephen Marino, and Leon J. Goodman. Rbe as a function of neutron energy. i. experimental observations. *Radiation Research*, 64(2):245–255, 1975.

[189] M. Belli, R. Cherubini, S. Finotto, G. Moschini, O. Sapora, G. Simone, and M.A. Tabocchini. RBE-LET relationship for the survival of V79 cells irradiated with low energy protons. *International Journal of Radiation Biology*, 55(1):93–104, 1989.

[190] RG Dale, B. Jones, and A. Cárabe-Fernández. Why more needs to be known about rbe effects in modern radiotherapy. *Applied Radiation and Isotopes*, 67(3):387–392, 2009.

[191] M. Krämer and M. Scholz. Treatment planning for heavy-ion radiotherapy: calculation and optimization of biologically effective dose. *Physics in medicine and biology*, 45(11):3319, 2000.

[192] Ben Phoenix, Stuart Green, Mark A. Hill, Bleddyn Jones, Andrew Mill, and David L. Stevens. Do the various radiations present in BNCT act synergistically? Cell survival experiments in mixed alpha-particle and gamma-ray fields. *Applied Radiation and Isotopes*, 67(7-8, Supplement 1):S318 – S320, 2009.